A FUNDAMENTAL STUDY OF SMOLDERING WITH EMPHASIS ON EXPERIMENTAL DESIGN FOR ZERO-G

NASA GRANT No. NAG-3-443, NASA LeRC

FINAL PROGRESS REPORT

Carlos Fernandez-Pello, P.I.
Patrick J. Pagni, Co-P.I.

Department of Mechanical Engineering
University of California, Berkeley
Berkeley, CA 94720

Submitted to:

NASA LEWIS RESEARCH CENTER
Space Experiments Division
Cleveland, OH 44135

August 1995

ABSTRACT

A research program to study smoldering combustion with emphasis on the design of an experiment to be conducted in the Space Shuttle was conducted at the Department of Mechanical Engineering, University of California Berkeley under NASA sponsorship. The motivation of the research is the interest in smoldering both as a fundamental combustion problem and as a serious fire risk. Research conducted included theoretical and experimental studies that have brought considerable new information about smolder combustion, the effect that buoyancy has on the process, and specific information for the design of a space experiment. Experiments were conducted at normal gravity, in opposed and forward mode of propagation and in the upward and downward direction to determine the effect and range of influence of gravity on smolder. Experiments were also conducted in microgravity, in a drop tower and in parabolic aircraft flights, where the brief microgravity periods were used to analyze transient aspects of the problem. Significant progress was made on the study of one-dimensional smolder, particularly in the opposed-flow configuration. These studies provided the background for a continuation research program currently underway on smoldering, also supported by NASA. They also provided enough information to design a small-scale space-based experiment and that was successfully conducted in the Spacelab Glovebox in the June 1992 USML-1/STS-50 mission of the Space Shuttle Columbia.

I. INTRODUCTION

Smoldering is defined as a non-flaming, surface combustion reaction, that propagates through the interior of porous combustible materials. The propagation of the smolder reaction is a complex phenomena involving processes related to the transport of heat and mass in a porous media, together with surface chemical reactions. Smoldering is a weakly reacting phenomena, and generally propagates very slowly. However, it can play an important role in the initiation of unwanted fires because of the potential rapid transition from the slow smoldering reaction to the flaming combustion of the material. Furthermore, smoldering is often difficult to detect and suppress because it may take place in the material interior and the porosity of the material may prevent the access of the extinguishing agent to the reaction zone. Thus, understanding of the physical and chemical mechanisms controlling smoldering is important not only because smoldering is a fundamental combustion process, but because such understanding can be critical to the prevention and control of destructive fires.

Smoldering is classified into opposed and forward configurations according to the direction in which the oxidizer flows toward the reaction zone. In opposed smolder, the oxidizer enters the reaction zone opposing the direction of propagation, and in forward smolder in the same direction. Since in the reference frame of the reaction zone the fuel and oxidizer enter the reaction zone from the same direction in opposed smolder and in the opposite direction in forward smolder, the former type of smolder has been also referred to as co-current smolder, and the latter as counter-current. The transport of mass can take place by mixed convection, forced and free, and by diffusion. This leads to a secondary classification of smoldering into convection driven and diffusion driven smolder. At normal gravity there is yet another classification into downward and upward smolder propagation.

Research conducted under this grant included theoretical and experimental studies of both opposed and forward smolder, that have brought considerable new information about smolder combustion and the effect that buoyancy has on the process. During the initial stages of the research program, emphasis was given to the development of a theoretical foundation for the program. Once the theoretical development reached a stage where comparison with experiments was deemed necessary, the emphasis was shifted to the experimental program. The objective of the experiments was to determine the effect of buoyancy (gravity) on smoldering, and to provide a data base for theoretical models verification. Experiments indicated that buoyancy had a small influence on the one-dimensional, co-current smoldering of cellulose and only at very low forced flow air velocities. It has a significant influence, however, when smolder occurs in a

2

gas-solid interface. Unfortunately, cellulose powder sediments and it is not possible to do upward burning experiments, or to significantly vary the void fraction in normal gravity. For this reason the research was switched to conducting the experiments with polyurethane foam.

Polyurethane foam, however, smolders only in a narrow range of conditions. After testing several ignition methods, a reliable ignition system was developed, and a vigorous ground based experimental program followed. A series of experiments in normal gravity for downward and upward, natural convection, co-current smoldering of polyurethane foam were completed. Another series of experiments were conducted at the NASA LeRC 2.2 seconds Drop-Tower to observe trends in the ignition characteristics of the foam, and to attempt to infer how smoldering will behave in microgravity. These tests were followed by another series of variable gravity smolder experiments conducted in the KC-135 and Lear-jet aircraft.

II. RESEARCH PROGRESS

The research program was planned to follow a progressive path aimed to acquire the information needed to design smolder experiments to be carried out in a space-based laboratory. The experiments would provide data, which in conjunction with theoretical models, would help to elucidate the mechanisms controlling smolder, and its potential behavior in a space environment. The research conducted under this grant is summarized below. References are given, to papers published or presented at meetings, that describe the work in more detail.

II.1 THEORY

During the initial stages of the research program efforts were concentrated on the development of theoretical models of smolder. Models of opposed (co-current) and forward (counter-current) smoldering under pure forced-flow, zero-gravity, conditions were developed [1,2,4]. The models describe the propagation of a smolder reaction through a porous solid fuel, and the resulting governing equations consist of the Darcy equation to describe the flow through the porous media, and the energy and species equations to describe the heat released at the reaction and the transport of heat and mass to and from the reaction. Because of the microgravity environment, it is assumed that the propagation of the smolder reaction is one-dimensional and steady. Radiation heat transfer is incorporated using the diffusion approximation and smolder combustion is modeled by a finite rate, one step reaction mechanism. Because the solid and the gas move at different velocities, both the smolder temperature, and the smolder velocity are eigenvalues.

3

The resulting dimensionless equations are similar to those governing the propagation of a laminar premixed flame for opposed smolder, and to a diffusion flame for forward smolder. From these non-dimensional equations the non-dimensional groups that control smoldering were identified for their use in the definition of the experiments [1,2,4]. The solution of the equations provided explicit expressions for the char oxidation velocity, and smolder reaction velocity and temperature. A global energy balance between the energy released in the reaction and the energy required to preheat the solid and the gas provides an explicit expression for the smolder velocity. The key predictions are that the smolder reaction temperature increases logarithmically and the smolder velocity linearly with the oxygen mass flux reaching the reaction.

II.2 EXPERIMENTS

Once the theoretical development reached a stage where comparison with experiments was deemed necessary, the emphasis was shifted to the development of the experimental aspect of the project. The scope of the experiments was the determination of how, and under what conditions, buoyancy (gravity) affects smoldering, and to provide a data base for comparison with theoretical models.

II.2.1 Cellulose Smoldering

Experiments were first conducted with powder cellulose as the combustible material [3,5,6] because it smolders easily and because there is considerable information about the subject in the technical literature. In the experiments buoyancy was modified primarily by changing the gas density through the ambient pressure. These experiments indicated that deep in the interior of the cellulose sample, buoyancy had a small influence on the one-dimensional, downward, opposed smoldering and only at very low forced-flow air velocities. It had a significant influence, however, when smolder occurred at the gas/solid interface, or if chimney-induced drafts were present in the experiments.

Cellulose powder sediments and it is not possible to do upward burning experiments, or to significantly vary the void fraction in normal gravity. For this reason the research was switched to conducting the experiments with a self-supporting porous fuel, specifically polyurethane foam.

II.2.2 Polyurethane Foam Smoldering

Polyurethane foam smolders only in a narrow range of conditions, extinguishing, melting, or flaming if these

4

conditions are not met. The determination of the range of conditions at which polyurethane foam smolders, and the development of an appropriate ignition method was a difficult and frustrating task that took a considerable amount of time to be resolved. Finally a reliable ignition system based on an electrically-heated Nichrome wire sandwiched in two layers of porous ceramic was developed. This development led to a very active and vigorous ground-based experimental program on the smoldering characteristics of polyurethane foam.

II.2.2.1 Natural Convection

A series of experiments in normal gravity for downward and upward, natural-convection smoldering of polyurethane foam was completed first [7]. The experiments showed that for the foam used, buoyancy influences the smolder reaction only for fuel heights of around 5 cm or smaller. For larger foam heights, normal-gravity buoyancy can not overcome the friction losses in the sample interior and generate convective flows, unless a chimney effect is created by the hot char left by the propagating smolder reaction or by external means (a duct located on top of the fuel, for example). Under these conditions the smolder velocity for both upward and downward smolder are similar. These results indicate that the air contained in the foam pores may be sufficient to sustain smolder. This result could be of particular importance if smoldering were to occur in a spacecraft, since microgravity provides an insulating environment and the heat from the smolder reaction, not being convectively removed, could lead to an enhancement of the smolder reaction, or even to the transition to flaming.

II.2.2.2 Forced Flow

The above experiments were followed by another series of experiments of forced flow smoldering, opposed and forward, [8]. In addition to providing information about the smolder process in forced flows, the experiments had the objective of determining the range of flow velocities at which buoyancy has a significant role in the smolder process. This was accomplished by comparing the results for upward and downward smoldering. Measurements conducted in these experiments included the smolder propagation velocity and reaction zone temperature as a function of the air flow velocity, the location of the smolder front along the sample, and the direction of smolder propagation (downward and upward).

The experimental results showed that there are some common characteristics to all the smolder configurations tested. All the experiments showed that three zones with distinct smolder characteristics can be identified along the foam sample. An initial zone near the igniter where the smolder process is

5

influenced by heat transfer from the igniter, an intermediate zone where smolder is self-sustained and free from external effects, and a third zone near the sample end that is strongly affected by convective currents. The smolder reaction propagation velocity and temperature generally have a direct correspondence and vary in each one of these three zones. The analysis of these variations confirmed that the smolder process is controlled by the competition between the supply of oxidizer to the reaction zone and the loss of heat from the reaction zone. However, the variation of the smolder velocity and temperature with the forced flow is quantitatively different for opposed and forward smoldering due to the different effect that the flow direction of the oxidizer and post-combustion gases have in each case.

Opposed Smoldering [8]: The variation with the opposed, forced air flow of the smolder propagation velocity and temperature shows that both parameters reach a maximum at flow velocities of approximately 2.5 mm/sec. At low flow velocities, oxygen depletion is the dominant factor controlling the smolder process, and the smolder velocity and temperatures are small. Increasing the flow velocity strengthens the smolder reaction due to the addition of oxidizer, which results in larger smolder velocities and temperatures. At even larger flow velocities convective cooling becomes dominant causing the weakening and final extinction of the smolder reaction. These competing mechanisms play a very important role in the end region of the sample where buoyancy-generated currents result in the strong enhancement of the reaction or in its extinction, depending on whether oxygen supply or convective cooling is the controlling smolder mechanism. Comparison between downward and upward smoldering indicates that gravity influences the smolder combustion of this type of foam for forced flow velocities smaller than 3 mm/sec, and sample sizes smaller than 50 mm.

Forward Smoldering [9]: The results of the dependence on the forced flow velocity of the smolder propagation velocity and temperature shows that in this case the smolder velocity always increases and the temperature decreases with the air flow rate, regardless of the sample location. These trends are the result of the hot post-combustion gases being convected ahead of the smolder front. Although they preheat the virgin material favoring the propagation of the reaction, they also dilute the oxidizer ahead of the reaction weakening it and reducing its temperature. For upward smoldering, transition to flaming was observed to occur in the char at the zone closer to the sample end and for air velocities of 15 mm/sec or larger. Comparison between upward and downward smoldering also showed that the effect of gravity takes place for air flow rates smaller than 3 mm/sec.

The differences observed between the opposed and forward smolder measurements can be explained by the differences in each case between the flow direction of the oxidizer and post-combustion gases. In the former case, the cold oxidizer flows opposite

6

to the smolder reaction propagation, and as the air velocity is increased at low flow velocities, the addition of oxidizer dominates the convective cooling and enhances the smolder reaction. At larger air velocities, however, convective cooling becomes dominant and the smolder velocity decreases as the air velocity is increased. In forward smoldering the oxidizer flows in the same direction as that of smolder propagation, and the hot post-combustion gases are convected to the virgin fuel ahead of the smolder front. The preheating of the virgin fuel results in an increase in the smolder velocity as the air flow rate is increased, even though the smolder temperature remains constant, or even decreases, due to the dilution of oxidizer by the post-combustion gases. Furthermore, the fresh oxidizer flows through the hot char, and since the char still contains a large amount of unburnt fuel secondary reaction may occur in the char, which under certain flow conditions can result in transition to flaming.

II.2.2.3 Micro-gravity smoldering

A series of smolder experiments were conducted at the NASA LeRC 2.2-seconds Drop Tower to observe trends in the ignition characteristics of the foam, and to attempt to infer how smoldering will behave in microgravity [10,12]. The parameter analyzed was the smolder reaction temperature variation with time, because the temperature itself, or the smolder velocity, do not change enough in 2.2 seconds to observe significant differences. The results for the temperature gradient variation with the flow velocity indicate that microgravity favors the initiation of smoldering, and that the upper range of flow velocities at which buoyancy plays a significant role on smoldering is around 2mm/sec, in approximate agreement with the normal gravity experiment.

A series of opposed flow smoldering experiments were also conducted in the KC-135 aircraft (30 secs of micro-g for up to 40 parabolas) to observe the effects of the variation of the gravity on the smolder process [11]. Although the microgravity period was too short to study steady smoldering in micro-gravity, the tests provided initial information about the process and permitted the observation of smolder trends as the gravity changes. The tests also complement the Drop Tower tests summarized above. The results show that buoyancy affects both the species transport and transfer of heat to and from the reaction zone. At the reaction zone, the former is dominant, which results in a decrease of the smolder temperature in microgravity. Away from the reaction zone the latter is dominant and the temperature increases due to the lack of convective cooling. All these effects are less noticeable as the flow velocity is increased, and as the reaction propagates toward the sample interior confirming that buoyancy is important at low flow velocities and near the sample ends. Another series of parabolic flight experiments have been conducted recently but

the results have not been analyzed with enough detail to report then at this time.

Finally, the information obtained from the ground experiments on the smoldering of polyurethane foam was used to design a small-scale experiment that was carried out in the USML-1/STS-50 mission of the Space Shuttle Columbia in June 1992. The size of the fuel specimen (a cylinder 5cm in diameter and 10 cm long) was determined by the constrains of the Glove-box where the experiments were conducted. Four tests were planned, two in still air and another two with a low-velocity air flowing around the sample. Two igniter configurations were designed, one with the igniter on the cylinder axis and the other with the igniter at one end of the cylinder.

III. PUBLICATIONS

1. Dosanjh, S., Pagni, P.J., and Fernandez-Pello, A.C., "Forced Cocurrent Smoldering Combustion," Combustion and Flame, 68, 131-142 (1987).

2. Dosanjh, S. and Pagni, P.J., "Forced Counter-Current Smoldering Combustion," Second AIME-JSME Thermal Engineering Joint Conference, Honolulu,Hawaii, March 1987.

3. Dosanjh, S., Peterson, J., Fernandez-Pello, A.C., and Pagni, P.J.,"Buoyancy Effects on Smoldering Combustion," Acta-Astronautica, No. 11/22, 689-696 (1986).

4. Dosanjh, S. "Smoldering Combustion Analysis," Ph.D. Thesis, Department of Mechanical Engineering, University of California, Berkeley, 1986.

5. Newhall, J.L., Fernandez-Pello, A.C., and Pagni, P.J., "Experimental Observations of the Effect of Pressure and Buoyancy on Co-Current Smoldering," J. of Fire and Materials,14, pp.145-150, 1989.

6. Newhall, J.L. "Experimental Observations of the Effect of Buoyancy on the rate of Co-Current Smolder Propagation in Cellulose", Masters Project, Department of Mechanical Engineering, University of California, Berkeley, 1988.

7. Torero, J., Kitano, M., and Fernandez-Pello, A.C., "Gravitational Effects on Co-Current Smoldering," 1990 Spring Meeting, Western States es Section and Canadian Section of the Combustion Institute, April 29-May2, Banff, Alberta, Canada, 1990.

8. Torero, J., Kitano, M. and Fernandez-Pello, A.C. "Mixed Flow Smoldering of Polyurethane Foam" 1990 Fall Technical Meeting,

Western States Section/Combustion Institute, San Diego, Ca. October 1990.

9. Torero, J. Kitano, M. and Fernandez-Pello, A.C. " Forward Smoldering of Polyurethane Foam" 1991 Spring Meeting, Western States Section/ Combustion Institute, Boulder, Co. March 1991.

10. Cantwell, E. and Fernandez-Pello, A.C., "Smoldering Combustion under Low Gravity," 28th Aerospace Meeting, January 8-11, Reno, NV, paper AIAA-90-0648, 1990.

11. Cantwell, E.R., and Fernandez-Pello, A.C."Smoldering Combustion under Low Gravity Conditions" 1990 Fall Technical Meeting, Western States Section/Combustion Institute, San Diego, Ca. October 1990. Also Poster # P245 Twenty- Third International Symposium on Combustion, Orleans, France, July 1990

APPENDIX

Papers Listed in the Publication Section

PAPER 1

"FORCED COCURRENT SMOLDERING COMBUSTION"

Dosanjh, S., Pagni, P.J., and Fernandez-Pello, A.C.

Forced Cocurrent Smoldering Combustion

SUDIP S. DOSANJH, PATRICK J. PAGNI, and A. CARLOS FERNANDEZ-PELLO

Mechanical Engineering Department, University of California, Berkeley, CA 94720

An analytic model of the propagation of smoldering combustion through a very porous solid fuel is presented. Here smoldering is initiated at the top of a long, radially insulated, uniform fuel cylinder, so that the smolder wave propagates downward, opposing an upward forced flow of oxidizer. Because the solid fuel and the gaseous oxidizer enter the reaction zone from the same direction, this configuration is referred to as cocurrent (or premixed-flame-like). It is assumed that the propagation of the smolder wave is one-dimensional and steady in a frame of reference moving with the wave. Buoyancy is included and shown to be negligible in the proposed application of a smoldering combustion experiment for use on the Space Shuttle. Radiation heat transfer is incorporated using the diffusion approximation and smoldering combustion is modeled by a finite rate, one-step reaction mechanism. Because the solid and the gas move at different velocities, both the downstream temperature, T_f, and the smolder velocity, v, are eigenvalues. The dimensionless equations are very similar to those governing the propagation of a laminar premixed flame. A straightforward extension of the activation energy asymptotics analysis presented by Williams for premixed flames yields an expression for a dimensionless eigenvalue determining T_f. A global energy balance provides a relation for the smolder velocity, v. Predictions are compared with the experimental findings of Rogers and Ohlemiller and with the numerical results of Ohlemiller, Bellan, and Rogers. Key results include (1) for a given solid fuel, T_f depends only on the initial oxygen mass flux, $\dot{m}_\alpha''$, and increases logarithmically with $\dot{m}_\alpha''$; (2) v increases linearly with $\dot{m}_\alpha''$ and at fixed $\dot{m}_\alpha''$, increasing the initial oxygen mass fraction, $Y_{\alpha i}$, increases v; (3) steady smolder propagation is possible only for $Y_{\alpha i} \geq c_{eff}(T_f - T_i)/Q$, with extinction occurring when all of the energy released in the reaction zone is used to heat the incoming gas. General explicit expressions for T_f and v are presented.

1. INTRODUCTION

Smoldering is defined as combustion without flame. The primary source of heat release is the heterogeneous oxidation of the solid [1]. This process occurs in several steps [2]. Oxygen diffuses to the surface of the solid where it is adsorbed. A highly exothermic reaction ensues on the surface. After the products of combustion (primarily CO_2, H_2O, and CO) are desorbed, they diffuse away from the surface. Many materials can sustain smoldering combustion. These include coal, cotton, dusts, paper, polyurethane foams, thermal insulation materials, and wood. If the material is sufficiently permeable, smoldering can occur well within the host. A self-supporting exothermic reaction zone can pass through the substance [1]. Oxygen reaches the reaction zone

by convection and diffusion. However, such a scenario is not valid for all porous materials. Upon being heated, some substances decompose into a "liquid" tar [3], restricting the flow of air and consequently inhibiting the propagation of such a smolder wave. Smoldering combustion can be prevented in some materials by adding sulfur [4, 5].

A schematic of the problem under consideration and the coordinate system used is shown in Fig. 1. A porous combustible solid with density ρ_{si}, temperature T_i, and void volume fraction ϕ is contained in a vertical cylinder. A gaseous oxidizer with an oxygen concentration Y_{oi}, a density ρ_{gi}, and an inlet velocity u_i flows upward through the solid. In the Appendix, buoyancy is shown to be negligible in the proposed application of a smoldering combustion experiment for use on the
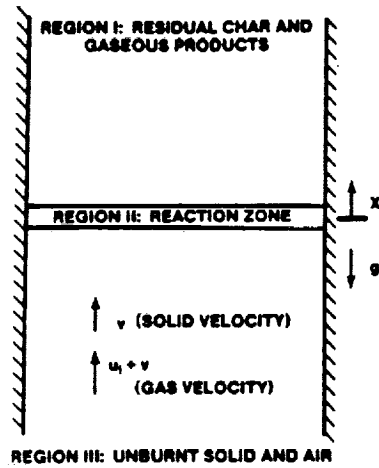
Fig. 1. Cocurrent smoldering combustion viewed in a frame of reference moving with the smolder wave.

TABLE I

Typical Smolder Characteristics [14]

Quantity of Interest	Magnitude
Smolder velocity, v	$O(0.01$ cm/s$)$
Initial gas velocity, u_i	$O(0.1$ cm/s$)$
Peak temperature, T_f	350–500°C
Smolder wave thickness	2–3 cm
Inverse equivalence ratio, r_{eq}	$O(0.03)$
Solid mass flux, $\dot{m}_s''$	$O(0.0004$ g/cm^2 s$)$
Gas mass flux, $\dot{m}_g''$	$O(0.0001$ g/cm^2 s$)$
Solid mass fraction, ϵ_s	$O(0.8)$
Gas mass fraction, ϵ_g	$O(0.2)$

Space Shuttle. A planar ignition source is used to initiate smoldering at the top of the solid. The smolder wave propagates downward opposing the upward flow of oxidizer. Because the oxidizer and the fuel enter the reaction zone from the same direction, this configuration is often referred to as cocurrent or premixed-flame-like. While all of the oxygen is consumed in the reaction zone, a considerable amount of solid remains [1]. The heat released in the reaction zone is transferred upstream, by conduction and radiation, providing the energy required to preheat the solid.

Some of the earliest work in the field of smoldering combustion was conducted by Palmer [6], who measured the rate of smolder spread in dust trains and heaps. Recently, several researchers have modeled smoldering combustion propagation. Smolder spread in horizontal, cylindrical, cellulose [7], and polyurethane [8] fuel elements has been examined. Leisch et al. [9] investigated smoldering combustion in horizontal dust layers. Kinbara et al. [10] studied the downward spread of smoldering through various cellulosic materials. Muramatsu et al. [11] scrutinized the evaporation-pyrolysis processes inside a smoldering cigarette. Kansa et al. [12] considered wood pyrolysis. The present study is intended to complement the earlier work of Ohlemiller et al. [13], who developed a large computer code to investigate unsteady smol-

der propagation in flexible polyurethane foams. Because their method required expensive finite-element calculations, Ohlemiller et al. concluded that a primary use of their model was to study the initiation of smoldering combustion.

A primary goal of this study is to use activation energy asymptotics to conduct a parametric investigation of cocurrent smoldering combustion. The dimensionless equations are very similar to those governing the propagation of a laminar premixed flame. A straightforward extension of the premixed flame analysis presented by Williams [2] yields an expression for a dimensionless eigenvalue, Λ, providing a relationship between the initial oxygen mass flux, $\dot{m}_{oi}'' = Y_{oi}\phi\rho_{gi}u_i$, and the final temperature, T_f. A global energy balance determines the smolder velocity, v. Both v and T_f are highly dependent on $\dot{m}_{oi}''$. This is due to the oxygen limited nature of cocurrent smoldering combustion. That is, all of the incoming oxygen is usually consumed and the total energy available is proportional to $\dot{m}_{oi}''$. Theoretical predictions are compared with the experimental findings of Rogers and Ohlemiller [14] and with the calculations of Ohlemiller et al. [13].

2. ANALYSIS

2.1. Governing Equations

Typical values of several key smolder characteristics, including the smolder velocity, v, and the peak temperature, T_f, are given in Table I. Many

fuels of interest are very porous, and consequently, conduction is a relatively poor mode of heat transfer [13]. Thus, radiation heat transfer is often important despite the relatively low temperatures encountered in smoldering combustion—peak temperatures are usually between 350 and 500° C [14]. Electron microscope photographs of two solid fuels, a GM-25 polyurethane foam and a packed bed of alpha-cellulose, are shown in Figs. 2A and 2B, respectively. Both of these materials have been used in recent experimental investigations [3, 7, 8, 14, 16] of smoldering combustion. While radiation is important in polyurethane foams, it is approximately negligible in tightly packed beds of alpha-cellulose. In the following analysis, radiation heat transfer is incorporated using a diffusion approximation.

Smoldering is modeled as a finite rate, one-step reaction,

$$1 \text{ g(Unburned Solid)} + n_o O_2,$$

$$\rightarrow n_s(\text{Ash}) + n_{gp}(\text{Gaseous Products}) + Qn_o, \quad (1)$$
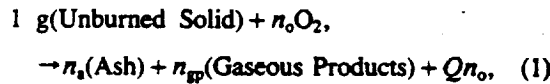
where the n values are stoichiometric coefficients (grams/gram of unburned solid). Ohlemiller and Lucca [15] reported that such a model adequately described the cocurrent smoldering of cellulosic insulation materials. Ohlemiller et al. [13] modeled the smoldering combustion of a polyurethane foam by using two global reactions. However, since the second reaction (oxidation) was much faster than the first reaction (pyrolysis), their two-step reaction mechanism can be well approximated by Eq. (1). The following asymptotic analysis can be modified to include a nonoxidative pyrolysis reaction. Because the amount of energy consumed by pyrolysis is much smaller than the amount released in the reaction zone, for steady smolder, such a reaction will only have a small effect on the temperature profiles.

Additionally, the solid phase is considered continuous with a constant void volume fraction. Cocurrent smoldering is assumed to be one-dimensional and steady in a frame of reference fixed on the smolder wave. Fick's law is used to model the diffusion of oxygen and the quantity $\rho_g D$ is assumed constant. The gas and the solid are presumed to be in local thermal equilibrium.

Energy transport due to concentration gradients, energy dissipated by viscosity, work done by body forces, and the kinetic energy of the gas phase have been ignored.

In a frame of reference moving with the smolder wave, $\dot{m}_s'' = (1 - \phi)\rho_s v$. Since the smolder velocity is usually at least an order of magnitude smaller than the gas phase velocity [13, 14], $\dot{m}_g'' \cong \phi\rho_g u$. This assumption allows $\dot{m}_{oi}''$ to be treated as a known quantity. The conservation of mass requires that $\dot{m}''$ $(= \dot{m}_s'' + \dot{m}_g'')$ remain constant. Mass flux fractions are defined by

$$\epsilon_s = \frac{\dot{m}_s''}{\dot{m}''}, \qquad \epsilon_g = \frac{\dot{m}_g''}{\dot{m}''}, \qquad (2a,2b)$$

$$\epsilon_{us} = \frac{Y_{us}\dot{m}_s''}{\dot{m}''}, \qquad (3)$$

$$\epsilon_o = \frac{1}{\dot{m}''}\left[\phi Y_o \rho_g u - \phi\rho_g D \frac{dY_o}{dx}\right]. \qquad (4)$$

Symbols are defined in the nomenclature. Equation (1) gives

$$\frac{d\epsilon_{us}}{dx} = \frac{1}{n_o}\frac{d\epsilon_o}{dx} = \frac{1}{(1-n_s)}\frac{d\epsilon_s}{dx} = -\frac{1}{(n_{gp}-n_o)}\frac{d\epsilon_g}{dx}. \qquad (5)$$

Species conservation for oxygen requires

$$\frac{d\epsilon_o}{dx} = -\frac{n_o}{\dot{m}''}\dot{r}'', \qquad (6)$$

and integrating the conservation of energy gives

$$\dot{m}'' c_{eff}(T - T_i) - (k_{eff} + k_{rad})\frac{dT}{dx} = Q\dot{m}''(\epsilon_{oi} - \epsilon_o), \qquad (7)$$

where Eq. (6) has been used to eliminate the reaction rate from Eq. (7). The effective thermal conductivity, $k_{eff} = \phi k_g + (1 - \phi)k_s$, accounts for heat transfer due to conduction in both gas and solid phases. Radiation heat transfer is incorporated using a temperature dependent conductivity [15, 17], $k_{rad} = 16\sigma l_r T^3/3$. The effective heat capacity, $c_{eff} = \epsilon_s c_s + \epsilon_g c_g$, is taken as constant.

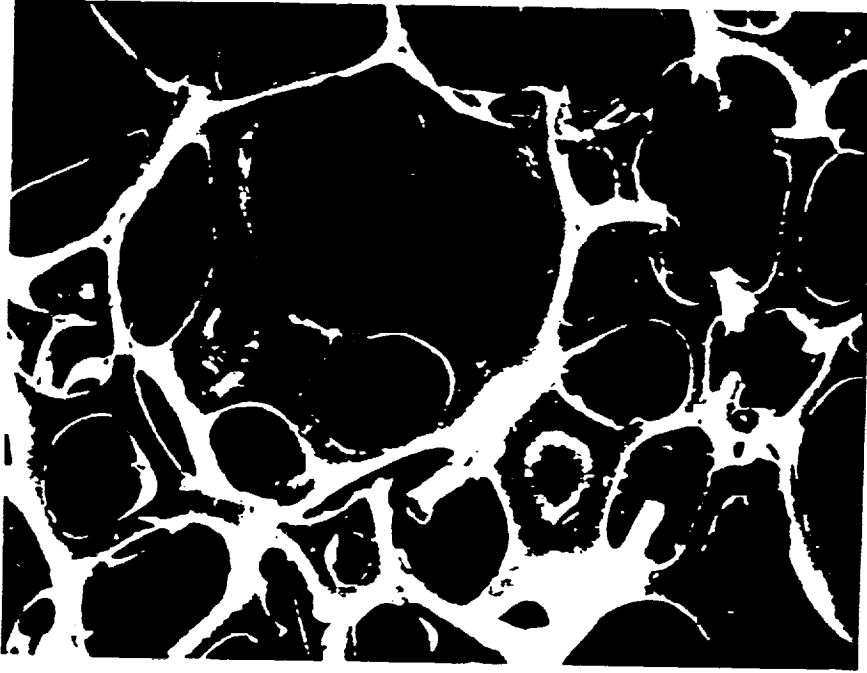The reaction rate, $\dot{r}''$, is assumed to depend on

Fig. 2A. Electron microscope photograph of a polyurethane foam.

the oxygen mass fraction, the solid fuel present, and the temperature in an Arrhenius form,

$$\dot{r}''' = Z(Y_o\rho_g)^a(Y_{us}\rho_s)^bT^ce^{-E/RT}, \qquad (8)$$

where a, b, and c are constants. The conservation of momentum, which is discussed in the Appendix, and the ideal gas equation of state, $P = \rho_g RT$, complete the preceding set of equations. Because pressure variations are small [1], the transport equations can be solved without considering the momentum equation. Properties of a polyurethane foam and an alpha-cellulose packing are given in Table II.

The following boundary conditions are imposed on Eqs. (4)–(6): as $x \to -\infty$, $\epsilon_o \to \epsilon_{oi}$; as $x \to +\infty$, $\epsilon_o \to 0$, $Y_o \to 0$, and $T \to T_f$. Two boundary conditions are imposed on Eq. (4). The second boundary condition, which requires that all of the incoming oxygen be consumed, will determine T_f.

Setting $T = T_f$, $\epsilon_o = 0$, and $dT/dx = 0$ in Eq. (7) gives

$$v = \frac{Q\dot{m}_{oi}''}{(1-\phi)\rho_{si}c_{eff}(T_f-T_i)} - \frac{\phi\rho_{gi}u_i}{(1-\phi)\rho_{si}}. \qquad (9)$$

After solving for T_f, Eq. (9) will be used to determine v.

2.2. Dimensionless Governing Equations

A characteristic distance, $x_c = k_{eff}/\dot{m}''c_{eff}$, is chosen by balancing convection and diffusion in the energy equation, thus eliminating one dimensionless parameter. Typically, $k_{eff} \sim 0.05$ W/m K, $\dot{m}'' \sim 0.005$ kg/m^2 s, and $c_{eff} \sim 1$ kJ/kg K, giving $x_c \sim 0.01$ m. Because the definition of x_c does not account for radiation, x_c is somewhat

Fig. 2B. Electron microscope photograph of alpha-cellulose.

TABLE II

Typical Properties of a Polyurethane Foam and a Packed Bed of Alpha-Cellulose

	Polyurethane[a]	Alpha-Cellulose[b]
ϕ	0.97	0.82
ρ_u [kg/m^3]	1150	620
c, [kJ/(kg K)]	1.7	0.84
k_{eff} [W/m K]	0.047	0.050
$k_{rad}(T_i)$ [W/m K]	0.005	−0
E [kJ/mol]	155 (140)[c]	180
Q [kJ/kg]	12,300 (7,600)	12,500
Z	10^{10} m^3/kg s	3×10^6 m$^{1.5}$/kg$^{0.5}$ K$^{0.5}$ s
a	1	0.5
b	1	1
c	0	0.5
n_{gy}/n_o	3.7	1.4

[a] Properties given in Ref. [13] are shown in parentheses whenever they are different from the value listed above.

[b] From Refs. [7, 16].

[c] Shown in the parentheses is the activation energy for the first reaction in the two-step model in Ref. [13].

smaller than the smolder wave thickness given in Table I. Since all of the oxygen is consumed, the oxygen mass flux and the oxygen mass fraction are normalized by their initial values (that is. $\bar{\epsilon}_o = \epsilon_o/\epsilon_{oi}$ and $\bar{Y}_o = Y_o/Y_{oi}$). A dimensionless temperature is defined by $\bar{T} = (T - T_i)/T_c$, where T_c is a characteristic temperature. Setting $T_c = T$, makes $\bar{T}$ an $O(1)$ quantity—see Table I.

The dimensionless parameters governing cocurrent smoldering are listed in Table III. Parameter ranges given in Table III were estimated from the properties tabulated in Table II. Note that the asymptotic analysis is only valid when the Zeldovich number, $\beta = \beta' \bar{T}_f/(1 + \bar{T}_f)^2$, is large ($\beta > 10$) [2], roughly corresponding to $\beta' > 50$. The dimensionless radiation conductivity. N_R, is artificially low because it is based on T_i rather than T_f. A critical value of the dimensionless heat release, D_c, below which solutions cease to exist, will be identified.

Dividing Eqs. (4) and (6) by Eq. (7) eliminates the spatial coordinate, $\bar{x}$. In terms of the new

Table III

Dimensionless Parameters Governing Forced Cocurrent Smoldering Combustion (in Addition to the Following Parameters, r_{eq}, a, b, and c Must Be Specified)

$D_c = \dfrac{QY_\alpha}{c_{eff}T_i}$	Dimensionless measure of the energy released in the reaction zone (varies from 0 to 40)
$Le = \dfrac{k_{eff}T_i}{\phi\rho_s DQY_\alpha}$	Modified Lewis number (varies from 0.05 to infinity)
$N_R = \dfrac{16\sigma l_r T_i^3}{3k_{eff}}$	Dimensionless radiation conductivity (usually less than 0.1)
$P_s = \left[\dfrac{n_{g}}{n_o} - 1\right] Y_\alpha$	Measures the amount of gas produced in the reaction zone (varies between 0.1 and 1.0)
$\beta' = \dfrac{E}{RT_i}$	Dimensionless activation energy (varies between 50 and 70)
$\bar\Lambda = \dfrac{n_o Z(RK_{eff})^{1+a}\rho_{si}^b T_i^{2a+c+2}\Gamma(1+a)}{m_\alpha''^2(EQ)^{1+a}(\phi D_i)^a}$	Dimensionless preexponential factor (usually lies between 10^8 and 10^{10})

coordinate, $\hat{T}$, the governing equations are

$$\frac{T - \hat{T}_f(1 - \bar\varepsilon_o)}{1 + N_R(1 + \hat{T})^3} \frac{d\bar\varepsilon_o}{d\hat{T}} = -\omega \tag{10}$$

and

$$\frac{T - \hat{T}_f(1 - \bar\varepsilon_o)}{Le\ \hat{T}_f[1 + N_R(1 + \hat{T})^3]} \frac{d\bar{Y}_o}{d\hat{T}}$$
$$= [1 + P_s(1 - \bar\varepsilon_o)]\ \bar{Y}_o - \bar\varepsilon_o. \tag{11}$$

The dimensionless reaction rate is given by

$$\omega = \Lambda \bar{Y}_o^a[1 - r_{eq}(1 - \bar\varepsilon_o)]^b(\hat{T} + 1)^{c-a}$$
$$\times \exp\left\{-\frac{\beta'(\hat{T}_f - \hat{T})}{(\hat{T} + 1)(\hat{T}_f + 1)}\right\}, \tag{12}$$

where

$$\Lambda = \frac{\bar\Lambda\beta'^{1+a}\hat{T}_f}{Le^a\ \Gamma(1+a)} \exp\left\{-\frac{\beta'}{1 + \hat{T}_f}\right\}. \tag{13}$$

In terms of $\hat{T}$, the boundary conditions are $\bar\varepsilon_o \to 1$ as $\hat{T} \to 0$ ($\hat{x} \to -\infty$); $\bar\varepsilon_o \to 0$ and $\bar{Y}_o \to 0$ as $\hat{T} \to \hat{T}_f$ ($\hat{x} \to +\infty$). After solving Eqs. (10) and (11),

the spatial coordinate, $\hat{x}(\hat{T})$, is determined by

$$\frac{1 + N_R(1 + \hat{T})^3}{\hat{T} - \hat{T}_f(1 - \bar\varepsilon_o)} \frac{d\hat{T}}{d\hat{x}} = 2. \tag{14}$$

Equation (9) gives a relationship between a dimensionless smolder velocity, $\bar{v} = v/v_c$, and the dimensionless final temperature, $\hat{T}_f = (T_f - T_i)/T_i$:

$$\bar{v} = \frac{1}{\hat{T}_f} - \frac{1}{D_c}. \tag{15}$$

A characteristic smolder velocity, $v_c = Qm_{oi}''/(1 - \phi)\rho_{si}c_{eff}T_i$, is chosen by balancing the energy released in the reaction zone and the energy required to preheat the solid, thus eliminating one parameter from the above equation.

3. ACTIVATION ENERGY ASYMPTOTICS

Typical values of the Zeldovich number, β, encountered in smoldering combustion are fairly large. From the argument of the exponential in Eq. (12), the reaction rate is significant only when $1 - \beta^{-1} < \hat{T}/\hat{T}_f < 1$, corresponding to the (inner) Region II in Fig. 1. The outer region consists of

the point $\hat{T} = \hat{T}_f$, Region I in Fig. 1, and Region III in Fig. 1, $0 < \hat{T}/\hat{T}_f < 1 - \beta^{-1}$. In the outer regions, the reaction rate is negligible and diffusion is balanced by convection. Because the inner region is very thin, diffusion dominates convection, and consequently, the source terms in the governing equations are balanced by diffusion.

In Region III, $\omega \sim 0$ and Eq. (10) yields $\hat{\epsilon}_o = 1$. Substituting $\hat{\epsilon}_o = 1$ into Eq. (11) and integrating once gives

$$\hat{Y}_o = 1 - \exp\left[-\mathrm{Le}\ \hat{T}_f \int_{\hat{T}}^{\hat{T}_f} \frac{1}{t} \right.$$

$$\times\ \left. [1 + N_R(1+t)^3]\, dt \right].\quad (16)$$

Note that the integral in the above equation diverges at $\hat{T} \to 0$. Therefore, $\hat{Y}_o \to 1$ as $\hat{T} \to 0$. A stretched variable is defined, $\xi = \beta(1 - \hat{T}/\hat{T}_f)$. Expanding $\hat{Y}_o$ and $\hat{\epsilon}_o$ in terms of $1/\beta$ gives $\hat{Y}_o = (1/\beta)\hat{Y}_o{}^1 + O(1/\beta^2)$ and $\hat{\epsilon}_o = \hat{\epsilon}_o{}^0 + O(1/\beta)$, respectively. Matching conditions are: $\hat{\epsilon}_o{}^0 \to 1$ as $\xi \to +\infty$; $\hat{\epsilon}_o{}^0 \to 0$ and $\hat{Y}_o{}^1 \to 0$ as $\xi \to 0$.

In the inner region, Eqs. (10)–(13) yield (to leading order)

$$\frac{\hat{\epsilon}_o{}^0}{1 + N_R(1 + \hat{T}_f)^3}\ \frac{d\hat{\epsilon}_o{}^0}{d\xi}$$

$$= \frac{\Lambda}{\beta^{1+a}} [\hat{Y}_o{}^1]^q [1 - r_{eq}(1 - \hat{\epsilon}_o{}^0)]^b e^{-\xi} \quad (17)$$

and

$$\frac{d\hat{Y}_o{}^1}{d\xi} = \mathrm{Le}\ \hat{T}_f[1 + N_R(1 + \hat{T}_f)^3]. \quad (18)$$

Integrating Eq. (18), substituting the resulting expression into Eq. (17), applying the matching conditions, and integrating once yield

$$\Lambda = \frac{\beta^{1+a}f(b, r_{eq})}{\mathrm{Le}^a\ \hat{T}_f{}^a[1 + N_R(1 + \hat{T}_f)^3]^{1+a}\Gamma(1+a)},\quad (19)$$

where

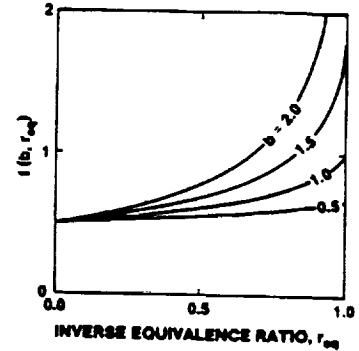$$f(b, r_{eq}) = \int_0^1 \frac{t\,dt}{[1 - r_{eq}(1 - t)]^b}.\quad (20)$$

Fig. 3. The function $f(b, r_{eq})$ plotted versus the inverse equivalence ratio, r_{eq}, for various values of b.

Because the oxygen consumption of a typical smolder wave is only a few percent of that required for stoichiometric burning, the inverse equivalence ratio, r_{eq}, is fairly small [13, 15]. As shown in Fig. 3, $f(b, r_{eq}) \to 1/2$ in the limit $r_{eq} \to 0$.

4. GENERAL SOLUTION

4.1. Fields

Because all of the incoming oxygen is consumed in the reaction zone, the total heat release is proportional to the initial oxygen mass flux, $\dot{m}_{oi}''$. Both the smolder velocity, v, and the final temperature, $\hat{T}_f$, are highly dependent on $\dot{m}_{oi}''$. Since $\hat{T}_f$ appears in Eqs. (10)–(12), (14), varying $\dot{m}_{oi}''$ affects the dimensionless oxygen mass fraction, $\hat{Y}_o(\hat{T})$, the dimensionless oxygen mass flux, $\hat{\epsilon}_o(\hat{T})$, and the dimensionless distance, $\hat{x}(\hat{T})$. These profiles depend on Le, N_R, r_{eq}, β', $\bar{\Lambda}$, a, b, and c. Since r_{eq} is usually small, the various profiles are weakly dependent on r_{eq} and b. Results presented in this section are for the limit $r_{eq} \to 0$, and consequently, the solutions are independent of both r_{eq} and b.

When $\hat{\epsilon}_o$ is plotted as a function of normalized temperature, $\hat{T}/\hat{T}_f$, the resulting curves depend on only two parameters, the Zeldovich number $\beta = \beta'\hat{T}_f/(1 + \hat{T}_f)^2$ and the constant a. As evidenced by Fig. 4, the incoming oxygen is consumed in a narrower region as β is increased. Also plotted in Fig. 4 is $\hat{Y}_o$ versus $\hat{T}/\hat{T}_f$, parameterized in Le, for $N_R = 0.1$, $\bar{\Lambda} = 10^{10}$, $a = 1$, and $c = 0$. The
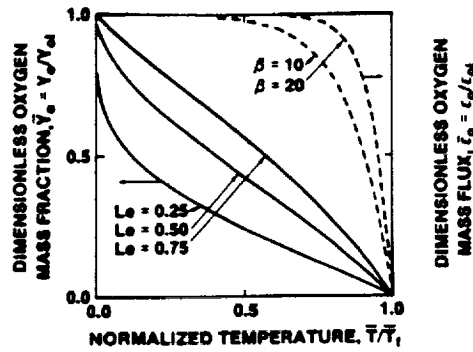
Fig. 4. Dimensionless oxygen mass fraction, $\bar{Y}_o = Y_o/Y_{oi}$, versus normalized temperature, T/T_f, with $N_R = 0.1$, $\beta' = 60$, $\bar{\Lambda} = 10^{10}$, $a = 1$, $c = 0$, and $r_{eq} = 0$. Also plotted is the dimensionless oxygen mass flux, $\bar{\epsilon}_o = \epsilon_o/\epsilon_{oi}$, versus T/T_f, for $a = 1$ and $r_{eq} = 0$. The dimensionless parameters are defined in Table II.

modified Lewis number, Le, measures the thermal thickness relative to oxygen diffusion thickness. The preceding analysis is valid when the diffusion thickness is much larger than the thickness of the reaction zone, roughly corresponding to Le $\ll \beta$. When Le $\sim \beta$, the dimensionless oxygen mass fraction is $O(1)$ in the reaction zone and smoldering is kinetically controlled [18]. For polyurethane, with $u_i = 0.2$ cm/s and $P_a = 1$ atm, the criterion for diffusion controlled smoldering is Y_{oi}

≥ 0.02. For a packed bed of alpha-cellulose, the criterion is $Y_{oi} \geq 0.01$.

After ascertaining the dependence of $\bar{\epsilon}_o$ on T, Eq. (14) can be used to determine T as a function of dimensionless distance, $\bar{x}$. Typical temperature profiles, parameterized in N_R and β', for $\bar{\Lambda} = 10^9$, $a = 1$, and $c = 0$, are shown in Fig. 5. Raising the dimensionless radiation conductivity, N_R, decreases the final temperature and increases the thermal thickness of smolder zone. On the other hand, increasing β leads to greater final temperatures. Note that $\bar{\epsilon}_o(\bar{x})$ and $\bar{Y}(\bar{x})$ can be constructed by combining Figs. 4 and 5. Results from such a calculation are shown in Fig. 6.

4.2. Final Temperature and Smolder Velocity

A key result of this analysis is $T_f(N_R, \beta', \bar{\Lambda}, a, c)$. In the limit $r_{eq} \rightarrow 0$, Eqs. (19) and (20) give

$$\bar{\Lambda}[1 + N_R(1 + \bar{T}_f)^3]^{1+a}(1 + \bar{T}_f)^{a+c+2}$$

$$\times \ e^{-\beta'/(1+\bar{T}_f)} = \frac{1}{2}. \tag{21}$$

A plot of $\bar{T}_f = (T_f - T_i)/T_i$ versus $\bar{\Lambda}$, parameterized in the dimensionless activation energy, β', and the dimensionless radiation conductivity, N_R, for $a = 1$ and $c = 0$, is shown in Fig. 7. As the

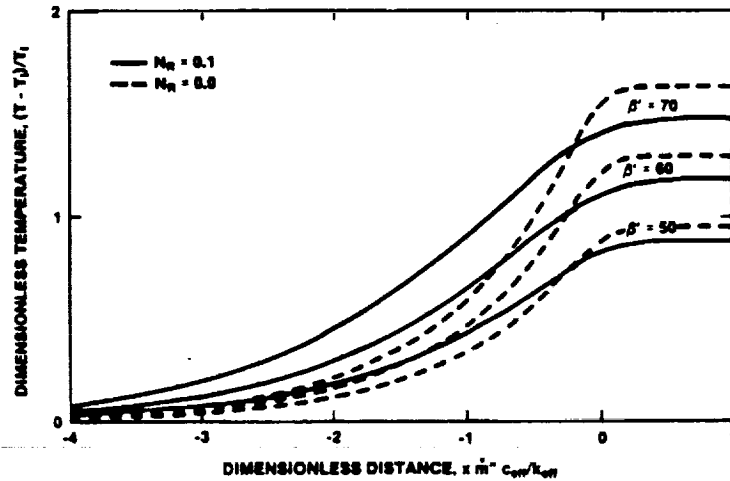Fig. 5. Dimensionless temperature, $\bar{T} = (T - T_i)/T_i$, versus dimensionless distance, $\bar{x} = x\dot{m}^a c_{eff}/k_{eff}$, with $\bar{\Lambda} = 10^{10}$, $a = 1$, $c = 0$, and $r_{eq} = 0$.
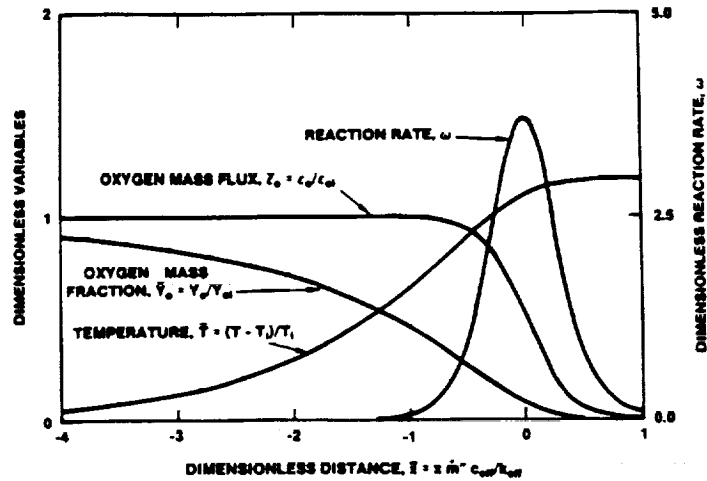
Fig. 6. Dimensionless variables, $\bar{Y}_o$, $\bar{\epsilon}_o$, and $\bar{T}$, and the dimensionless reaction rate, ω, versus dimensionless distance, $\bar{x}$, with $\beta' = 60$, $\bar{\Lambda} = 10^{10}$, $Le = 0.5$, $N_R = 0.1$, $r_{eq} = 0$, $a = 1$, and $c = 0$.
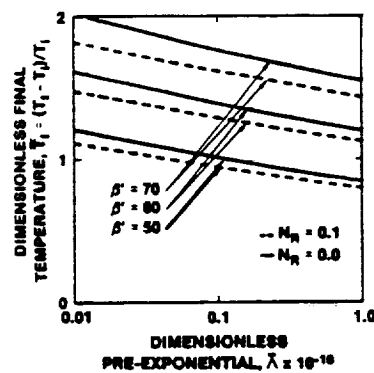

Fig. 7. Dimensionless final temperature, $\bar{T}_f = (T_f - T_i)/T_i$, versus the dimensionless preexponential factor, $\bar{\Lambda}$, with $a = 1$, $c = 0$, and $r_{eq} = 0$.

Fig. 8. Downstream temperatures in polyurethane predicted by the present analytic model, for the properties listed in Table I (—) and those given by Ohlemiller et al (-··-), measured by Rogers and Ohlemiller, and calculated by Ohlemiller et al. (○). Measurements are for the following conditions: u_i = 0.04 cm/s, Y_{oi} = 0.23 (+), and Y_{oi} = 0.44 (△): u_i = 0.15 cm/s, Y_{oi} = 0.44 (×). Also shown in the figure are predictions for cellulose (–).

reaction rate is increased, by either raising the preexponential, $\bar{\Lambda}$, or lowering the activation energy, β', $\bar{T}_f$ decreases and the smolder velocity, $\bar{v}$, which is inversely proportional to $\bar{T}_f$, increases. That is, the material burns faster when the reaction rate is higher.

For a given fuel, $\bar{T}_f$ decreases logarithmically with $\bar{\Lambda}$. Therefore, $\bar{T}_f$ increases logarithmically with the initial oxygen mass flux, $\dot{m}''_{oi}$, as shown in Fig. 8. Also indicated are measurements by Rogers and Ohlemiller [14] and calculations by

Ohlemiller et al. [13] for polyurethane. Ohlemiller et al. attributed the discrepancy between their predictions and experiments to uncertainty in the base parameter set (see Table II). When their parameters are used in this model, as shown by the dot-dash line in Fig. 8, predicted values of T_f are close to those calculated by Ohlemiller et al. Results from this study indicate that the parame-

ters in Table II are a better choice, for they give much closer agreement between predictions (solid line) and measurements. The dashed line in Fig. 8 gives the final temperature for alpha-cellulose.

As shown in Eq. (15), the dimensionless smolder velocity depends only on D_c and $\hat{T}_f$. The dimensionless parameter, D_c, which measures the total energy released in the reaction zone relative to the amount of energy required to raise the temperature of the gas from T_i to T_f, contains the experimentally observed dependence of v on Y_{oi}. For a given fuel and a fixed initial oxygen mass flux, $\dot{m}_{oi}''$, increasing Y_{oi} raises D_c, leading to higher smolder velocities. This dependence of $\bar{v}$ on D_c is fairly weak except near extinction. For Y_{oi} near 0.23, D_c is on the order of 10 and therefore, as a first approximation, $\bar{v} \sim 1/\hat{T}_f$. Because T_f varies slowly with $\dot{m}_{oi}''$, v is approximately proportional to $\dot{m}_{oi}''$ (recall that $v_c \sim \dot{m}_{oi}''$). Figure 9 illustrates the dependence of $\bar{v}$ on $\bar{\Lambda}$ for polyurethane. Overall, there is good agreement between the smolder velocities predicted by this model and those measured by Rogers and Ohlemiller [14].

Extinction occurs when $v = 0$, corresponding to $T_f = D_c$. That is, extinction occurs when all of the energy released is used to heat the incoming gas. Steady smoldering combustion is possible only when $Y_{oi} \geq c_{eff}(T_f - T_i)/Q$. For polyurethane, with $u_i = 0.2$ cm/s and $P_a = 1$ atm, this criterion requires that $Y_{oi} \geq 0.05$. Note that the presence of heat losses from the sides of the cylinder will raise this critical value of Y_{oi}.

5. CONCLUSIONS

An analytical model of cocurrent (premixed-flame-like) smoldering combustion has been developed. Smoldering was assumed to be one-dimensional and steady in a frame of reference fixed on the smolder front. Radiation heat transfer was incorporated using a diffusion approximation and smoldering was modeled using a one-step reaction mechanism.

Key results include (1) for a given fuel, the final temperature depends only on the initial oxygen mass flux, $\dot{m}_{oi}''$, increasing logarithmically with $\dot{m}_{oi}''$; (2) the smolder velocity, v, is linearly dependent on $\dot{m}_{oi}''$ and at fixed $\dot{m}_{oi}''$, increases with
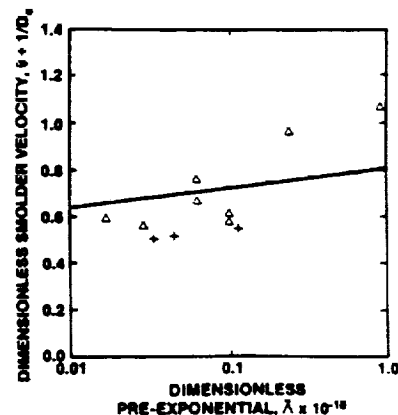

Fig. 9. Dimensionless smolder velocity, $\bar{v} + 1/D_c$, versus the dimensionless preexponential, $\bar{\Lambda}$, for polyurethane. Smolder velocities predicted by the present analytic model (—), measured by Rogers and Ohlemiller (△), and calculated by Ohlemiller et al. (+) are shown.

initial oxygen mass fraction, Y_{oi}; and (3) steady smolder propagation is possible only for $Y_{oi} \geq c_{eff}(T_f - T_i)/Q$, with extinction occurring when all of the energy released in the reaction zone is used to heat the incoming gas.

The preceding analysis can be modified to allow for several second-order effects. Heat losses from the sides of the cylinder will affect the extinction criterion, increasing the critical value of Y_{oi} below which steady solutions cease to exist. When properties are allowed to vary, the equations determining v and T_f will still be valid, with the properties appearing in these equations evaluated at T_f [2]. As discussed earlier, a nonoxidative pyrolysis reaction can also be included in the analysis. However, for steady smolder, the presence of such a reaction will only have a small effect on the temperature profiles.

APPENDIX: INFLUENCE OF BUOYANCY

Because the temperature field and hence the buoyancy varies as the smolder wave spreads, u_i may not be known a priori. The quasi-steady conservation of momentum for this system is

$$\phi \frac{dP}{dx} = -\mu a_d u + \phi(\rho_{gi} - \rho_g)g. \tag{22}$$

Integrating Eq. (22) yields

$$\int_{h-L}^{h} \mu a_d u \, dx = \phi \, \Delta P + \phi \int_{h-L}^{h} g(\rho_{gi} - \rho_g) \, dx,$$

$$(23)$$

where h is the length of Region I in Fig. 1, L is the total length of Regions I–III, and $\Delta P = P_i - P_f$ is the pressure drop across the solid, excluding changes in hydrostatic pressure. While the flow resistance, a_d, is lower in the char layer, the gas velocity, u, is higher. Therefore, it is assumed that the quantity $a_d u$ remains approximately constant at $a_d u_i$. A step change in ρ_g from ρ_{gi} to ρ_{gf} occurs at $x = 0$. The initial velocity is then approximated as

$$u_i = \frac{\phi \, \Delta P}{\mu a_d L} + \frac{\phi g \rho_{gi} h T_f}{\mu a_d L (1 + T_f)}.$$

$$(24)$$

Buoyancy can be neglected when $g\rho_{gi}h/\Delta P \ll (1 + T_f)/T_f$. At STP, $\rho_{gi} \sim 1$ kg/m^3 and $T_f \sim 1$, so that at sea level, with $g = 9.8$ m/s^2, $\Delta P/h \gg 5$ Pa/m suffices while in orbit; with $g \sim 10^{-3}$ m/s^2, $\Delta P/h \gg 5 \times 10^{-4}$ Pa/m will suffice. On the other hand, for polyurethane, buoyancy is negligible if the forced $u_i \gg 4 \times 10^{-4}$ m/s at sea level and if $u_i \gg 4 \times 10^{-8}$ m/s in orbit. When $\Delta P/g\rho_{gi}h \ll T_f/(1 + T_f)$, $u_i \sim g\rho_{gi}$. Since the smolder velocity is proportional to the oxygen mass flux, $v \sim Y_{oi}\rho_{gi}u_i \sim Y_{oi}g\rho_{gi}^2$. This result agrees with the experimental finding [16] that v is proportional to P_a^2 for buoyancy driven systems.

NOMENCLATURE

a_d	Darcy coefficient
c	heat capacity
c_{eff}	effective heat capacity, $\epsilon_s c_s + \epsilon_g c_g$
D	mass diffusivity of oxygen in air
D_c	dimensionless energy release per mass of O_2, $QY_{oi}/c_{eff}T_i$
g	gravitational acceleration
h	distance over which buoyancy acts
k_{eff}	conductivity due to conduction, $\phi k_g + (1 - \phi)k_s$

k_{rad}	conductivity due to radiation, $16\sigma l_r T^3/3$
l_r	radiation path length
L	height of the solid fuel
Le	modified Lewis number (see Table III)
$\dot{m}''$	mass flux
N_R	dimensionless radiation conductivity, (see Table III)
n	stoichiometric coefficients
P	pressure
P_g	dimensionless gas production parameter (see Table III)
Q	energy released per mass of O_2 consumed
$\dot{r}''$	reaction rate
r_{eq}	inverse equivalence ratio, $\epsilon_{oi}/n_o\epsilon_{usi}$
T	temperature
u	mass averaged velocity of the gas phase
v	smolder velocity
Y	mass fraction
x	spatial coordinate
Z	preexponential factor in the reaction rate
β	Zeldovich number, $E(T_f - T_i)/RT_f^2$
β'	dimensionless activation energy, E/RT_i
Λ	dimensionless eigenvalue
$\bar{\Lambda}$	dimensionless preexponential (see Table III)
ϵ	mass flux fraction
μ	dynamic viscosity
ξ	stretched coordinate, $\beta(1 - T/T_f)$
ρ	density
σ	Stephan–Boltzmann constant
ϕ	void volume/total volume

Subscripts

a	ash
c	characteristic
f	final value ($x = +\infty$)
g	gas phase
gp	gaseous products
i	initial value ($x = -\infty$)
o	oxygen
s	solid phase
us	unburned solid

REFERENCES

1. Ohlemiller, T. J., *Prog. Energy Combust. Sci.* 11:277–310 (1986).

2. Williams, F. A., *Combustion Theory*, 2nd Edition, Benjamin/Cummings, Menlo Park, 1985.

3. Ohlemiller, T. J., and Rogers, F. E., *J. Fire Flamm.* 9:489-509 (1978).

4. Gann, R. G., Earl, W. L., Manka, M. J., and Miles, L. B., *18th Symposium (International) on Combustion,* The Combustion Institute, Pittsburgh, 1981, p. 571.

5. McCarter, R., *J. Consumer Prod. Flamm.* 4:346-358 (1977).

6. Palmer, K. N., *Combust. Flame* 1:129-153 (1957).

7. Moussa, N. A., Toong, T. Y., and Garris, C. A., *16th Symposium (International) on Combustion,* The Combustion Institute, Pittsburgh, 1976, p. 1447.

8. Ortiz-Molina, M. G., Toong, T. Y., Moussa, N. A., and Tesoro, G. C., *Seventeenth Symposium (International) on Combustion,* The Combustion Institute, Pittsburgh, 1979, p. 1191.

9. Leisch, S. O., Kauffman, C. W., and Sichel, M., *20th Symposium (International) on Combustion,* The Combustion Institute, Pittsburgh, 1984.

10. Kinbara, T., Endo, H., and Sega, S., *11th Symposium (International) on Combustion,* The Combustion Institute, Pittsburgh, 1966, p. 525.

11. Muramatsu, M., Umemura, S., and Okado, T., *Combust. Flame* 36:245-262 (1979).

12. Kansa, E. J., Perlee, H. E., and Chaiken, R. F., *Combust. Flame* 29:311-324 (1977).

13. Ohlemiller, T. J., Bellan, J., and Rogers, F. E., *Combust. Flame* 36:197-215 (1979).

14. Rogers, F. E., and Ohlemiller, T. J., *J. Fire Flamm.* 11:32-44 (1980).

15. Ohlemiller, T. J., and Lucca, D. A., *Combust. Flame* 54:131-147 (1983).

16. Dosanjh, S. S., Peterson, J., Fernandez-Pello, A. C., and Pagni, P. J., *Acta Astronautica IAF-85 Stockholm Special Issue: Microgravity Materials and Fluid Sciences,* 1986.

17. Tong, T. W., and Tien, C. L., *J. Thermal Insulation* 4:27-44 (1980).

18. Williams, F. A., *16th Symposium (International) on Combustion,* The Combustion Institute, Pittsburgh, 1976, p. 1281.

PAPER 2

"FORCED COUNTER-CURRENT SMOLDERING COMBUSTION"
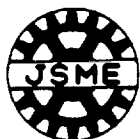
Dosanjh, S. and Pagni, P.J.

Proceedings of the 1987 ASME•JSME Thermal Engineering Joint Conference

Honolulu, Hawaii
March 22–27, 1987

Editors
P. J. MARTO – ASME
I. TANASAWA – JSME

FORCED COUNTERCURRENT SMOLDERING COMBUSTION

S. S. Dosanjh* and P. J. Pagni
Mechanical Engineering Department
University of California
Berkeley, California

*Currently at Sandia National Laboratories, Albuquerque, New Mexico

ABSTRACT

A model of smoldering combustion propagation through very porous solid fuels is presented. Here smoldering is initiated at the bottom of a long, radially infinite fuel bed, so that the smolder wave propagates upwards, in the same direction as the forced flow of oxidizer. Because the solid fuel and the gaseous oxidizer enter the reaction zone from opposite directions, this configuration is referred to as countercurrent, diffusion-flame-like or reverse. The proposed application is an experiment for use on the Space Shuttle. Due to the microgravity environment, it is assumed that the propagation of the smolder wave is one-dimensional. Radiation heat transfer is incorporated using a diffusion approximation and smoldering is represented utilizing a two-step mechanism consisting of a pyrolysis reaction followed by a char oxidation reaction. An infinite reaction rate approximation is used to model the oxidation reaction zone and it is assumed pyrolysis occurs at a known temperature, T_p. Because the two reaction fronts move at different velocities, countercurrent smolder propagation is unsteady. Two cases are considered: (1) no ash residue; and (2) an ash layer building below the smolder wave. The residual ash serves as insulation and its presence leads to higher peak temperatures. Explicit expressions are derived for the char oxidation velocity, v, the maximum temperature, T_m, and the pyrolysis front velocity, v_p. Key results include: (1) in the absence of radial heat losses, v_p approaches a constant value which is different from v; (2A) for the no residual ash case, in limit of long time ($t \to \infty$), T_m is determined by balancing the energy released in the oxidation region with the energy required to preheat the gas and the energy lost as radiation; (2B) when an ash layer builds below the smolder wave, radiation losses are negligible in the limit $t \to \infty$, and T_m is higher than in the no ash case; and (3) self-sustained countercurrent smoldering combustion is not possible when the energy convected by the gas phase is insufficient to drive the pyrolysis front.

NOMENCLATURE

a_d	Darcy coefficient
c	heat capacity
D_{co}	dimensionless energy release, $QY_{oi}/c_g T_i$
D_{cp}	dimensionless pyrolysis energy, $Q_p/c_s T_i$
h	ash height
k	thermal conductivity
k_{eff}	conductivity due to conduction, $\delta k_g + (1-\delta)k_s$
k_{rad}	conductivity due to radiation, $16\sigma \ell_r T_i^3/3$
ℓ	ratio of thermal conductivities, k_g/k_{eff}
ℓ_r	radiation heat length
L	distance between the oxidation zone and the pyrolysis front
Le	modified Lewis number
$\dot{m}''$	mass flux
M_i	molecular weight of species i
N_R	dimensionless radiation conductivity, $16\sigma \ell_r T_i^3/3k_{eff}$
P	pressure
Q	energy released per mass of O_2 consumed
Q_E	dimensionless external heat flux, $\dot{q}_e/QY_{oi}\dot{m}_{gi}$
Q_p	energy consumed per gram of unburnt solid
Q_R	dimensionless radiation losses, $\varepsilon\sigma T_i^4/QY_{oi}\dot{m}_{gi}$
s_a	dimensionless stoichiometric coefficient, $\nu_a M_a/\nu_{us}M_{us}$
s_c	dimensionless stoichiometric coefficient, $\nu_c M_c/\nu_{us}M_{us}$
T	temperature
u	mass averaged velocity of the gas phase
v	smolder velocity
V	dimensionless smolder velocity, $\nu_{us}M_{us}Y_{oi}C_s/\nu_o M_o c_g$
x	spatial coordinate
Y	mass fraction
ε	emissivity
ν	stoichiometric coefficient
ρ	density
σ	Stephan-Boltzmann constant
τ	ratio of gas to solid response times, $\rho_{gi}c_g/(1-\delta)\rho_{si}c_s$
δ	void volume / total volume

1. INTRODUCTION

Smoldering, which is defined as combustion without flame, can occur in many materials, including coal [1,2], cotton [3,4], paper [5-7], polyurethane foams [8], wood [9,10], thermal insulation materials [11] anc various dusts [12,13]. If the host material is sufficiently permeable, a self-supporting exothermic reaction zone can pass through the substance [14]. Oxygen reaches the reaction zone by convection and diffusion. However, some materials decompose into a "liquid" tar [14] upon being heated, restricting the flow of air and inhibiting the propagation of a smolder wave through the material. Smoldering combustion can be prevented in some materials by adding sulfur [15].

Schematics of the problems under consideration are presented in Figs. 1A and 1B. A gaseous oxidizer, with an oxygen concentration, Y_{oi}, and an inlet velocity, u_i, flows upward through a porous combustible medium which has a void volume fraction, ϕ. The solid and gas fractions begin with densities, ρ_{si} and ρ_{gi}, respectively. At t=0, both the solid and the gas are at a uniform temperature, T_i. Smoldering is initiated at the bottom of the material by applying an external heat flux, q_e, for $0 < t < t_e$. The smolder wave propagates upwards, in the same direction as the forced flow of oxidizer. In a frame of reference moving with the smolder zone, the solid and the oxidizer enter the reaction region from opposite directions. Consequently, this configuration is referred to as countercurrent or diffusion-flame-like. It is also called forward smolder since the reaction zone moves in the oxidizer flow direction.
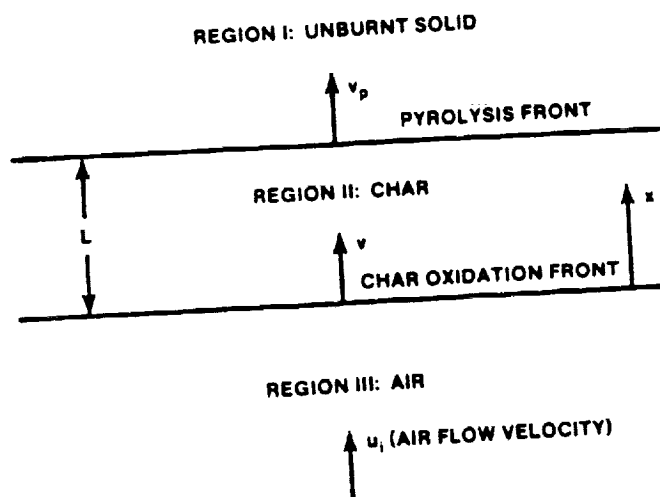
REGION I: UNBURNT SOLID

REGION I: UNBURNT SOLID
v_p
PYROLYSIS FRONT
REGION II: CHAR
x
L
v
CHAR OXIDATION FRONT
REGION III: AIR
u_i (AIR FLOW VELOCITY)

FIG 1A: Schematic of countercurrent smoldering for Case I (no residual ash).

REGION I: UNBURNT SOLID
v_p
PYROLYSIS FRONT
REGION II: CHAR
x
L
v
CHAR OXIDATION FRONT
h
REGION III: RESIDUAL ASH
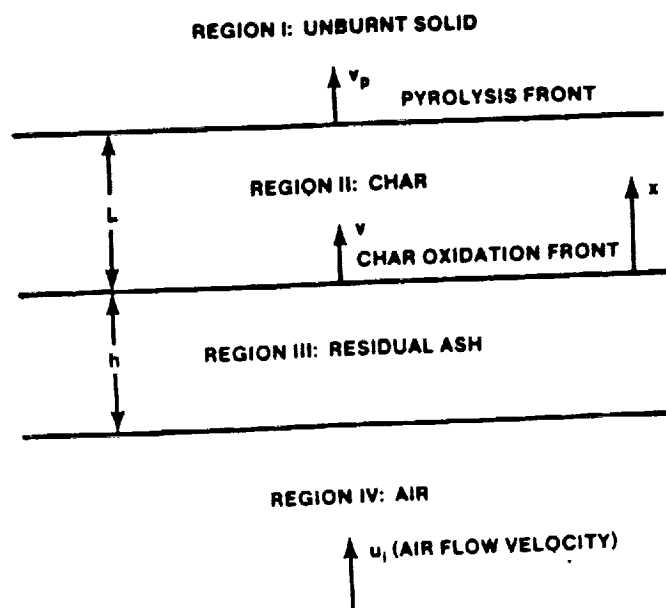REGION IV: AIR
u_i (AIR FLOW VELOCITY)

FIG. 1B: Schematic of countercurrent smoldering for Case II (an ash layer building below the smolder wave).

Relatively little attention has been given to smoldering combustion in the countercurrent configuration [14]. Ohlemiller and Lucca [16] conducted an experimental investigation using cellulosic insulation as a fuel. In a related study, Summerfield et al [17] presented a one-dimensional numerical model of smolder spread in a cigarette during steady draw. Two reactions were included, pyrolysis and char oxidation. Because the wrapping paper burns back, a significant amount of air bypasses the hottest part of the char oxidation region. Consequently, cigarette smolder is more complicated than the countercurrent smoldering scenarios depicted in Figs. 1A and 1B. Winslow [18] investigated countercurrent propagation within the context of coal gasification in the packed bed utilizing an unsteady, one-dimensional model. Different gas and solid temperatures were used and concentrations of eight chemical species, two forms of water (surface and interior), coal and char were calculated. Due to the complexity of these solutions, it is difficult to determine which mechanisms dominate the movement of the six reaction fronts.

A model of unsteady countercurrent smoldering combustion propagation is presented in this study. Smoldering combustion is represented with a two-step reaction mechanism consisting of a char oxidation reaction and a pyrolysis reaction. An infinite reaction rate approximation is used to model the oxidation reaction zone and it is assumed pyrolysis occurs at a known temperature, T_p. Because the two reaction fronts move at different velocities, countercurrent smolder propagation is unsteady. Two cases are considered: no ash residue (see Fig. 1A), $v_a M_a = 0$, and an ash layer building below the smolder wave (see Fig. 1B), $v_a M_a \neq 0$. The residual ash serves as insulation, leading to higher peak temperatures. The range of validity of the solutions is identified and explicit expressions are derived, in the limit of long time, for the char oxidation velocity, v, the pyrolysis front velocity, v_p, and the maximum temperature, T_m.
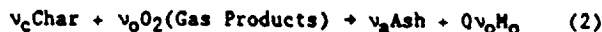
2. ANALYSIS

2.1 Assumptions

The scenario depicted in Fig. 1 is not a realistic representation of the countercurrent smoldering combustion of all solid fuels. For some solids will collapse downwards as the smolder wave propagates. In this study, it is assumed that the solid remains stationary in a frame of reference fixed in the laboratory. If the fuel consists of small, loosely packed, solid particles, this assumption is only valid in a microgravity environment. Smoldering combustion is represented by a two-step reaction mechanism.

$$\nu_{us}(\text{Unburnt Solid}) + Q_p \nu_{us} M_{us} \to \nu_c \text{Char} + \nu_{gp1}(\text{Gas Products}) \quad (1)$$

and

$$\nu_c \text{Char} + \nu_o O_2(\text{Gas Products}) \to \nu_a \text{Ash} + Q\nu_o M_o \quad (2)$$

where Q_p is the energy required to pyrolyse one gram of unburnt solid and Q is the energy released per gram of O_2 consumed. Char oxidation is modeled using an infinite reaction rate approximation. It is assumed that the pyrolysis reaction occurs at a known temperature, T_p. This is a reasonable approximation for many solids of interest [19-21]. For alpha-cellulose, $T_p=300^\circ C$ [19]. Alternatively, pyrolysis can be modeled using Arrhenius-type kinetics [17,18,20]. Such an approach leads to numerical calculations and requires the specification of kinetic constants whose values are sometimes ambiguous [19].

The char oxidation zone moves at a constant speed, v, which is determined by the rate at which oxygen reaches the reaction region, while the pyrolysis front moves at a velocity, v_p, which is several times larger than v. Because the pyrolysis reaction is endothermic [14], motion of the pyrolysis front is highly dependent on heat transfer from the oxidation zone, where the energy required to sustain smoldering is released. Energy is transferred to the pyrolysis zone by conduction, radiation and gas phase convection. Typical values of several smolder characteristics, including the maximum temperature, T_m, the oxidation velocity, v, and the pyrolysis speed, v_p, are given in Table I.

TABLE I
Order of magnitude estimates for several smolder characteristics.

Quantity of Interest	Magnitude[a]
forced gas velocity, u_i	$(1-5) \times 10^{-3}$ m/sec
oxidation velocity, v	$(1-3) \times 10^{-5}$ m/sec
pyrolysis front velocity, v_p	$(5-15) \times 10^{-5}$ m/sec
maximum temperature, T_m	$800-900^\circ K$

a. Measurements by Ohlemiller and Lucca [16].

Because the solid fuel and the gaseous oxidizer enter the oxidation zone from opposite directions, all of the char is consumed in accordance with Eq.(2) before the oxidation zone moves forward. Therefore, the oxidation velocity, v, is proportional the the initial oxgen mass flux, with the proportionality constant determined by stoichiometric considerations [14,16]. Because v is several orders of magnitude smaller than the gas velocity, u_i, the oxygen mass flux (in a frame of reference moving with the oxidation zone) is approximately, $Y_{oi}\phi\rho_{gi}u_i$ [16]. Thus,

$$V = \frac{\nu_{us}M_{us}}{\nu_o M_o} \frac{Y_{oi}\rho_{gi}u_i}{(1-\phi)\rho_{si}} \quad (3)$$

Typically, $Y_{oi}\sim0.23$, $u_i\sim0.005$ m/s, $\rho_{gi}\sim1$ kg/m^3, and $(1-\phi)\rho_{si}\sim40$ kg/m^3, resulting in oxidation velocities on the order of 10^{-5} m/s. For the same conditions, smolder velocities encountered in cocurrent smoldering are more than 50 times larger [16]. In a frame of reference moving with the oxidation zone, the gas phase mass flux, $\dot{m}_g''$, is an order of magnitude larger than the solid phase mass flux, $\dot{m}_s''$. Setting $Y_{oi}=0.23$ and representing oxidation with the reaction, $C+O_2$, Eq. (3) yields $\dot{m}_s''/\dot{m}_g''\sim0.08$. Neglecting terms involving $\dot{m}_s''$ considerably simplifies the governing equations. Also, since the solid density based on total volume, $(1-\phi)\rho_{si}$, is much greater than $\phi\rho_{gi}$, the energy stored in the gas phase is negligible when compared with that stored in the solid phase [8,17].

Additionally, the solid phase is assumed continuous with a constant void volume fraction. The propagation of the smolder wave is approximately one-dimensional. Fick's Law is used to model the diffusion of oxygen. Radiation heat transfer is incorporated utilizing the diffusion limit. The gas and the solid are presumed to be in local thermal equilibrium. Energy transport due to concentration gradients, energy dissipated by viscosity, work done by body forces and the kinetic energy of the gas phase have been ignored. The quantity, $\rho_g D$, is taken to be constant. This is a reasonable assumption because the mass diffusivity of oxygen in the air, D, increases with temperature and decreases with pressure [22]. It is also assumed that properties, such as the gas phase thermal conductivity, k_g, the solid phase thermal conductivity, k_s, the gas specific heat, c_g, and the solid specific heat, c_s, remain constant.

2.2 CASE I: NO RESIDUAL ASH

2.2.1 Governing Equations

After the initiation of smoldering, the coordinate system moves with the char oxidation region. For $x>0$ (Regions I and II in Fig. 1A), the conservation of energy requires

$$(1-\phi)\rho_s c_s \frac{\partial T}{\partial t} + \dot{m}_g'' c_g \frac{\partial T}{\partial x} = \frac{\partial}{\partial x} [k_{eff} + k_{rad}] \frac{\partial T}{\partial x}, \quad (4)$$

where the effective thermal conductivity, $k_{eff}=\phi k_g + (1-\phi)k_g$, accounts for heat transfer due to conduction in both phases. Radiation heat transfer is incorporated using the temperature dependent conductivity, $k_{rad}=16\sigma\ell_r T^3/3$, where ℓ_r is the radiation path length. For $x<0$ (Region III in Fig. 1A),

$$\rho_g c_g \frac{\partial T}{\partial t} + \dot{m}_g'' c_g \frac{\partial T}{\partial x} = k_g \frac{\partial^2 T}{\partial x^2} . \quad (5)$$

Since all of the oxygen is consumed, $Y_o=0$ for $x>0$. For $x<0$, conservation of species for oxygen yields

$$\rho_g \frac{\partial Y_o}{\partial t} + \dot{m}_g'' \frac{\partial Y_o}{\partial x} = \rho_g D \frac{\partial^2 Y_o}{\partial x^2} . \quad (6)$$

Conservation of gas mass gives

$$[1 + (\phi-1)H(x)] \frac{\partial \rho}{\partial t} + \frac{\partial \dot{m}_g''}{\partial x} = 0 , \quad (7)$$

where $H(x)$ is the Heaviside function, which vanishes for $x<0$ and is equal to 1 for $x>0$. Noting that all of the incoming solid is consumed in the oxidation zone, Eq. (1) yields

167

$$\rho_s = \begin{cases} [1 - \dfrac{\nu_{gp1} M_{gp1}}{\nu_{us} M_{us}} H(L-x)]\rho_{si} \text{ ,for } x>0 & (8) \\ 0 \text{ , for } x<0 \end{cases}$$

Because the pressure changes by only a small amount for these very porous systems [14], the ideal gas law gives $\rho_g RT = P_s$, thus completing the preceding set of equations.

The following boundary conditions are imposed on Eqs. (4-7): as $x \to -\infty$, $T \to T_i$, $Y \to Y_{oi}$ and $\ddot{m}_g \to \ddot{m}_{gi}$; as $x \to +\infty$, $dT/dx \to 0$. The temperature is continuous across both interfaces. Because $\ddot{m}_s \ll \ddot{m}_g$, $\ddot{m}_g$ is approximately continuous across both interfaces. It is assumed that smoldering begins when the temperature of the x=0 interface reaches a critical value, $T_{ig} > T_p > T_i$. However, only an approximate value for T_{ig} is needed since the solutions are independent of the initial conditions as $t \to \infty$. Conservation of energy at the x=0 interface gives

$$[k_{eff} + \frac{16}{3} \sigma \ell_r T_m^3] \frac{\partial T}{\partial x}\Big|_{x=0^+} + k_g \frac{\partial T}{\partial x}\Big|_{x=0^-}$$

$$+ \epsilon \sigma(T_m^4 - T_i^4) + Q\rho_g D \frac{\partial Y_o}{\partial x}\Big|_{x=0^-} \quad H(T_m - T_{ig})$$

$$- \ddot{q}_e H(t_e - t) , \qquad (9)$$

where T_m is the temperature at x=0. Thus, the maximum temperature, T_m, is determined by balancing the energy transported downstream, by conduction and radiation, and the energy conducted upstream, radiation heat losses from the x=0 interface, the energy released in the oxidation zone and the external heat flux. Motion of the pyrolysis front is calculated by equating the energy consumed by pyrolysis and the net energy transported to the pyrolysis zone, giving

$$v_p = \frac{[k_{eff} + \frac{16}{3} \sigma \ell_r T_p^3]}{(1-\delta)\rho_{si} Q_p} \left[\frac{\partial T}{\partial x}\Big|_{x=L^+} - \frac{\partial T}{\partial x}\Big|_{x=L} \right], \quad (10)$$

where $v_p = dL/dt + v$ and L is the distance between the two reaction regions. Initially, both the temperature the the oxygen concentration are uniform. That is, $T(x,0) = T_i$ and $Y_o(x,0) = Y_{oi}$. After smoldering is initiated, $Y_o(0,t) = 0$.

2.2.2 Dimensionless Governing Equations

A dimensionless temperature is defined by $\bar{T} = (T - T_i)/T_c$. Setting $T_c = T_i$ makes T of order one and eliminates the parameter, T_c/T_i, which arises from the nonlinear terms in the governing equations. The oxygen mass fraction, Y_o, the gas density, ρ_g, and the gas mass flux, $\ddot{m}_g$, are normalized by their initial values. A characteristic distance, $x_c = k_{eff}/\ddot{m}_{gi} C_g$ are chosen by balancing terms in Eq. (4). Typically, $u_i \sim 0.005$m/sec, $\rho_{gi} \sim 1$ kg/m^3, $(1-\delta)\rho_{si} \sim 40$ kg/m^3, $c_s \sim c_g \sim 1$ kJ/kg K, and $k_{eff} \sim 0.05$ W/m K, giving $x_c \sim 0.01$ m and $t_c \sim 80$ sec. Thus, the ratio, $x_c/t_c \sim 0.013$ cm/sec, is of the same order as v_p (see Table I). This is to be expected because v_p is determined by heat transfer considerations and both x_c and t_c were chosen to make terms in the energy equation of order one.

For $x>0$, conservation of energy requires

$$\bar{\rho}_s \frac{\partial \bar{T}}{\partial t} + \ddot{m}_g \frac{\partial \bar{T}}{\partial x} = \frac{\partial}{\partial x} [1 + N_r(1+\bar{T})^3] \frac{\partial \bar{T}}{\partial x} , \qquad (11)$$

and for $x<0$,

$$\tau \bar{\rho}_g \frac{\partial \bar{T}}{\partial t} + \ddot{m}_g \frac{\partial \bar{T}}{\partial x} = \frac{\partial^2 \bar{T}}{\partial x^2} . \qquad (12)$$

Since all of the oxygen is consumed, $\bar{Y}_o = 0$ for $\bar{x} > 0$. For $\bar{x} < 0$, conservation of species for oxygen yields

$$\tau \bar{\rho}_g \frac{\partial \bar{Y}_o}{\partial t} + \ddot{m}_g \frac{\partial \bar{Y}_o}{\partial x} = \frac{1}{Le} \frac{\partial^2 \bar{Y}_o}{\partial x^2} . \qquad (13)$$

Conservation of gas mass requires

$$\tau[1-(1-\delta)H(\bar{x})] \frac{\partial \bar{\rho}_g}{\partial t} + \frac{\partial \ddot{m}_g}{\partial x} = 0 . \qquad (14)$$

Equation (8) yields

$$\bar{\rho}_s = \begin{cases} 1 - (1-s_c) H (\bar{L}-\bar{X}) \text{ , for } \bar{x}>0 \\ 0, \text{ for } \bar{x}<0 \end{cases} \qquad (15)$$

In dimensionless form, the ideal gas equation of state is $\bar{\rho}_g(1+\bar{T}) = 1$. The dimensionless smolder velocity, $V = vt_c/x_c$, equals after the onset of smoldering and zero beforehand.

The following boundary conditions are imposed on Eqs. (11-14): as $\bar{x} \to -\infty$, $\bar{T} \to 0$, $\bar{Y}_o \to 1$ and $\ddot{m}_g \to 1$; as $\bar{x} \to +\infty$, $d\bar{T}/d\bar{x} \to 0$. Both temperature and the gas mass flux are continuous across the interfaces. Conservation of energy across the $\bar{x}=0$ interface gives

$$\frac{1}{D_{co}} [1 + N_R(1+\bar{T}_m)^3] \frac{\partial \bar{T}}{\partial x}\Big|_{\bar{x}=0^+} - \frac{\ell}{D_{co}} \frac{\partial \bar{T}}{\partial x}\Big|_{\bar{x}=0^-}$$

$$Q_R[(1+\bar{T}_m)^4 - 1] + \frac{1}{Le} \frac{\partial \bar{Y}_o}{\partial x}\Big|_{\bar{x}=0^-} \quad H(\bar{T}_m - \bar{T}_{ig})$$

$$- Q_g H(\bar{t}_e - \bar{t}) , \qquad (16)$$

where $\bar{T}_m$ is the temperature at $\bar{x}=0_\pm$. The temperature of the pyrolysis zone is held fixed, $\bar{T}(\bar{L},t) = \bar{T}_p$, and the motion of this front is determined by

$$\bar{v}_p = \frac{d\bar{L}}{dt} + V$$

$$= \frac{1}{D_{cp}} [1 + N_R(1+\bar{T})^3] \left[\frac{\partial \bar{T}}{\partial x}\Big|_{\bar{x}=\bar{L}^+} - \frac{\partial \bar{T}}{\partial x}\Big|_{\bar{x}=\bar{L}^-} \right] . \qquad (17)$$

Initially, $\bar{T}(\bar{x},0) = 0$ and $\bar{Y}_o(\bar{x},0) = 1$. After smoldering is initiated $\bar{Y}_o(0,\bar{t}) = 0$.

The dimensionless parameters appearing in the preceding equations and typical values of these parameters, estimated from properties provided in refs. [8,16,23-25], are given in Table II. The quantity, τ, represents the ratio of the gas phase response time to the solid phase response time and is always less than 0.04 for the fuels of interest. As discussed in the following section, this fact leads to considerable simplification in the governing equations because solutions in Region III in Fig. 1A are steady when τ is small.

TABLE II

Dimensionless parameters governing forced countercurrent smoldering combustion. In addition to the following parameters, the void volume fraction, δ, the irradiation time, $\bar{t}_e$, the ignition temperature, $\bar{T}_{ig}$, and the pyrolysis temperature, $\bar{T}_p$, must be specified.

Parameter	Physical Meaning
$D_{co} = \dfrac{Q Y_{oi}}{c_g T_i}$	Dimensionless measure of the heat released per mass of oxygen consumed (varies from 0 to 20)
$D_{cp} = \dfrac{Q_p}{c_s T_i}$	Dimensionless measure of the energy consumed by pyrolysis (varies from 0.25 to 1)
$\ell = \dfrac{k_g}{k_{eff}}$	Dimensionless thermal thickness in Region III (varies from 0.5 and 0.7)
$Le = \dfrac{k_{eff}}{\rho_g D c_g}$	Modified Lewis number (usually lies between 1.9 and 3.0)
$N_R = \dfrac{16 \sigma \ell_r T_i^3}{3 \, k_{eff}}$	Dimensionless radiation conductivity (less than 0.1)
$Q_E = \dfrac{\dot{q}_e''}{Q Y_{oi} \dot{m}_{gi}''}$	External heat flux measured relative to the total energy released in the reaction zone
$Q_R = \dfrac{\varepsilon \sigma T_i^4}{Q Y_{oi} \dot{m}_{gi}''}$	Dimensionless measure of the energy radiated to the surroundings (varies from 0.005 to infinity)
$S_a = \dfrac{\nu_a M_a}{\nu_{us} M_{us}}$	Stoichiometric coefficient
$S_c = \dfrac{\nu_c M_c}{\nu_{us} M_{us}}$	Stoichiometric coefficient (varies between 0.3 and 0.4)
$V = \dfrac{\nu_{us} M_{us}}{\nu_o M_o} \dfrac{Y_{oi} c_s}{c_g}$	Dimensionless char oxidation velocity (varies from 0 to 1)
$\tau = \dfrac{\rho_{gi} c_g}{(1-\theta)\rho_{si} c_s}$	Gas phase response time divided by the solid phase response time (less than 0.04)

2.2.3 Quasi-Steady Equations

Terms in Eqs. (12-14) involving time derivatives can be neglected because τ is always less than 0.04. This result is in agreement with the findings of Ohlemiller and others [8,14,17], who reported that the gas phase can be considered quasi-steady in many smoldering combustion applications. Setting τ equal to zero in Eq. (14), integrating once, and combining with Eq. (11),

$$\bar{\rho}_s \frac{\partial \bar{T}}{\partial t} + \frac{\partial \bar{T}}{\partial x} = \frac{\partial}{\partial x}\left[1 + N_r(1+\bar{T})^3\right]\frac{\partial \bar{T}}{\partial x} . \tag{18}$$

Equation (12) yields an explicit expressions for the temperature in Region III in fig. 1A (x<0),

$$\bar{T} = \bar{T}_m \, e^{x/\ell} . \tag{19}$$

After smoldering is initiated, Eq. (13) gives

$$\bar{Y}_o = 1 - e^{Le\,\bar{x}} . \tag{20}$$

Combining Eqs. (16,19,20),

$$\left[1 + N_R(1+\bar{T}_m)^3\right]\frac{\partial \bar{T}}{\partial x}\bigg|_{x=0^+} = \bar{T}_m + Q_R D_{co}\left[(1+\bar{T}_m)^4 - 1\right]$$

$$- D_{co} H(\bar{T}_m - \bar{T}_{ig}) - D_{co} Q_E H(\bar{t}_e - t) . \tag{21}$$

Equation (21) determines $\bar{T}_m$ while $\bar{v}_p$ is given by Eq. (17).

2.3 CASE II: ASH LAYER BUILDING BELOW SMOLDER WAVE

After the initiation of smoldering, the coordinate system moves with the char oxidation zone. As the oxidation front propagates upward, an ash layer of height, $h(t)=vt$, builds below the smolder wave - see Fig. 1B. Because the governing equations for Case II are very similar to those for Case I, only dimensionless equations are presented in this section. Relevant dimensionless variables are defined in the preceding section and the dimensionless parameters appearing in the following equations are listed in Table II. As discussed previously, the gas phase response time is much smaller than the solid phase response time (that is, $\tau \ll 1$). Consequently, the temperature in Region IV in Fig. 1B, the oxygen concentration, and the gas phase mass flux profiles are steady. Conservation of energy in Regions I through III in Fig. 1B again gives Eq. (18), while in Region IV

$$\bar{T} = \bar{T}_h \, e^{x/\ell} . \tag{22}$$

The temperature at $\bar{x}=-h$, $\bar{T}_h(\bar{t})$, will be determined by applying the conservation of energy at the $\bar{x}=-h$ interface. After smolder initiation, conservation of species for oxygen yields

$$\bar{Y}_o = \begin{cases} 0 & , \text{ for } \bar{x}>0 \\ 1 - e^{\bar{x}Le} & , \text{ for } -\bar{h} < x < 0 \\ 1 - e^{\bar{h}Le/6} e^{(\bar{h}+x)Le} & , \text{ for } \bar{x} < -\bar{h} \end{cases} \tag{23}$$

Equations (1,2) determine the solid density,

$$\bar{\rho}_s = \begin{cases} 1 - (1-s_c) \, H(\bar{L}-\bar{X}) & , \text{ for } \bar{x}>0 \\ s_c & , \text{ for } -\bar{h}<\bar{x}<0 \\ 0 & , \text{ for } \bar{x}<-\bar{h} \end{cases} \tag{24}$$

The following boundary conditions are imposed on Eq. 18: as $\bar{x}\to-\infty$, $\bar{T}\to 0$; as $\bar{x}\to+\infty$, $d\bar{T}/dx\to 0$. The temperature is continuous across all of the interfaces. Before smolder initiation, conservation of energy across the $\bar{x}=0$ interface requires

$$\left[1 + N_R(1+\bar{T}_m)^3\right]\frac{\partial \bar{T}}{\partial x}\bigg|_{x=0^+} = \bar{T}_m + Q_R D_{co}\left[(1+\bar{T}_m)^4 - 1\right]$$

$$- Q_E D_{co} H(\bar{t}_e - \bar{t}) . \tag{25}$$

After initiation, conditions at $\bar{x}=-h$ and $\bar{x}=0$ are

$$\left[1 + N_R(1+\bar{T}_h)^3\right]\frac{\partial \bar{T}}{\partial x}\bigg|_{x=0^+} = \bar{T}_h + Q_R D_{co}\left[(1+\bar{T}_h)^4 - 1\right]$$

$$- Q_E D_{co} H(\bar{t}_e - \bar{t}) . \tag{26}$$

and

$$\left[1 + N_R(1+\bar{T}_m)^3\right]\left[\frac{\partial \bar{T}}{\partial x}\bigg|_{x=0^-} - \frac{\partial \bar{T}}{\partial x}\bigg|_{x=0^+}\right] = D_{co} , \tag{27}$$

respectively. Equations (26,27) determine $\bar{T}_h$ and T_m. Motion of the pyrolysis front is still governed by Eq. (17). Consideration of an ash layer introduces one additional parameter, s_a.

3. SOLUTIONS

3.1 CASE I: NO RESIDUAL ASH

Techniques for solving partial differential equations with moving interfaces have been developed within the context of freezing and thawing in cold climates [26] and the charring of solids during a fire [19]. The time-explicit finite difference scheme presented by Lundarini [26] is utilized to solve Eqs. (17,18,21). Temperature profiles after the onset of smoldering for typical values of the dimensionless parameters are shown in Fig. 2. The maximum temperature, $\bar{T}_m$, reaches a steady value before $\bar{t}=2.5$. A plot of $\bar{T}_m(\bar{t})/\bar{T}_m(\infty))$ is given in Fig. 3 for two cases: (1) the external heat flux is turned off at $\bar{t}=\bar{t}_e=1.0$ (solid line); (2) the heat flux is turned off immediately after smolder initiation (dashed line). Radiation and conduction heat transfer from the oxidation zone to the pyrolysis front becomes small when the dimensionless distance between the two reaction regions is large - that is, when $L\gg1$. Neglecting terms on the left hand side of Eq. (21), as $t\to\infty$,

$$Q_R D_{co} [(1+\bar{T}_m)^4 - 1] + \bar{T}_m = D_{co} \qquad (28)$$

Because $Q_R D_{co}$ is usually greater than 0.15 and $\bar{T}_m \sim 2$, the first term on the left hand side of the above equation is an order of magnitude larger than the second and consequently, $\bar{T}_m \sim Q^{-1/4}-1$, or in dimensional form, $T_m = (Q\dot{m}_{oi}/c\sigma)^{1/4}$. Thus, as a first approximation, the peak temperature is determined by balancing the heat released in the reaction zone and radiation heat losses from the x=0 interface. Typically, Q~12.3 kJ/gm of O_2, $Y_{oi}\sim0.23$, $\dot{m}_{gi}\sim0.006$ kg/m^2s and $\epsilon\sim0.9$, giving $T_m\sim490°C$. Because a small portion of the energy released is used to preheat the incoming gas, the peak temperature will be slightly lower than this value.

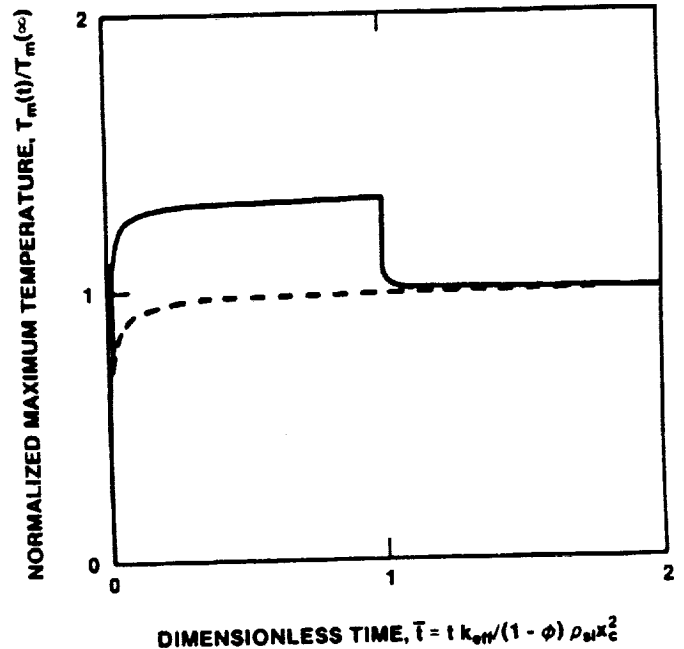DIMENSIONLESS TIME, $\bar{t} = t k_{eff}/(1 - \phi) \rho_{si} x_c^2$

FIG. 3: Normalized maximum temperature, $\bar{T}_m(\bar{t})/\bar{T}_m(\infty)$, versus dimensionless time, $\bar{t}$, for two cases: (1) the external heat flux turned off at $\bar{t}=\bar{t}_e=1$ (—); (2) the external heat flux turned off immediately after smolder initiation (--). With $D_{co}=12$, $D_{cp}=0.3$, $\ell=0.7$, $N_R=0$, $Q_e=1$, $Q_R=0.02$, $s_c=0.3$, $V=0.2$, and $\bar{T}_p=\bar{T}_{ig}=1$.

A plot of $\bar{T}_m$ versus $Q_R D_{co}$ for various values of D_{co} is shown in Fig. 4. Smoldering will only occur when $\bar{T}_p(-1) < \bar{T} < \bar{T}_{flame}$, where $\bar{T}_{flame}$ is a critical temperature above the flaming is observed. Figure 4 also demonstrates the relationship between the ignition temperature, $\bar{T}_{ig}$, and the minimum external heat flux, Q_g, that will produce smoldering (replace $\bar{T}$ with $\bar{T}_{ig}$ and D_{co} with $Q_{g,min}D_{co}$). Note that $Q_{g,min}$ is found by setting $\bar{T}_m=\bar{T}_{ig}$ and $d\bar{T}/dx|_{x=0^+}=0$ in Eq. (21), giving

$$Q_{g,min} D_{co} = \bar{T}_m + Q_R D_{co} [(1+\bar{T}_m)^4 -1] . \qquad (29)$$

when either the ignition temperature, $\bar{T}_{ig}$, or the radiation heat losses, $Q_R D_{co}$, increase, a greater amount of energy must be supplied to the bottom of the material to produce smoldering.
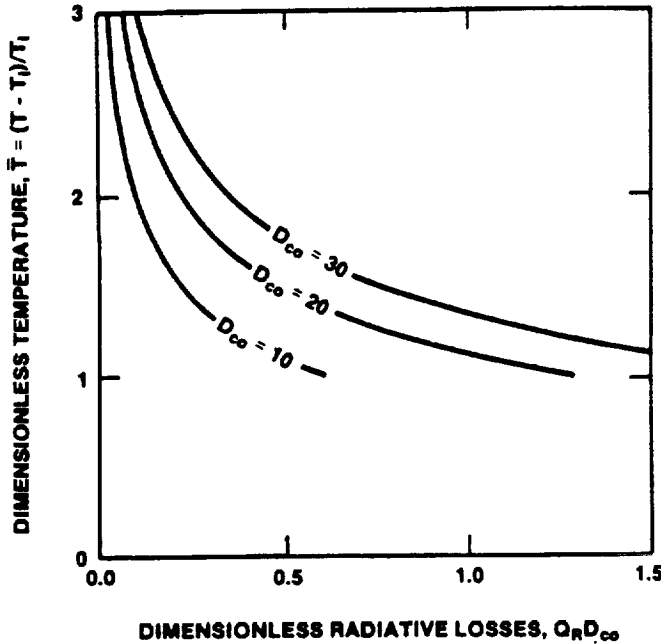
FIG. 2: Dimensionless temperature, T, versus dimensionless distance, $\bar{x}$, at various values of dimensionless time, $\bar{t}$, for Case I, with $D_{co}=12.0$, $D_{cp}=0.3$, $\ell=0.7$, $N_R=0$, $Q_g=1.0$, $Q_R=0.021$, $s_c=0.3$, $V=0.2$, $\bar{t}_e=1.0$, $\bar{T}_p=1.0$ and $\bar{T}_{ig}=1.0$.

DIMENSIONLESS RADIATIVE LOSSES, $Q_R D_{co}$

FIG. 4: Setting $\bar{T}$ equal to the dimensionless maximum temperature, $\bar{T}_m$, gives $\bar{T}_m$ versus dimensionless radiative losses, $Q_R D_{co}$, parameterized in the dimensionless heat release, D_{co}. Setting $\bar{T}$ equal to the ignition temperature, $\bar{T}_{ig}$, and replacing D_{co} with $Q_{g,min} D_{co}$ gives $\bar{T}_{ig}$ versus $Q_R D_{co}$ for various $Q_{g,min} D_{co}$.

Integrating Eq. (11) from $\bar{x}=0$ to $\bar{x}=\bar{L}$ and combining the resulting expression with Eq. (17) provides an expression for $\bar{v}_p$,

$$\bar{v}_p = \frac{1}{D_{cp}} \left\{ (\bar{T}_m - \bar{T}_p) - [1 + N_R(1 + \bar{T}_m)^3] \left.\frac{\partial \bar{T}}{\partial \bar{x}}\right|_{\bar{x}=0^+} \right.$$

$$- s_c \frac{\partial}{\partial t} \int_0^{\bar{L}} \bar{T} \, d\bar{x} + s_c \bar{T}_p \frac{d\bar{L}}{dt}$$

$$\left. + [1 + N_R(1 + \bar{T}_m)^3] \left.\frac{\partial \bar{T}}{\partial \bar{x}}\right|_{\bar{x}=\bar{L}^+} \right\} \quad (30)$$

Of the energy that is transferred downstream from the char oxidation zone (see the first two terms on the right hand side of the above equation), only a portion is consumed in the pyrolysis reaction region. Most of the energy is stored in the hot char in Region II in Fig. 1A [14], a small fraction is used to preheat the unburnt solid in Region I and the remainder is consumed in pyrolysis. In the limit $\bar{t} \to \infty$, radiative and conductive heat transfer downstream from both reaction regions is negligible, and Eq. (30) gives

$$\bar{v}_p + \frac{s_c}{D_{cp}} \left\{ \frac{\partial}{\partial t} \int_0^{\bar{L}} \bar{T} \, d\bar{x} - \bar{T}_p \frac{d\bar{L}}{dt} \right\} = \frac{1}{D_{cp}} (\bar{T}_m - \bar{T}_p) \quad (31)$$

Thus, energy consumed in the pyrolysis zone and stored by the hot char is supplied only by gas phase convection in the limit $\bar{t} \to \infty$. A reasonable approximation for the second term on the left hand side of the above equation is

$$\frac{\partial}{\partial t} \int_0^{\bar{L}} \bar{T} \, d\bar{x} - \bar{T}_p \frac{d\bar{L}}{dt} = (\bar{T}_m - \bar{T}_p) \frac{d\bar{L}}{dt} . \quad (32)$$

Combining Eqs. (31,32), gives

$$\bar{v}_p = \frac{d\bar{L}}{dt} + v = \frac{(\bar{T}_m - \bar{T}_p) - D_{cp} v}{s_c(\bar{T}_m - \bar{T}_p) + D_{cp}} + v . \quad (33)$$

As $\bar{t} \to \infty$, the pyrolysis velocity approaches a constant value which, in general, differs from the char oxidation speed. Because the two reaction fronts move at different velocities, no steady solutions exist and countercurrent smolder propagation is inherently unsteady. Predicted $v_p(t \to \infty)$ are compared with measurements by Ohlemiller and Lucca [16] in Fig. 5.
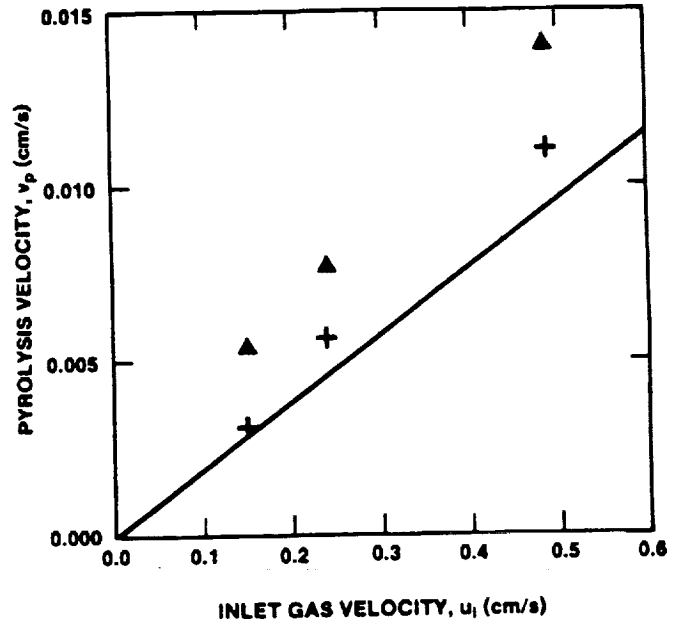

INLET GAS VELOCITY, u_i (cm/s)

FIG 5: Predicted (—) pyrolysis front velocities, $v_p(t \to \infty)$, versus initial gas velocity, u_i, for cellulosic insulation with $(1-\phi)\rho_{si} = 34$ kg/m^3, $c_s = 2.4$ kJ/kg, $Q_p = 0.37$ kJ/gm, $s_c = 0.3$, $\bar{T}_m = 1.8$ and $\bar{T}_p = 1$. Shown are measurements [16] between thermocouples 1 and 2 (Δ) and between 2 and 3 (+) – thermocouples 1, 2 and 3, were placed 7.5 cm, 10.1 cm and 11.4 cm, from the bottom, respectively.

Self-sustaining countercurrent smoldering is not possible when $dL/dt < 0$, corresponding to

$$\frac{c_g(T_m - T_p)}{Q_p} < Y_{oi} \frac{v_{us} H_{us}}{v_o H_o} \quad (34)$$

Solutions do not exist when the energy convected downstream from the oxidation zone is insufficient to drive the pyrolysis front.

3.3.2 Case II: An Ash Layer Builds Below Smolder Wave

Results presented in this section are restricted to small values of the stoichiometric coefficient, s_a. In Region III in Fig. 1B ($-h < x < 0$), the term involving the time derivative in Eq. (22) is small when $s_a \ll 1$ (note that $\bar{\rho}_s = s_a$ in Region III). Thus, $\bar{T}$ is steady in Region III when $s_a \ll 1$. When the thickness of the ash layer is

much greater than x_c, radiation heat losses from below are negligible. The residual ash serves as insulation, leading to high peak temperatures. The dimensionless temperature of the oxidation zone, $\bar{T}_m$, approaches D_{co} as $\bar{t}\to\infty$. For Y_{oi}–0.2, T_m–2,500°C. Such high temperatures will produce flaming combustion in most materials of interest [14]. In the absence of radial heat losses, temperatures encountered in the countercurrent configuration are much higher than those in cocurrent smolder. This is due to the role of gas phase convection. For countercurrent smolder, hot gases produced in the reaction zone flow into the unburnt solid, preheating the incoming fuel. While in cocurrent smolder, gas phase convection carries energy out of the system. When an ash layer builds below the smolder zone, Eq. (33) still determines the pyrolysis velocity, $\bar{v}_n(\bar{t}\to\infty)$. Because $\bar{T}_m\to D_{co}$, Eq. (33) now gives

$$\frac{d\bar{L}}{d\bar{t}} = \frac{\dfrac{D_{cp}}{D_{co}} - v}{1 + \dfrac{D_{cp}}{D_{co}}} \quad . \tag{35}$$

Since D_{co}/D_{cp} is fairly large, on the order of 10, Eq. (35) yields $d\bar{L}/d\bar{t}$–1. In dimensional form, $dL/dt = \rho_{gi}u_i c_g/(1-\delta)\rho_{si}c_s$. Typically, u_i–5 X 10^{-3} m/s, $(1-\delta)\rho_{si}/\rho_{gi}$–40 and c_s–c_g, giving dL/dt–10^{-4} m/s. Note that v–3 X 10^{-5} m/s for this case, so v_p–1.3 X 10^{-4} cm/s.

4. CONCLUSIONS

A model of unsteady, countercurrent smoldering combustion propagation has been developed. The proposed application is an experiment for use on the Space Shuttle. Due to the microgravity environment, it was assumed that the propagation of the smolder wave was one-dimensional. Radiation heat transfer was incorporated using a diffusion approximation. Smoldering combustion was represented using a two step mechanism, which included a pyrolysis reaction and a char oxidation reaction. A "flame" sheet approximation was used to model the oxidation zone and it was assumed pyrolysis occurs at a known temperature, T_p. In general, the two reaction fronts move at different velocities and countercurrent smolder propagation was unsteady. Two cases were considered: (1) no residual ash, $v_a M_a$–0, and complete consumption of the char; and (2) an ash layer forming beneath the oxidation zone, due to either production of ash during oxidation, $v_a M_a$–0, or leakage of char through the reaction zone.

Explicit expressions were derived for the char oxidation velocity, v, the maximum temperature, T_m, and the pyrolysis front velocity, v_p, in the limit of long time. Key results included: (1) in the absence of radial heat losses, v_p approaches a constant value which is, in general, different from v; (2A) for the no residual ash case, in limit of long time, T_m is determined by a balance among the energy released in the oxidation region, the energy required to preheat the gas and radiation heat losses; (2B) when an ash layer builds below the smolder wave, radiation heat losses from the bottom are negligible in the limit $t\to\infty$ and T_m is higher than in the no ash case; and (3) self-sustained countercurrent smoldering combustion is only possible when $c_g(T_m-T_p)/Q_p\geq Y_{oi} v_{us} M_{us}/v_o M_o$, i.e. solutions cease to exist when the energy convected by the gas phase is insufficient to drive the pyrolysis front.

The need for further experimental investigation of countercurrent smoldering cannot be overemphasized. Such experiments are necessary both to test the present model and to guide future theoretical work. Especially important is the transition to flaming combustion. Results from this study indicate that such a transition is more likely in materials which form a residual ash. It is anticipated that these materials will be readily identified experimentally.

REFERENCES

1. Beshty, B. S., "A Mathematical Model for the Combustion of a Porous Carbon Particle," Combustion and Flame, 32, p. 295, 1978.

2. Gann, R. G. and Chent, I. T., "Flow Study of Smoldering Charcoal Combustion," American Chemical Society, 172nd National Meeting, Division of Organic Coatings and Plastics, Report #20, 1976.

3. Donaldson, D. T., Yeadon, D. A. and Harper, R. J., "Smoldering Phenomenon Associated with Cotton," Textile Research Journal, 53, p. 160, 1983.

4. McCarter, R. J., "Smoldering Combustion of Cotton and Rayon," Journal of Consumer Product Flammability, 4, p. 346, 1977.

5. Kinbara, T., Endo, H. and Sega, S., "Downward Propagation of Smoldering through Solid Materials," Eleventh Symposium (International) on Combustion, the Combustion Institute, p. 525, 1967.

6. Moussa, N.A., Toong, T. Y. and Garris, C. A., "Mechanism of Smoldering of Cellulosic Materials," Sixteenth Symposium (International) on Combustion, The Combustion Institute, p. 1447, 1976.

7. Dosanjh, S. S., Peterson, J., Fernandez-Pello, A. C. and Pagni, P. J., "Bouyancy Effects on Smoldering Combustion," Acta Astronautica IAF-85 Stockholm Special Issue: Microgravity Materials and Fluid Sciences, 1985.

8. Ohlemiller, T. J., Bellan, J., and Rogers, F. E., "A Model of Smoldering Combustion Applied to Flexible Polyurethane Foams," Combustion and Flame, 36, p. 197, 1979.

9. McCarter, R. J., "Smoldering Combustion of Wood Fibers: Cause and Prevention," Journal of Fire and Flammability, 9, p. 119, 1978.

10. Kansa, E. J., Perlee, H. E. and Chaiken, R. F., "Mathematical Model of Wood Pyrolysis Including Internal Forced Convection," Combustion and Flame, 29, p. 311, 1977.

11. Day, M. and Wiles, D. M., "Combustibility of Loose Fiber Fill Cellulose Insulation: The Role of Borax and Boric Acid" Journal of Thermal Insulation, 2, p. 30, 1978.

12. Cohen, L. and Luft, N. V., "Combustion of Dust Layers in Still Air," Fuel, 34, p. 154, 1954.

13. Palmer, K. N., "smoldering Combustion in Dusts and Fibrous Materials," Combustion and Flame, 1, p. 14, 1957.

14. Ohlemiller, T. J., "Modeling of Smoldering Combustion Propagation," Progress in Energy and Combustion Science, 11, p. 277, 1986.

15. Gann, R. G., Earl, V. L., Manka, M. J. and Miles, L. B., "Mechanism of Cellulose Smoldering Retardance by Sulfur," Eighteenth Symposium (International) on Combustion, The Combustion Institute, p. 571, 1981.

16. Ohlemiller, T. J. and Lucca, D. A., "An Experimental Comparison of Forward and Reverse Combustion," Combustion and Flame, 54, p. 131, 1983.

17. Summerfield, M., Ohlemiller, T. J. and Sandusky, H. V., "A Thermophysical Mathematical Model of Steady-Draw Smoking and Predictions of Overall Cigarette Behavior," Combustion and Flame, p. 263, 1978.

18. Winslov, A.M., Numerical Model of Coal Gasification in a Packed Bed," Sixteenth Symposium (Internatuional) on Combustion, The Combustion Institute, p. 503, 1976.

19. Kanury, A. M., "Rate of Charring Combustion in a Fire," Fourteenth Symposium (International) on Combustion, The Combustion Institute, p. 1131, 1972.

20. Delichatsios, M. A. and de Ris, J., "An Analytic Model for the Pyrolysis of Charring Materials," Factory Mutual Research Corporation, May 1983.

21. Kanury, A. M., Introduction to Combustion Phenomena, Gordon and Breach Science Publishers, 1975.

22. Hirschefelder, J. O., Curtis, C. F. and Bird, R. B., Molecular Theory of Gases and Liquids, John Wiley and Sons, 1954.

23. Shafizadeh, F. and Bradbury, A. G. V., "Smoldering Combustion of Cellulosic Materials," Journal of Thermal Insulation, 2, p. 141, 1979.

24. Rogers, F. E. and Ohlemiller, T. J., "Cellulosic Insulation Material - I: Overall Degradation Kinetics and Reaction Rates," Combustion Science and Technology, 24, p. 129, 1980.

25. Tye, R. P., "Heat Transmission in Cellulosic Fiber Insulation Materials," Journal of Testing and Evaluation, 2, p. 176, 1974.

26. Lunardini, V. J., Heat Transfer in Cold Climates, Van Nostrand Reinhold Company, pp. 471-529, 1981.

PAPER 3

"BUOYANCY EFFECTS ON SMOLDERING COMBUSTION"

Dosanjh, S., Peterson, J., Fernandez-Pello, A.C., and Pagni, P.J.

BUOYANCY EFFECTS ON SMOLDERING COMBUSTION†

S. Dosanjh, J. Peterson, A. C. Fernandez-Pello and P. J. Pagni

Department of Mechanical Engineering, University of California, Berkeley, CA 94720, U.S.A.

Abstract—A theoretical and experimental study is carried out to determine the effect of buoyancy on the rate of spread of a cocurrent smolder reaction through a porous combustible material. Since buoyant forces are proportional to the product $g(\rho_g - \rho_s)$, they can be controlled experimentally by varying either the gravitational acceleration, g, or the density difference, $\rho_g - \rho_s$. The latter approach was followed in the present work. Measurements are performed of the smolder spread rate through porous α-cellulose (0.83 void fraction) as a function of the ambient air pressure. The experiments are carried out in a pressure vessel for ambient pressures ranging from 0.5 to 1.2 atm. The rate of spread was obtained from the temperature histories of thermocouples placed at fixed intervals along the fuel centerline. The smolder velocity was found to increase as the ambient pressure was increased. Extinction was found to occur when the buoyancy forces could not overcome the drag forces, indicating that at least for the present experimental conditions transport by diffusion cannot, by itself, support the spread of a smolder reaction. This conclusion is particularly important for outer space conditions where gravity and consequently buoyancy could be negligible. In the analysis, which assumes one-dimensional processes, the transport equations are solved to give the smolder spread rate as a function of the inlet oxygen mass flux. This mass flux is then estimated by balancing buoyancy and drag forces. Assuming that the smolder chemical reaction is only weakly dependent on pressure, the analysis finally predicts a smolder velocity dependence of the form $v \sim Y_{ox} g \rho_g^2 \sim Pa^2$, i.e. is proportional to the ambient pressure squared. Good qualitative agreement is found between the theoretical predictions and the experimental results.

1. INTRODUCTION

Smoldering combustion, which is defined as burning and smoking (that is, combustion) without flame, is present in a variety of combustion processes ranging from the burning of porous building materials to underground coal combustion. The host for the smoldering process is a porous combustible material. It is at the surface of this material where a heterogeneous chemical reaction takes place. Smoldering involves complex processes related to fluid mechanics and heat transfer in a porous media together with surface chemical reactions. Chemically, the porous combustible material is a hydrocarbon (for example, cellulose or polyurethane) which can sustain surface reactions and produce enthalpy and desorbing species—primarily CO_2, H_2 and CO. It usually undergoes considerable chemical change as the smolder wave propagates through the material from virgin bulk to slightly heated and pyrolytic material to largely carbonaceous char and ash behind the wave. The slower the wave propagates, the more complete its decomposition and combustion. Once established, self-sustaining smoldering well within this bulk can be difficult to extinguish.

†Paper IAF-85-289 presented at the *36th Congress of the International Astronautical Federation*, Stockholm, Sweden, 7–12 October, 1985.

When smoldering is initiated at the top of the material in a natural convection environment, the reaction zone travels downward, in the direction opposite to the buoyantly induced flow of air. Because the fuel and the oxygen enter the reaction zone from the same direction, this configuration is often referred to as cocurrent. Smoldering combustion is an oxygen-limited phenomenon[1,2]. Since, in most cases, all of the available oxygen is consumed, the total heat release is approximately proportional to the incoming oxygen mass flux. Increasing the buoyancy force increases the gas velocity, leading to higher temperatures and faster reaction rates[2]. For this reason, the rate at which a self-sustaining smolder wave passes through a porous material is very dependent on the magnitude of the buoyancy force relative to the magnitude of the drag forces.

Some of the earliest work in smoldering combustion was undertaken by Palmer[3], who measured the rate of smolder spread in dust trains and heaps. Since then, a number of experimental and theoretical investigations have appeared in the literature. Topics of research include smolder propagation in cigarettes[4,5], coal[6,7], polyurethane foams[8–10], wood[11–13] and wood products[14]. Smoldering combustion in the cocurrent configuration has been investigated experimentally with polyurethane foam[15] and loose-fill cellulose insulation[16] used as fuels. These materials exhibited similar smolder char-

acteristics. Raising either the oxygen concentration or the gas velocity led to higher burning rates.

The objective of the present work is to study, both experimentally and theoretically, the effect of buoyancy on cocurrent smoldering combustion. Buoyant forces, which are proportional to the product† $g(\rho_g - \rho_s)$, can be controlled experimentally by varying either the gravitational acceleration, g, or the density difference $\rho_g - \rho_s$. The latter approach is followed in the work presented here. By changing the ambient pressure, the density of the gas and consequently the buoyant force is varied. The rate of smolder spread through porous cellulose is measured for air pressures ranging from 0.5 to 1.2 atmospheres. The smolder velocity is found to increase as the ambient pressure is increased.

A model of cocurrent smoldering combustion under free flow conditions is also developed. In one dimension, the local gas velocity is determined from the conservation of mass—as a function of the inlet gas velocity (u_i). Since the pressure varies by a small amount over distances comparable to the thickness of the smolder wave[1,17], the transport equations can be solved before considering the momentum equation. Solution of these equations provides the rate of smolder spread as a function of u_i. The quantity, u_i is then estimated by using an integral momentum analysis. The predicted smolder velocities are in qualitative agreement with the measurements.

2. MATHEMATICAL FORMULATION

A schematic of the problem under consideration is presented in Fig. 1. A porous combustible solid with density ρ_{si}, temperature T_i, and void fraction ϕ, is contained in a vertical cylinder. Smoldering is initiated at the top of the porous material using a planar ignition source. The smolder wave propagates downward opposing a buoyantly driven upward flow of oxidizer. The gaseous oxidizer has an oxygen concentration Y_{oi} and a density ρ_g. While all of the oxygen is consumed in the reaction zone, a considerable amount of solid remains. In a frame of reference moving with the reaction zone, the solid fuel and the oxidizer enter the smolder wave with velocities v and $u_i + v$, respectively.

Over distances comparable to the smolder wave thickness, variations in pressure can be taken as a perturbation[1,2,17]. That is, $P = Pa + p$, where p/Pa is small quantity. In one dimension, the conservation of gas mass determines the gas velocity as a function of the inlet velocity (u_i). To leading order, the transport equations can be solved before considering the momentum equation. The transport equations are formulated in this section and a solution is presented in Section 3. The smolder velocity and the peak temperature are functions of u_i. The determination of u_i is discussed in Section 4.

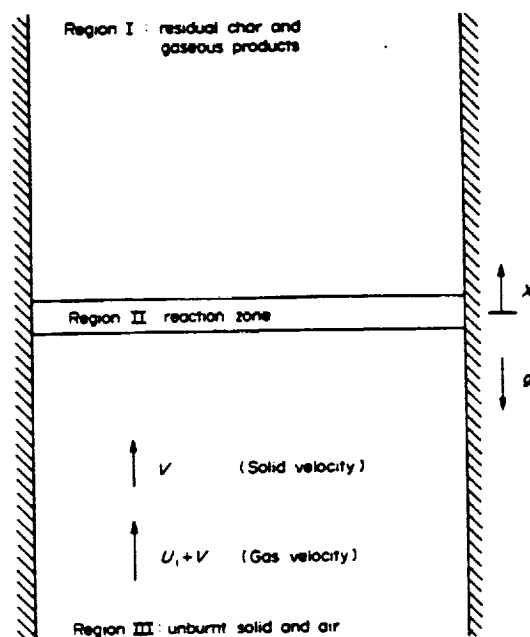†Nomenclature is given in Appendix at end of paper.

Fig. 1. Schematic of cocurrent smoldering combustion viewed in a frame of reference moving with the reaction zone.

Assumptions made in the following analysis include:

1. The propagation of the smolder wave is one-dimensional and quasi-steady in a frame of reference moving with the smolder wave.

2. The gas phase and the solid phase are in local thermal equilibrium (that is, $T_s = T_g$).

3. Radiation heat transfer can be modelled using a diffusion approximation.

4. The smolder chemical reaction is of the form

$$v_{us}(\text{unburnt solid}) + v_o O_2 \rightarrow v_a(\text{ash})$$

$$+ v_{gp}(\text{gaseous products}) \quad (1)$$

5. Thermophysical properties are constant.

In a frame of reference moving with the smolder wave, solid and gas phase mass fluxes are (symbols are defined in the Appendix and Tables 1 and 2)

$$m_s = (1 - \phi)\rho_s v, \quad (2)$$

$$m_g = \phi \rho_g(u + v). \quad (3)$$

The conservation of mass requires

$$m = m_s + m_g = \text{constant} \quad (4)$$

Phase and species mass flux fractions are defined, as follows,

$$\epsilon_s = m_s/m, \quad (5)$$

$$\epsilon_g = m_g/m, \quad (6)$$

$$\epsilon_{us} = Y_{us} m_s/m, \quad (7)$$

$$\epsilon_o = \frac{\phi Y_o \rho_g(u + v + V_o)}{m}, \quad (8)$$

Table 1. Dimensionless groups

$\alpha = \dfrac{T_f - T_i}{T_f}$	Change in temperature divided by the final temperature
$\beta = \dfrac{E}{RT_f^2}(T_f - T_i)$	Zeldovich number
$\Lambda = \dfrac{kZ(Y_\alpha \rho_{gl})^r \rho_{vi}^b T_f^f}{m^2 c E_\alpha \beta^a} \exp(-E/RT_f)$	Damkohler group
$\pi_1 = \dfrac{k_f E_p}{\phi \rho_g Dc}$	Modified Lewis number
$\pi_2 = \left(\dfrac{v_{gp} M_{gp}}{v_o M_o} - 1\right) Y_\alpha$	Fractional increase of the gas phase mass flux
$\pi_3 = \dfrac{k}{k + k_{rad} T_f^3} = \dfrac{k}{k_f}$	Ratio of the thermal conductivity to the effective thermal conductivity (radiation and conduction)
$\phi_{eq} = \dfrac{v_o M_o}{v_{us} M_{us}} \dfrac{\epsilon_{usi}}{\epsilon_{oi}}$	Equivalence ratio

where V_o is the diffusion velocity of the oxygen. Equation (1) gives the following relationships between these flux fractions

$$\frac{1}{v_{us} M_{us}} \frac{d\epsilon_{us}}{dx} = \frac{1}{v_o M_o} \frac{d\epsilon_o}{dx} = \frac{1}{(v_{us} M_{us} - v_a M_a)} \frac{d\epsilon_s}{dx}$$

$$= \frac{1}{(v_{gp} M_{gp} - v_a M_a)} \frac{d\epsilon_g}{dx}. \quad (9)$$

Distances are measured relative to k_f/mc, where $k_f = k + k_{rad} T_f^3$ is the effective thermal conductivity. A dimensionless temperature is defined as,

$$T = \frac{T - T_i}{T_f - T_i}. \quad (10)$$

Since all of the incoming oxygen is consumed in the reaction zone, ρg, ϵ_o and Y_o are nondimensionalized by their initial values (Table 2).

In dimensionless form, the transport equations are [17]:

Conservation of oxygen

$$\frac{d\epsilon_o}{d\bar{x}} = -w. \quad (11)$$

Table 2. Dimensionless variables

$\bar{\epsilon}_o = \dfrac{\epsilon_o}{\epsilon_{oi}}$	Dimensionless oxygen mass flux
$\bar{\rho}_g = \dfrac{\rho_g}{\rho_{gp}}$	Dimensionless gas density
$\bar{T} = \dfrac{T - T_i}{T_f - T_i}$	Dimensionless temperature
$\bar{u} = \dfrac{u}{u_c}$	Dimensionless gas velocity
$\bar{Y}_o = \dfrac{Y_o}{Y_{oi}}$	Dimensionless oxygen concentration

Fick's Law

$$\frac{1}{\pi_1} \frac{d\bar{Y}_o}{d\bar{x}} = [1 + \pi_2(1 - \bar{\epsilon}_o)] \bar{Y}_o - \bar{\epsilon}_o. \quad (12)$$

Conservation of energy

$$\{\pi_3 + (1 - \pi_3)[1 - \alpha(1 - \bar{T})]^3\} \frac{d\bar{T}}{d\bar{x}}$$

$$= \bar{T} - (1 - \bar{\epsilon}_o). \quad (13)$$

Auxilliary relations (Arrhenius type reaction rate)

$$w = (\beta \bar{Y}_o)^a \left[1 - \frac{1}{\phi_{eq}}(1 - \bar{\epsilon}_o)\right]^b [1 - \alpha(1 - \bar{T})]^f \cdot$$

$$\times \exp\left(-\frac{\beta(1 - \bar{T})}{[1 - \alpha(1 - \bar{T})]}\right) \quad (14)$$

The dimensionless groups and variables are given in Tables 1 and 2 respectively. Dividing eqns (11, 12) by eqn. (13), the spatial coordinate $\bar{x}$ can be eliminated. In terms of the new coordinate $\bar{T}$, the boundary conditions are

as $\bar{T} \to 0$	$\bar{\epsilon}_o \to 1$	(15)
as $\bar{T} \to 1$	$\bar{\epsilon}_o \to 0$	(16)
	$\bar{Y}_o \to 0$	

3. AN ASYMPTOTIC SOLUTION OF THE TRANSPORT EQUATIONS

For cellulose, the Zeldovich number, β, is on the order of fifteen[14]. Because of Arrhenius-type dependence of the reaction rate on temperature, relatively small changes in temperature can lead to large changes in the reaction rate. Under such circumstances, it is reasonable to assume that the oxidation

reaction is confined to a thin region[18]. This region acts as a source for energy and a sink for oxygen. The reaction zone is, in essence, a derivative layer. Temperature and oxygen concentration vary continuously across this layer, while their derivatives undergo a discontinuous change.

Since region II (Fig. 1) is fairly thin. the source terms in the governing equations are balanced by diffusion. In the outer regions (regions I and III), convection and diffusion balance. The smolder velocity and the maximum temperature are determined by matching the inner solution with the outer solutions. The details of this matching process are available in [17]. The following results are pertinent to this study.

$$\frac{Q\epsilon_{oi}}{C(T_f - T_i)} = 1,$$ (17)

$$A = \frac{f(\phi_{eq})}{\pi_1^2 \Gamma(1 + a)},$$ (18)

where

$$f(\phi_{eq}) = \int_0^1 \frac{t \, dt}{\left[1 - \frac{1}{\phi_{eq}}(1 - t)\right]^b}.$$ (19)

Equations (17, 18) determine v and T_f as functions of u_i. As illustrated in Figs 2 and 3, both v and T_f increase as the inlet oxygen mass flux $(Y_\alpha \phi \rho_\beta u_i)$ is increased.

4. CONSIDERATION OF THE MOMENTUM EQUATION

The inlet gas phase velocity (u_i) is determined from an integral momentum analysis. A characteristic gas phase velocity is defined by balancing buoyancy forces and drag forces.

$$u_c = \frac{\phi \rho_\beta g}{\mu a_{di}},$$ (20)
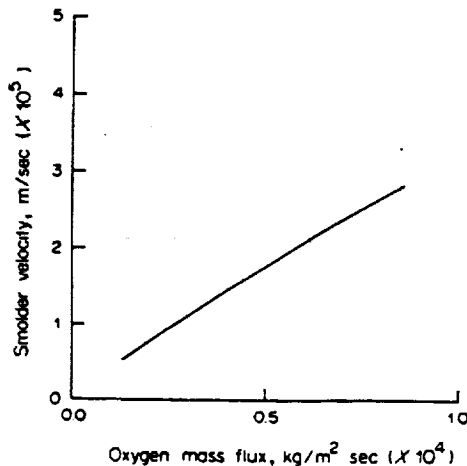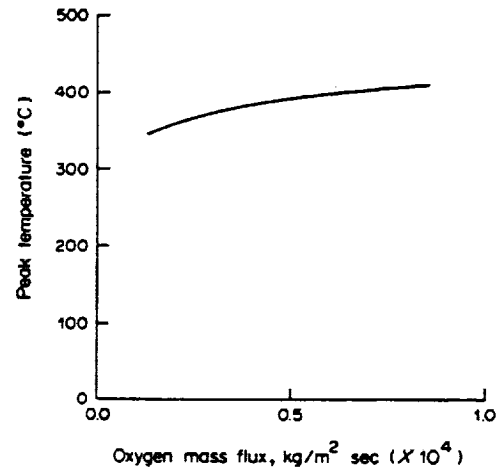
Fig. 3. Final temperature. T_f. as a function of the inlet oxygen mass flux. $\phi Y_\alpha \rho_\beta u_i$.

where μa_d is the proportionally constant in Darcy's Law. The gas density. ρ_g, is nondimensionalized by ρ_β.

In the absence of an imposed pressure gradient, the conservation of momentum requires (see Nomenclature section in Appendix):

$$\int_{-\hbar}^{\hbar_o - \hbar} \bar{a}_d \bar{u} \, dx = \int_{-\hbar}^{\hbar_o - \hbar + L} (1 - \bar{\rho}_g) \, d\bar{x},$$ (21)

where L is the chimney height, h is the height of the virgin solid and $h_o - h$ is the char height. While the flow resistance, a_d, is lower in the char layer, the gas phase velocity is higher. The latter is due to both gas generation and expansion in the reaction zone. Therefore, it is reasonable to assume that $a_d u$ remains approximately constant. Using this assumption, eqn (21) yields the following relationship between μ_i and α (which depends on T_f),

$$u_i = \alpha \left[1 + \frac{L - h}{h_o}\right].$$ (22)

Fig. 2. Smolder velocity. r. as a function of the inlet oxygen mass flux. $\phi Y_\alpha \rho_\beta u_i$.
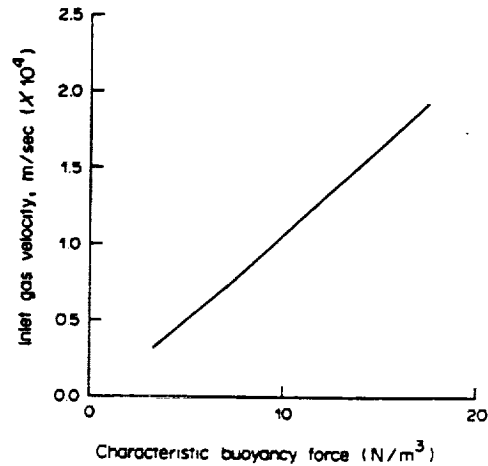
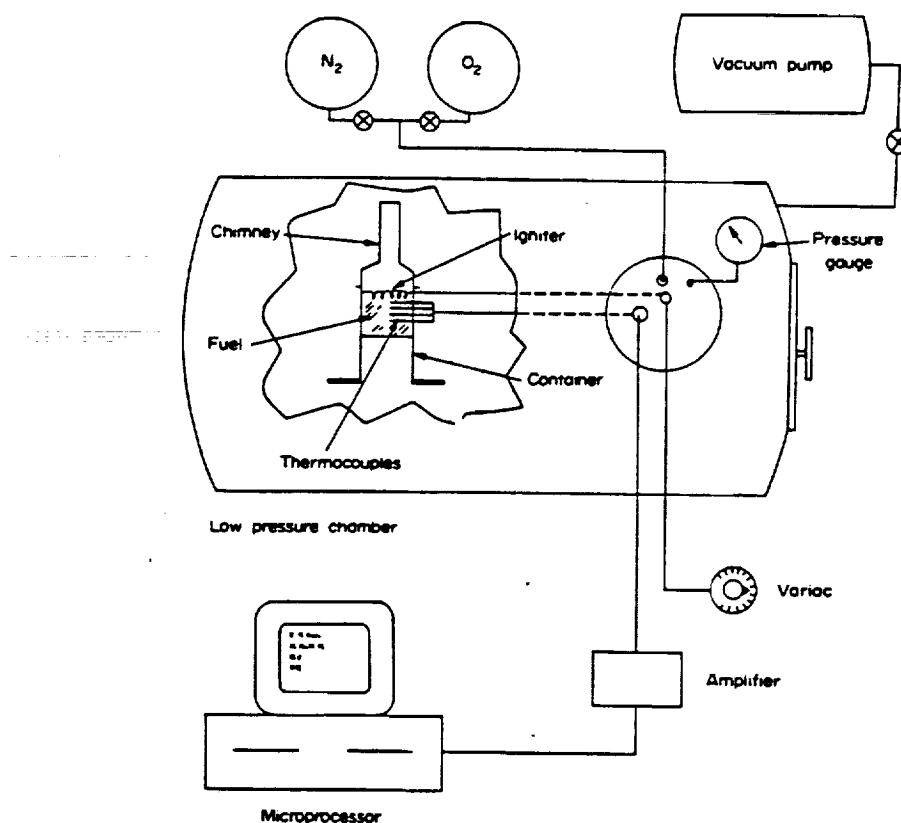Fig. 4. Inlet gas velocity. u_i. as a function of a characteristic buoyancy force. $g \rho_\beta$.

Fig. 5. Schematic diagram of the experimental installation.

Equations (17, 18, 22) determine v, T_f and u_i. As illustrated by Fig. 4, u_i is approximately proportional to the characteristic buoyancy force $g\rho_{gi}$. Since the smolder velocity is proportional to the oxygen mass flux,

$$v \sim Y_{oi}\rho_{gi}u_i \sim Y_{oi}g\,\rho_{gi}^2. \qquad (23)$$

Assuming that the reaction rate of the smolder reaction is independent of pressure, it can be deduced from the above expression that the smolder velocity is proportional to the ambient pressure squared, that is $v \sim Pa^2$. Since the reaction rate for most fuels is only weakly dependent on pressure, it is expected that the above velocity/pressure dependence will be valid at least for relatively small variations of the ambient pressure. However, if the ambient pressure is reduced considerably, the reaction rate and temperature will decrease to the point that extinction will occur. The reduction of the flow of oxygen to the reaction zone due to both the decrease in pressure and post-combustion temperature, i.e. decrease in buoyancy, will also add to the onset of extinction.

5. EXPERIMENT

Experiments are performed to determine the effect

of ambient pressure, and consequently of buoyancy, on the rate of smolder spread through a porous combustible material. A schematic diagram of the experimental installation is shown in Fig. 5. The experiments are carried out in a cylindrical pressure vessel 1.8 m in diameter and 3.3 m long. A vacuum pump or a compressor is used to set the vessel pressure below or above atmospheric pressure. The oxygen concentration in the vessel can be varied by adding oxygen or nitrogen from pressurized bottles. Acrylic windows located at opposite sides of the vessel provide optical access to the test area. The fuel/container unit is held by a frame in the middle of the test area, avoiding the obstruction of the flow of air in and around the fuel container.

The porous fuel is contained in a vertical Pyrex cylinder 0.07 m in diameter and 0.16 m long. These dimensions, in particular the cylinder diameter, are selected to reduce to a minimum, the depletion of oxygen in the vessel during the fuel combustion process, while ensuring a one-dimensional smolder spread process in a region of at least 2 cm in diameter around the cylinder axis. Small holes placed longitudinally along the side of the cylinder allow the positioning of thermocouples or gas sampling probes in the porous material. A nichrome wire electrical

igniter can be positioned at the top or bottom of the cylindrical container to initiate the smoldering process at either end of the cylinder. As an alternative ignition method, an easily ignitable fuel (cellulose soaked in heptane for example) is thinly spread on top of the porous material and ignited with a small pilot flame or spark. The flaming combustion of the volatile fuel initiates the smoldering combustion of the porous combustible. A chimney 0.33 m long and 0.03 m in diameter, tapered at the bottom to a diameter of 0.07 m is fitted on top of the fuel container. The chimney is used to both enhance the buoyancy driven flow of oxidizer through the porous fuel and to prevent the diffusion of air to the top surface of the combustible material. The fuel container and the chimney are insulated with a fiber-glass jacket to reduce heat losses to the environment.

The rate of smoldering spread is measured from the temperature histories of thermocouples embedded in the porous fuel and with their junction placed at fixed distances along the cylinder axis. Four Chromel-Alumel thermocouples 0.8 mm in diameter, are embedded in the porous fuel at 5 or 10 mm apart. The emf from the thermocouples is amplified to volt levels and processed in a real time data acquisition microcomputer. With the fuel temperature histories, the rate of spread of the smolder reaction is calculated from the time lapse of reaction zone arrival to two consecutive thermocouples, and the known distance between the thermocouples. The arrival of the smolder reaction zone at the thermocouple position is characterized by a maximum in the temperature profile. Under most experimental conditions this maximum is not sharply defined, which introduces inaccuracies in the definition of the smolder front arrival time and consequently in the calculation of the smoldering spread rate. In spite of this problem, the thermocouple probing method is considered to be the most practical and accurate method to measure the rate of smolder spread.

6. RESULTS AND COMPARISON

The experiments presented in this work were carried out using α-Cellulose powder as porous combustible material. A preweighted amount of cellulose is loosely packed in the cylindrical container filling a constant volume, therefore keeping an approximately constant void fraction. The cellulose is supported at the bottom by a wire mesh which is attached to the cylinder surface 40 mm from the cylinder top. The upper cellulose surface is kept flush with the top cylinder rim. The 40 mm cellulose bed height was found to be the maximum at which the present experimental set up could operate. For larger heights, the pressure drop in the system is apparently too large to be overcome by the chimney generated buoyancy, particularly at the lower pressures tested. The resulting induced flow of air is not large enough to sustain the progress of the smolder reaction. Al-

Fig. 6. Electron microscope photograph showing the structure of the α-cellular (× 300).

though longer fuel beds could be tested by increasing the chimney height, it was decided that a 40 mm fuel height was sufficient to provide the information sought in this work. All the experiments were performed with an approximately constant cellulose void fraction of 0.82. The void fraction was estimated from the measured weight, occupied volume and a cellulose density of $0.62 \times 10^3 \text{ kg/m}^3$. An example of the structure of the cellulose used in the experiments is shown in the photograph of Fig. 6, taken with an Electron Microscope at a magnification of × 400. It is seen that the material is formed primarily by long, interlaced, cellulose fibers. Photographs, as the one shown in Fig. 6, can be used to approximately estimate the Darcy coefficient of the porous fuel.

The measured rates of smolder spread through the cellulose are presented in Fig. 7 for several ambient air pressures. For the measurements, the four thermocouples were placed, in most cases, 5 mm apart from each other with the first thermocouple located 15 mm from the top cellulose surface. In a few tests, the thermocouples were positioned at distances 10 mm apart. The smolder velocities presented in Fig. 7 were calculated from the outputs of the second and
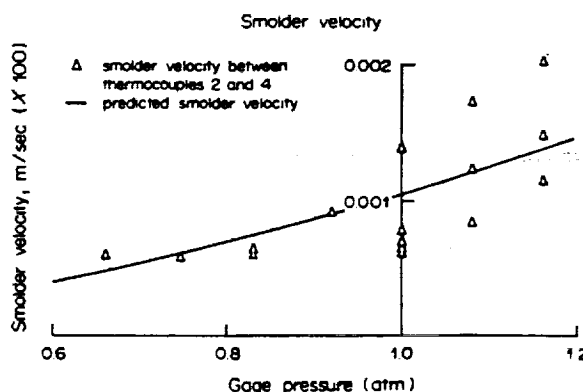

Fig. 7. Measured and predicted smolder velocity, v, as a function of the ambient pressure, Pa.

fourth thermocouples, because they seemed to provide the most reproducible data. As it is seen from the results of the figure, there is scatter in the measurements, particularly at higher pressures. We believe that this is primarily the result of inaccuracies in the determination of the arrival of the smoldering front at the thermocouple location. This is more noticeable at higher pressures because the smolder velocity is higher. The scatter in the data may be also the result of small variations in the cellulose void fraction and location of the thermocouples. For comparison purposes, the theoretically predicted smolder velocity is also presented in Fig. 7. For the theoretical calculations, the Darcy coefficient is selected such that at atmospheric pressure the theoretical prediction agrees with the average measured smolder velocity. Approximate estimation of the Darcy coefficient from the Electron Microscope photographs (Fig. 6) gives values for the smolder velocity that are approx. 30% lower than those presented in Fig. 7. Although the comparison between theory and experiments can only be considered here as qualitative, it is seen from Fig. 7 that the theoretical model predicts very well the general trend of the experimental results, with the smoldering velocity decreasing as the ambient pressure decreases. This is the result of the decrease of the flow rate of air through the system as the pressure, and consequently the buoyancy, is decreased.

An interesting experimental observation is that the smolder reaction does not spread at ambient pressures below 0.6 atm. We believe that this is primarily due to the inability of the oxygen to reach the reaction zone because at this pressure the buoyant forces cannot overcome the pressure losses. The decrease of the reaction rate due to the decrease in pressure is probably another factor that contributes to the extinction, or lack of spread, of the smolder reaction. The present theoretical model is not capable of predicting extinction and, thus, cannot be used to predict this experimental result. An important conclusion of this experimental observation is that, at least for α-cellulose with void fractions equal to or larger than the one used here and for air as oxidizer, smolder combustion will not take place if species diffusion is the only mechanism to transport the oxidizer to the reaction zone. This result could be particularly important for the potential development of smolder combustion process under micro-gravity conditions, in space vehicles for example, since buoyancy forces would be negligible and the flow of oxidizer would have to be driven by diffusion or forced.

In Fig. 8 the predicted and measured peak temperature are presented as a function of the ambient pressure. It is seen that there is good qualitative agreement between experiments and theory, although the predicted temperatures are lower than the measured ones. This result is probably due to the simplified chemical kinetic model used in the theory. The complex chemical reactions taking place at the

fuel surface are simply modeled with a one step reaction with an Arrhenius type reaction rate. Furthermore, the values of the activation energy and pre-exponential factor used to calculate the reaction rate are not accurately known. Selection of a larger value of the activation energy or the pre-exponential factor could result in a better quantitative agreement between theory and experiment.

7. CONCLUDING REMARKS

Theoretically predicted rates of smolder spread and peak reaction temperatures during the natural convection, cocurrent, smoldering combustion of porous cellulose in air at varied ambient pressures agree well, at least qualitatively, with the experimental results for ambient pressures that do not differ considerably from the atmospheric value. The quantitative differences appear to be due primarily to simplifications used in the modeling of the chemical reactions taking place at the fuel surface, to uncertainties in the value of key process parameters such as activation energy, pre-exponential factor, Darcy coefficient and void fraction, and to experimental errors because of difficulties in measuring accurately the rate of smolder spread.

It is found that the presence of a steady flow of oxidizer toward the reaction zone is of critical importance for the progress of the reaction zone. Both the smolder velocity and reaction temperature are strong functions of the oxidizer flow rate, increasing with it. Extinction is observed to occur if the flow rate is below a critical value. This indicates that, at least for cellulose with void fraction as the one tested in this work or higher, diffusion of oxidizer toward the reaction zone is not a sufficient transport mechanism to sustain the cocurrent smolder combustion process.
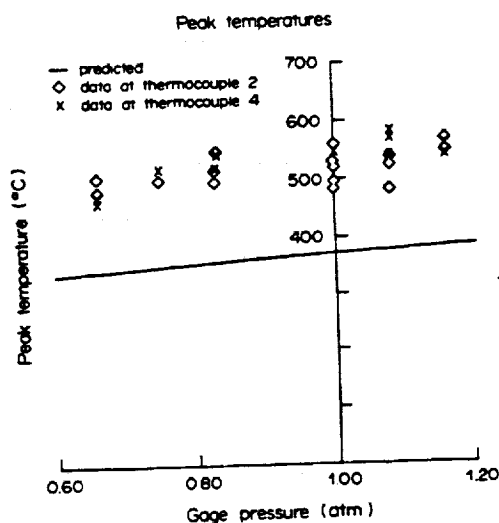

Fig. 8. Measured and predicted reaction zone peak temperature, T_f, as a function of the ambient pressure.

This result is particularly important for natural convection smoldering combustion under microgravity conditions since buoyancy forces are very small and the oxidizer can only be transported to the reaction zone by diffusion. The present results suggest that for smolder combustion to occur in a microgravity environment, the flow of oxidizer must be forced through the fuel, or the porous fuel must have, among others, a large void fraction, a small Darcy coefficient, a low activation energy and a large effective thermal conductivity, that is, properties that favor the transport of heat and mass by diffusion and that present minimum obstruction to the free flow of gases.

The present work, however, can be only viewed as preliminary. Theoretical predictions and detailed experiments of the smolder extinction process are necessary. Experiments with other porous fuels, and in particular the accurate determination of the conditions at which smolder combustion would occur in a microgravity environment are also necessary.

REFERENCES

1. T. J. Ohlemiller, Modeling of smoldering combustion propagation. NBSIR 84-2895 (1984).
2. T. J. Ohlemiller, J. Bellan and F. E. Rogers, A model of smoldering combustion applied to flexible polyurethane foams. *Combust. Flame* **36**, 197-215 (1979).
3. K. N. Palmer, Smoldering combustion in dusts and fibrous materials. *Combust. Flame* **1**, 14-17 (1957).
4. M. Muramatsu, S. Umemura and T. Okado, Mathematical model of evaporation-pyrolysis processes inside a naturally smoldering cigarette. *Combust. Flame* **36**, 245-262 (1977).
5. R. R. Baker, Combustion and thermal decomposition regions inside a burning cigarette. *Combust. Flame* **30**, 21-32 (1977).
6. B. S. Beshty, A mathematical model for the combustion of a porous carbon particle. *Combust. Flame* **32**, 295-311 (1978).
7. R. G. Gann and I. T. Cheng. Flow study of smoldering charcoal combustion. American Chemical Society, 172nd National Meeting, Division of Organic Coatings and Plastics, Report No. 20 (1976).
8. T. J. Ohlemiller and F. E. Rogers. A survey of several factors influencing smoldering combustion in flexible and rigid polymer foams. *J. Fire Flammab.* **9**, 489-509 (1978).
9. F. E. Rogers and T. J. Ohlemiller. Studies of the smoldering combustion of flexible polyurethane cushioning materials. *J. Fire Flammab.* **9**, 5-13 (1978).
10. R. J. McCarter, Smoldering combustion of polyurethane foam. *J. Consumer Prod. Flammab.* **3**, 128-140 (1976).
11. R. J. McCarter, Smoldering combustion of wood fibers: cause and prevention. *J. Fire Flammab.* **9**, 119-126 (1978).
12. E. J. Kansa, H. E. Perlee and R. F. Chaiken. Mathematical model of wood pyrolysis including internal forced convection. *Combust. Flame* **29**, 311-324 (1977).
13. K. Kailasanath and B. T. Zinn, Theoretical investigation of the smoldering combustion of porous solids. Presented at the *Fluids Engineering Conference* (1981).
14. N. A. Moussa, T. Y. Toong and C. A. Garris, Mechanism of smoldering of cellulosic materials. *Sixteenth Symposium (International) on Combustion*, The Combustion Institute, pp. 1447-1457 (1976).
15. F. E. Rogers and T. J. Ohlemiller, Smolder characteristics of flexible polyurethane foams. *J. Fire Flammab.* **11**, 32-44 (1980).
16. T. J. Ohlemiller and D. A. Lucca, An experimental comparison of forward and reverse combustion. *Combust. Flame* **54**, 131-147 (1983).
17. S. S. Dosanjh, P. J. Pagni and A. C. Fernandez-Pello, Forced cocurrent smoldering combustion. *Combust. Flame*, In press (1986).
18. F. A. Williams, *Combustion Theory*, Second edn. Benjamin/Cummings (1985).

APPENDIX

Nomenclature

a_d = Darcy coefficient
c = Heat capacity
D = Mass diffusivity of oxygen in air
E = Activation energy
g = Gravitational acceleration
h = Height of the virgin solid
k = Effective thermal conductivity of the solid and the gas = $\phi k_g + (1 - \phi)k_s$
m = Mass flux
M_i = Molecular weight of species i
P = Pressure
Q = Energy released per mass of oxygen consumed
T = Temperature
u = Velocity of the gas phase
v = Smolder velocity
V_i = Diffusion velocity of gas species i
Y_o = Density of the oxygen/density of the gas phase
Y_{us} = Density of the unburnt solid/density of the solid
Z = Pre-exponential factor

Greek letters

β = Zel'dovich number
ϵ = Mass flux fraction
ρ = Density
μ = Dynamic viscosity
v_{ij} = Stoichiometric coefficient
ϕ = Void volume/total volume
ϕ_{eq} = Equivalence ratio

Subscripts

a = Ash
f = Final value ($x = +\infty$)
g = Gas phase
gp = Gaseous products
i = Initial value ($x = -\infty$)
s = Solid phase
us = Unburnt solid

PAPER 4

"SMOLDERING COMBUSTION ANALYSIS"

Dosanjh, S.

Smoldering Combustion Analyses

By

Sudip Singh Dosanjh

B.S. (University of California) 1982
M.S. (University of California) 1984

DISSERTATION

Submitted in partial satisfaction of the requirements for the degree of

DOCTOR OF PHILOSOPHY

in

Engineering

in the

GRADUATE DIVISION

OF THE

UNIVERSITY OF CALIFORNIA, BERKELEY

Approved: ...*Patrick J. Pag* ———............ *7/3/96*......
              Chairman   Date

...*A.C.F.-Pely*............................ *7/7/86*...

....

....

Smoldering Combustion Analyses

by

Sudip S. Dosanjh
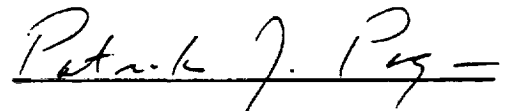
ABSTRACT

Smoldering combustion propagation through very porous solid materials is examined. The proposed application is an experiment for use on the Space Shuttle. Due to the microgravity environment, smolder propagation is assumed to be one-dimensional. Two configurations are considered: (1) cocurrent, premixed-flame-like or reverse ; (2) counter-current, diffusion-flame-like or forward.

In cocurrent smoldering combustion, both forced and free flow are analytically represented. It is assumed that the propagation of the smolder wave is steady in a frame of reference moving with the wave. Smoldering is described by a finite-rate, one-step, oxidation reaction and radiation heat transfer is incorporated using a diffusion approximation. The dimensionless equations are very similar to those governing the propagation of a laminar premixed flame. A straightforward extension of the activation energy asymptotics analysis presented by Williams yields an expression for a dimensionless eigenvalue, Λ , thus determining the final temperature, T_f. A global energy balance then determines the smolder velocity, v. Explicit expressions are derived for the smolder velocity, v, and the final temperature, T_f. An approximate extinction criterion

is identified.

A model of unsteady, forced, countercurrent smoldering combustion is also presented. Smoldering is represented utilizing a two step mechanism consisting of a pyrolysis reaction followed by a char oxidation reaction. A "flame" sheet approximation is used to model the oxidation reaction. It is assumed that pyrolysis occurs at a known temperature, T_p. Because the two reaction zones move at different velocities, countercurrent smoldering is unsteady. Two cases are considered: (1) no residual ash, $y_a M_a = 0$, and (2) an ash layer forming beneath the oxidation zone, $y_a M_a \neq 0$. The residual ash serves as insulation, and its presence leads to higher peak temperatures. Explicit expressions are derived for the oxidation velocity, v, the maximum temperature, T_m, and the pyrolysis front velocity, v_p.

Patrick J. Pagni
Chairman, Thesis Committee

ACKNOWLEDGEMENTS

I would like to thank Professor Patrick J. Pagni for his encouragement and guidance. His caring support during my studies is deeply appreciated.

This work would not have been possible without my parents love and encouragement.

Special thanks to my wife Lynn for her love and patience.

CONTENTS

CHAPTER 1

INTRODUCTION

1.1 PHENOMENON OF INTEREST

Smoldering is defined as a heterogeneous oxidation zone propagating through a porous fuel [1]. Oxygen diffuses to the surface of the solid where it is adsorbed [2]. A highly exothermic reaction ensues. The products of combustion (primarily CO_2, H_2O and CO) desorb and diffuse away from the surface. Many materials can sustain smoldering. These include coal [3,4], cotton [5,6], paper [7], polyurethane foams [8-11], wood [12-14], thermal insulation materials [15] and various dusts [16,17]. If the host material is sufficiently permeable, smoldering is not necessarily confined to its outer surface. A self-supporting exothermic reaction zone can pass through the substance [1]. Oxygen reaches the reaction zone by convection and diffusion. However, such a scenario is not valid for all porous materials. Upon being heated, some substances decompose into a "liquid" tar [8], restricting the flow of air through the material and consequently inhibiting the propagation of such a smolder wave. Smoldering combustion can be prevented in some materials by adding sulfur [6,18].

There are two distinct classifications for the one-dimensional propagation of a smolder wave - see Figs. 1-1 and 1-2. The reaction zone travels downward when smoldering
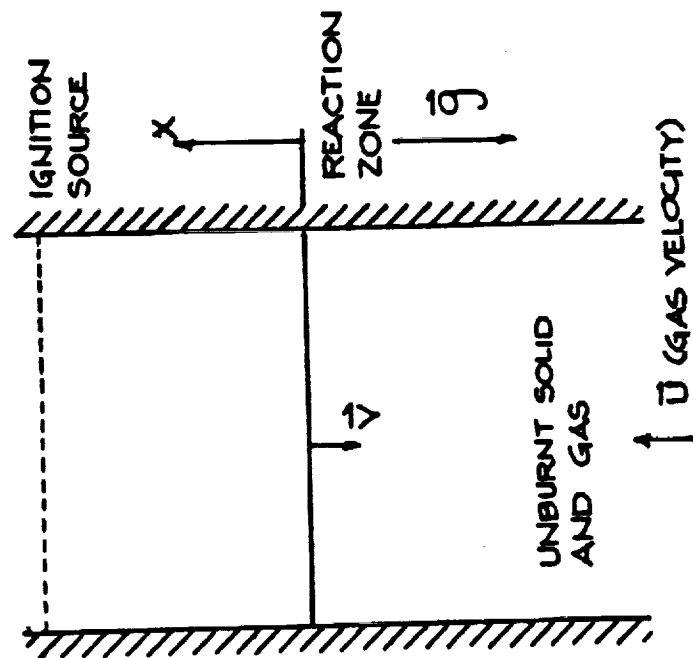
FIG. 1-2: Countercurrent, forward
or diffusion-flame-like.

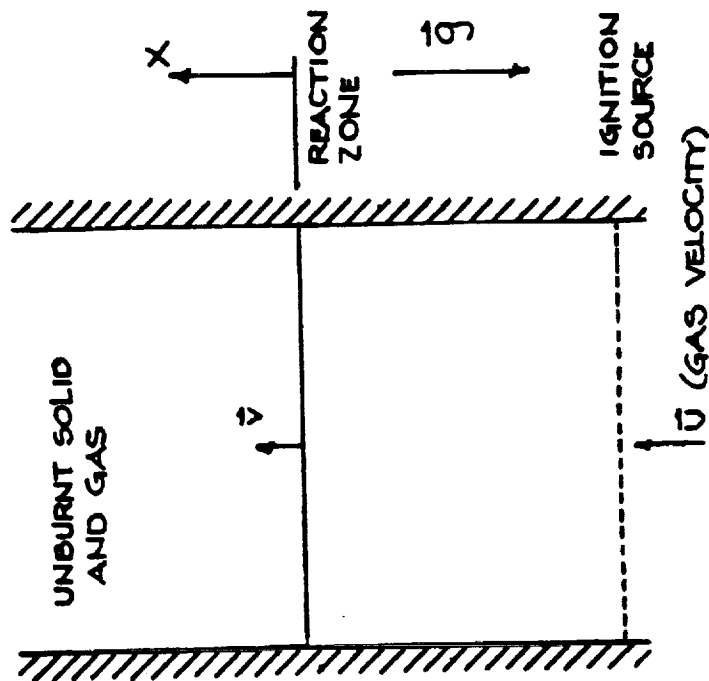FIG. 1-1: Cocurrent, reverse
or premixed-flame-like.

is initiated at the top of the material, moving in the direction opposite to the flow of air, corresponding to reverse smolder. This configuration is also referred to as cocurrent or premixed-flame-like because the fuel and the air enter the reaction zone from the same direction. On the other hand, the reaction zone travels upwards when smoldering is initiated at the bottom, moving in the same direction as the air flow, corresponding to forward smolder. In this case the fuel and the air enter the oxidation zone from opposite directions. This configuration is also referred to as countercurrent or diffusion-flame-like.

If the inlet gas velocity, u_i, is held fixed, smolder propagation in the cocurrent configuration becomes steady and the burning velocity reaches a constant value [2,19,20]. While almost all of the oxygen reaching the reaction zone is consumed, a considerable amount of solid remains behind in the form of a residual ash. This ash serves as insulation, letting fairly weak smolder waves propagate [20]. Because all the available oxygen is consumed, the amount of heat released in the oxidation zone is proportional to the oxygen mass flux, $\dot{m}''_{oi}$. The smolder velocity is highly dependent on $\dot{m}''_{oi}$, increasing linearly with $\dot{m}''_{oi}$. On the other hand, the peak temperature is only weakly dependent on $\dot{m}''_{oi}$, increasing logarithmically with m_{oi} [2,20,21].

Smolder propagation in the countercurrent configuration is unsteady [19]. This unsteady behavior is due to the presence of two reaction regions. A pyrolysis reaction zone

moves upwards through the solid leaving behind a fairly black char. Oxidation of this char in a thin zone provides the energy required to sustain smoldering [19]. As in a diffusion flame, all of the available fuel and oxygen is consumed in the oxidation zone [2,19]. Therefore, the char oxidation speed is fairly constant and is proportional to the incoming oxygen mass flux, with the proportionality constant determined from stoichiometric conditions. Because the pyrolysis reaction is endothermic, the motion of the pyrolysis front is very dependent on heat transfer from the oxidation zone. In the absence of heat losses from the sides of the cylinder, the pyrolysis front velocity approaches a constant value, which is, in general, several times larger than the char oxidation speed [19]. Consequently, countercurrent smolder propagation is inherently unsteady.

Another important difference between the two configurations is the direction in which energy is convected by the gas. In the cocurrent configuration, hot gases produced in the reaction region flow into the burnt solid. Consequently, heat transfer by radiation and conduction must provide the energy required to preheat the unburnt solid. In the countercurrent configuration, energy convected by the gas phase raises the temperature of the unburnt material. Therefore, in the absence of heat losses, temperatures encountered in the countercurrent configuration are higher than those encountered in cocurrent smolder.

1.2 RELATED STUDIES

Early work in smoldering combustion was conducted by Palmer [17], who measured the rate of smolder spread in various dust trains and heaps. Since then, researchers have studied smolder propagation in a wide variety of configurations. Cocurrent smoldering combustion has been examined experimentally using polyurethane foams [22], cellulosic insulation materials [19] and packed beds of alpha-cellulose fibers [23] as fuels. Ohlemiller et al [20] developed a large computer code to investigate unsteady, cocurrent, smolder propagation in flexible polyurethane foams. A pulse of radiation was used to initiate smoldering at the top of the porous fuel. Two reactions (pyrolysis and oxidation) were included in the analysis. The solid and the gas were presumed to be in local thermal equilibrium (that is, $T_s = T_g$) and radiation heat transfer was incorporated using a two-flux model. Because their method required expensive finite element calculations, Ohlemiller et al concluded that a primary use of this model is to study the initiation of smoldering combustion.

Relatively little attention has been given to smoldering combustion in the countercurrent configuration [1]. Ohlemiller and Lucca [19] conducted an experimental investigation of this problem using cellulosic insulation as a fuel. Summerfield et al [24] presented a one-dimensional numerical model of smolder spread in a cigarette during steady draw. Two reactions were included, pyrolysis and char

oxidation. Because the wrapping paper burns back, a significant amount of air bypasses the hottest part of the char oxidation region. Consequently, cigarette smolder is much more complicated than the countercurrent smoldering scenario depicted in Fig. 2-2.

Several researchers [25-27] have investigated countercurrent propagation within the context of coal gasification in a packed bed. A large number of reactions were included in these analyses. One of the most complete numerical solutions was presented by Winslow [25]. In his unsteady, one-dimensional model, different gas and solid temperatures were used and concentrations of eight chemical species, two forms of water (surface and interior), coal and char were calculated. Good agreement between measurements and calculations was reported. However, due to the complexity of the solutions, it is difficult to determine which mechanisms dominate the movement of the six reaction fronts.

Steady smolder spread in horizontal, cylindrical, alpha-cellulose and polyurethane, fuel elements was examined by Moussa et al [28] and Ortiz-Molina et al [29], respectively. The gas and the solid were assumed to be in local thermal equilibrium. The material was divided into two regions, an isothermal char-oxidation zone, the length of which was determined empirically, and a pyrolysis zone. Two competing reactions were used to model pyrolysis. Good agreement between the predicted and measured extinction

limit was reported.

Muramatsu [30] formulated a model of evaporation-pyrolysis processes inside a cigarette. No attempt was made to model the burning region. Energy convected by the gas phase was considered negligible and the smolder speed was determined experimentally. Since the burning velocity was known a priori, the mathematical formulation was an initial value problem and a Runge-Kutta integration technique was used. Another study concerned with modeling the smoldering of cigarettes was carried out by Baker [31]. Empirically determined temperature profiles and gas species concentrations were used to find the net rate of chemical production of heat and the consumption of oxygen.

Recently, Leisch et al [32] modelled the steady smoldering combustion of dust layers in a quiescent atmosphere. Two reactions (pyrolysis and char oxidation) were considered. The oxygen supply was considered uniform. Consequently, there was no need to consider gas species equations. The smolder velocity, which is an eigenvalue of the problem, was determined by a trial and error numerical integration.

A fairly complete mathematical formulation of the smoldering combustion of a porous solid comprised of spherical particles was presented by Ohlemiller [1]. Packed bed correlations were used to describe heat and mass transfer between the particles and the bulk gas. Because the particle pores are small, the motion of the gas within the

pores is independent of the motion of the gas outside the pores. Mixing in the bulk gas phase is assumed to be vigorous enough so that the properties of the gas phase are uniform over distances comparable to the size of a typical particle. Consequently, the temperature and species concentration profiles in the particles are spherically symmetric. Since energy and species equations must be solved for each particle present, the primary use of this model is to elucidate the physics of smoldering combustion. There is virtually no hope of obtaining solutions to these equations.

Ohlemiller also presented a set of equations governing smolder propagation for cases in which distances characteristic of changes in temperature and species concentration are much larger than the diameter of a typical particle. The solid and the gas within the pores can be treated as one component and the gas outside the pores as the other component. The formulation consists of two energy equations, one equation for each solid phase species, two equations for each gas phase species and a momentum equation.

1.3 THE PRESENT CONTRIBUTION

Activation energy asymptotics are used to study forced cocurrent smoldering combustion in Chapter 2. It is assumed that the propagation of the smolder wave is one-dimensional and steady in a frame of reference moving with the reaction zone. Smoldering is represented using a finite-rate, one-

step reaction. A non-oxidative pyrolysis reaction can be included in the analysis. However, for steady smolder, the presence of such a reaction will have only a small effect on the temperature profiles. The dimensionless equations are very similar to those governing the propagation of a laminar premixed flame. A straightforward extension of premixed flame analyses [2,33] yields an expression for a dimensionless eigenvalue, Λ, thus providing a relationship between the initial oxygen mass flux, $\dot{m}''_{oi} = Y_{oi} \phi \rho_{gi} u_i$, and the final temperature, T_f. A global energy balance then determines the smolder velocity, v. Theoretical predictions are compared with the experimental findings of Rogers and Ohlemiller [21] and with the calculations of Ohlemiller et al [20].

A model of unsteady countercurrent smoldering combustion propagation is developed in Chapter 3. Smoldering combustion is represented using a two-step mechanism consisting of a pyrolysis reaction followed by a char oxidation reaction. A "flame" sheet approximation is used to model the oxidation reaction zone and it is assumed pyrolysis occurs at a known temperature, T_p. Because the two reaction fronts move at different velocities, countercurrent smolder propagation is unsteady. Two cases are considered: (1) no ash residue ; and (2) an ash layer building below the smolder wave. The residual ash serves as insulation, leading to much higher peak temperatures. The range of validity of the solutions is identified and explicit expressions are

derived for the char oxidation velocity, v, the pyrolysis front velocity, v_p, and the maximum temperature, T_m, in the limit of long time. Predictions are compared with measurements by Ohlemiller and Lucca [19].

In Chapter 4, the effect of buoyancy on cocurrent smoldering combustion is investigated both experimentally and theoretically. Buoyant forces, which are proportional to the product, $g(\rho_{gi}-\rho_g)$, can be controlled experimentally by varying either the gravitational acceleration, g, or the density difference, $\rho_{gi}-\rho_g$. The latter approach is followed in the work presented here. By changing the ambient pressure, the density of the gas and consequently, the buoyancy force, is varied. The rate of smolder spread through a packing of alpha-cellulose is measured for air pressures ranging from 0.5 to 1.2 atmospheres.

A model of cocurrent smoldering combustion under free flow conditions is also presented in Chapter 4. In one dimension, the gas velocity is determined from the conservation of mass - as a function of the inlet gas velocity, u_i. Since the pressure varies by a small amount over distances comparable the thickness of the smolder wave [1], the transport equations can be solved before considering the momentum equation. Explicit expressions for the smolder velocity, v, and the final temperature, T_f, are derived by using activation energy asymptotics. Both eigenvalues, v and T_f, are functions of u_i. The quantity, u_i, is then estimated by using an integral momentum

analysis. The smolder velocity is found to increase as the ambient pressure was increased. Good agreement between predictions and experiments is observed.

A series of ground based experiments designed to test the predictions of the present models are proposed in Chapter 5. Possible comparisons between measurements and the theory are discussed. It is anticipated that these comparisons will establish the range of validity of key assumptions in the analyses (such as the one-dimensional propagation approximation) and will hopefully lead to improvements in the current theory.

CHAPTER 2

FORCED COCURRENT SMOLDERING COMBUSTION

2.1 INTRODUCTION

A schematic of the problem under consideration is shown
in Fig. 2-1. A gaseous oxidizer with an initial oxygen
concentration, Y_{oi}, an inlet velocity, u_i, and an initial
temperature, T_i, flows upwards through a porous combustible
solid with void volume fraction ϕ . The solid and gas
fractions have initial densities, ρ_{si} and ρ_{gi}, respectively.
Buoyancy is included and shown to be negligible in the
proposed application of a smoldering combustion experiment
for use on the Space Shuttle. A planar ignition source is
used to initiate smoldering at the top of the solid. The
smolder wave propagates downward opposing the upward flow of
oxidizer. Because the oxidizer and the fuel enter the
reaction zone from the same direction, this configuration is
often referred to as cocurrent or premixed-flame-like. While
all of the oxygen is consumed in the reaction zone, a
considerable amount of solid remains [1]. Energy released in
the reaction zone is transferred upstream by conduction and
radiation, providing the energy required to preheat the
solid and the gas.

Smoldering combustion in the cocurrent configuration
has been investigated experimentally using polyurethane foam
[9], cellulosic insulation [19] and alpha-cellulose [23], as

REGION I: RESIDUAL CHAR AND
GASEOUS PRODUCTS

X

REGION II: REACTION ZONE

g

V   (SOLID VELOCITY)

U_i+V   (GAS VELOCITY)
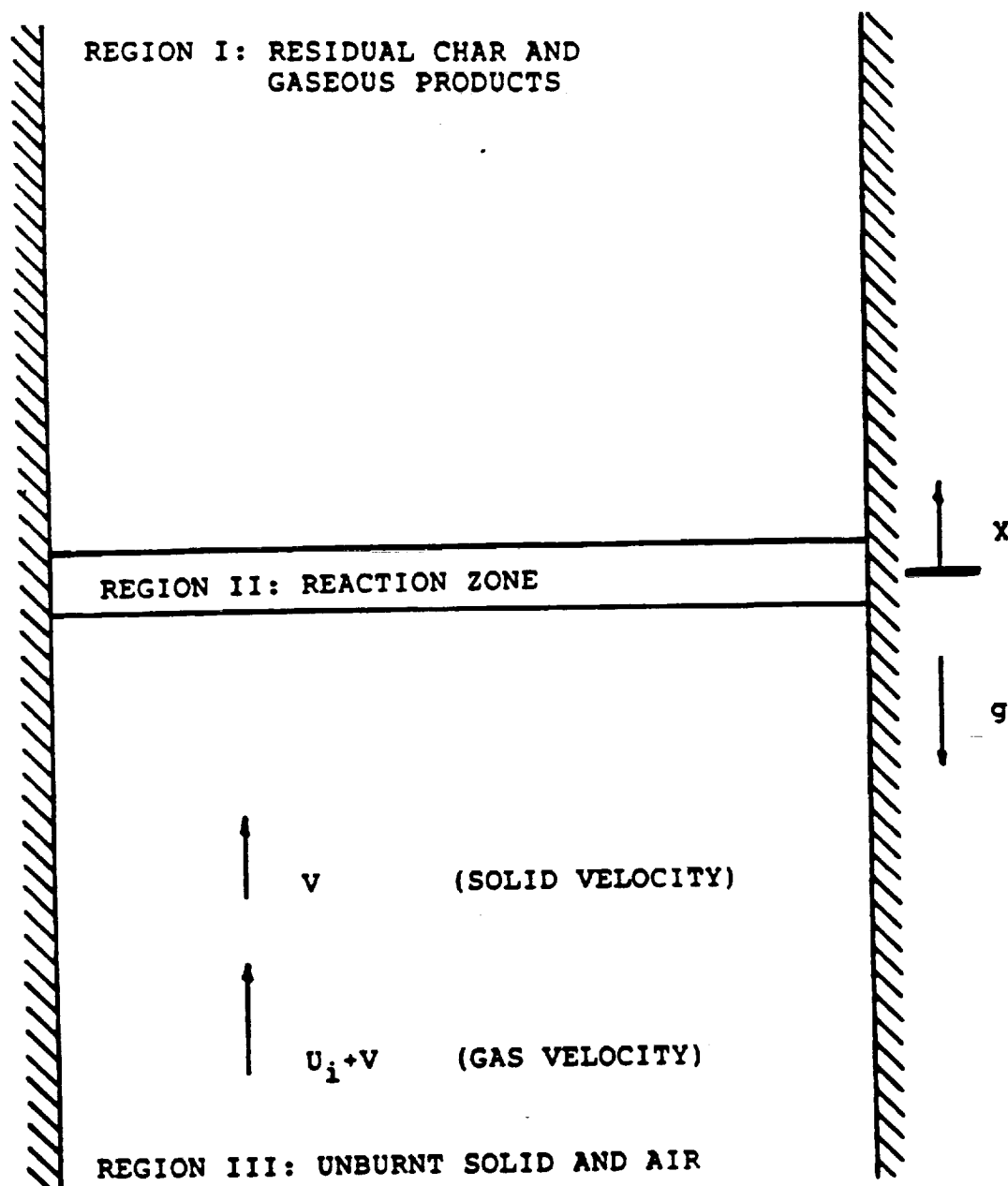
REGION III: UNBURNT SOLID AND AIR

FIG. 2-1: Cocurrent smoldering combustion viewed in a frame
of reference moving with the smolder wave.

fuels. The present study is intended to compliment the
earlier work of Ohlemiller et al [20], who developed a large
computer code to investigate unsteady, one-dimensional,
cocurrent smolder propagation in flexible polyurethane
foams. Because their method required expensive finite-
element calculations, Ohlemiller et al concluded that a
primary use of their model was to study the initiation of
smoldering combustion.

A primary goal of this study is to use activation
energy asymptotics to conduct a parametric investigation of
cocurrent smoldering combustion. The dimensionless equations
are very similar to those governing the propagation of a
laminar premixed flame. A straightforward extension of the
premixed flame analysis presented by Williams [2] yields an
expression for a dimensionless eigenvalue, Λ, providing a
relationship between the initial oxygen mass flux, $\dot{m}''_{oi} =$
$\phi Y_{oi} \rho_{gi} u_i$, and the final temperature, T_f. The smolder
velocity, v, is then determined by balancing the energy
released in the oxidation zone with the energy required to
preheat the solid and the gas from T_i to T_f. Both v and T_f
are highly dependent on $\dot{m}''_{oi}$. This is due to the oxygen
limited nature of cocurrent smoldering combustion. That is,
all of the incoming oxygen is usually consumed and the total
energy available is proportional to $\dot{m}''_{oi}$. Theoretical pre-
dictions are compared with the experimental findings of
Rogers and Ohlemiller [9] and with the calculations of
Ohlemiller et al [20]. The influence of buoyancy is

TABLE 2-I: Typical smolder characteristics.

Quantity of Interest	Magnitude[a]
smolder velocity, v	$\mathcal{O}(0.01$ cm/sec$)$
initial gas velocity, u_i	$\mathcal{O}(0.1$ cm/sec$)$
peak temperature, T_f	350-500 C
smolder wave thickness	2-3 cm
inverse equivalence ratio, r_{eq}	$\mathcal{O}(0.03)$
solid mass flux, $\dot{m}_{si}''$	$\mathcal{O}(0.0004$ gm/cm^{2}s$)$
gas mass flux, $\dot{m}_{gi}''$	$\mathcal{O}(0.0001$ gm/cm^{2}s$)$
solid mass fraction, ϵ_s	$\mathcal{O}(0.8)$
gass mass fraction, ϵ_g	$\mathcal{O}(0.2)$

a. Order of magnitude estimates given in refs.[9,20].

500 μ m
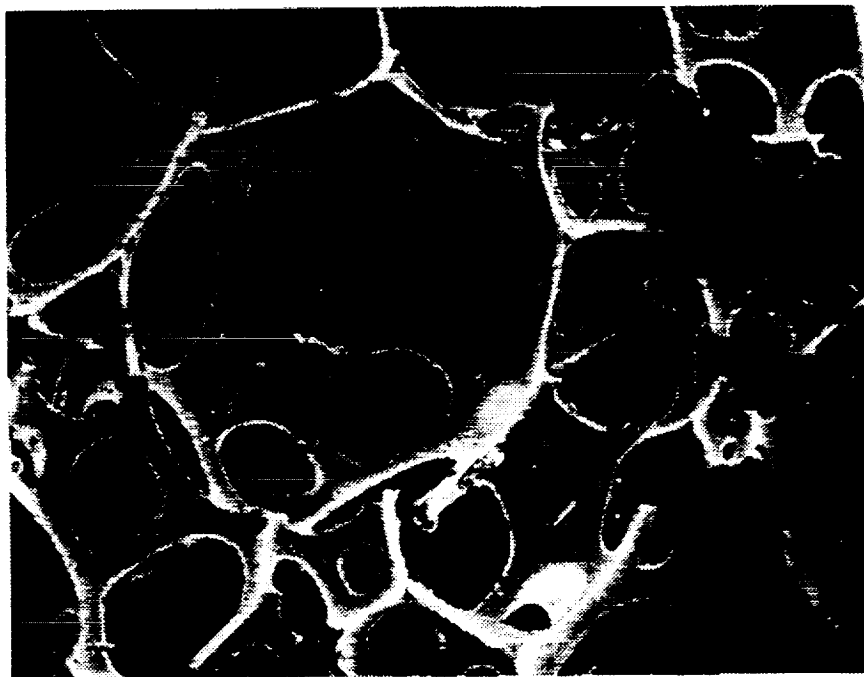
FIG. 2-2a: Electron microscope photograph of a GM-25
polyurethane foam.

100 μm

FIG. 2-2b: Electron microscope photograph of an alpha-cellulose fuel bed.

discussed in section 2.5.
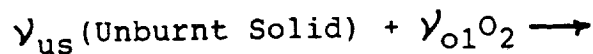
2.2 ANALYSIS

2.2.1 Assumptions

Typical values of several key smolder characteristics, including the smolder velocity, v, and the peak temperature, T_f, are given in given in Table 2-I. Electron microscope photographs of two solid fuels, a GM-25 polyurethane foam and a packed bed of alpha-cellulose, are shown in Figs. 2-2A and 2-2B, respectively. Both of these materials have been used in recent experimental investigations [9,20,21,28,29] of smoldering combustion. The polyurethane foam is composed of large contiguous bubbles whose diameters are on the order of several hundred microns. On the other hand, the alpha-cellulose is formed by interlaced fibers, roughly one-hundred microns long and ten microns in diameter.

Many fuels of interest are very porous, and consequently, conduction is a relatively poor mode of heat transfer [19]. Thus, radiation heat transfer is often important despite the relatively low temperatures encountered in smoldering combustion - peak temperatures are usually between 350 and 500°C [20]. While radiation is important in polyurethane foams, it is approximately negligible in tightly packed beds of alpha-cellulose. In the following analysis, a diffusion approximation is utilized to model radiation heat transfer. That is, the radiation heat flux is incorporated using a temperature dependent conductivity [34-36].
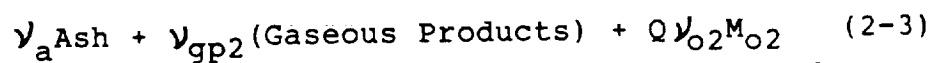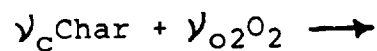
Smoldering combustion is represented by a finite rate, one-step reaction,

$$\gamma_{us}(\text{Unburnt Solid}) + \gamma_o O_2 \longrightarrow$$

$$\gamma_a \text{Ash} + \gamma_{gp}(\text{Gaseous Products}) + Q\gamma_o M_o \quad . \quad (2\text{-}1)$$
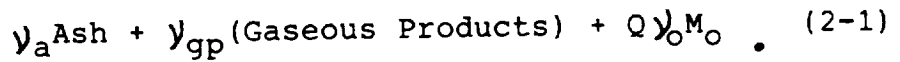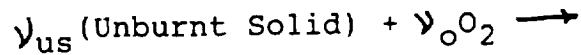
Reaction mechanisms for alpa-cellulose, GM-25 polyurethane foam, wood dust and cellulosic insulation are discussed in Appendix A. Ohlemiller and Lucca [19] reported that a one-step oxidation reaction adequately describes the cocurrent smoldering of cellulosic insulation materials. Ohlemiller et al [20] modelled the smoldering combustion of a polyurethane foam by utilizing two global reactions,
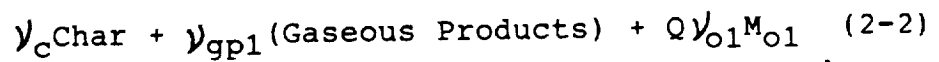
$$\gamma_{us}(\text{Unburnt Solid}) + \gamma_{o1} O_2 \longrightarrow$$

$$\gamma_c \text{Char} + \gamma_{gp1}(\text{Gaseous Products}) + Q\gamma_{o1} M_{o1} \quad (2\text{-}2)$$

and

$$\gamma_c \text{Char} + \gamma_{o2} O_2 \longrightarrow$$

$$\gamma_a \text{Ash} + \gamma_{gp2}(\text{Gaseous Products}) + Q\gamma_{o2} M_{o2} \quad (2\text{-}3)$$

However, since the second reaction (oxidation) was much faster than the first reaction (pyrolysis), their two step reaction mechanism can be well approximated by Eq.(2-1). The following asymptotic analysis can be modified to include a non-oxidative pyrolysis reaction. Because the amount of energy consumed by pyrolysis is much smaller than the amount released in the reaction zone, for steady smolder, the

presence of such a reaction will have a small effect on the temperature profiles.

Additionally, the solid phase is considered continuous with a constant void volume fraction. Propagation of the smolder wave is assumed to be one-dimensional and steady in a frame of reference moving with the smolder wave. Fick's Law is used to model the diffusion of oxygen. The gas and the solid are presumed to be in local thermal equilibrium. A criterion for checking the validity of this equilibrium approximation is derived in Appendix B. Energy transport due to concentration gradients, energy dissipated by viscosity, work done by body forces and the kinetic energy of the gas phase have been ignored. Because the mass diffusivity of oxygen in air, D, increases with temperature and decreases with pressure [37], the quantity, $\rho_g D$, is taken to be constant. It is also assumed that properties, such as the gas phase thermal conductivity, k_g, the solid phase thermal conductivity, k_s, the gas phase specific heat, c_g, and the solid phase specific heat, c_s, remain constant.

2.2.2 Governing Equations

Equations governing heat and mass transfer in a porous medium are derived in Appendix C. In a frame of reference moving with the smolder wave, $\dot{m}_s'' = (1-\phi)\rho_s v$. Since the smolder velocity is usually at least an order of magnitude smaller than the gas phase velocity [9,19,20], $\dot{m}_g'' \sim \phi \rho_g u$. This assumption allows $\dot{m}_{oi}''$ to be treated as a known quantity. The conservation of mass requires that $\dot{m}''$ ($= \dot{m}_s'' + \dot{m}_g''$)

remain constant. Mass flux fractions are defined by:

$$\epsilon_{s,g} = \frac{\dot{m}''_{s,g}}{\dot{m}''} , \qquad (2\text{-}4)$$

$$\epsilon_{us} = Y_{us}\frac{\dot{m}''_s}{\dot{m}''} , \qquad (2\text{-}5)$$

$$\epsilon_o = \frac{1}{\dot{m}''}\left[\phi Y_o \rho_g u - \phi \rho_g D \frac{dY_o}{dx}\right] . \qquad (2\text{-}6)$$

Symbols are defined in the nomenclature. Equation (2-1) gives

$$\frac{1}{\nu_{us}M_{us}}\frac{d\epsilon_{us}}{dx} = \frac{1}{\nu_o M_o}\frac{d\epsilon_o}{dx} = \frac{1}{(\nu_{us}M_{us}-\nu_a M_o)}\frac{d\epsilon_s}{dx} = \frac{-1}{(\nu_{gp}M_{gp}-\nu_o M_o)}\frac{d\epsilon_g}{dx} . \qquad (2\text{-}7)$$

Species conservation for oxygen requires

$$\frac{d\epsilon_o}{dx} = -\frac{\nu_o M_o}{\dot{m}''}\dot{r}''' , \qquad (2\text{-}8)$$

and integrating the conservation of energy gives

$$\dot{m}''C_{eff}(T-T_i) - (k_{eff}+k_{rad})\frac{dT}{dx} = Q\dot{m}''(\epsilon_{oi}-\epsilon_o) , \qquad (2\text{-}9)$$

where Eq.(2-8) has been used to eliminate the reaction rate from Eq.(2-9). The effective thermal conductivity, $k_{eff}= \phi k_g+(1-\phi)k_s$, accounts for heat transfer due to conduction in both gas and solid phases. Radiation heat transfer is incorporated using a temperature dependent conductivity,

TABLE 2-II: Typical properties of a polyurethane foam and a packed bed of alpha-cellulose.

	polyurethane[a]	alpha-cellulose[c]
ϕ	0.97	0.90
ρ_{si} [kg/m^3]	1150	620
c_s [kJ/(kg K)]	1.7	0.84
k_{eff} [W/m K]	0.047	0.050
$k_{rad}(T_i)$ [W/m K]	0.005	0
E [kJ/mole]	155 (140)[b]	180
Q [kJ/kg]	12,300 (7,600)	12,500
Z	$10^{10} m^3/kg\ s$	$3 \times 10^6 m^{1.5}/kg^{0.5}K^{0.5}s$
a	1	0.5
b	1	1
c	0	0.5
$\dfrac{\nu_{gp}M_{gp}}{\nu_o M_o}$	3.7	1.4

a. Properties given in refs. [20,39]. The value given by Ohlemiller et al [20] is shown in parenthesis whenever it differs from the value listed above.

b. Shown in the parenthesis is the activation energy for the first reaction in the two-step model in ref. [20].

c. Properties given in refs. [21,28,40].

$k_{rad}=16\sigma\ell_r T^3/3$. For simplicity, it is assumed that an effective heat capacity, $c_{eff}=\epsilon_s c_s + \epsilon_g c_g$, remains constant.

The reaction rate, $\dot{r}'''$, is assumed to depend on the oxygen mass fraction, the solid fuel present and the temperature in an Arrhenius form,

$$\dot{r}''' = Z\left(Y_o \rho_g\right)^a \left(Y_{us}\rho_s\right)^b T^c\, e^{-E/RT}, \qquad (2\text{-}10)$$

where a, b and c are arbitrary constants. The oxygen mass fraction is determined from the definition of the oxygen mass flux, Eq. (2-6). The conservation of momentum, which is discussed in the appendix, and an equation of state, $P=\rho_g RT$, complete the preceding set of equations. Because the pressure varies by a small amount [1], the transport equations can be solved before considering the momentum equation. Properties of a polyurethane foam and a packing of alpha-cellulose are given in Table 2-II.

The following boundary conditions are imposed on Eqs. (2-6,2-8,2-9):

$$\text{as}\quad x \rightarrow -\infty \qquad \epsilon_o \rightarrow \epsilon_{oi} \qquad\qquad (2\text{-}11)$$

$$\text{as}\quad x \rightarrow +\infty \quad \begin{cases} \epsilon_o \rightarrow 0 \\ Y_o \rightarrow 0 \\ T \rightarrow T_f \end{cases} \qquad (2\text{-}12)$$

Two boundary conditions are imposed on Eq. (2-6). The second

TABLE 2-III: Dimensionless parameters governing forced cocurrent smoldering combustion. In addition to the following parameters, r_{eq}, a, b, and c must be specified.

$$D_c = \frac{Q Y_{oi}}{C_{eff} T_i}$$

Dimensionless measure of the energy released in the reaction zone (varies from 0 to 40)

$$L_e = \frac{k_{eff} T_i}{\phi \, \rho_g D Q Y_{oi}}$$

Modified Lewis number (varies from 0.05 to infinity)

$$N_R = \frac{16 \, \sigma \, \ell_r T_i^3}{3 \, K_{eff}}$$

Dimensionless radiation conductivity (usually less than 0.1)

$$P_g = \left(\frac{\nu_{gp} M_{gp}}{\nu_o M_o} - 1 \right) Y_{oi}$$

Measures the amount of gas produced in the reaction zone (varies between 0.1 and 1.0)

$$\beta' = \frac{E}{R T_i}$$

Dimensionless activation energy (varies between 50 and 70)

$$\tilde{\Lambda} = \frac{\nu_o M_o Z (R K_{eff})^{1+a} \rho_{si}^b T_i^{2a+cr^2} \Gamma(1+a)}{\dot{m}_{oi}''^2 (F Q)^{1+a} (\phi D_i)^a}$$

Dimensionless pre-exponential factor (usually lies between 10^8 and 10^{10})

boundary condition, which requires that all of the incoming oxygen be consumed, will determine T_f. Setting $T=T_f$, $\epsilon_o=0$ and $dT/dx=0$ in Eq.(2-9) gives

$$V = \frac{Q \dot{m}_{oi}''}{(1-\phi)\rho_{si}c_{eff}(T_f-T_i)} - \frac{\phi \rho_{gi} u_i}{(1-\phi)\rho_{si}}$$

(2-13)

After solving for T_f, Eq.(2-13) will determine v.

2.2.3 Dimensionless Governing Equations

A characteristic distance, $x_c = k_{eff}/\dot{m}''c_{eff}$, is chosen by balancing convection and diffusion in the energy equation, thus eliminating one dimensionless parameter. Typically, $k_{eff} \sim 0.05$ W/m K, $\dot{m}'' \sim 0.005$ kg/m^{2}s, and $c_{eff} \sim 1$ kJ/kg K, giving $x_c \sim 0.01$ m. Because the definition of x_c does not account for radiation, x_c is somewhat smaller than the smolder wave thickness given in Table 2-I. Since all of the oxygen is consumed, the oxygen mass flux and the oxygen mass fraction are normalized by their initial values. A dimensionless temperature is defined by $\bar{T} = (T-T_i)/T_c$. Setting $T_c = T_i$ eliminates the parameter, T_c/T_i, which arises from the nonlinear terms in the governing equations. This choice for T_c also makes $\bar{T}$ an O(1) quantity - see Table 2-I.

The dimensionless parameters governing cocurrent smoldering are listed in Table III. Parameter ranges given in Table 2-III were estimated from the properties tabulated in Table 2-II. Note that the asymptotic analysis is only valid when the Zeldovich number, $\beta = \beta' \bar{T}_f/(1+\bar{T}_f)^2$, is large ($\beta > 10$) [2], roughly corresponding to $\beta' > 50$. The

dimensionless radiation conductivity, N_R, is artificially low because it is based on T_i rather than T_f. A critical value of the dimensionless heat release, D_c, below which steady solutions cease to exist, will be identified.

Dividing Eqs. (2-6 and 2-8) by Eq. (2-9) eliminates the spatial coordinate, $\bar{x}$. In terms of the new coordinate, $\bar{T}$, the governing equations are

$$\frac{\bar{T} - \bar{T}_f(1-\bar{\varepsilon}_0)}{1 + N_R(1+\bar{T})^3} \frac{d\bar{\varepsilon}_0}{d\bar{T}} = -\omega \; , \tag{2-14}$$

and

$$\frac{\bar{T} - \bar{T}_f(1-\bar{\varepsilon}_0)}{Le\,\bar{T}_f\left[1 + N_R(1+\bar{T})^3\right]} \frac{d\bar{Y}_0}{d\bar{T}} = \left[1 + P_g(1-\bar{\varepsilon}_0)\right]\bar{Y}_0 - \bar{\varepsilon}_0 \; . \tag{2-15}$$

The dimensionless reaction rate is given by

$$\omega = \Lambda\,\bar{Y}_0^{\,a}\left[1 - r_{eq}(1-\bar{\varepsilon}_0)\right]^b (\bar{T}+1)^{c-a} \exp\left\{-\frac{\beta'(\bar{T}_f-\bar{T})}{(\bar{T}+1)(\bar{T}_f+1)}\right\} , \tag{2-16}$$

where

$$\Lambda = \frac{\tilde{\Lambda}\,\beta'^{\,1+a}\,\bar{T}_f}{Le^a\,\Gamma(1+a)} \exp\left\{-\frac{\beta'}{1+\bar{T}_f}\right\} . \tag{2-17}$$

In terms of $\bar{T}$, the boundary conditions are:

as $\bar{T} \to 0 \;\; (\bar{x} \to -\infty)$ $\bar{\varepsilon}_0 \to 1$ $\qquad$ (2-18)

as $\bar{T} \to \bar{T}_f \;\; (\bar{x} \to +\infty)$ $\qquad \begin{cases} \bar{\varepsilon}_0 \to 0 \\ \bar{Y}_0 \to 0 \end{cases}$ $\qquad$ (2-19)

After solving Eqs. (2-14 and 2-15), the spatial coordinate,

$\bar{x}(\bar{T})$, is determined by

$$\frac{1 + N_R(1+\bar{T})^3}{\bar{T} - \bar{T}_f(1-\mathcal{E}_0)} \frac{d\bar{T}}{d\bar{x}} = 1 \quad .$$

(2-20)

Eq.(2-13) gives a relationship between a dimensionless smolder velocity, $\bar{V}=v/v_c$, and the dimensionless final temperature, $\bar{T}_f=(T_f-T_i)/T_i$,

$$\bar{V} = \frac{1}{\bar{T}_f} - \frac{1}{\mathcal{D}_c} \quad ,$$

(2-21)

where a characteristic smolder velocity,

$$v_c = \frac{Q\,\dot{m}''_{oi}}{(1-\emptyset)\rho_{si}C_{eff}T_i} \quad ,$$

(2-22)

is chosen by balancing the energy released in the reaction zone and the energy required to preheat the solid, thus eliminating one parameter from the above equation.

2.3 ACTIVATION ENERGY ASYMPTOTICS

Typical values of the Zeldovich number, β, encountered in smoldering combustion are fairly large. From the argument of the exponential in Eq.(2-16), the reaction rate is significant only when $1- \beta^{-1} \lesssim \bar{T}/\bar{T}_f \leq 1$, corresponding to the (inner) Region II in Fig.1. The outer region consists of the point $\bar{T}= \bar{T}_f$, Region I in Fig.1, and Region III in Fig.1, $0 \leq \bar{T}/\bar{T}_f \lesssim 1- \beta^{-1}$. In the outer regions, the reaction rate is negligible and diffusion is balanced by convection. Because

the inner region is very thin, diffusion dominates convection, and consequently, the source terms in the governing equations are balanced by diffusion.

In Region III, $\omega \sim 0$ and Eq.(2-14) yields $\overline{\epsilon}_0 = 1$. Substituting $\overline{\epsilon}_0 = 1$ into Eq.(2-15) and integrating once gives

$$\overline{Y}_0 = 1 - \exp\left[-Le\overline{T}_f \int_{\overline{T}}^{\overline{T}_f} \frac{1}{\eta}\left[1 + N_R(1+\eta)^3\right] d\eta\right]. \tag{2-23}$$

For $N_R = 0$, Eq.(2-23) gives $\overline{Y}_0 = 1 - \overline{T}^{Le}$. Note that the integral in Eq.(2-23) diverges as $\overline{T} \to 0$. Therefore, $\overline{Y}_0 \to 1$ as $\overline{T} \to 0$. A stretched variable is defined, $\zeta = \beta(1 - \overline{T}/\overline{T}_f)$. Expanding $\overline{Y}_0$ and $\overline{\epsilon}_0$ in terms of $1/\beta$ gives

$$\overline{Y}_0 = \left(\frac{1}{\beta}\right)\overline{Y}_0^1 + \Theta\left(\frac{1}{\beta^2}\right), \tag{2-24}$$

and

$$\overline{\epsilon}_0 = \overline{\epsilon}_0^0 + \Theta\left(\frac{1}{\beta}\right). \tag{2-25}$$

Matching conditions are:

$$\text{as } \zeta \to +\infty \quad \overline{\epsilon}_0^0 \to 1 \tag{2-26}$$

$$\text{as } \zeta \to 0 \quad \begin{cases} \overline{\epsilon}_0^0 \to 0 \\ \overline{Y}_0 \to 0 \end{cases} \tag{2-27}$$

In the inner region, Eqs.(2-14,2-15,2-16,2-17) yield (to leading order)

$$\frac{\overline{\epsilon}_0^0}{1 + N_R(1+\overline{T}_f)^3} \frac{d\overline{\epsilon}_0^0}{d\zeta} = \frac{\Lambda}{\beta^{1+\alpha}}\left[\overline{Y}_0^1\right]^\alpha \left[1 - r_{eq}(1-\overline{\epsilon}_0^0)\right]^b e^{-\zeta} \tag{2-28}$$

and
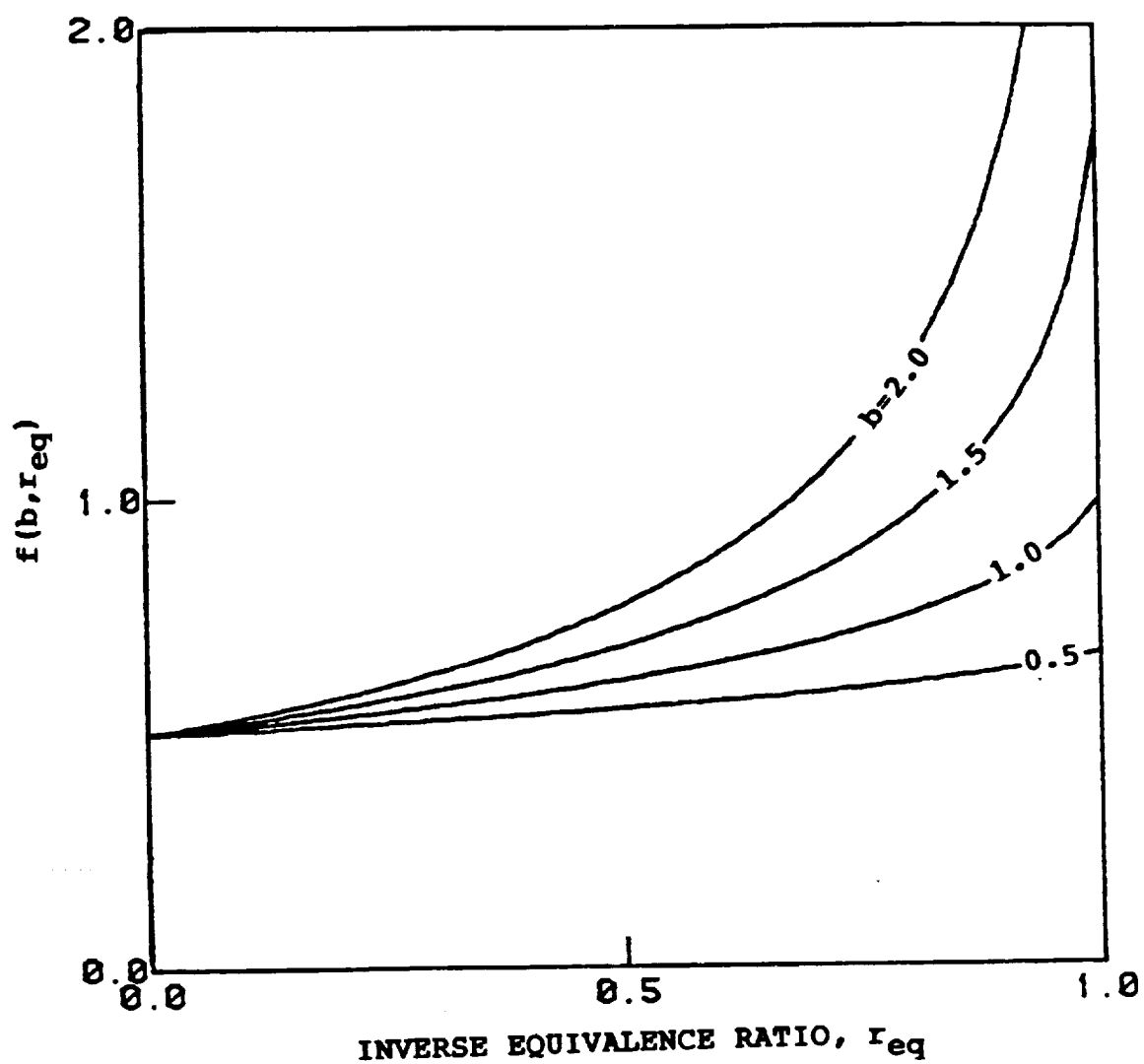
FIG. 2-3: The function $f(b, r_{eq})$ plotted versus the inverse equivalence ratio, r_{eq}, for various values of b.

$$\frac{d\overline{Y_o}}{d\xi} = Le \, \overline{T_f} \left[1 + N_R (1 + \overline{T_f})^3 \right].$$

(2-29)

Integrating Eq.(2-29), substituting the resulting expression into Eq.(2-28), applying the matching conditions and integrating once yields

$$\Lambda = \frac{\beta^{1+a} \, f(b, r_{eq})}{Le^a \, \overline{T_f}^a \left[1 + N_R (1 + \overline{T_f})^3 \right]^{1+a} \Gamma(1+a)} \, ,$$

(2-30)

where

$$f(b, r_{eq}) = \int_0^1 \frac{t \, dt}{\left[1 - r_{eq} (1 - t) \right]^b} \, .$$

(2-31)

Because the oxygen consumption of a typical smolder wave is only a few percent of that required for stoichiometeric burning, the inverse equivalence ratio, $r_{eq} = \nu_{us} M_{us} \epsilon_{oi} / \nu_o M_o \epsilon_{usi}$, is fairly small [19,20]. As shown in Fig. 2-3, $f(b, r_{eq}) \rightarrow 1/2$ in the limit $r_{eq} \rightarrow 0$.

2.4 GENERAL SOLUTION

2.4.1 Fields

Because all of the incoming oxygen is consumed in the reaction zone, the total heat release is proportional to the initial oxygen mass flux, $\dot{m}''_{oi}$. Both the smolder velocity, v, and the final temperature, T_f, are highly dependent on $\dot{m}''_{oi}$. Since $\overline{T}_f$ appears in Eqs.(2-14,2-15,2-16,2-20), varying $\dot{m}''_{oi}$ affects the dimensionless oxygen mass fraction, $\overline{Y}_o(\overline{T})$, the dimensionless oxygen mass flux, $\overline{\epsilon}_o(\overline{T})$, and the
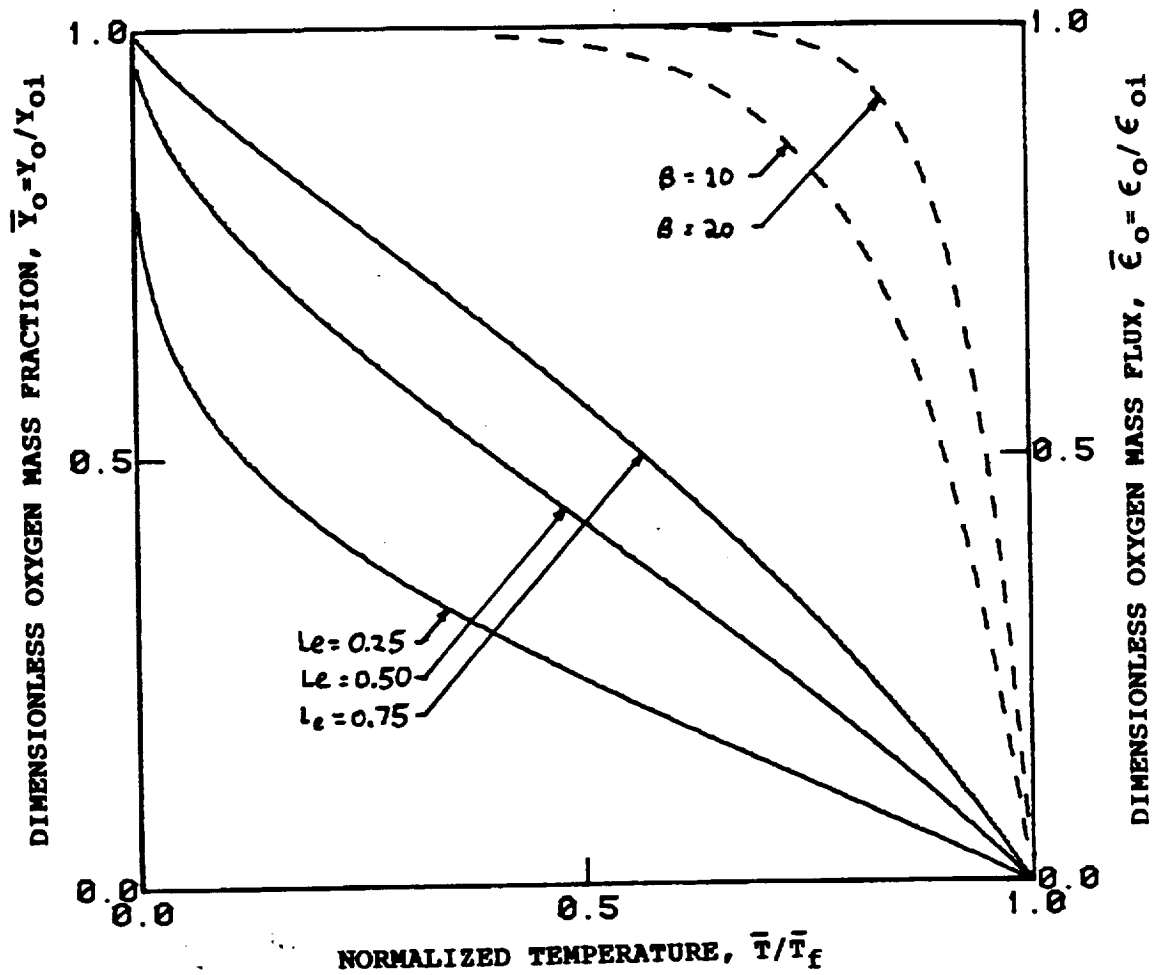
FIG. 2-4: Dimensionless oxygen mass fraction, $\overline{Y}_o = Y_o/Y_{oi}$, versus normalized temperature, $\overline{T}/\overline{T}_f$, with $N_R = 0.1$, $\beta' = 60$, $\widetilde{\mathcal{A}} = 10^{10}$, $a=1$, $c=0$ and $r_{eq} = 0$. Also plotted is the dimensionless oxygen mass flux, $\overline{\epsilon}_o = \epsilon_o/\epsilon_{oi}$, versus $\overline{T}/\overline{T}_f$, for $a=1$ and $r_{eq} = 0$. The dimensionless parameters are defined in Table 2-III.

dimensionless distance, $\overline{x}(\overline{T})$. These profiles depend on Le, N_R, r_{eq}, β', $\widetilde{\Lambda}$, a, b and c. Since r_{eq} is usually small, the various profiles are weakly dependent on r_{eq} and b. Results presented in the following discussion are for the limit $r_{eq} \to 0$, and consequently, the solutions are independent of both r_{eq} and b.

When $\overline{\epsilon}_o$ is plotted as a function of normalized temperature, $\overline{T}/\overline{T}_f$, the resulting curves depend on only two parameters, the Zeldovich number, $\beta = \beta' \overline{T}_f / (1 + \overline{T}_f)^2$, and the constant, a. As evidenced by Fig. 2-4, the incoming oxygen is consumed in a narrower region as β is increased. Also plotted in Fig. 2-4 is $\overline{Y}_o$ versus $\overline{T}/\overline{T}_f$, parameterized in Le, for $N_R= 0.1$, $\widetilde{\Lambda} = 10^{10}$, a=1 and c=0. The modified Lewis number, Le, measures the thermal thickness relative to oxygen diffusion thickness. The preceding analysis only valid when the diffusion thickness is much larger than the thickness of the reaction zone, roughly corresponding to Le $<< \beta$. When Le $\sim \beta$, the dimensionless oxygen mass fraction is O(1) in the reaction zone and smoldering is kinetically controlled [38]. For polyurethane, with $u_i=0.2$ cm/s and $P_a=1$ atm, the criterion for diffusion controlled smoldering is $Y_{oi}>>0.02$. For a packed bed of alpha-cellulose, the criterion is $Y_{oi}>>0.01$.

After ascertaining the dependence of $\overline{\epsilon}_o$ on $\overline{T}$, Eq.(2-20) is utilized to determine $\overline{T}$ as a function of the dimensionless distance, $\overline{x}$. Typical temperature profiles,
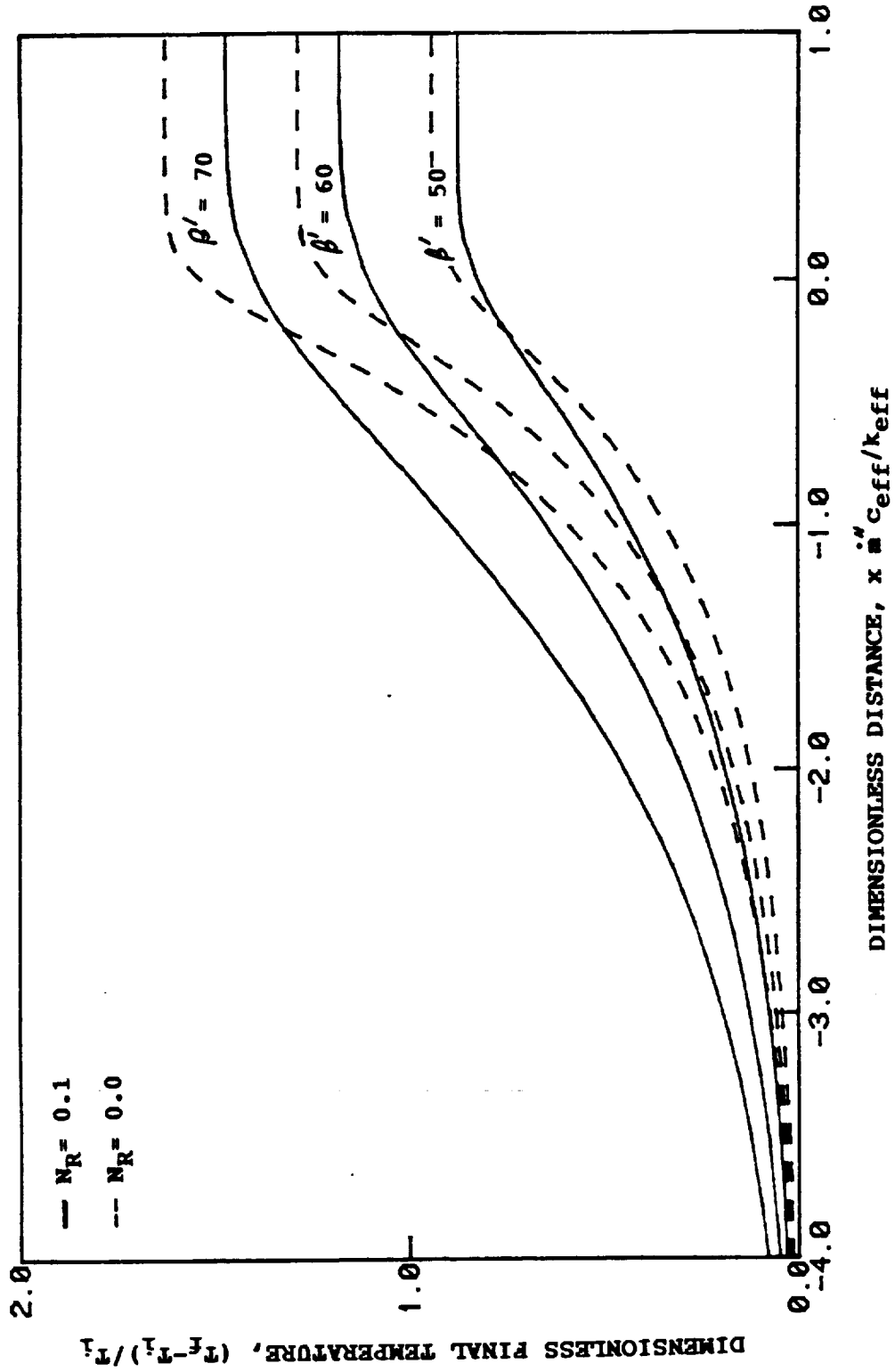
FIG. 2-5: Dimensionless temperature, $\bar{T}=(T-T_i)/T_i$, versus dimensionless distance, $\bar{x}=x\,\dot{m}''c_{eff}/k_{eff}$, with $\widehat{\Lambda}=10^{10}$, $a=1$, $c=0$, and $r_{eq}=0$.

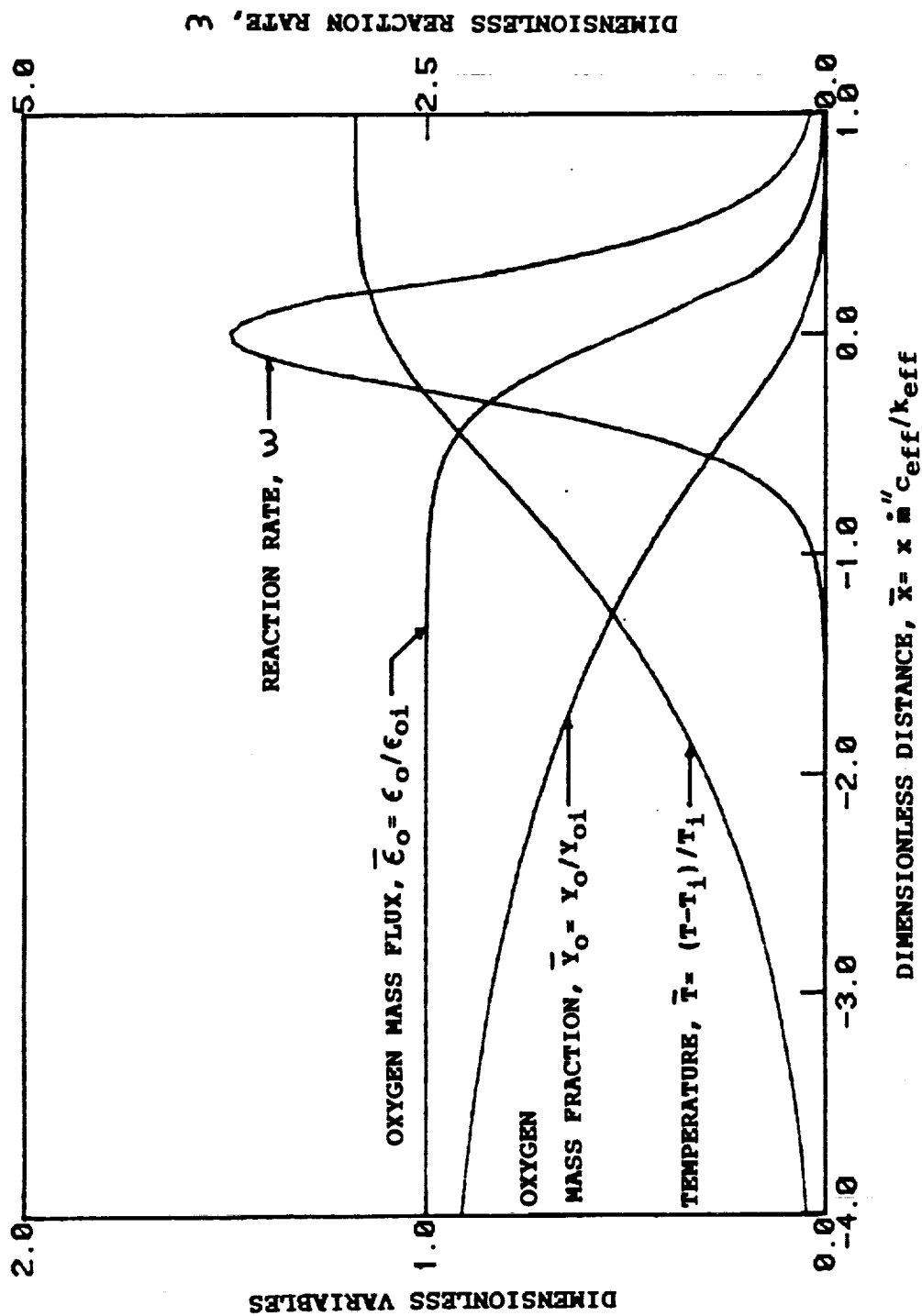FIG. 2-6: Dimensionless variables, $\bar{Y}_o$, $\bar{\epsilon}_o$, and $\bar{T}$, and the dimensionless reaction rate, ω, versus dimensionless distance, $\bar{x} = x \dot{m} c_{eff}''/k_{eff}$, with $\beta' = 60$, $\tilde{\Lambda} = 10^{10}$, $Le = 0.5$, $N_R = 0.1$, $r_{eq} = 0$, $a = 1$ and $c = 0$.

parameterized in N_R and β', for $\tilde{\Lambda} = 10^9$, a=1 and c=0, are shown in Fig. 2-5. Raising the dimensionless radiation conductivity, N_R, decreases the final temperature and increases the thermal thickness of smolder zone. On the other hand, increasing β leads to greater final temperatures. Note that $\bar{\epsilon}_o(\bar{x})$ and $\bar{Y}_o(\bar{x})$ can be constructed by combining Figs. 2-4 and 2-5. Results from such a calculation are shown in Fig. 2-6.

At this point in the analysis, quantities of secondary interest, such as the gas phase velocity, u_i, can be calculated. Integrating Eq.(2-7) and utilizing Eqs.(2-4,2-11) gives

$$\bar{u} = \left[1 + \bar{T}\right]\left[1 + P_g(1 - \bar{\epsilon}_o)\right], \qquad (2\text{-}32)$$

where a normalized gas velocity, $\bar{u} = u/u_i$, has been defined. Over most of the domain, $\bar{u}$ increases linearly with $\bar{T}$ due to gas phase expansion. However, as $\bar{T}$ approaches $\bar{T}_f$, $\bar{u}$ increases dramatically because of gas generation in the reaction zone. In the limit $r_{eq} \to 0$, $\bar{u}$ depends on four parameters, β', a, P_g, and $\bar{T}_f$. Setting $\bar{T} = \bar{T}_f$ and $\bar{\epsilon}_o = 0$, Eq.(2-32) yields

$$\bar{u}_f = \left[1 + \bar{T}_f\right]\left[1 + P_g\right], \qquad (2\text{-}33)$$

thus determining the final velocity, $\bar{u}_f$.
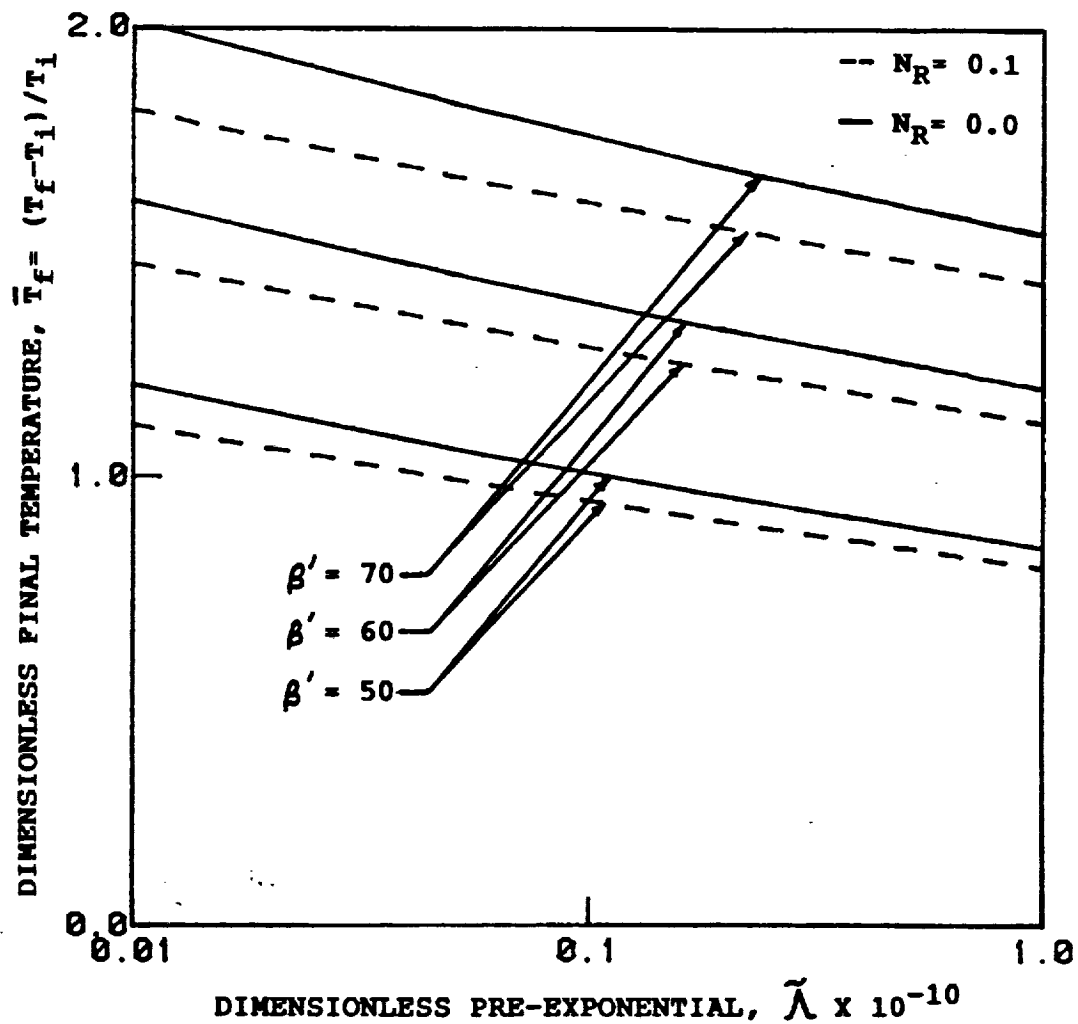
FIG. 2-7: Dimensionless final temperature, $\overline{T}_f = (T_f - T_i)/T_i$, versus the dimensionless pre-exponential factor, $\widetilde{\Lambda}$, with a=1, c=0, and $r_{eq}=0$.
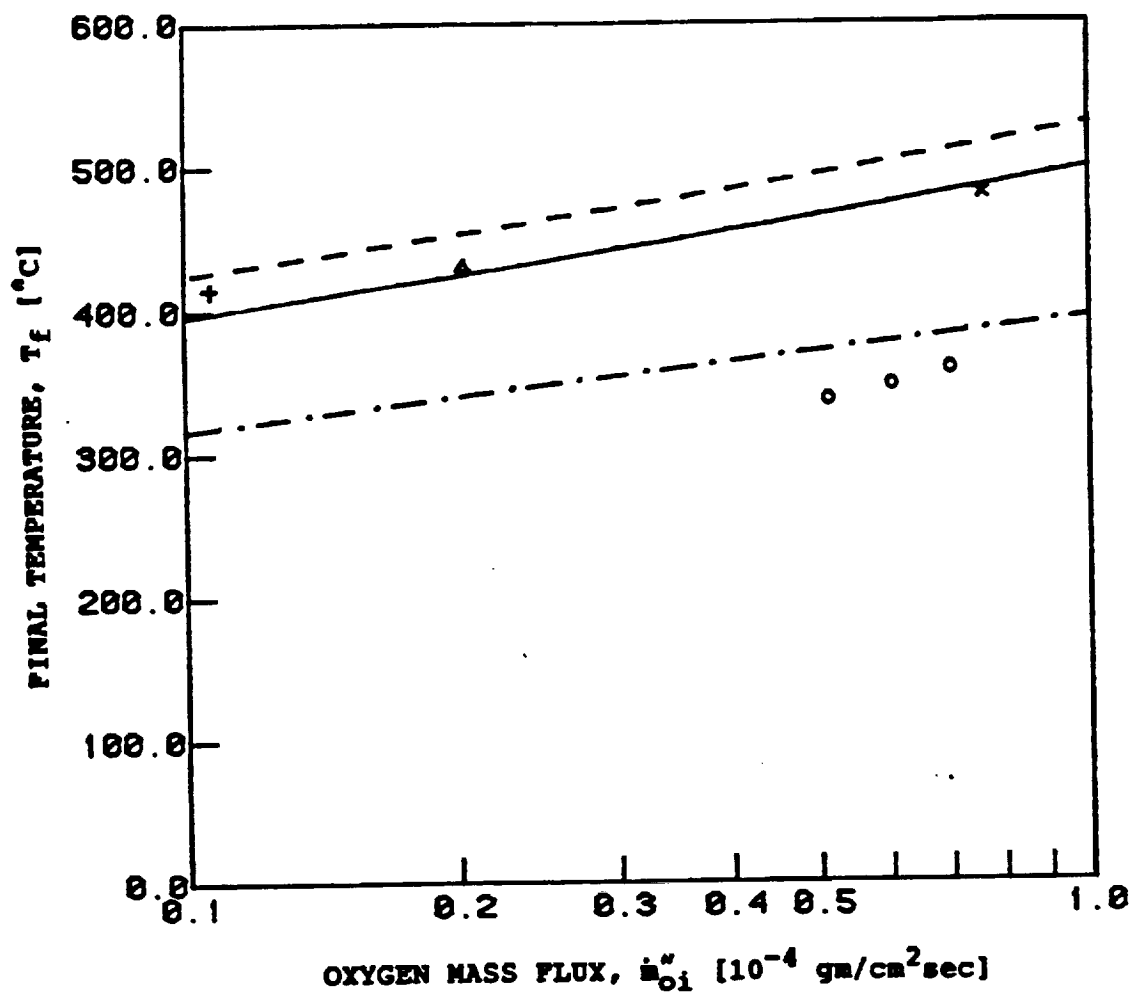
FIG. 2-8: Downstream temperatures in polyurethane predicted by the present analytic model, for the properties listed in Table 2-II (——) and those given by Ohlemiller et al (-•-), measured by Rogers and Ohlemiller and calculated by Ohlemiller et al (O). Measurements are for the following conditions: $u_i=0.04$ cm/s, $Y_{oi}=$ 0.23 (+) and $Y_{oi}=0.44$ (▲); $u_i=0.15$ cm/s, $Y_{oi}=0.44$ (x). Also shown in the figure are predictions for cellulose (-—).

2.4.2 Final Temperature and Smolder Velocity

A key result of this analysis is $\overline{T}_f(N_R, \beta', \widetilde{\Lambda}, a, c)$. In the limit $r_{eq} \to 0$, Eqs.(2-30 and 2-31) give

$$\widetilde{\Lambda}\left[1 + N_R(1 + \overline{T}_f)^3\right]^{1+a}(1 + \overline{T}_f)^{a+c+2} e^{-\beta'/(1+\overline{T}_f)} = \frac{1}{2} \quad . \qquad (2-34)$$

A plot of $\overline{T}_f = (T_f - T_i)/T_i$ versus $\widetilde{\Lambda}$, parameterized in the dimensionless activation energy, β', and the dimensionless radiation conductivity, N_R, for $a=1$ and $c=0$, is shown in Fig.2-7. As the reaction rate is increased, by either raising the pre-exponential, $\widetilde{\Lambda}$, or lowering the activation energy, β', $\overline{T}_f$ decreases and the smolder velocity, $\overline{v}$, which is inversely proportional to $\overline{T}_f$, increases. That is, the material burns faster when the reaction rate is higher.

For a given fuel, $\overline{T}_f$ decreases logarithmically with $\widetilde{\Lambda}$. Therefore, T_f increases logarithmically with the initial oxygen mass flux, $\dot{m}''_{oi}$, as shown in Fig. 2-8. Also indicated are measurements by Rogers and Ohlemiller [9] and calculations by Ohlemiller et al [20] for polyurethane. Ohlemiller et al attributed the discrepancy between their predictions and experiments to uncertainty in the base parameter set (see Table 2-II). When their parameters are used in this model, as shown by the dot dash line in Fig. 2-8, predicted values of $\overline{T}_f$ are close to those calculated by Ohlemiller et al. Results from this study indicate that the parameters in Table 2-II are a better choice, for they give much closer agreement between predictions (solid line) and
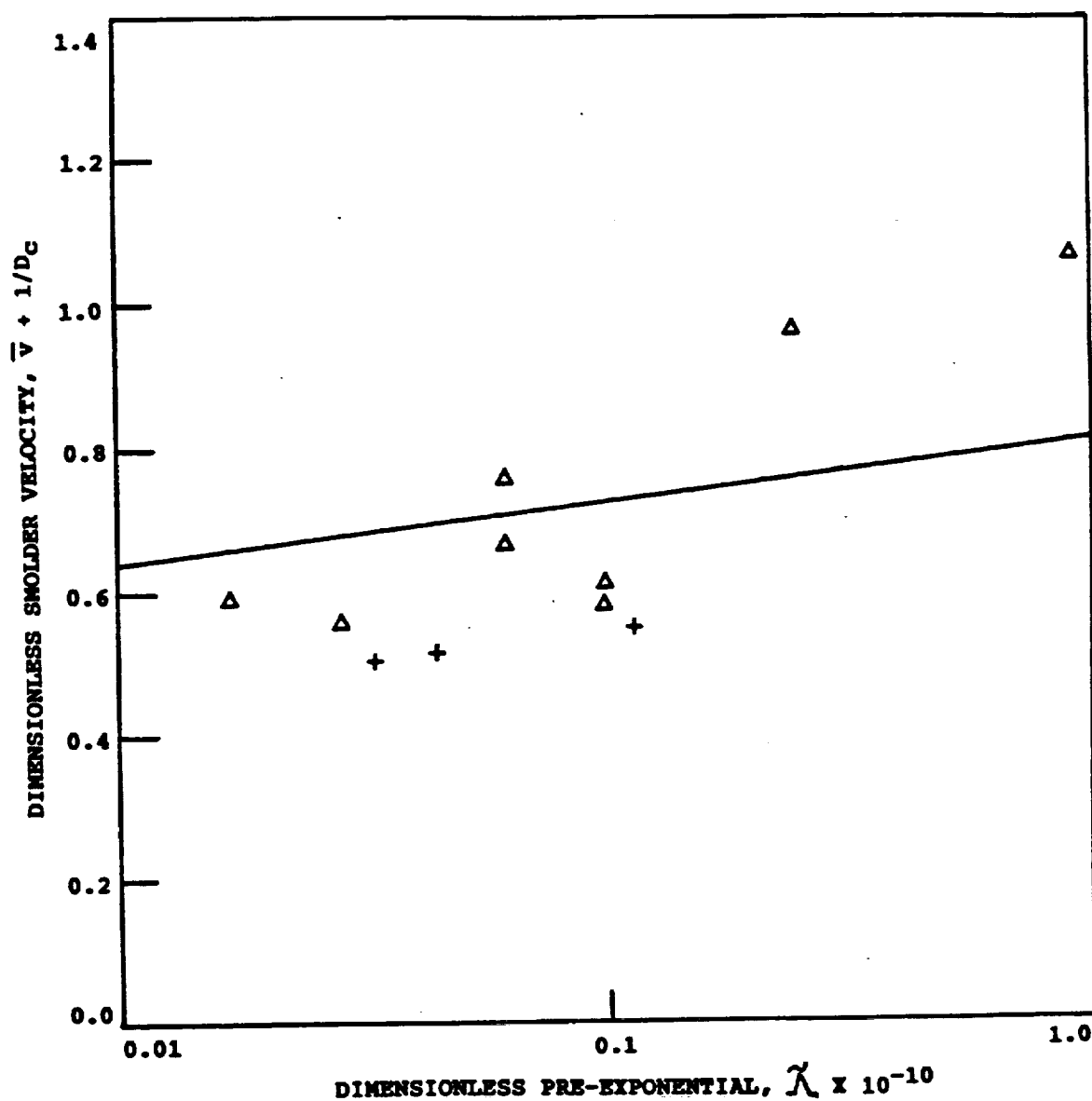
FIG. 2-9: Dimensionless smolder velocity, $\bar{v}+1/D_c$, versus the dimensionless pre-exponential, $\tilde{\Lambda}$, for polyurethane. Smolder velocities predicted by the present analytic model (——), measured by Rogers and Ohlemiller (▲) and calculated by Ohlemiller et al (+) are shown.

measurements. The dashed line in Fig. 2-8 gives the final temperature for alpha-cellulose.

As shown in Eq.(2-21), the dimensionless smolder velocity depends only on D_c and $\bar{T}_f$. The dimensionless parameter, D_c, which measures the total energy released in the reaction zone relative to the amount of energy required to raise the temperature of the gas from $\bar{T}_i$ to $\bar{T}_f$, contains the experimentally observed dependence of $\bar{v}$ on Y_{oi}. For a given fuel and a fixed initial oxygen mass flux, $\dot{m}''_{oi}$, increasing Y_{oi} raises D_c, leading to higher smolder velocities. This dependence of $\bar{v}$ on D_c is fairly weak except near extinction. For Y_{oi} near 0.23, D_c is on the order of 10 and therefore, as a first approximation, $\bar{v} \sim 1/\bar{T}_f$. Because T_f varies slowly with $\dot{m}''_{oi}$, v is approximately proportional to $\dot{m}''_{oi}$ (recall that $v_c \sim \dot{m}''_{oi}$). Figure 2-9 illustrates the dependence of $\bar{v}$ on $\tilde{\Lambda}$ for polyurethane. Overall, there is good agreement between the smolder velocities predicted by this model and those measured by Rogers and Ohlemiller [9].

Extinction occurs when $\bar{v}=0$, corresponding to $\bar{T}_f = D_c$. That is, extinction occurs when all of the energy released is used to heat the incoming gas. Steady smoldering combustion is possible only when $Y_{oi} \geq c_{eff}(T_f-T_i)/Q$. For polyurethane, with $u_i=0.2$ cm/s and $P_a=1$ atm, this criterion requires that $Y_{oi} \geq 0.05$. While for alpha-cellulose this criterion is $Y_{oi} \geq 0.03$. Note that the presence of heat losses from the sides of the cylinder will raise this critical value of Y_{oi}. When the smolder wave is close to the top of

the material, heat losses from the top will also have an important effect on the extinction criterion [20].

2.5 INFLUENCE OF BUOYANCY

Because the temperature field and hence the buoyancy varies as the smolder wave spreads, u_i may not be known a priori. The quasi-steady conservation of momentum for this system is

$$\phi \frac{dP}{dx} = -\mu a_d u + \phi g (\rho_{gi} - \rho_g) . \tag{2-35}$$

Integrating Eq.(2-35) yields

$$\int_{h-L}^{h} \mu a_d u \, dx = \phi \Delta P + \phi \int_{h-L}^{h} g (\rho_{gi} - \rho_g) dx , \tag{2-36}$$

where h is the length of region I in Fig. 2-1, L is the total length of regions I-III and $\Delta P = P_i - P_f$ is the pressure drop across the solid, excluding changes in hydrostatic pressure. While the flow resistance, a_d, is lower in the char layer, the gas velocity, u, is higher. Therefore, it is assumed that the quantity $a_d u$ remains approximately constant at $a_d u_i$. A step change in ρ_g from ρ_{gi} to ρ_{gf} occurs at x=0. The initial velocity is then approximated as

$$u_i = \frac{\phi \Delta P}{\mu a_d L} + \frac{\phi g \rho_{gi} h \overline{T_f}}{\mu a_d L (1 + \overline{T_f})} \tag{2-37}$$

Buoyancy can be neglected when $g \rho_{gi} h / \Delta P \ll (1 + \overline{T}_f) / \overline{T}_f$. At

STP, $\rho_{gi} \sim 1$ kg/m^3 and $\bar{T}_f \sim 1$, so that at sea level, with g= 9.8 m/s^2, Δ P/h >> 5 Pa/m suffices while in orbit, with g $\cong$ 10^{-3} m/s^2, ΔP/h >> 5x10^{-4} Pa/m will suffice. On the other hand, for polyurethane, buoyancy is negligible if the forced u_i >> 4x10^{-4}m/s at sea level and if u_i >> 4x10^{-8}m/s in orbit. When Δ P/gρ_{gi}h << $\bar{T}_f$/(1+$\bar{T}_f$), $u_i \sim$ gρ_{gi}. Since the smolder velocity is proportional to the oxygen mass flux, v $\sim$ $Y_{oi}\rho_{gi}u_i \sim Y_{oi}g\rho_{gi}$. This result agrees with the experimental finding (see Chapter 4) that v is proportional to $P_a^{\bar{2}}$ for buoyancy driven systems.

2.6 CONCLUSIONS

An analytic model of cocurrent (premixed flame-like) smoldering combustion propagation has been developed. Buoyancy was included and shown to be negligible in the proposed application of a cocurrent smoldering experiment for use on the Space Shuttle. Because of the microgravity environment, propagation of the smolder wave was assumed to be one-dimensional and steady in a frame of reference moving with the smolder wave. Radiation heat transfer was incorporated using a diffusion approximation and smoldering was modelled using a one-step reaction mechanism.

Key results include: (1) for a given fuel, the final temperature depends only on the initial oxygen mass flux, $\dot{m}''_{oi}$, increasing logarithmically with $\dot{m}''_{oi}$; (2) the smolder velocity, v, is linearly dependent on $\dot{m}''_{oi}$ and at fixed $\dot{m}''_{oi}$, increasing the initial oxygen mass fraction, Y_{oi}, increases

v ; and (3) steady smolder propagation is possible only for $Y_{oi} \geq c_{eff}(T_f - T_i)/Q$, with extinction occurring when all of the energy released in the reaction zone is used to heat the incoming gas.

The preceding analysis can be modified to allow for several second order effects. Heat losses from the sides of the cylinder will affect the extinction criterion, increasing the critical value of Y_{oi} below which steady solutions cease to exist. When properties are allowed to vary, the equations determining v and T_f will still be valid, with the properties appearing in these equations evaluated at T_f [2,33]. As discussed earlier, a non-oxidative pyrolysis reaction can also be included in the analysis. However, for steady smolder, the presence of such a reaction will only have a small effect on the temperature profiles.

CHAPTER 3

FORCED COUNTERCURRENT SMOLDERING COMBUSTION

3.1 INTRODUCTION

Schematics of the problems under consideration are
presented in Figs. 3-1A and 3-1B. A gaseous oxidizer, with
an oxygen concentration, Y_{oi}, and an inlet velocity, u_i,
flows upward through a porous combustible medium which has a
void volume fraction, $\emptyset$. The solid and gas fractions begin
with densities, ρ_{si} and ρ_{gi}, respectively. At t=0, both the
solid and the gas are at a uniform temperature, T_i.
Smoldering is initiated at the bottom of the material by
applying an external heat flux, q_e, for $0 < t < t_e$. The smolder
wave propagates upwards, in the same direction as the forced
flow of oxidizer. In a frame of reference moving with the
smolder zone, the solid and the oxidizer enter the reaction
region from opposite directions. Consequently, this
configuration is referred to as countercurrent or diffusion-
flame-like. It is also called forward smolder since the
reaction zone moves in the oxidizer flow direction.

A model of unsteady, forced, countercurrent smoldering
combustion propagation is presented in this chapter.
Smoldering combustion is represented with a two-step
reaction mechanism consisting of a char oxidation reaction
and a pyrolysis reaction. A "flame" sheet approximation is
used to model the oxidation reaction zone and it is assumed

REGION I: UNBURNT SOLID

v_p Pyrolysis Front

L REGION II: CHAR X

v Char Oxidation Front

REGION III: AIR

U_i (air flow velocity)

FIG. 3-1A: Schematic of countercurrent smoldering for Case I (no residual ash).

C-2.

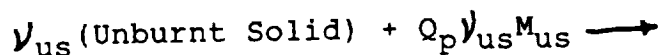REGION I: UNBURNT SOLID

v_p Pyrolysis Front

L

REGION II: CHAR

X

v Char Oxidation Front

h

REGION III: RESIDUAL ASH

REGION IV: AIR

U_i (air flow velocity)
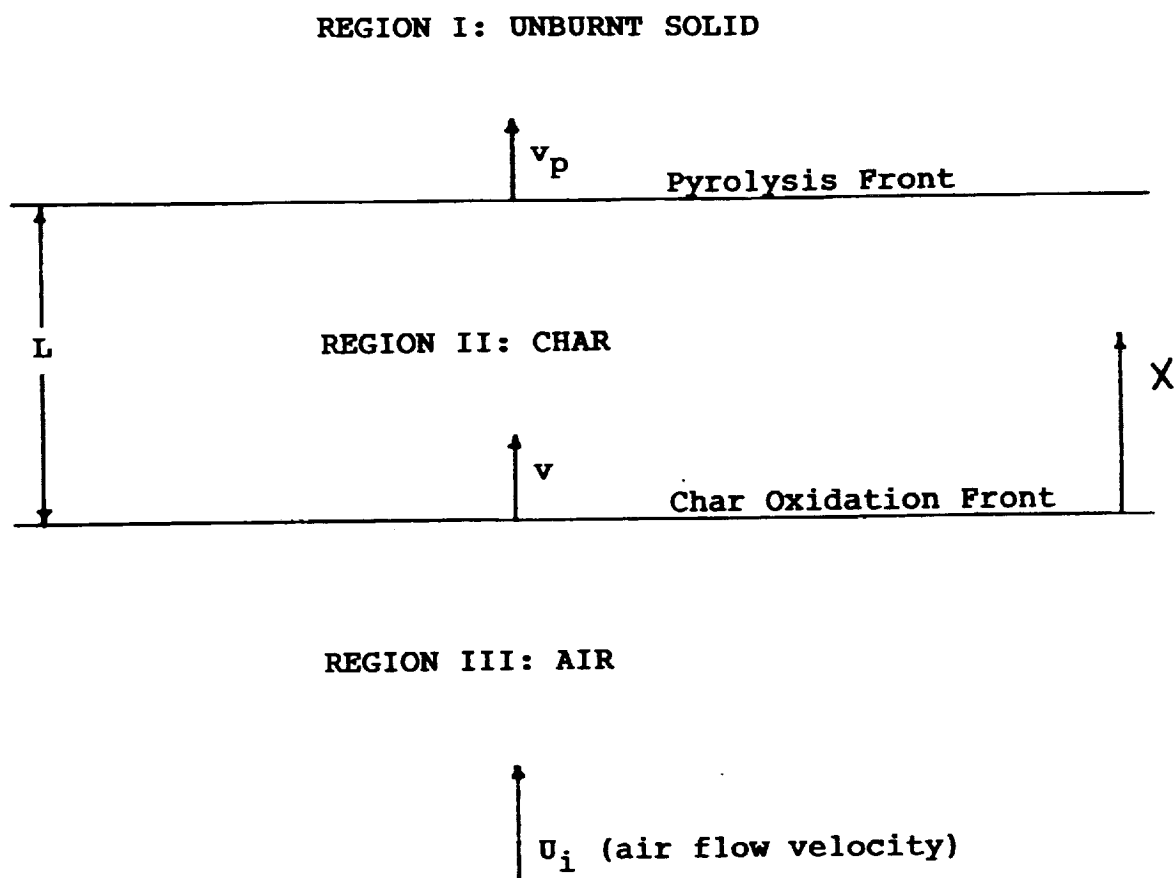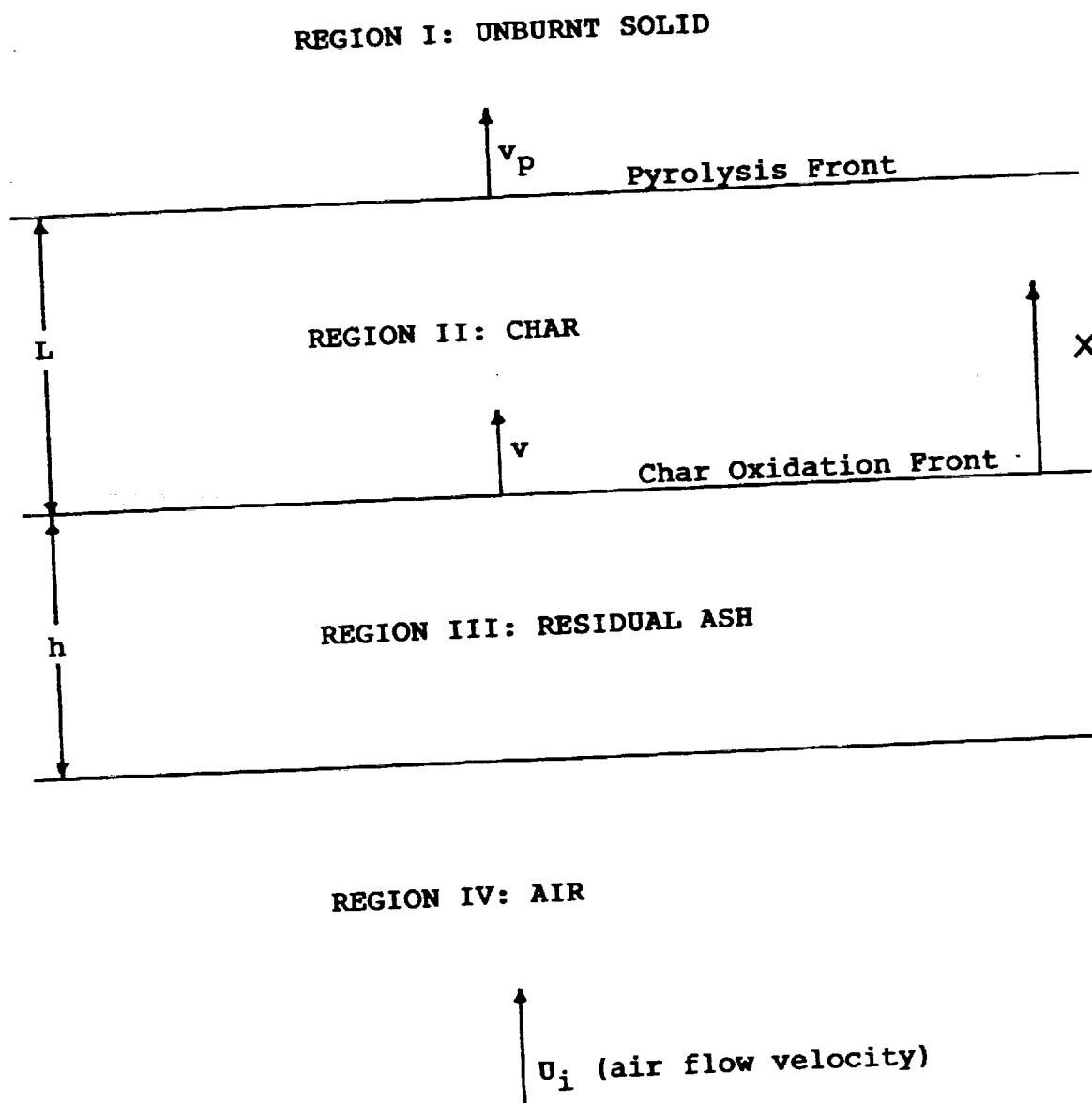
FIG. 3-1B: Schematic of countercurrent smoldering for Case II (an ash layer building below the smolder wave).

pyrolysis occurs at a known temperature, T_p. Because the two reaction fronts move at different velocities, countercurrent smolder propagation is unsteady. Two cases are considered: no ash residue (see Fig. 3-1A), $y_a M_a = 0$, and an ash layer building below the smolder wave (see Fig. 3-1B), $y_a M_a \neq 0$. The residual ash serves as insulation and its presence leads to higher peak temperatures. The range of validity of the solutions is identified and explicit expressions are derived, in the limit of long time, for the char oxidation velocity, v, the pyrolysis front velocity, v_p, and the maximum temperature, T_m.

3.2 ANALYSIS

3.2.1 Assumptions

The scenario depicted in Fig. 3-1 is not a realistic representation of the countercurrent smoldering combustion of all solid fuels. Some solids will collapse downwards as the smolder wave propagates. In this study, it is assumed that the solid remains stationary in a frame of reference fixed in the laboratory. If the fuel consists of small, loosely packed, solid particles, this assumption is only valid in a microgravity environment. Smoldering combustion is represented by a two-step reaction mechanism,

$$y_{us}(\text{Unburnt Solid}) + Q_p y_{us} M_{us} \longrightarrow$$

$$y_c \text{Char} + y_{gp1}(\text{Gas Products}) \qquad (3-1)$$

and

$$\nu_c \text{Char} + \nu_o O_2 \longrightarrow$$
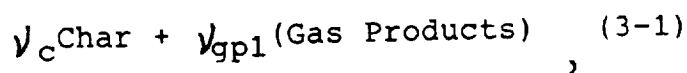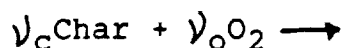
$$\nu_{gp2} (\text{Gas Products}) + \nu_a \text{Ash} + Q\nu_o M_o \quad (3\text{-}2)$$

where Q_p is the energy required to pyrolyse one gram of unburnt solid and Q is the energy released per gram of O_2 consumed. Char oxidation is modeled using a "flame sheet" assumption. It is assumed that the pyrolysis reaction occurs at a known temperature, T_p. This is a reasonable approximation for many solids of interest [41,42,44]. For alpha-cellulose, $T_p = 300°C$ [41]. Alternatively, pyrolysis can be modeled using Arrhenius-type kinetics [24,25,41]. Such an approach leads to numerical calculations and requires the specification of kinetic constants whose values are sometimes ambiguous [41].

The char oxidation zone moves at a constant speed, v, which is determined by the rate at which oxygen reaches the reaction region, while the pyrolysis front moves at a velocity, v_p, which is several times larger than v. Because the pyrolysis reaction is endothermic [1], motion of the pyrolysis front is highly dependent on heat transfer from the oxidation zone, where the energy required to sustain smoldering is released. Energy is transferred to the pyrolysis zone by conduction, radiation and gas phase convection. Typical values of several smolder characteristics, including the maximum temperature, T_m, the oxidation velocity, v, and the pyrolysis speed, v_p, are given in Table 3-I.

TABLE 3-I: Order of magnitude estimates for several smolder characteristics.

Quantity of Interest	Magnitude[a]
forced gas velocity, u_i	$(1-5) \times 10^{-3}$ m/sec
oxidation velocity, v	$(1-3) \times 10^{-5}$ m/sec
pyrolysis front velocity, v_p	$(5-15) \times 10^{-5}$ m/sec
maximum temperature, T_m	$800-900\,°K$

a. Measurements by Ohlemiller and Lucca [19].

Because the solid fuel and the gaseous oxidizer enter the oxidation zone from opposite directions, all of the char is consumed in accordance with Eq.(2) before the oxidation zone moves forward. Therefore, the oxidation velocity, v, is proportional to the initial oxygen mass flux, with the proportionality constant determined by stoichiometry [1,19]. Because v is several orders of magnitude smaller than the gas velocity, u_i, the oxygen mass flux in a frame of reference moving with the oxidation zone is approximately, $Y_{oi}\,\phi\,\rho_{gi}u_i$ [16]. Thus,

$$ V = \frac{\nu_{us}M_{us}}{\nu_o M_o}\,\frac{Y_{oi}\,\rho_{gi}\,u_i}{(1-\phi)\rho_{si}} \cdot \tag{3-3} $$

Typically, $Y_{oi} \sim 0.23$, $u_i \sim 0.005$ m/s, $\rho_{gi} \sim 1$ kg/m^3, and $(1-\phi)\rho_{si} \sim 40$ kg/m^3, resulting in oxidation velocities on the order of 10^{-5} m/s. For the same conditions, smolder

velocities encountered in cocurrent smoldering are more than 50 times larger [19]. In a frame of reference moving with the oxidation zone, the gas phase mass flux, $\dot{m}_g''$, is an order of magnitude larger than the solid phase mass flux, $\dot{m}_s''$. Setting $Y_{oi}=0.23$ and representing oxidation with the reaction, $C+O_2 \rightarrow CO_2$, Eq. (3-3) yields $\dot{m}_s''/\dot{m}_g'' \approx 0.08$. Neglecting terms involving $\dot{m}_s''$ considerably simplifys the governing equations. Also, since the solid density based on total volume, $(1-\phi)\rho_{si}$, is much greater than $\phi\rho_{gi}$, the energy stored in the gas phase is negligible when compared with that stored in the solid phase [20,24].

Additionally, the solid phase is assumed continuous with a constant void volume fraction. The propagation of the smolder wave is approximated as one-dimensional. Fick's Law is used to model the diffusion of oxygen. Radiation heat transfer is incorporated using the diffusion limit. The gas and the solid are assumed to be in local thermal equilibrium. Energy transport due to concentration gradients, energy dissipated by viscosity, work done by body forces and the kinetic energy of the gas phase have been ignored. The quantity, $\rho_g D$, is taken to be constant. This is a reasonable assumption because the mass diffusivity of oxygen in air, D, increases with temperature and decreases with pressure [37]. It is also assumed that properties, such as the gas phase thermal conductivity, k_g, the solid phase thermal conductivity, k_s, the gas specific heat, c_g, and the solid specific heat, c_s, remain constant.

2.2 CASE I: No Residual Ash

2.2.1 Governing Equations

After the initiation of smoldering, the coordinate system moves with the char oxidation region. In this moving frame of reference, solutions are steady in Region III (x<0) in Fig. 3-1A. For x>0 (Regions I and II in Fig. 3-1A), the conservation of energy requires

$$(1-\phi)\rho_s c_s \frac{\partial T}{\partial t} + \dot{m}_g'' c_g \frac{\partial T}{\partial x} = \frac{\partial}{\partial x}\left[k_{eff} + k_{rad}\right]\frac{\partial T}{\partial x} , \quad (3-4)$$

where the effective thermal conductivity, $k_{eff} = \phi k_g + (1-\phi)k_s$, accounts for heat transfer due to conduction in both phases. Radiation heat transfer is incorporated using a temperature dependent conductivity, $k_{rad} = 16\sigma \ell_r T^3/3$, where ℓ_r is the radiation path length. For x<0 (Region III in Fig.3-1A),

$$\rho_g c_g \frac{\partial T}{\partial t} + \dot{m}_g'' c_g \frac{\partial T}{\partial x} = k_g \frac{\partial^2 T}{\partial x^2} , \quad (3-5)$$

Since all of the oxygen is consumed, $Y_o=0$ for x>0. For x<0, conservation of species for oxygen yields

$$\rho_g \frac{\partial Y_o}{\partial t} + \dot{m}_g'' \frac{\partial Y_o}{\partial x} = \rho_g D \frac{\partial^2 Y_o}{\partial x^2} . \quad (3-6)$$

Conservation of gas mass gives

$$\left[1 + (\phi-1) H(x)\right]\frac{\partial \rho_g}{\partial t} + \frac{\partial \dot{m}_g''}{\partial x} = 0 , \quad (3-7)$$

where H(x) is the Heaviside function, which vanishes for x<0 and is equal to 1 for x>0. Noting that all of the incoming solid is consumed in the oxidation zone, Eq.(3-1) yields

$$\rho_s = \begin{cases} \left[1 - \dfrac{\nu_{gp1} M_{gp1}}{\nu_{us} M_{us}} H(L-x) \right] \rho_{si} & \text{, for } x > 0 \\ 0 & \text{, for } x < 0 \end{cases} \quad (3-8)$$

Because the pressure changes by only a small amount for these very porous systems [1], the ideal gas law gives $\rho_g RT = P_a$, thus completing the preceding set of equations.

The following boundary conditions are imposed on Eqs.(3-4 to 3-7): as $x \to -\infty$, $T \to T_i$, $Y \to Y_{oi}$ and $\dot{m}_g'' \to \dot{m}_{gi}''$; as $x \to +\infty$, $dT/dx \to 0$. The temperature is continuous across both interfaces. Because $\dot{m}_s'' << \dot{m}_g''$, $\dot{m}_g''$ is approximately continuous across both interfaces. It is assumed that smoldering begins when the temperature of the x=0 interface reaches a critical value, $T_{ig} > T_p > T_i$. However, only an approximate value for T_{ig} is needed since the solutions are independent of the initial conditions as $t \to \infty$. Conservation of energy at the x=0 interface gives

$$\left[K_{eff} + \frac{16}{3} \sigma \ell_r T_m^3 \right] \frac{\partial T}{\partial x} \bigg|_{x=0^+} = K_g \frac{\partial T}{\partial x} \bigg|_{x \to 0^-} + \varepsilon \sigma (T_m^4 - T_i^4)$$

$$+ Q \rho_g D \frac{\partial Y_o}{\partial x} \bigg|_{x=0^-} H(T_m - T_{ig}) - \dot{q}_e'' H(t_e - t), \quad (3-9)$$

where T_m is the temperature at x=0. Thus, the maximum temperature, T_m, is determined by balancing the energy transported downstream, by conduction and radiation, and the

energy conducted upstream, radiation heat losses from the x=0 interface, the energy released in the oxidation zone and the external heat flux. Motion of the pyrolysis front is calculated by equating the energy consumed by pyrolysis and the net energy transported to the pyrolysis zone, giving

$$V_p = \frac{\left[K_{eff} + \frac{16}{3} \sigma \ell_r T_p^3 \right]}{(1-\phi) \rho_{si} \, Q_p} \left[\left. \frac{\partial T}{\partial x} \right|_{x=L^+} - \left. \frac{\partial T}{\partial x} \right|_{x=L^-} \right], \qquad (3\text{-}10)$$

where v_p= dL/dt+v and L is the distance between the two reaction regions. Initially, both the temperature and the oxygen concentration are uniform. That is, $T(x,0)=T_i$ and $Y_o(x,0)= Y_{oi}$. After smoldering is initiated, $Y_o(0,t)=0$.

2.2.2 Dimensionless Governing Equations

A dimensionless temperature is defined by $\overline{T}=(T-T_i)/T_c$. Setting $T_c=T_i$ makes $\overline{T}$ of order one and eliminates the parameter, T_c/T_i, which arises from the nonlinear terms in the governing equations. The oxygen mass fraction, Y_o, the gas density, ρ_g, and the gas mass flux, $\dot{m}_g''$, are normalized by their initial values. A characteristic distance,

$$X_c = \frac{K_{eff}}{\dot{m}_{gi}'' C_g}, \qquad (3\text{-}11)$$

and a characteristic time,

$$t_c = \frac{x_c^2 (1-\phi) \rho_{si} C_s}{K_{eff}}, \qquad (3\text{-}12)$$

are chosen by balancing terms in Eq.(3-4). Typically,

$u_i \sim 0.005$ m/sec, $\rho_{gi} \sim 1$ kg/m^3, $(1-\phi)\rho_{si} \sim 40$ kg/m^3, $c_s \sim c_g$ 1 kJ/kg K, and $k_{eff} \sim 0.05$ W/m K, giving $x_c \sim 0.01$ m and $t_c \sim 80$ sec. Thus, the ratio, $x_c/t_c \sim 0.013$ cm/sec, is of the same order as v_p (see Table 3-I). This is to be expected because v_p is determined by heat transfer considerations and both x_c and t_c were chosen to make terms in the energy equation of order one.

For $\bar{x} > 0$, conservation of energy requires

$$\bar{\rho_s} \frac{\partial \bar{T}}{\partial \bar{t}} + \bar{m_g} \frac{\partial \bar{T}}{\partial \bar{x}} = \frac{\partial}{\partial \bar{x}} \left[1 + N_R (1 + \bar{T})^3 \right] \frac{\partial \bar{T}}{\partial \bar{x}} , \qquad (3\text{-}13)$$

and for $\bar{x} < 0$,

$$\tau \bar{\rho_g} \frac{\partial \bar{T}}{\partial \bar{t}} + \bar{m_g} \frac{\partial \bar{T}}{\partial \bar{x}} = \ell \frac{\partial^2 \bar{T}}{\partial \bar{x}^2} . \qquad (3\text{-}14)$$

Since all of the oxygen is consumed, $\bar{Y}_0 = 0$ for $\bar{x} > 0$. For $\bar{x} < 0$, conservation of species for oxygen yields

$$\tau \bar{\rho_g} \frac{\partial \bar{Y_0}}{\partial \bar{t}} + \bar{m_g} \frac{\partial \bar{Y_0}}{\partial \bar{x}} = \frac{1}{Le} \frac{\partial^2 \bar{Y_0}}{\partial \bar{x}^2} . \qquad (3\text{-}15)$$

Conservation of gas mass requires

$$\tau \left[1 - (1-\phi) H(\bar{x}) \right] \frac{\partial \bar{\rho_g}}{\partial \bar{t}} + \frac{\partial \bar{m_g}}{\partial \bar{x}} = 0 . \qquad (3\text{-}16)$$

Equation (3-8) yields

$$\bar{\rho_s} = \begin{cases} 1 - (1 - S_c) H(\bar{L} - \bar{x}) , & \text{for } \bar{x} > 0 \\ 0 , & \text{for } \bar{x} < 0 \end{cases} \qquad (3\text{-}17)$$

TABLE 3-II: Dimensionless parameters governing forced countercurrent smoldering combustion. In addition to the following parameters, the void volume fraction, , the irradiation time, t_e, the ignition temperature, T_{ig}, and the pyrolysis temperature, T_p, must be specified.

$$D_{co} = \frac{QY_{oi}}{C_s T_i}$$	Dimensionless measure of the heat released per mass of oxygen consumed (varies from 0 to 20)
$$D_{cp} = \frac{Q_p}{C_s T_i}$$	Dimensionless measure of the energy consumed by pyrolysis (varies from 0.25 to 1)
$$\ell = \frac{K_g}{K_{eff}}$$	Dimensionless thermal thickness in Region III (varies from 0.5 and 0.7)
$$Le = \frac{K_{eff}}{\rho_g D C_g}$$	Modified Lewis number (usually lies between 1.9 and 3.0)
$$N_R = \frac{16\sigma \ell_r T_i^3}{3 K_{eff}}$$	Dimensionless radiation conductivity (less than 0.1)
$$Q_R = \frac{\dot{q}_e''}{Q \dot{m}_{oi}''}$$	External heat flux measured relative to the total energy released in the reaction zone
$$Q_E = \frac{\varepsilon \sigma T_i^4}{Q \dot{m}_{oi}''}$$	Dimensionless measure of the energy radiated to the surroundings (varies from 0.005 to infinity)
$$S_a = \frac{\nu_a M_a}{\nu_{us} M_{us}}$$	Stoichiometric coefficient - ash
$$S_c = \frac{\nu_c M_c}{\nu_{us} M_{us}}$$	Stoichiometric coefficient - char (varies between 0.3 and 0.4)

TABLE 3-II: (cont.)

$$V = \frac{\nu_{us} M_{us}}{\nu_0 M_0} \frac{Y_{0i} C_s}{C_g}$$

Dimensionless char oxidation velocity (varies from 0 to 1)

$$\tau = \frac{\rho_{gi} C_g}{(1-\phi)\rho_{si} C_s}$$

Gas phase response time divided by the solid phase response time (less than 0.04)

In dimensionless form, the ideal gas equation of state is $\overline{\rho}_g(1+\overline{T})=1$. The dimensionless smolder velocity, $\overline{v}= vt_c/x_c$, equals V after the onset of smoldering and is zero beforehand.

The following boundary conditions are imposed on Eqs. (3-13 through 3-16): as $\overline{x}\rightarrow-\infty$, $\overline{T}\rightarrow 0$, $\overline{Y}_o\rightarrow 1$ and $\overline{m}_g\rightarrow 1$; as $\overline{x}\rightarrow+\infty$, $d\overline{T}/d\overline{x}\rightarrow 0$. Both temperature and the gas mass flux are continuous across the interfaces. Conservation of energy across the $\overline{x}=0$ interface gives

$$\frac{1}{D_{co}}\left[1+N_R(1+\overline{T}_m)^3\right]\frac{\partial\overline{T}}{\partial\overline{x}}\bigg|_{\overline{x}=0^+} = \frac{\ell}{D_{co}}\frac{\partial\overline{T}}{\partial\overline{x}}\bigg|_{\overline{x}=0^-} + Q_R\left[(1+\overline{T}_m)^4-1\right]$$

$$+ \frac{1}{Le}\frac{\partial\overline{Y}_o}{\partial\overline{x}}\bigg|_{\overline{x}=0^-} H\cdot(\overline{T}_m-\overline{T}_{ig})-Q_f H(\overline{t}_e-\overline{t}), \quad (3\text{-}18)$$

where $\overline{T}_m$ is the temperature at $\overline{x}=0$. The temperature of the pyrolysis zone is held fixed, $\overline{T}(\overline{L},\overline{t})= \overline{T}_p$, and the motion of this front is determined by

$$\overline{V}_p = \frac{d\overline{L}}{d\overline{t}}+V = \frac{1}{D_{cp}}\left[1+N_R(1+\overline{T}_p)^3\right]\left[\frac{\partial\overline{T}}{\partial\overline{x}}\bigg|_{\overline{x}=\overline{L}^+} - \frac{\partial\overline{T}}{\partial\overline{x}}\bigg|_{\overline{x}=\overline{L}^-}\right] \quad (3\text{-}19)$$

Initially, $\overline{T}(\overline{x},0)= 0$ and $Y_o(x,0)= 1$. After smoldering is initiated, $Y_o(0,t)=0$.

The dimensionless parameters appearing in the preceding equations and typical values of these parameters, estimated from properties provided in the literature [19,20,45-48], are given in Table 3-II. The quantity, τ, represents the

ratio of the gas phase response time to the solid phase response time and is always less than 0.04 for the fuels of interest. As discussed in the following section, this fact leads to considerable simplification in the governing equations because solutions in Region III in Fig. 3-1A are steady when τ is small.

2.2.3 Quasi-Steady Equations

Terms in Eqs.(3-14 through 3-16) involving time derivatives can be neglected because τ is always less than 0.04. This result is in agreement with the findings of Ohlemiller and others [1,20,24], who reported that the gas phase can be considered quasi-steady in many smoldering combustion applications. Setting τ equal to zero in Eq. (3-16), integrating once, and combining with Eq.(3-13),

$$\bar{\rho}_s \frac{\partial \bar{T}}{\partial \bar{t}} + \frac{\partial \bar{T}}{\partial \bar{x}} = \frac{\partial}{\partial \bar{x}} \left[1 + N_R (1+\bar{T})^3 \right] \frac{\partial \bar{T}}{\partial \bar{x}} . \tag{3-20}$$

Equation (3-14) yields an explicit expressions for the temperature in Region III in Fig. 1A ($\bar{x}<0$),

$$\bar{T} = \bar{T}_m \, e^{\bar{x}/\ell} . \tag{3-21}$$

After smoldering is initiated, Eq. (3-15) gives

$$\bar{Y}_o = 1 - e^{\text{Le} \, \bar{x}} . \tag{3-22}$$

Combining Eqs.(3-18,3-21,3-22),

$$\left[1 + N_R(1+\bar{T}_m)^3\right]\frac{\partial \bar{T}}{\partial \bar{x}}\bigg|_{\bar{x}=0^+} = \bar{T}_m + Q_R \mathcal{D}_{co}\left[(1+\bar{T}_m)^4 - 1\right]$$

$$- \mathcal{D}_{co} H(\bar{T}_m - \bar{T}_{ig}) - \mathcal{D}_{co} Q_E H(\bar{t}_e - \bar{t}) . \quad (3-23)$$

Equation (3-23) determines $\bar{T}_m$ while $\bar{v}_p$ is given by Eq.(3-19).

2.3 CASE II: Ash Layer Building Below Smolder Wave

After the initiation of smoldering, the coordinate system moves with the char oxidation zone. As the oxidation front propagates upward, an ash layer of height, h(t)=vt, builds below the smolder wave - see Fig. 3-1B. Because the governing equations for Case II are very similar to those for Case I, only dimensionless equations are presented in this section. Relevant dimensionless variables are defined in the preceding section and the dimensionless parameters appearing in the following equations are listed in Table II. As discussed previously, the gas phase response time is much smaller than the solid phase response time (that is, $\mathcal{T} \ll 1$). Consequently, the temperature in Region IV in Fig. 3-1B, the oxygen concentration, and the gas phase mass flux profiles are steady. Conservation of energy in Regions I through III in Fig. 3-1B gives

$$\bar{\rho}_s \frac{\partial \bar{T}}{\partial \bar{t}} + \frac{\partial \bar{T}}{\partial \bar{x}} = \frac{\partial}{\partial \bar{x}}\left[1 + N_R(1+\bar{T})^3\right]\frac{\partial \bar{T}}{\partial \bar{x}} , \quad (3-24)$$

while in Region IV,

$$\overline{T} = \overline{T}_h \, e^{\overline{x}/\ell} \ .$$

(3-25)

The temperature at $\overline{x} = -\overline{h}$, $\overline{T}_h(\overline{t})$, will be determined by applying the conservation of energy at the $\overline{x} = -\overline{h}$ interface. After smolder initiation, conservation of species for oxygen yields

$$\overline{Y}_0 = \begin{cases} 0 \ , & \text{for } \overline{x} > 0 \\[2mm] 1 - e^{\overline{x} \, Le} \ , & \text{for } -\overline{h} < \overline{x} < 0 \\[2mm] 1 - e^{\overline{h} \, Le/\phi} \, e^{(\overline{h} + \overline{x}) Le} \ , & \text{for } \overline{x} < -\overline{h} \end{cases}$$

(3-25)

Equations (3-1,3-2) determine the solid density,

$$\overline{\rho}_s = \begin{cases} 1 - (1 - S_c) H(\overline{L} - \overline{x}) \ , & \text{for } \overline{x} > 0 \\[2mm] S_a \ , & \text{for } -\overline{h} < \overline{x} < 0 \\[2mm] 0 \ , & \text{for } \overline{x} < -\overline{h} \end{cases}$$

(3-27)

The following boundary conditions are imposed on Eq.(3-24): as $\overline{x} \rightarrow -\infty$, $\overline{T} \rightarrow 0$; as $\overline{x} \rightarrow +0$, $d\overline{T}/d\overline{x} \rightarrow 0$. The temperature is continuous across all of the interfaces. Before smolder initiation, conservation of energy across the $\overline{x} = 0$ interface requires

$$\left[1 + N_R (1 + \overline{T}_m)^3 \right] \frac{\partial \overline{T}}{\partial \overline{x}} \bigg|_{\overline{x}=0^+} = \overline{T}_m + Q_R \mathcal{D}_{c_0} \left[(1 + \overline{T}_m)^4 - 1 \right]$$

$$- Q_E \mathcal{D}_{c_0} \, H(\overline{T}_e - \overline{t}) \ ,$$

(3-26)
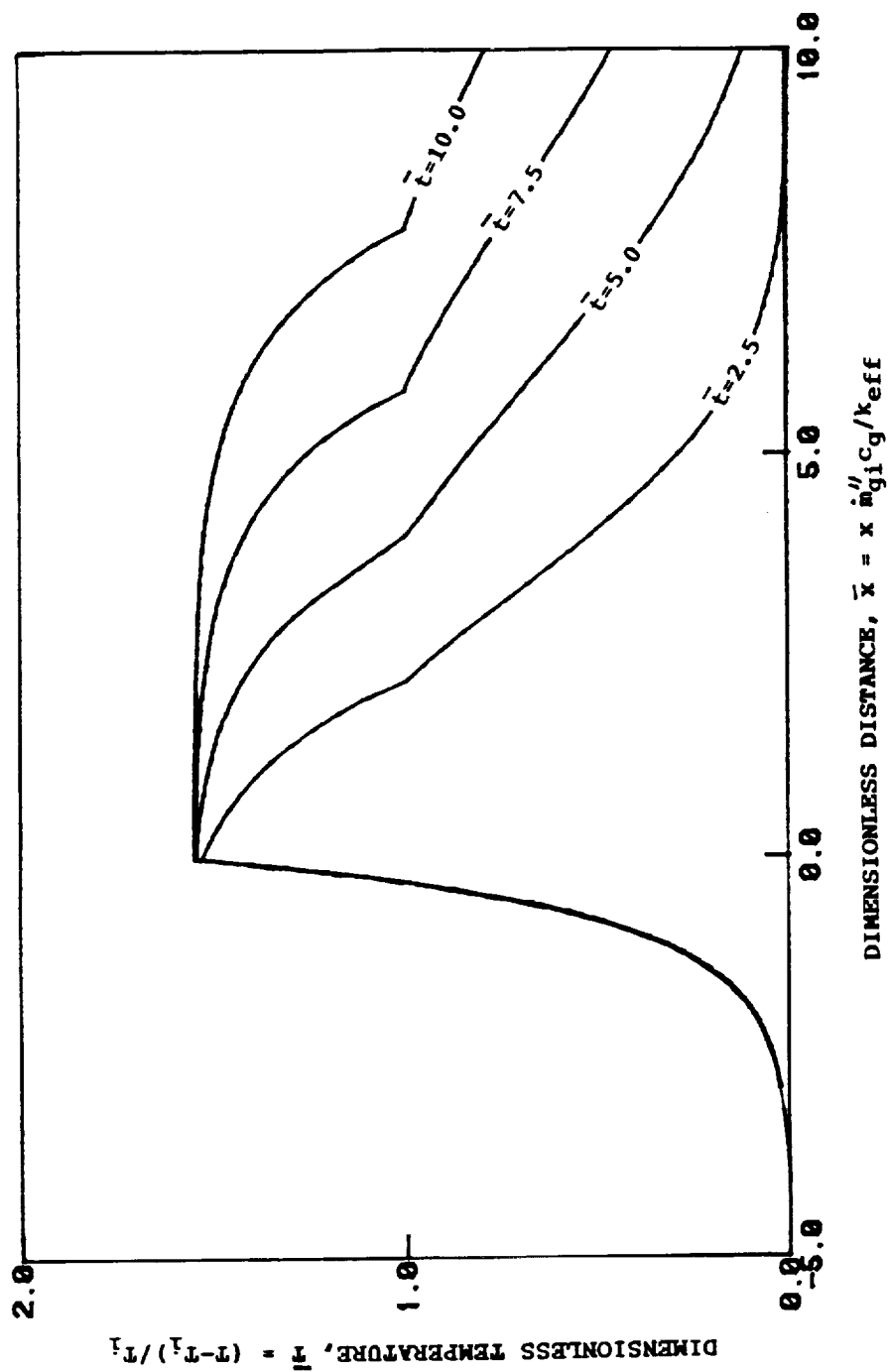
FIG. 3-2: Dimensionless temperature, $\bar{T}$, versus dimensionless distance, $\bar{x}$, at various dimensionless times, $\bar{t}$, for Case I, with $D_{CO}=12.0$, $D_{CP}=0.3$, $\ell=0.7$, $N_R=0$, $Q_E=1.0$, $Q_R=0.021$, $s_C=0.3$, $V=0.2$, $\bar{t}_e=1.0$, and $\bar{T}_{ig}=\bar{T}_p=1.0$.
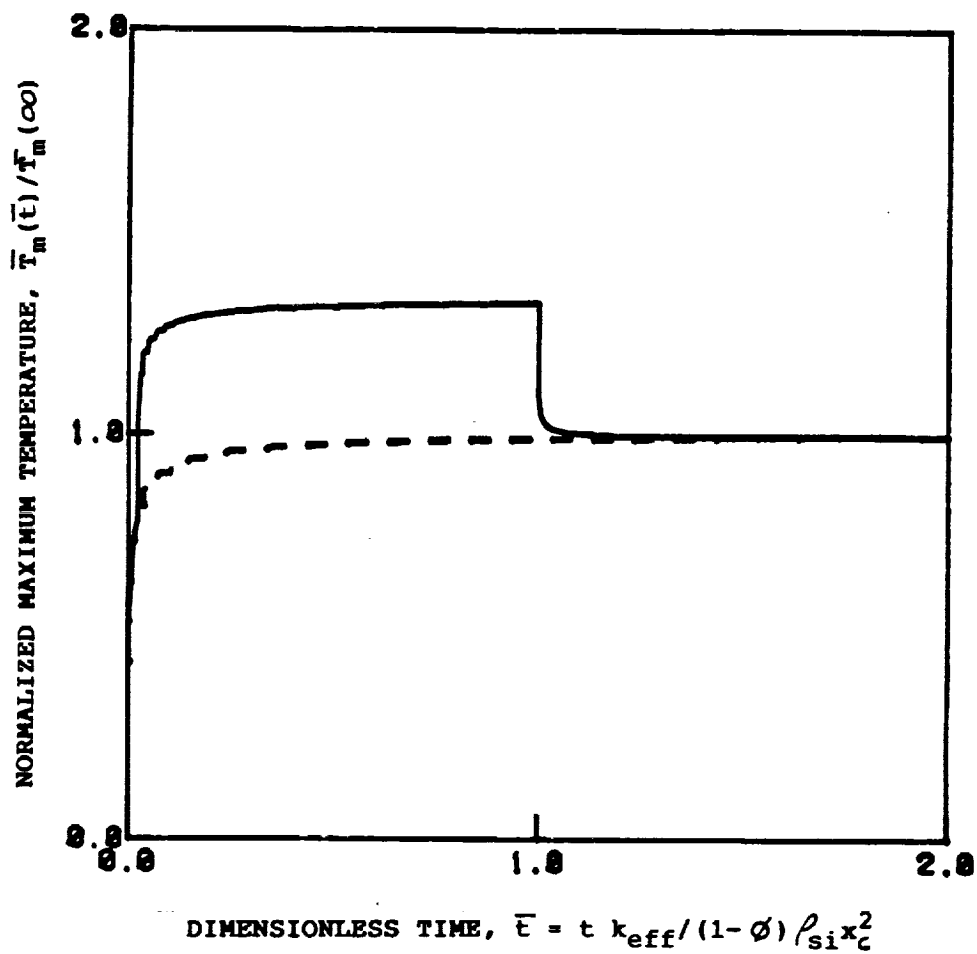
FIG. 3-3: Normalized maximum temperature, $\overline{T}_m(\overline{t})/\overline{T}_m(\infty)$, versus dimensionless time, $\overline{t}$, for: (1) the external heat flux turned off at $\overline{t}=\overline{t}_e=1$ (—) ; (2) the external heat flux turned off immediately after smolder initiation (--). With $D_{co}=12$, $D_{cp}=0.3$, $\ell=0.7$, $N_R=0$, $Q_E=1$, $Q_R=0.02$, $s_c=0.3$, $V=0.2$, and $\overline{T}_p=\overline{T}_{ig}=1$.

After initiation, conditions at $\bar{x}=-\bar{h}$ and $\bar{x}=0$ are

$$\left[1 + N_R(1+\bar{T}_h)^3\right]\frac{\partial\bar{T}}{\partial\bar{x}}\bigg|_{\bar{x}=0^+} = \bar{T}_h + Q_R D_{\infty}\left[(1+\bar{T}_h)^4 - 1\right]$$

$$- Q_E D_{co} H(\bar{t}_e - \bar{t}), \qquad (3\text{-}29)$$

and

$$\left[1 + N_R(1+\bar{T}_m)^3\right]\left[\frac{\partial\bar{T}}{\partial\bar{x}}\bigg|_{\bar{x}=0^-} - \frac{\partial\bar{T}}{\partial\bar{x}}\bigg|_{\bar{x}=0^+}\right] = D_{co}, \qquad (3\text{-}30)$$

respectively. Equations (3-29,3-30) determine $\bar{T}_h$ and $\bar{T}_m$. Motion of the pyrolysis front is still governed by Eq. (3-19). Consideration of an ash layer introduces one additional parameter, s_a.

3.3 SOLUTIONS

3.3.1 CASE I: No Residual Ash

Techniques for solving partial differential equations with moving interfaces have been developed within the context of freezing and thawing in cold climates [44] and the charring of solids during a fire [41]. The time-explicit finite difference scheme presented by Lundarini [44] is utilized to solve Eqs. (3-20,3-21,3-24). Temperature profiles after the onset of smoldering for typical values of the dimensionless parameters are shown in Fig. 3-2. The maximum temperature, $\bar{T}_m$, reaches a steady value before $\bar{t}=2.5$. A plot of $\bar{T}_m(\bar{t})/\bar{T}_m(\infty)$ is given in Fig. 3-3 for two cases: (1) the
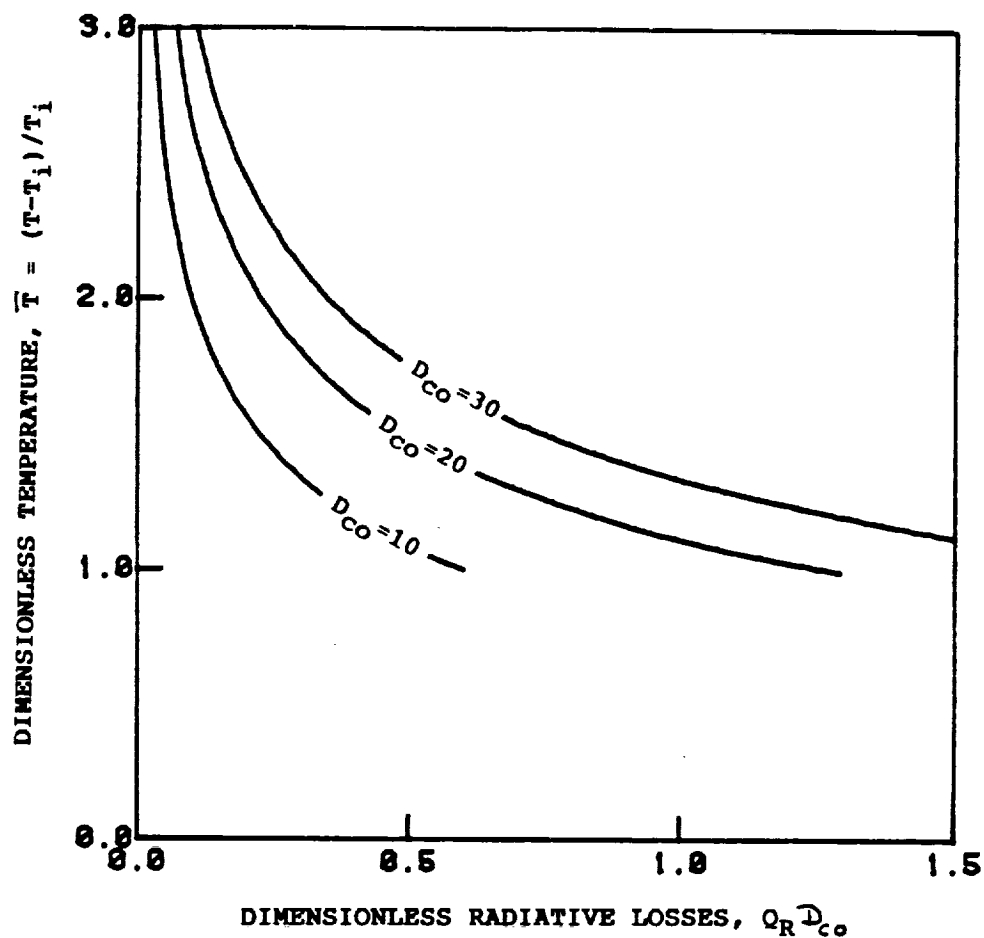
FIG. 3-4: Setting $\overline{T}$ equal to the dimensionless maximum temperature, $\overline{T}_m$, gives $\overline{T}_m$ versus dimensionless radiative losses, $Q_R D_{co}$, parameterized in the dimensionless heat release, D_{co}. Setting $\overline{T}$ equal to the ignition temperature, $\overline{T}_{ig}$, and replacing D_{co} with $Q_{E,min} D_{co}$ (the minimum external heat flux that will produce smoldering) gives $\overline{T}_{ig}$ versus $Q_R D_{co}$ for various $Q_{E,min} D_{co}$.

external heat flux is turned off at $\bar{t}=\bar{t}_e=1.0$ (solid line) ;
(2) the heat flux is turned off immediately after smolder
initiation (dashed line). Radiation and conduction heat
transfer from the oxidation zone to the pyrolysis front
becomes small when the dimensionless distance between the
two reaction regions is large - that is, when $\bar{L} \gg 1$.
Neglecting terms on the left hand side of Eq.(3-23), as
$\bar{t} \to \infty$,

$$Q_R D_{co}\left[(1+\bar{T}_m)^4 - 1\right] + \bar{T}_m = D_{co} .$$

(3-31)

Because $Q_R D_{co}$ is usually greater than 0.15 and $\bar{T}_m \sim 2$, the
first term on the left hand side of the above equation is an
order of magnitude larger than the second and consequently,
$\bar{T}_m \approx Q_R^{-1/4} - 1$, or in dimensional form, $T_m \approx (Q\dot{m}_{oi}''/ \epsilon\sigma)^{1/4}$. Thus,
as a first approximation, the peak temperature is determined
by balancing the heat released in the reaction zone and
radiation heat losses from the x=0 interface. Typically, $Q \sim$
12.3 kJ/gm of O_2, $Y_{oi} \sim 0.23$, $\dot{m}_{gi}'' \sim 0.006$ kg/m^{2}s and $\epsilon \sim 0.9$,
giving $T_m \sim 490^\circ$C. Because a small portion of the energy
released is used to preheat the incoming gas, the peak
temperature will be slightly lower than this value.

A plot of $\bar{T}_m$ versus $Q_R D_{co}$ for various values of D_{co} is
shown in Fig. 3-4. Smoldering will only occur when $\bar{T}_p(\cong 1) <$
$\bar{T} < \bar{T}_{flame}$, where $\bar{T}_{flame}$ is a critical temperature above
which flaming is observed. Figure 4 also demonstrates the
relationship between the ignition temperature, $\bar{T}_{ig}$, and the

minimum external heat flux, $Q_{E,min}$, that will produce smoldering (replace $\overline{T}$ with $\overline{T}_{ig}$ and D_{co} with $Q_{E,min}D_{co}$). Note that $Q_{E,min}$ is found by setting $\overline{T}_m=\overline{T}_{ig}$ and $d\overline{T}/d\overline{x}\big|_{\overline{x}=0^+}= 0$ in Eq.(3-23), giving

$$Q_{E,min} D_{co} = \overline{T}_m + Q_R D_{co}\left[(1+\overline{T}_m)^4 - 1\right] . \qquad (3\text{-}32)$$

When either the ignition temperature, $\overline{T}_{ig}$, or the radiation heat losses, $Q_R D_{co}$, increase, a greater amount of energy must be supplied to the bottom of the material to produce smoldering.

Integrating Eq.(3-13) from $\overline{x}=0$ to $\overline{x}=\overline{L}$ and combining the resulting expression with Eq.(3-19) provides an expression for $\overline{v}_p$,

$$\overline{v}_p = \frac{1}{D_{cp}}\left\{ (\overline{T}_m-\overline{T}_p) - \left[1+N_R(1+\overline{T}_m)^3\right]\frac{\partial\overline{T}}{\partial\overline{x}}\bigg|_{\overline{x}=0^+} - S_c\frac{\partial}{\partial\overline{t}}\int_0^{\overline{L}}\overline{T}\,d\overline{x} \right.$$
$$\left. + S_c\overline{T}_p\frac{d\overline{L}}{d\overline{t}} + \left[1+N_R(1+\overline{T}_p)^3\right]\frac{\partial\overline{T}}{\partial\overline{x}}\bigg|_{\overline{x}=\overline{L}^+} \right\} \qquad (3\text{-}33)$$

Of the energy that is transferred downstream from the char oxidation zone (see the first two terms on the right hand side of the above equation), only a portion is consumed in the pyrolysis reaction region. Most of the energy is stored in the hot char in Region II in Fig. 3-1A [1], a small fraction is used to preheat the unburnt solid in Region I and the remainder is consumed in pyrolysis. As $\overline{t}\to\infty$,
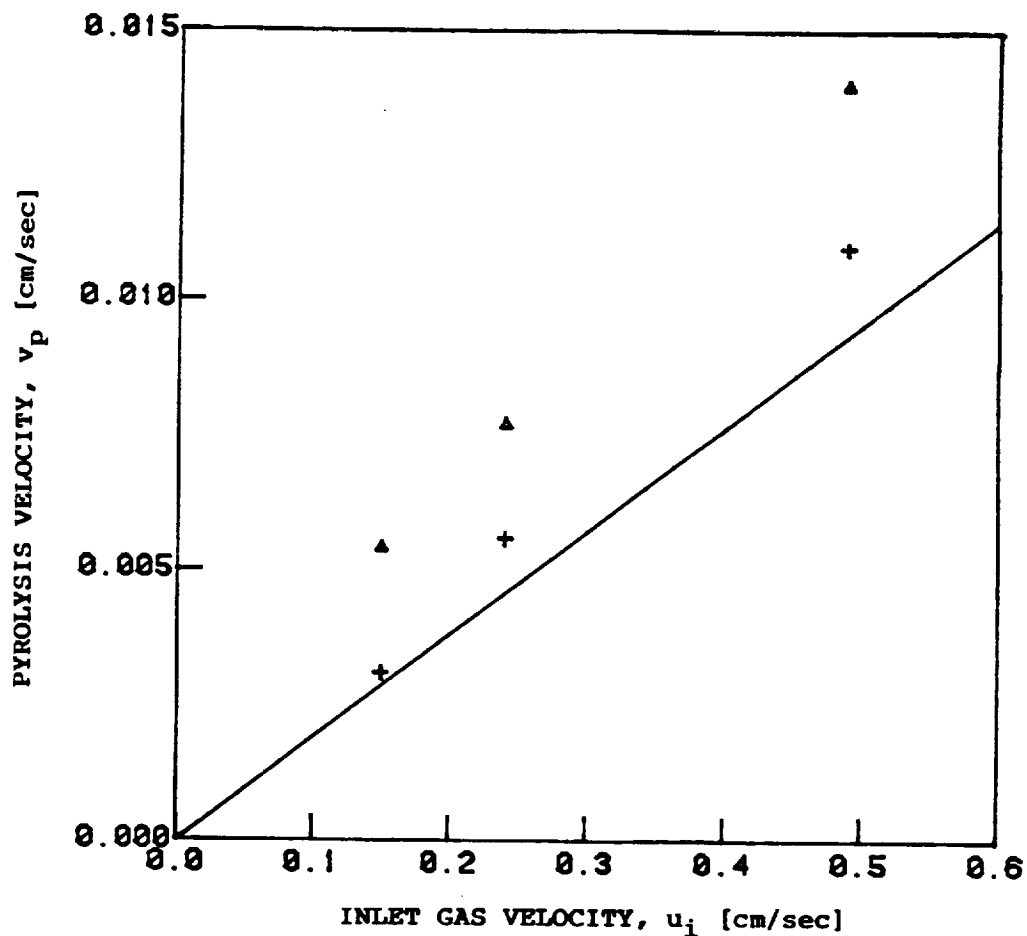
FIG. 3-5: Predicted (—) pyrolysis velocities, $v_p(t \to \infty)$, versus initial gas velocity, u_i, for cellulosic insulation with $(1-\phi)\rho_{si}=34$ kg/m^3, $c_s=2.4$ kJ/kg, $Q_p=0.37$ kJ/gm, $s_c=0.3$, $\overline{T}_m=1.8$ and $\overline{T}_p=1$. Shown are measurements [19] between thermocouples 1 and 2 (Δ) and between 2 and 3 (+) - thermocouples 1,2 and 3, were placed 7.5 cm, 10.1 cm and 11.4 cm, from the bottom, respectively.

radiative and conductive heat transfer downstream from both
reaction regions is negligible, and Eq.(3-34) gives

$$\bar{V}_p + \frac{S_c}{\mathcal{D}_{cp}} \left\{ \frac{\partial}{\partial \bar{t}} \int_0^{\bar{L}} \bar{T} d\bar{x} - \bar{T}_p \frac{d\bar{L}}{d\bar{x}} \right\} = \frac{1}{\mathcal{D}_{cp}} (\bar{T}_m - \bar{T}_p) \qquad (3\text{-}35)$$

Thus, energy consumed in the pyrolysis zone and stored by
the hot char is supplied only by gas phase convection in the
limit $\bar{t} \rightarrow \infty$. A reasonable approximation for the second term
on the left hand side of the above equation is

$$\frac{\partial}{\partial \bar{t}} \int_0^{\bar{L}} \bar{T} d\bar{x} - \bar{T}_p \frac{d\bar{L}}{d\bar{t}} = (\bar{T}_m - \bar{T}_p) \frac{d\bar{L}}{d\bar{t}} \qquad (3\text{-}36)$$

Combining Eqs.(3-35,3-36), gives

$$\bar{V}_p = \frac{d\bar{L}}{d\bar{t}} + V = \frac{(\bar{T}_m - \bar{T}_p) - \mathcal{D}_{cp} V}{S_c (\bar{T}_m - \bar{T}_p) + \mathcal{D}_{cp}} + V \qquad (3\text{-}37)$$

As $\bar{t} \rightarrow \infty$, the pyrolysis velocity approaches a constant value
which, in general, differs from the char oxidation speed.
Because the two reaction fronts move at different
velocities, no steady solutions exist and countercurrent
smolder propagation is inherently unsteady. Predicted
$\bar{V}_p(\bar{t} \rightarrow \infty)$ are compared with measurements by Ohlemiller and
Lucca [19] in Fig. 3-5.

Self-sustaining countercurrent smoldering is not
possible when $d\bar{L}/d\bar{t} < 0$, corresponding to

$$\frac{C_g (T_m - T_p)}{Q_p} < Y_{oi} \frac{\nu_{us} M_{us}}{\nu_o M_o} \qquad (3\text{-}38)$$

Solutions do not exist when the energy convected downstream from the oxidation zone is insufficient to drive the pyrolysis front.

3.3.2 CASE II: An Ash Layer Builds Below Smolder Wave

Results presented in this section are restricted to small values of the stoichiometric coefficient, s_a. In Region III in Fig. 3-1B ($-\bar{h}<\bar{x}<0$), the term involving the time derivative in Eq.(3-24) is small when $s_a \ll 1$ (note that $\bar{\rho}_s = s_a$ in Region III). Thus, $\bar{T}$ is steady in Region III when $s_a \ll 1$. When the thickness of the ash layer is much greater than x_c, radiation heat losses from below are negligible. The residual ash serves as insulation, leading to high peak temperatures. The dimensionless temperature of the oxidation zone, $\bar{T}_m$, approaches D_{co} as $\bar{t} \to \infty$. For $Y_{oi} \sim 0.2$, $T_m \sim 2,500$ C. Such high temperatures will produce flaming combustion in most materials of interest [1]. In the absence of radial heat losses, temperatures encountered in the countercurrent configuration are much higher than those in cocurrent smolder. This is due to the role of gas phase convection. For countercurrent smolder, hot gases produced in the reaction zone flow into the unburnt solid, serving to preheat the incoming fuel. While in cocurrent smolder, gas phase convection carries energy out of the system. When an ash layer builds below the smolder zone, Eq.(3-37) still determines the pyrolysis velocity, $\bar{v}_p(\bar{t} \to \infty)$. Because $\bar{T}_m$ D_{co}, Eq.(3-37) now gives

$$\frac{d\overline{L}}{d\overline{t}} = \frac{D_{cp} - D_{co}V}{D_{cp} + D_{co}} \quad .$$

(3-39)

Since D_{co}/D_{cp} is fairly large, on the order of 10, Eq.(3-39) yields $d\overline{L}/d\overline{t} \approx 1$. In dimensional form,

$$\frac{dL}{dt} \sim \frac{\rho_{gi} u_i c_g}{(1-\phi)\rho_{si} c_s} \quad .$$

(3-40)

Typically, $u_i \sim 5 \times 10^{-3}$ m/s, $(1-\phi)\rho_{si}/\rho_{gi} \sim 40$ and $c_s \sim c_g$, giving $dL/dt \sim 10^{-4}$ m/s. Note that $v \sim 3 \times 10^{-05}$ m/s for this case, so $v_p \sim 1.3 \times 10^{-4}$ cm/s.

3.4 CONCLUSIONS

A model of unsteady, countercurrent smoldering combustion propagation has been developed. The proposed application is an experiment for use on the Space Shuttle. Due to the microgravity environment, propagation of the smolder wave was assumed to be one-dimensional. Radiation heat transfer was incorporated using a diffusion approximation. Smoldering combustion was represented using a two step mechanism, which consisted of a pyrolysis reaction followed by a char oxidation reaction. A "flame" sheet approximation was used to model the oxidation zone and it was assumed pyrolysis occurs at a known temperature, T_p. In general, the two reaction fronts moved at different velocities and countercurrent smolder propagation was unsteady. Two cases were considered: (1) no residual ash,

$y_a M_a = 0$, and complete consumption of the char ; and (2) an ash layer forming beneath the oxidation zone, due to either production of ash during oxidation, $y_a M_a \neq 0$, or leakage of char through the reaction zone.

Explicit expressions were derived for the char oxidation velocity, v, the maximum temperature, T_m, and the pyrolysis front velocity, v_p, in the limit of long time. Key results included: (1) v is linearly proportional to inlet oxygen mass flux, with the proportionality constant determined from stoichiometry ; (2) in the absence of radial heat losses, v_p approaches a constant value which is, in general, different from v ; (3A) for the no residual ash case in limit of long time, T_m is determined by a balance among the energy released in the oxidation region, the energy required to preheat the gas and radiation heat losses ; (3B) when an ash layer builds below the smolder wave, radiation heat losses from the bottom are negligible in the limit $t \to \infty$ and T_m is higher than in the no ash case ; and (4) self-sustained countercurrent smoldering combustion is only possible when $c_g (T_m - T_p)/Q_p > Y_{oi} v_{us} M_{us}/y_o M_o$, i.e. solutions cease to exist when the energy convected by the gas phase is insufficient to drive the pyrolysis front.

The need for further experimental investigation of countercurrent smoldering cannot be overemphasized. Such experiments are necessary both to test the present model and

to guide future theoretical work. Especially important is the transition to flaming combustion. Results from this study indicate that such a transition is more likely in materials which form a residual ash. It is anticipated that these materials will be readily identified experimentally.

CHAPTER 4

FREE COCURRENT SMOLDERING COMBUSTION

4.1 INTRODUCTION

A schematic of the problem under consideration is shown in Fig. 4-1. The free cocurrent smoldering analysis presented in this chapter is very similar to the forced flow study in Chapter 2. The only difference is that in free flow, the inlet gas velocity, u_i, is determined by balancing buoyancy and drag forces while in forced flow, u_i is known a priori. Cocurrent smolder propagation under free flow conditions is highly dependent on the magnitude of the . buoyant forces due to the oxygen-limited nature of smoldering combustion [19,20]. Since all of the oxygen reaching the reaction zone is consumed, the total heat release is approximately proportional to the incoming oxygen mass flux, $\dot{m}''_{oi}$. Increasing the buoyancy force increases u_i, raising $\dot{m}''_{oi}$ and leading to higher temperatures and faster smolder spread [19].

Buoyant forces, which are proportional to the product $g(\rho_{gi} - \rho_g)$, can be controlled experimentally by varying either the gravitational acceleration, g, or the density difference, $\rho_{gi} - \rho_g$. The latter approach is followed in the work presented here. By changing the ambient pressure, the density of the gas and consequently the buoyancy force is varied. The rate of smolder spread through the porous fuel
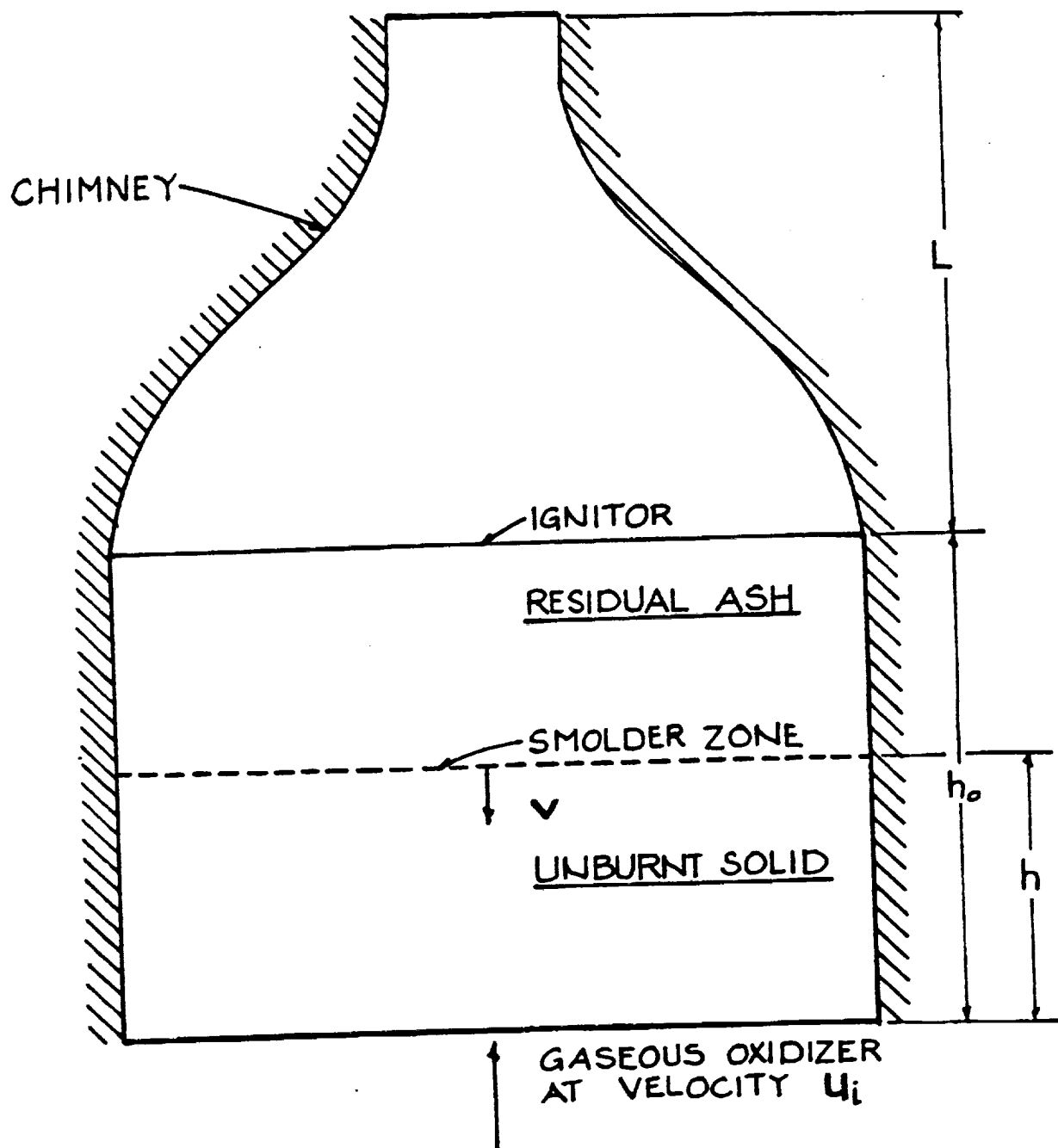
FIG. 4-1: Configuration of interest.

(alpha-cellulose) is obtained from the temperature histories of thermocouples placed at fixed intervals along the centerline of the material. A chimney, which fits on top of the fuel container (see Fig. 4-1), enhances the buoyantly driven flow of oxidizer through the porous fuel and prevents the diffusion of air to the top surface of the combustible material. Both the smolder velocity and the peak temperature are found to increase as the ambient pressure is increased.

A model of cocurrent smoldering combustion under free flow conditions is also presented. In one dimension, the gas velocity is determined from the conservation of gas mass - as a function of the inlet gas velocity, u_i. Because the pressure varies by a small amount over distances comparable the thickness of the smolder wave in the very porous fuels of interest [1], the transport equations can be solved before considering the momentum equation. Explicit expressions for the smolder velocity, v, and the final temperature, T_f, were derived in Chapter 2 by using activation energy asymptotics. Both eigenvalues, v and T_f, are functions of u_i. The quantity, u_i, is estimated by using an integral momentum analysis. Good agreement between the predictions and the measurements is observed.

4.2 ANALYSIS

4.2.1 Governing Equations

Equations (2-4 through 2-13) govern cocurrent smolder propagation. Typical properties of a bed of alpha-cellulose

TABLE 4-I: Properties of a packed bed of alpha-cellulose.[a]

ϕ	0.82
ρ_{si} [kg/m^3]	620
c_s [kJ/(kg K)]	0.84
k_{eff} [W/m K]	0.050
$k_{rad}(T_i)$ [W/m K]	~0
E [kJ/mole]	180
Q [kJ/kg]	12,500
$\mu\, a_d$ [10^{5}Newton-s/m^4]	3.0 [b] (3.7)[c]
z [10^{6}m$^{1.5}$/kg$^{0.5}$K$^{0.5}$s]	3 [d]
a	0.5
b	1
c	0.5
$\dfrac{\nu_{gp} M_{gp}}{\nu_o M_o}$	1.4

a. Properties given in refs. [28,40].

b. Darcy drag coefficient determined by matching predicted
   and measured smolder velocities for cocurrent smoldering
   of a 4 cm packed bed of alpha-cellulose (under free flow
   conditions).

c. Shown in paranthesis is the Darcy drag coefficient
   determined by direct measurement [49].

d. Pre-exponential factor determined by matching predicted
   and measured final temperatures for cocurrent smoldering
   of a 4 cm packed bed of alpha-cellulose (under free flow
   conditions).

are given in Table 4-I. The oxygen mass flux, which appears in the boundary condition in Eq. (2-11), is not known a priori in free flow because it depends on the inlet gas velocity, u_i.   A global momentum analysis is used to determine u_i in this section. In the absence of an imposed pressure gradient, the conservation of momentum requires

$$\int_{-h}^{h_o-h+L} \mu a_d u \, dx = \int_{-h}^{h_o-h+L} \phi g (\rho_{gi} - \rho_g) \, dx \, ,$$ (4-1)

where L is the chimney height, h is the height of the virgin solid and h_o-h is the char height - see Fig. 4-1. The quantity, μa_d, is the proportionality constant in Darcy's Law. While the flow resistance, a_d, is lower in the char layer, the gas phase velocity is higher. The latter is due to both gas expansion and generation in the reaction zone. Therefore, it is assumed that $a_d u$ remains constant. A step change in ρ_g from ρ_{gi} to ρ_{gf} occurs at x=0. Assuming that the flow resistance in the solid is much larger than the resistance in the chimney, the dimensionless initial velocity, $\bar{u}_i = u_i / u_c$, is given by

$$\bar{u}_i = \frac{\bar{T}_f}{1 + \bar{T}_f} \, ,$$ (4-2)

where a characteristic velocity,

$$u_c = \frac{\phi g \rho_{gi}}{\mu a_d} \left[1 + \frac{L-h}{h_o} \right] \, ,$$ (4-3)

TABLE 4-II: Dimensionless parameters affecting the smolder velocity, the final temperature and the gas velocity. In addition to the following parameters, r_{eq}, a, b, and c must be specified.

$$D_c = \frac{Q Y_{oi}}{c_{eff} T_i}$$	Dimensionless measure of the energy released in the reaction zone (varies from 0 to 40)
$$N_R = \frac{16 \sigma \ell_r T_i^3}{3 K_{eff}}$$	Dimensionless radiation conductivity (usually less than 0.1)
$$\beta' = \frac{E}{R T_i}$$	Dimensionless activation energy (varies between 50 and 70)
$$\tilde{\Lambda} = \frac{\nu_o M_o Z (R K_{eff})^{1+a} \rho_{si}^b T_i^{2a+cr^2} \Gamma(1+a)}{(\phi Y_{oi} \rho_{gi} u_i)^2 (EQ)^{1+a} (\phi D_i)^a}$$	Dimensionless pre-exponential factor (usually lies between 10^8 and 10^{10})

has been chosen by balancing buoyancy forces and drag forces. In the experiments presented here, $L/h_o \sim 10$. When $L \gg h_o$, Eq.(4-3) yields,

$$u_c = \frac{\phi g \rho_{gi} L}{\mu a_d h_o} \tag{4-4}$$

4.2.2 Asymptotic Solution of the Transport Equations

For cellulose, the Zel'dovich number, $\beta = \beta' \bar{T}_f / (1+\bar{T}_f)^2$, is on the order of fifteen [28]. Because of the Arrhenius-type dependence of the reaction rate on temperature, relatively small changes in temperature can lead to large changes in the reaction rate. Under such circumstances, it is reasonable to assume that the oxidation reaction is confined to a thin region in which the source terms in the governing equations are balanced by diffusion [2,3]. In the outer regions, convection and diffusion balance. The final temperature is determined by matching the inner solution with the outer solutions. The details of this matching process are available in Chapter 2. Dimensionless parameters governing cocurrent smolder propagation under free flow conditions are listed in Table 4-II. The dimensionless final temperature, $\bar{T}_f = (T_f - T_i)/T_i$, is determined by

$$\lambda \left[1 + N_R (1+\bar{T}_f^3) \right]^{1+a} (1+\bar{T}_f)^{a+c+2} e^{-\frac{\beta'}{1+\bar{T}_f}} = \bar{u}_i^2 f(b, r_{eq}) \tag{4-5}$$

where

$$f(b, r_{eq}) = \int_0^1 \frac{t\, dt}{\left[1 - r_{eq}(1-t) \right]^b} \tag{4-6}$$
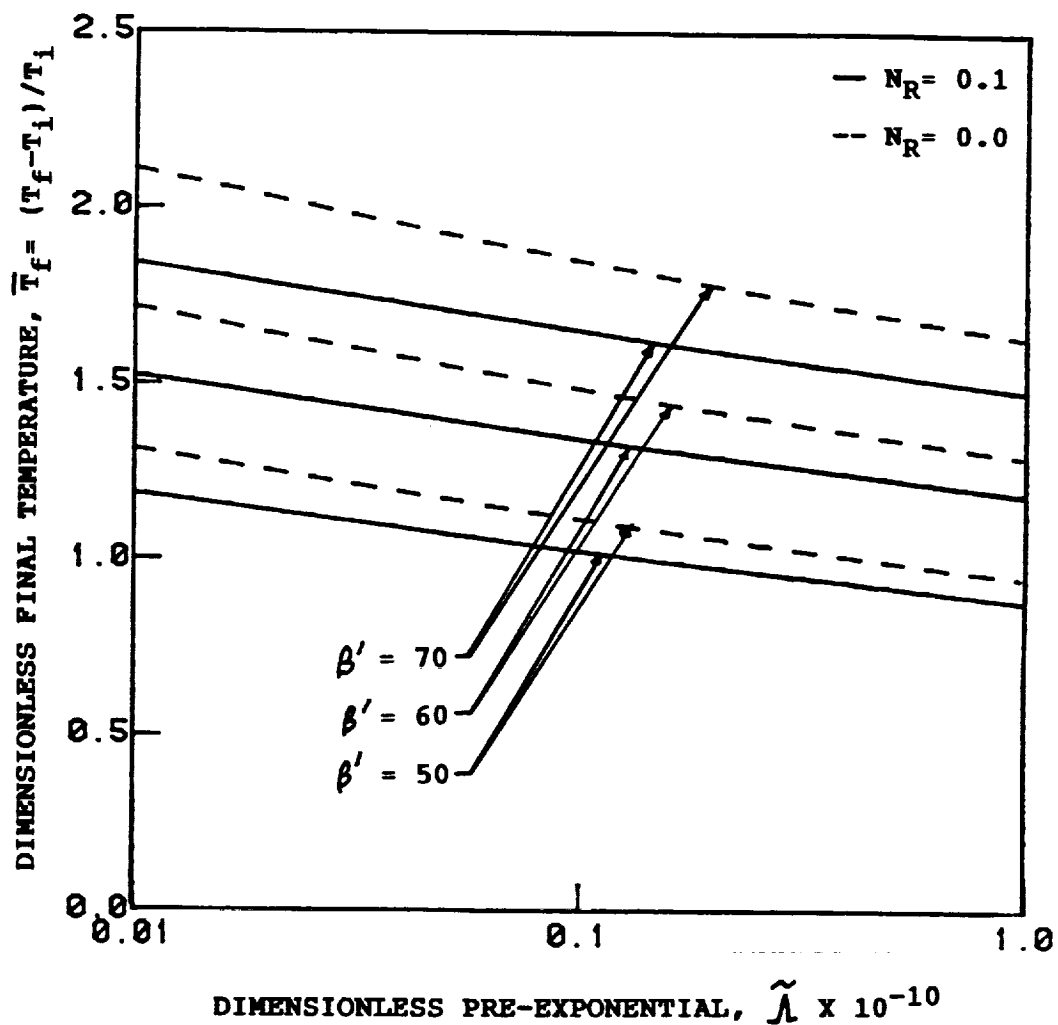
FIG. 4-2: Dimensionless final temperature, $\overline{T}_f$, versus the dimensionless pre-exponential, $\widetilde{\Lambda}$, parameterized in the dimensionless activation energy, β', and the dimensionless radiation conductivity, N_R, with a=0.5, c=0.5 and r_{eq}=0.
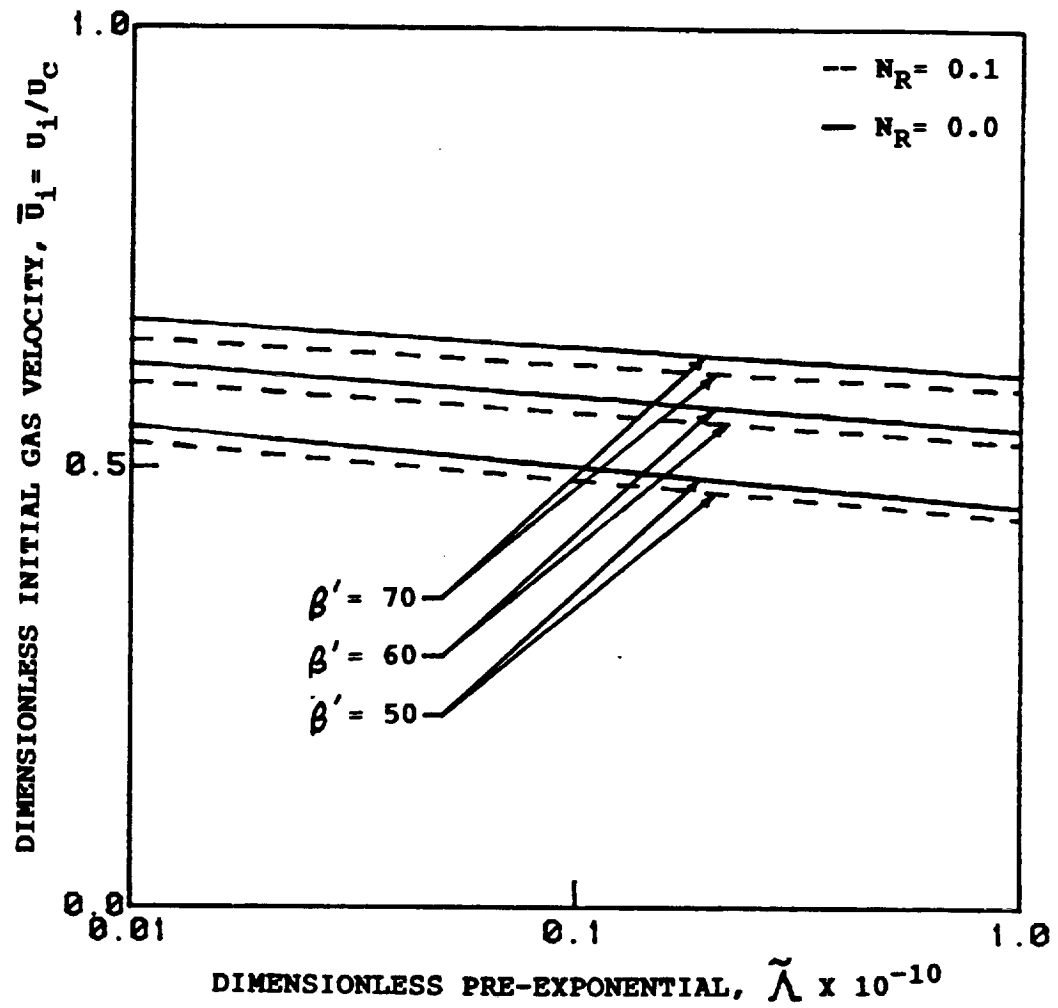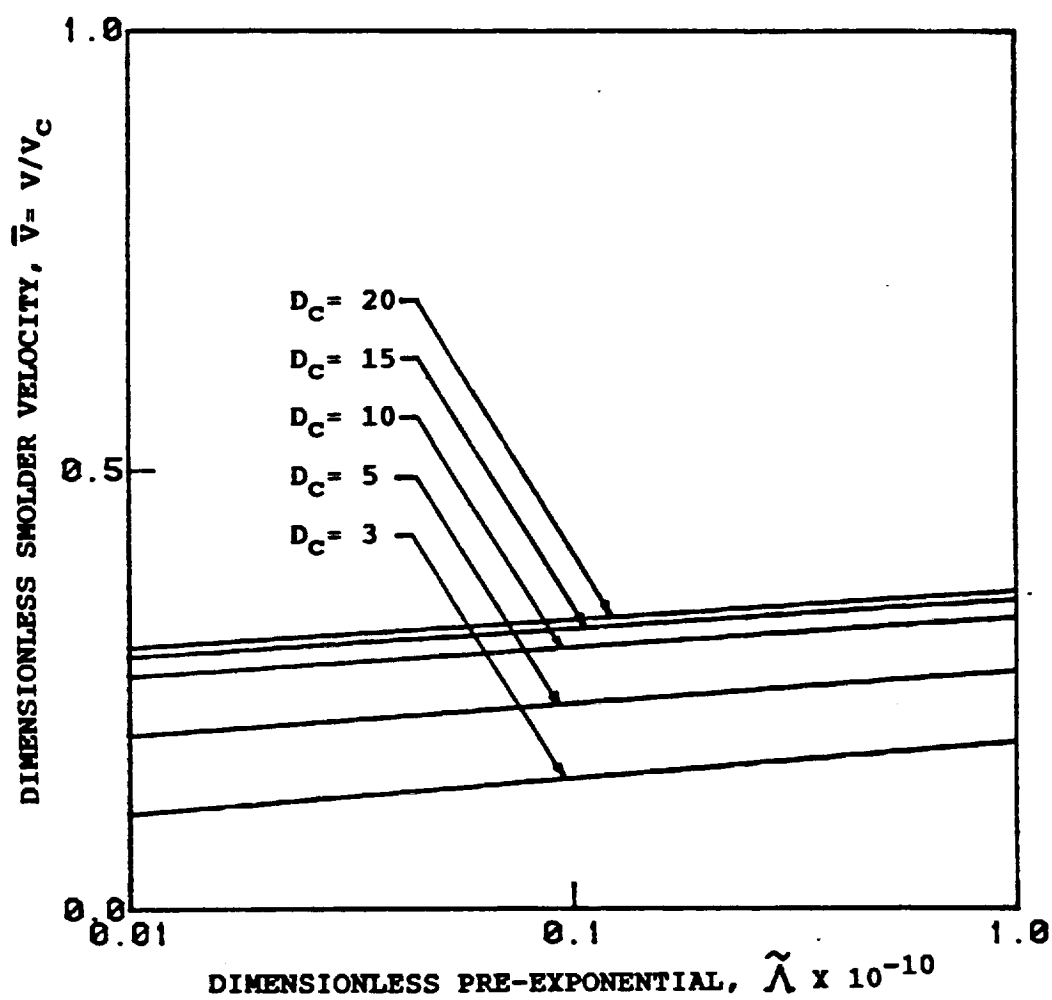
FIG. 4-3: Normalized initial gas velocity, $\bar{u}_i$, versus the dimensionless pre-exponential, $\tilde{\Lambda}$, parameterized in the dimensionless activation energy, β', and the dimensionless radiation conductivity, N_R, with $a=0.5$, $c=0.5$ and $r_{eq}=0$.

Equations (4-2,4-5,4-6) determine $\overline{T}_f$ and $\overline{u}_i$. In most cocurrent smolder combustion applications, the inverse equivalence ratio, $r_{eq} = \mathcal{Y}_{us} M_{us} \mathcal{E}_{oi} / \mathcal{Y}_o M_o \mathcal{E}_{usi}$, is small [9,19,20]. As $r_{eq} \rightarrow 0$, $f(b, r_{eq}) \rightarrow 0.5$.

4.2.3 Final Temperature, Initial Gas Velocity, and Smolder Velocity

For small values of the inverse equivalence ratio, r_{eq}, the dimensionless final temperature, $\overline{T}_f$, and the normalized initial gas velocity, $\overline{u}_i$, are independent of the constant, b, and r_{eq}. In the limit $r_{eq} \rightarrow 0$, both $\overline{T}_f$ and $\overline{u}_i$ depend on five parameters, the dimensionless radiation conductivity, N_R, the dimensionless activation energy, β', the dimensionless pre-exponential, $\tilde{\Lambda}$, and the constants, a and c — see Eqs.(4-2,4-5,4-6). Figure 4-2 illustrates the variation of $\overline{T}_f$ with N_R, β', and $\tilde{\Lambda}$, for a= 0.5 and c= 0.5. Note that $\overline{T}_f$ decreases logarithmically with $\tilde{\Lambda}$. Thus, for a given fuel, T_f depends only on the characteristic oxygen mass flux, $\dot{m}''_{oc} \sim Y_{oi} \rho_{gi} u_c$, increasing logarithmically with $\dot{m}''_{oc}$. Buoyancy affects T_f through u_c, which is proportional to the product, $g\rho_{gi}$. Consequently, $\dot{m}''_{oc}$ is proportional to the square of the ambient pressure — that is, $\dot{m}''_{oc} \sim gP_a^2$.

As shown in Fig. 4-3, $\overline{u}_i$ is weakly dependent on $\tilde{\Lambda}$ and N_R. For a particular fuel, u_i, is fairly constant. Over a wide range of conditions, $\overline{u}_i \simeq 0.6 \pm 0.1$. That is, setting $\overline{u}_i$ equal to 0.6 usually introduces less than a 15% error. As a first approximation, $u_i \approx 0.6 u_c$, where u_c is determined from Eq.(4-4). Consequently, u_i is approximately proportional to

FIG. 4-4: Normalized smolder velocity, v, versus the dimensionless pre-exponential, $\tilde{\Lambda}$, parameterized in the dimensionless heat release, D_c, with β'=70, a=0.5, c=0.5, N_R=0 and r_{eq}=0.

the characteristic buoyancy force, $g\rho_{gi}$.

A normalized smolder velocity, $\bar{v}=v/v_c$, is given by

$$\bar{v} = \bar{u}_i \left[\frac{1}{\bar{T}_f} - \frac{1}{D_c} \right] , \tag{4-7}$$

where a characteristic smolder velocity,

$$v_c = \frac{Q \dot{m}''_{oi}}{(1-\phi)\rho_{si} C_{eff} T_i} , \tag{4-8}$$

is defined by the balancing the energy released in the reaction zone and the energy required to raise the temperature of the solid from T_i to T_f. For a given solid fuel, $\bar{v}$ is affected by two parameters, the dimensionless pre-exponential, $\tilde{\Lambda}$, which is inversely proportional to $\dot{m}''_{oc}$ ($=Y_{oi}\rho_{gi}u_c$), and the dimensionless heat release, D_c, which is proportional to Y_{oi}. A plot of $\bar{v}$ versus $\tilde{\Lambda}$, parameterized in D_c, with $\beta'=70$, a=0.5, c=0.5, $N_R=0$, and $r_{eq}=0$, is shown in Fig. 4-4. Decreasing D_c leads to lower values of $\bar{v}$. Smoldering extinguishes when $D_c=\bar{T}_f$, corresponding to $\bar{v}=0$. Because $\bar{v}$ varies slowly with $\tilde{\Lambda}$, $v \sim v_c$. Using Eqs.(4-4,4-8),

$$v \approx \frac{Q Y_{oi} g \phi^2 \rho_{gi}^2 L}{(1-\phi)\rho_{si} C_{eff} T_i \mu a_d h_o} . \tag{4-9}$$

The smolder velocity varies quadratically with the ambient pressure and varies linearly with the gravitational acceleration (that is, $v \sim gP_a^2$).
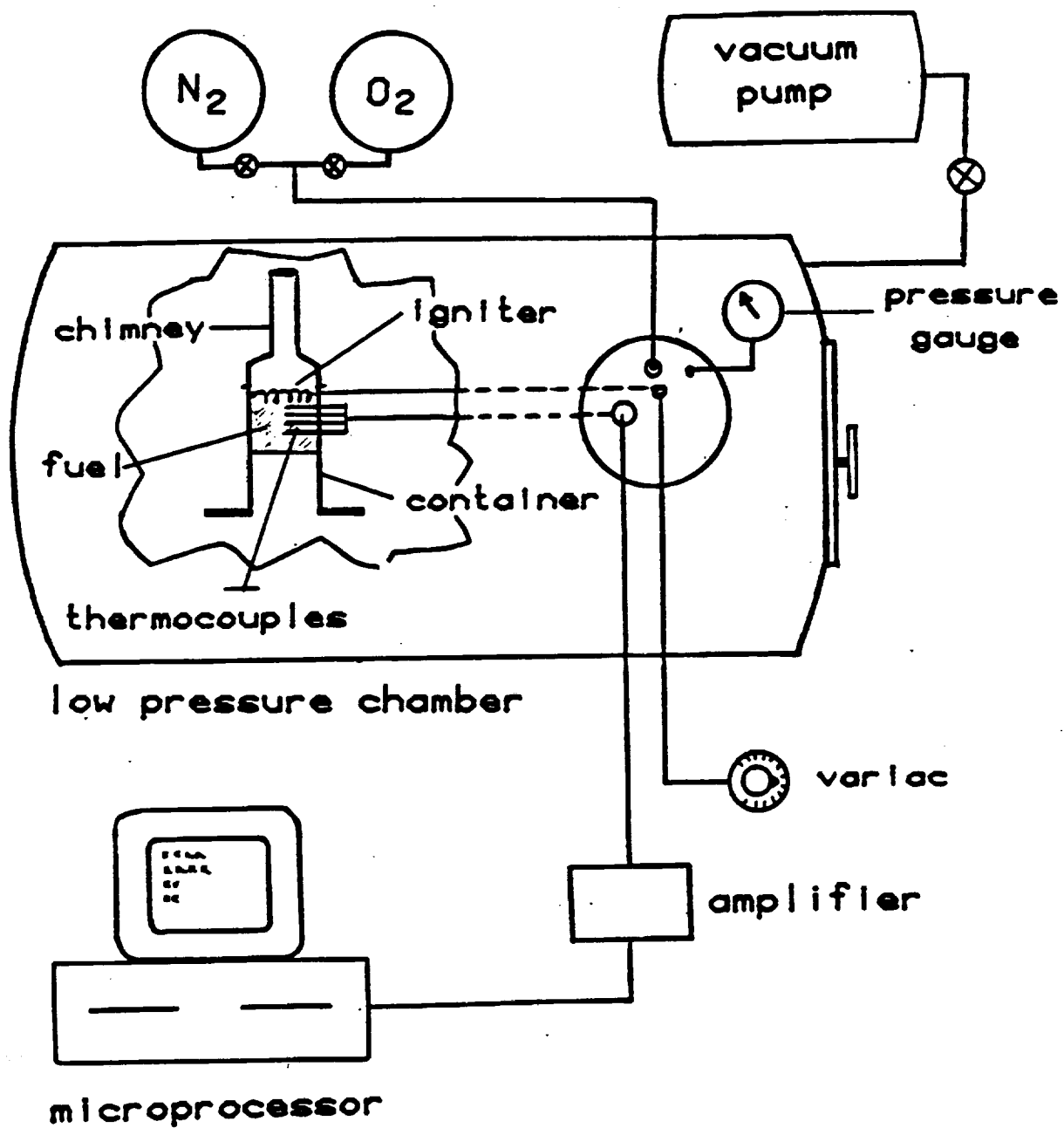
FIG. 4-5: Experimental installation.

4.3 EXPERIMENTS

Experiments are performed to determine the effect of ambient pressure, and consequently of buoyancy, on the rate of smolder spread through a porous combustible material. A schematic diagram of the experimental installation is shown in Fig. 4-5. The experiments are carried out in a cylindrical pressure vessel, 1.8 m in diameter and 3.3 m long. A vacuum pump or a compressor is used to set the vessel pressure below or above atmospheric pressure. The oxygen concentration in the vessel can be varied by adding oxygen or nitrogen from pressurized bottles. Acrylic windows located at opposite sides of the vessel provide optical access to the test area. The fuel/container unit is held by a frame in the middle of the test area, avoiding obstruction of the flow of air in and around the fuel container.

The porous fuel is contained in a vertical Pyrex cylinder, 0.07 m in diameter and 0.16 m long. These dimensions, in particular the cylinder diameter, are selected to reduce to a minimum, the depletion of oxygen in the vessel during the fuel combustion process, while ensuring a one-dimensional smolder spread process in a region of at least 2 cm in diameter around the cylinder axis. Small holes placed longitudinally along the side of the cylinder allow the positioning of thermocouples or gas sampling probes in the porous material. A nichrome wire electrical ignitor can be positioned at the top or the bottom of the cylindrical container to initiate the

smoldering process. As an alternative ignition method, an easily ignitable fuel (for example, cellulose soaked in heptane) is thinly spread on top of the porous material and ignited with a small pilot flame or a spark. Flaming combustion of the volatile fuel initiates the smoldering combustion of the porous combustible. A chimney, 0.33 m long and 0.03 m in diameter, tapered at the bottom to a diameter of 0.07 m is fitted on top of the fuel container. The chimney is used to both enhance the buoyantly driven flow of oxidizer through the porous fuel and to prevent the diffusion of air to the top surface of the combustible material. The fuel container and the chimney are insulated with a fiber-glass jacket to reduce heat losses to the environment.

The rate at which smoldering spreads is measured from temperature histories of the thermocouples embedded in the porous fuel with their junction placed at fixed distances along the cylinder axis. Four Chromel-Alumel thermocouples, 0.8 mm in diameter, are embedded in the porous fuel at 5 or 10 mm apart. The emf from the thermocouples is amplified to volt levels and processed in a real time acquisition microcomputer. With the fuel temperature histories, the rate of spread of smoldering combustion is calculated from the time lapse of reaction zone arrival to two consecutive thermocouples, and the known distance between thermocouples. The arrival of the smolder reaction zone at the thermocouple

position is characterized by a maximum in the temperature profile. Under most experimental conditions this maximum is not sharply defined, introducing inaccuracies in the definition of the smolder front arrival time and consequently in the calculation of the smoldering spread rate. In spite of this problem, the thermocouple probing method is considered one of the most accurate methods to measure the rate of smolder spread.

4.4 RESULTS AND COMPARISON

Results presented in this work are from experiments conducted using alpha-cellulose powder as a porous combustible fuel. A fixed amount (by weight) of alpha-cellulose was loosely packed in the cylindrical container filling a constant volume, thereby keeping an approximately constant void volume fraction. The cellulose was supported at the bottom by a wire mesh which was attached to the cylinder surface 40 mm from the top of the cylinder. The upper cellulose surface was kept flush with the top cylinder rim. This 40 mm cellulose bed height was found to be the maximum at which the present experimental configuration could operate. For larger bed heights, the pressure drop through the porous solid is too large to be overcome by the chimney generated buoyancy, particularly at pressures below atmospheric. The resulting buoyantly induced flow of air is not large enough to sustain the progress of the smolder reaction. Although longer fuel beds could be tested by increasing the chimney height, the 40 mm fuel height is
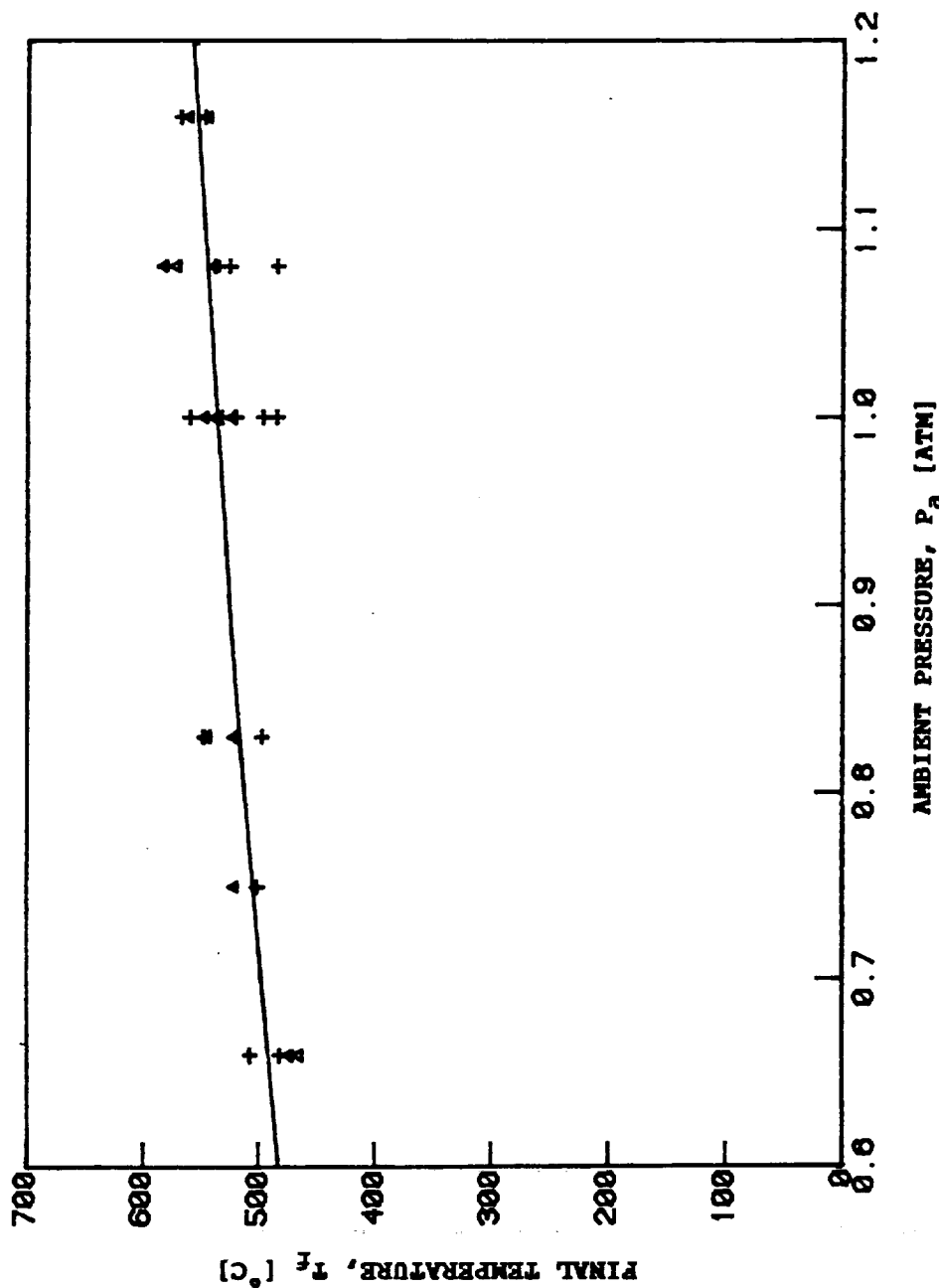
FIG. 4-6: Predicted (——) peak temperature, T_f, versus ambient pressure, P_a, for a 4 cm bed of alpha-cellulose with the properties given in Table 4-I. Measurements for two thermocouple locations, number two (+) and number four (▲), are also shown.

sufficient to provide the information sought in this work. All of the experiments were conducted with an approximately constant void volume fraction of 0.82. The void volume fraction was estimated from weight of the alpha-cellulose, the volume it occupies and the cellulose density given in Table 4-I. After coating the alpha-cellulose with a thin layer of gold, an electron microscope was used to investigate the structure of the material. At a magnification of 300 X, it was seen that the material is formed by long, interlaced, cellulose fibers. In the absence of reliable experimental data, photographs, such as the one shown Chapter 2, can be used to estimate various properties, including the Darcy drag coefficient, a_d, and the radiation path length, ℓ_r.

Measured peak temperatures at two thermocouple locations are presented in Fig. 4-6, for various values of the ambient air pressure. For these measurements, four thermocouples were placed, in most cases, 5 mm apart from each other with the first thermocouple located 15 mm from the top of the cellulose surface. In a few tests, the thermocouples were positioned at distances 10 mm apart. Peak temperatures predicted by the theoretical model, with the parameters given in Table 4-I, are also shown in Fig. 4-6. The value of the activation energy given in Table 4-I was suggested by Moussa et al [28], who modelled smolder spread in horizontal, cylindrical, cellulose fuel elements. Because
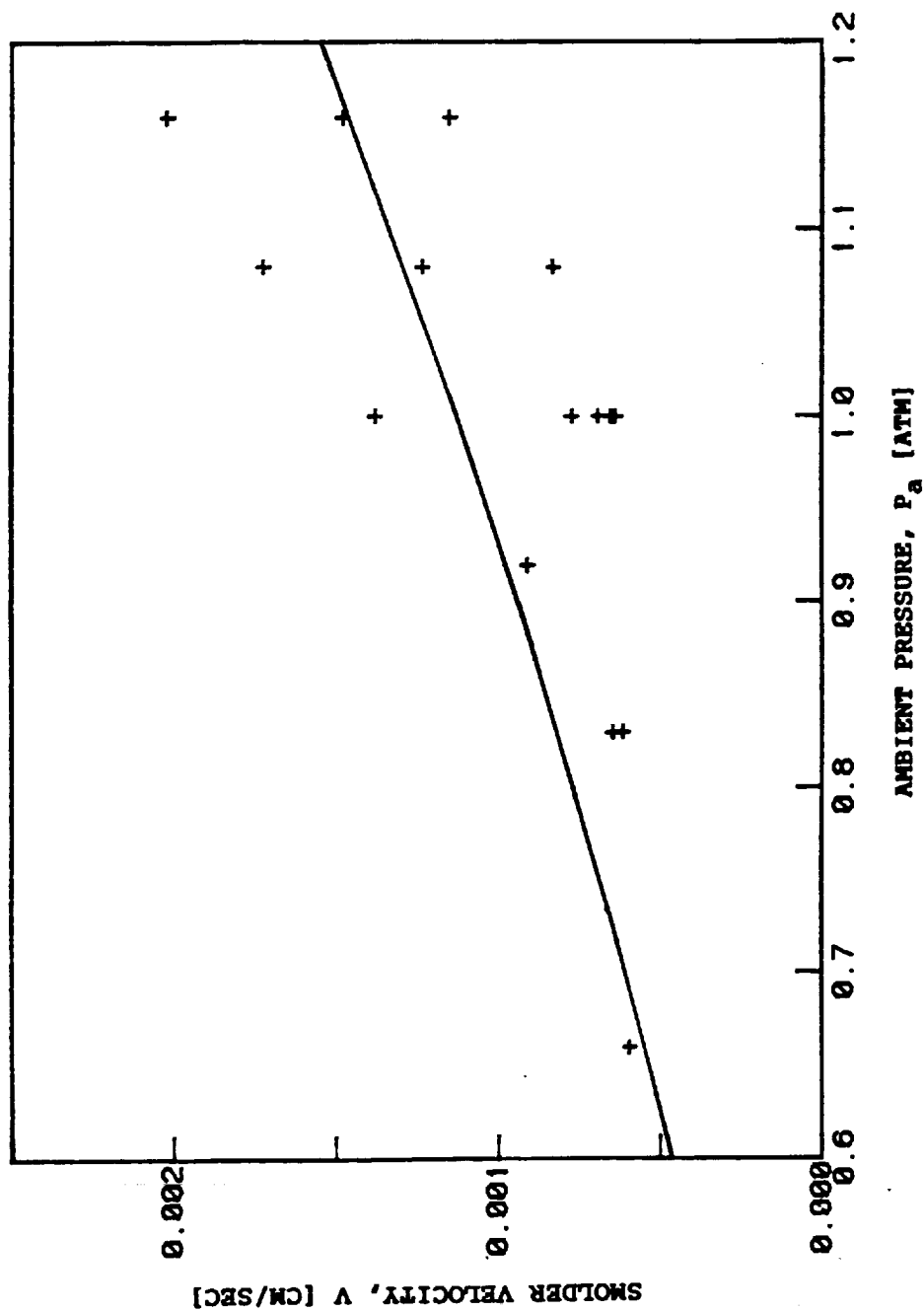
FIG. 4-7: Measured (+) and predicted (——) smolder

velocities, v, plotted versus ambient pressure, P_a, for a 4 cm

bed of alpha-cellulose with the properties given in Table 4-I.

char oxidation occurs on the outer surface of the cylinder, Moussa et al represented the reaction rate by an overall Arrhenius expression based on the surface area of the cylinder. Consequently, there is some uncertainty in the precise value of the pre-exponential factor in Eq.(2-10), for this reaction rate expression is based on a volumetric basis and the oxidation reaction occurs well within the outer boundaries of the porous solid. The value of the pre-exponential factor given in Table 4-I was selected by matching calculated and measured peak temperatures at one point. Because the distance over which buoyancy acts is much larger than the thickness of the alpha-cellulose bed, the peak temperature is fairly constant as smolder wave propagates. As shown in Fig. 4-6, there is very little difference between the peak temperatures at the second and fourth thermocouples. Overall, there is good qualitative agreement between the peak temperatures predicted by the theoretical model and those determined from experiments.

Measured rates of smolder spread through the alpha-cellulose bed are presented in Fig. 4-7 for several ambient air pressures. The smolder velocities were calculated from the outputs of the second and fourth thermocouples, which were placed 20 mm and 30 mm below the top surface of the cellulose bed, respectively. These thermocouples were chosen because they provided the most reproducible data. As is seen from the experimental data plotted in Fig. 4-7, there is scatter in the measurements, particularly at the higher

ambient pressures. This scatter is primarily attributable to inaccuracies in the determination of the time at which the smoldering front arrives at the thermocouple location in question. These errors are especially noticeable at higher pressures because the smolder velocity is higher. Small variations in the cellulose void volume fraction and uncertainty in the precise location of the thermocouples also contribute to the scatter in the data.

For comparison purposes, theoretically predicted smolder velocities are also presented in Fig. 4-7. Because of uncertainty in the Darcy drag coefficient during smolder propagation, the value used in these calculations was selected by matching the predicted and measured smolder velocities at one point. Although the comparison between theory and experiments can only be viewed as qualitative, it is seen from Fig. 4-7 that the theoretical model predicts very well the general trend of the experimental results, with slower smolder spread as the ambient pressure decreases. As discussed earlier, both the total heat release and the smolder velocity are proportional to inlet oxygen mass flux. Diminishing either the gas velocity or the density of the oxygen reduces the amount of oxygen reaching the reaction zone, leading to smaller smolder velocities. Decreasing the ambient pressure has two major effects. Firstly, the buoyancy force is lessened, leading to lower air flow velocities. Secondly, the density of oxygen is
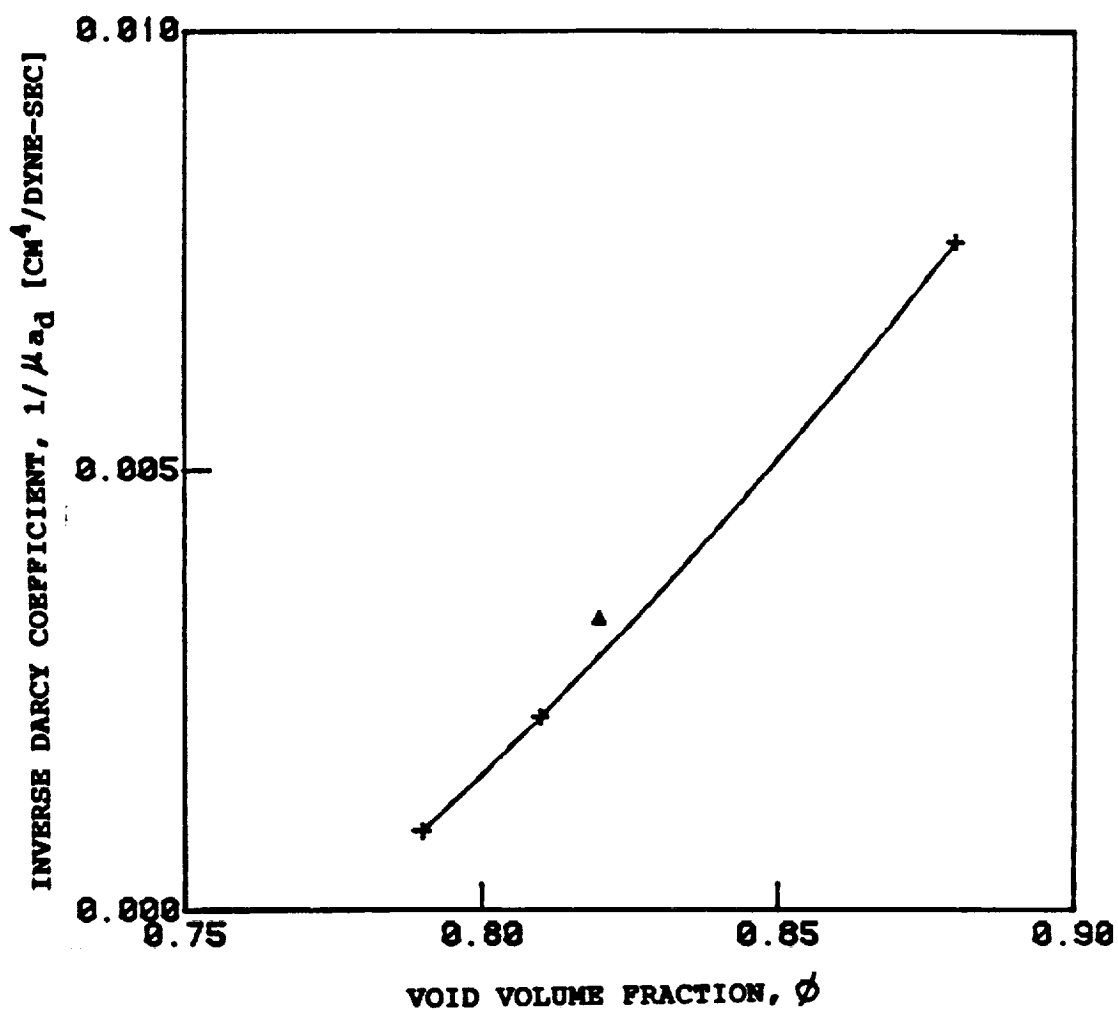
FIG. 4-8: Measured (+) inverse Darcy coefficients, $1/\mu a_d$, for various void volume fractions, ϕ, and a quadratic fit (—) through the data. Also shown is the theoretical value ($\blacktriangle$) obtained by matching predicted and measured smolder velocities.

reduced. Consequently, the smolder velocity decreases quadratically with the ambient pressure. Measurements for an alpha-cellulose bed support this hypothesis - see Fig. 4-7.

Experimentally determined Darcy drag coefficients are exhibited in Fig. 4-8 for several values of the void volume fraction [49]. These experiments were conducted in the absence of combustion. A fixed amount (by weight) of alpha-cellulose was placed in a bed of roughly the same depth (40 mm) as that used in the smoldering combustion experiments. The Darcy coefficient was estimated by imposing several known pressure drops through the porous solid and measuring the resulting air flow velocities. Also shown in Fig. 4-8 is the value of the Darcy coefficient calculated by matching predicted and measured smolder velocities for a void volume fraction of 0.82. This value is in close agreement with the direct measurements, supporting the hypothesis that the product of the Darcy drag coefficient and the gas velocity, $a_d u$, remains constant - see section 4.2.1.

An interesting experimental observation is that smoldering combustion does not spread at ambient pressures below 0.6 atmospheres. Recall that the extinction limit proposed in section 4.2.3 predicts that, for a given initial oxygen mass flux, there is a critical oxygen concentration below which steady solutions do not exist. Smolder propagation will cease when all of energy released in the reaction zone is used to heat the incoming gas. However, because heat losses have been ignored in the analysis, this

limit does not give a critical ambient pressure below which smoldering extinguishes. The total heat released in the reaction zone decreases quadratically with the ambient pressure. When the heat release is of the same order of magnitude as the heat losses, smoldering propagation will stop. This result is also valid for laminar premixed flames [2,33].

Therefore, there exists a critical oxygen flow rate, which depends on the magnitude of the heat losses, below which smoldering extinguishes. For the experimental apparatus employed in this study, utilizing an alpha-cellulose fuel with void volume fractions equal to or smaller than the one used here and an air oxidizer, smoldering combustion will not take place if species diffusion is the only mechanism to transport the oxidizer to the reaction zone. This result is especially important for the potential development of the smoldering combustion process under micro-gravity conditions, in space vehicles for example, since buoyancy forces are negligible. Under such circumstances, cocurrent smoldering combustion will extinguish unless the oxidizer is transported by a forced air flow.

4.5 CONCLUSIONS

A model of one-dimensional, steady, cocurrent smoldering combustion under free flow conditions has been

developed. Smoldering was represented using a finite-rate, one-step reaction mechanism. Explicit expressions for the smolder velocity, the final temperature and the initial gas velocity were derived. Smolder velocities and peak temperatures predicted by the theory for a packing of alpha-cellulose were compared with experimental results for values of the ambient pressure ranging from 0.6 to 1.2 atmospheres. Primarily because of difficulty in accurately determining the time at which the smolder front reaches a particular thermocouple location, there is scatter in the experimental data. This scatter is especially noticeable at pressures above atmospheric. Overall, there is good qualitative agreement between predictions and measurements.

Smoldering combustion propagation is highly dependent on a steady flow of oxidizer reaching the reaction zone. Both experiments and theory suggest that the smolder velocity increases approximately linearly with the oxygen mass flux, while the final temperature increases fairly slowly (in fact, logarithmically) with this flow rate. Extinction is observed to occur if the flow rate is below a critical value. This indicates that, at least for alpha-cellulose with void volume fractions equal to or smaller than the one tested in this work, diffusion of oxidizer toward the reaction zone is not a sufficient transport mechanism to sustain the cocurrent smoldering combustion process. This result is particularly important for natural convection smoldering combustion under microgravity

conditions since buoyancy forces are very small, and the oxidizer can only be transported to the reaction zone by diffusion. The present study suggests that for cocurrent smoldering combustion to occur in a microgravity environment, a flow of oxidizer must either be forced through the fuel, or the porous fuel must have a large void volume fraction, a small Darcy coefficient, a low activation energy and a large effective thermal conductivity. That is, the solid fuel must present minimum obstruction to the free flow of gases, and it should possess properties that favor the transport of heat and mass by diffusion.

However, the present work can only be viewed as preliminary. Heat losses from the sides of the cylinder must be included in the analysis to accurately predict the extinguishment of cocurrent smoldering combustion. A detailed experimental investigation of the smolder extinction process is needed. Experiments with other porous fuels must be undertaken to determine the generality of the conclusions reached in this study. In particular, accurate determination of the conditions at which smoldering combustion will occur in a microgravity environment is necessary.

CHAPTER 5

FUTURE RESEARCH

5.1 INTRODUCTION

Further theoretical and experimental investigation of both cocurrent and countercurrent smoldering combustion is anticipated. The goal of this research program is to design a smoldering experiment for use on the Space Shuttle. The current ground based experimental program will be continued through the next grant period. Before making further refinements in the theory, measurements are needed to test the current analytical models. Of particular interest is the one-dimensional propagation assumption. It is anticipated that purely 1-d propagation will only be possible in a microgravity environment. After establishing the range of validity of the 1-d approximation, simplifications in the chemistry and the effect of variable properties will be scrutinized. Comparisons between theory and experiments will hopefully lead to refinements in the current analytical models. A discussion of the proposed experiments and possible comparisons between existing theory and future measurements follows.

Many materials can sustain smoldering combustion. Smoldering has been observed in coal [3,4], cotton [5,6], paper [7], wood [12-14], thermal insulation materials [15] and various dusts [16,17]. Additionally, smoldering

combustion can occur in different foams, including PU16 [29] and PT34 [29] foams, Product Research Committee foams GM-21 [29] and GM-25 [20], all of which are flexible polyurethane foams, and the rigid isocyanurate foam designated GM-41 [19]. However, GM-21 and PT34 foams will undergo self-sustained smoldering only when they are covered with cotton fabric [29]. A discussion of the ability of rigid and flexible polymer foams to smolder is given by Ohlemiller and Rogers [9]. Because comparisons between theory and measurements are sought, only materials whose properties are readily available in the literature will be utilized as fuels in the proposed experiments. Detailed smolder reaction mechanisms are available for alpha-cellulose [28], a GM-25 flexible polyurethane foam [20], wood dust [32] and cellulosic insulation materials [46]. These mechanisms are discussed in Appendix A.

Several researchers [19,22,23] have investigated smoldering combustion in the cocurrent configuration experimentally. Rogers and Ohlemiller [22] measured the smolder velocity, v, and the final temperature, T_f, in a PRC GM-25 polyurethane foam. While holding the ambient pressure, P_a, fixed at 1 atm, the initial oxygen mass fraction, Y_{oi}, was varied from 0.18 to 0.44 for two values of the initial gas velocity, u_i, 0.04 and 0.15 cm/sec. Resulting v ranged from 0.0056 to 0.022 cm/sec, and increased approximately linearly with the initial oxygen mass flux, $\dot{m}_{oi}''$. The final

temperature, T_f, increased slowly with $\dot{m}_{oi}''$, varying from 410 to 490°C. Ohlemiller and Lucca [19] studied the cocurrent smoldering of cellulosic insulation materials and of a polyisocyanurate polymer, PRC foam GM-41. The latter was mechanically ground into particles with a mean diameter of several hundred microns. Both Y_{oi} and P_a were held fixed at 0.23 and 1 atm, respectively, while u_i was varied from 0.04 to 0.77 cm/sec, yielding v ranging 0.004 to 0.04 cm/sec. Dosanjh et al [23] considered the free cocurrent smoldering of a packing of alpha-cellulose fibers. While fixing Y_{oi} at 0.23, P_a changed from 0.5 to 1.2 atm, giving v between 0.0007 and 0.002 cm/sec.

Relatively little attention has been given to smoldering combustion in the countercurrent configuration [1]. Ohlemiller and Lucca [19], who studied the countercurrent smoldering of cellulosic insulation, measured the char oxidation velocity, v, the pyrolysis front velocity, v_p, and the maximum temperature, T_m, as u_i changed from 0.15 to 0.49 cm/sec, with Y_{oi} and P_a fixed at 0.23 and 1 atm, respectively. Both v, which ranged from 0.001 to 0.0029 cm/sec, and v_p, which varied from 0.003 to 0.014 cm/sec, increased roughly linearly with u_i, while T_m, which fell between 540 and 590°C, was independent of u_i.

The need for detailed experimental study of the transition of smoldering to flaming is clear. Because interest in smoldering is in large measure due to fire safety concerns, a good fundamental understanding of the

transition to flaming is essential. Unfortunately, very little is known about this phenomenon. In a recent review article, Ohlemiller [1] states that "transition to flaming has only been superficially explored experimentally and not modeled at all." In passing, Rogers and Ohlemiller [22] noted that flaming was observed during the cocurrent combustion of a GM-25 polyurethane foam when Y_{oi} was above 0.6 and extinction occurred for Y_{oi} below 0.1. However, no data was presented to support these claims. Moussa et al [28] and Ortiz-Molina et al [29], who studied smolder spread in horizontal, cylindrical, alpha-cellulose and polyurethane fuel elements, reported that flaming occurred when the oxygen partial pressure was raised above a critical value. This critical value decreased as the oxygen mole fraction was increased.

5.2 EXPERIMENTS

Experiments will be performed on cocurrent and countercurrent smoldering combustion of porous fuels under forced flow conditions. These experiments will take place in a large pressure chamber in which variations in gravity can be simulated by varying the buoyancy force, $g(\rho_{gi} - \rho_g)$, by changing the ambient pressure, P_a – note that the gas density is linearly related to P_a through the ideal gas law. The porous fuel is placed in a vertical pyrex cylinder, $\gtrsim 10$ cm in diameter and $\gtrsim 20$ cm tall. Thermocouples placed approximately one centimeter apart along the centerline of

this cylinder are used to determine the temperature histories inside the cylinder. Reaction zone propagation velocities are obtained from these temperature histories and the known distances between thermocouples. Forced flow conditions will be generated using a small scale combustion tunnel which will be totally contained within the pressure chamber. This tunnel consists of a small settling chamber connected to the test section by a converging nozzle. The flow of oxidizer is induced with a low power compressor. The flow is controlled and metered with a mass flow controller activated by a microcomputer (which is also utilized for data acquisition). An electrically heated wire grid is to be used as a planar ignition source.

Reaction zone propagation speeds and peak temperatures will be determined for a wide range of conditions. Several materials, including alpha-cellulose beds at different packing densities and polyurethane foams, will be utilized as fuels. The inlet gas velocity, u_i, the initial oxygen mass fraction, Y_{oi}, and the ambient pressure, P_a, will be varied independently. As discussed in the introduction, the effect of modifying Y_{oi} and u_i on propagation velocities and peak temperatures has been studied previously [19,22]. Consequently, the emphasis of the proposed experiments will be on quantifying the effect of altering P_a. Only P_a greater than 0.5 atm will be considered, for at very low pressures the reaction rates are strongly dependent on P_a. As P_a decreases, buoyant forces, which are proportional to P_a,

become less important. It is anticipated that there will be better agreement between theory and measurements at lower values of P_a because, strictly speaking, the one-dimensional propagation assumption is only valid in a microgravity environment. Moreover, comparisons between measurements and predictions at various P_a will establish the range of validity of the one-dimensional propagation approximation.

Extinction of smoldering can be investigated in both configurations. Unlike countercurrent smolder, smoldering in the cocurrent configuration becomes steady in a relatively short period of time [19]. Consequently, initial experiments will focus on the cocurrent configuration. An extinction limit will be identified by performing experiments at a wide range conditions and noting when smoldering extinguishes. When the results of these experiments are plotted in the three dimensional space consisting of the regions $Y_{oi}>0$, $u_i>0$ and $P_a>0$, an extinction surface can be defined for each fuel under consideration. For a given fuel, self-sustained smoldering combustion is only possible for points above its extinction surface. Determination of such an surface requires considerable trial and error. However, considerable simplification is possible, for in the one-dimensional propagation models neither u_i nor P_a appear independently, only their product appears. Therefore, when two or three dimensional effects are unimportant, the extinction surface collapses onto a line in the coordinate system with axes $Y_{oi}>0$ and $u_iP_a>0$. Future experiments will

identify critical values of P_a below which smoldering
extinguishes by fixing Y_{oi} (and u_i) and lowering P_a until
extinction occurs. This critical value of P_a will decrease
as Y_{oi} increases.

At the opposite extreme, raising either Y_{oi}, u_i or P_a
can lead to flaming combustion. The transition of smoldering
to flaming will be studied experimentally in both
configurations. In the countercurrent configuration, flaming
is much more likely when a residual ash forms beneath the
the smolder wave. This residual ash serves as insulation,
and its formation leads to considerably higher temperatures.
Different porous fuels will be classified according to their
ability to produce such an ash. For each fuel under
consideration, an attempt will be made to identify a
critical temperature, T_{flame}, above which flaming combustion
is observed. Provided that such a critical temperature can
be identified, the analytical models developed in Chapters 2
and 3 can be used to determine a flaming limit by setting
the peak temperature predicted by these models equal to
T_{flame}. Determination of such a limit is discussed in the
following section.

5.3 COMPARISONS WITH THEORY

Possible comparisons between the measurements described
in the previous section and the existing theory are
discussed in this section. In the forced countercurrent
smoldering experiments, the char oxidation velocity, v, the
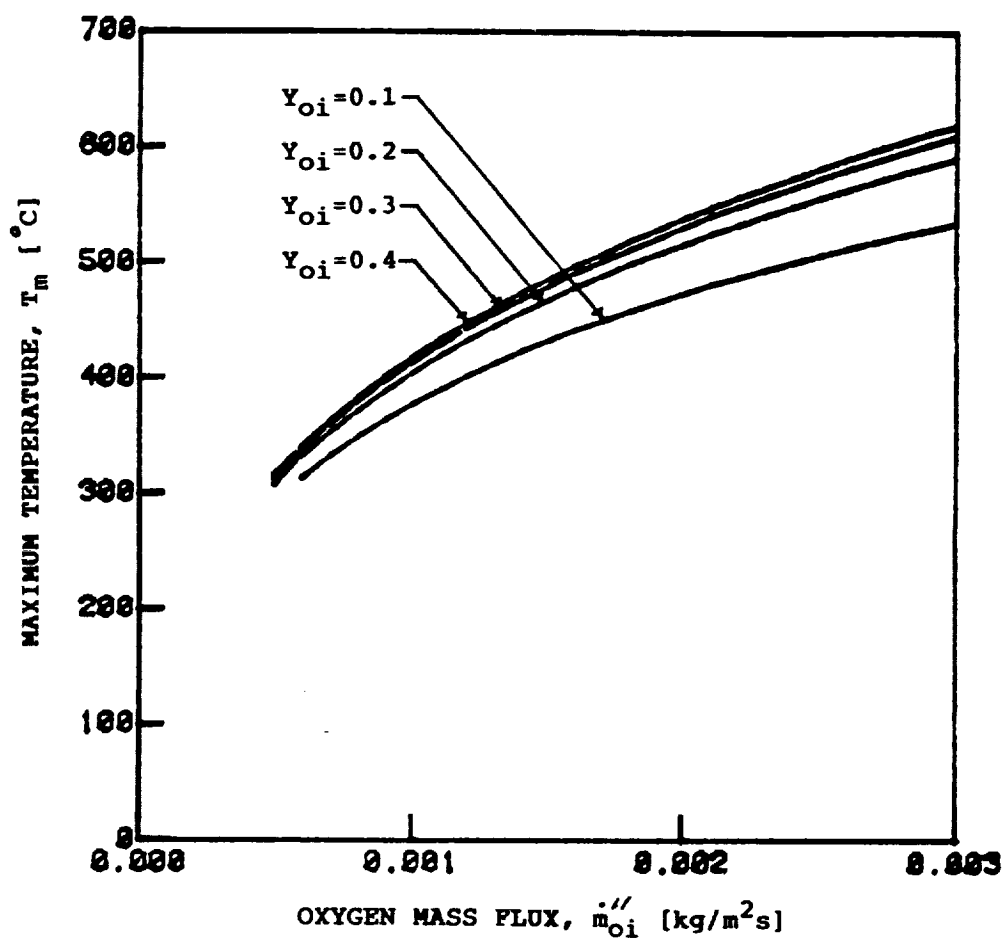
FIG. 5-1: Maximum temperature, $\overline{T}_m(\overline{t} \to \infty)$, as a function of inlet oxygen mass flux, $\dot{m}''_{oi}$, parameterized in the initial oxygen concentration, Y_{oi}, with Q=12 kJ/gm of O_2 and $\mathcal{E}$ =0.9.

pyrolysis front velocity, v_p, and the maximum temperature, T_m, are to be measured as a function of P_a at various fixed values of u_i and Y_{oi}. These measurements will be compared with the theoretical results presented in Chapter 3. For one-dimensional countercurrent smolder, the dimensionless oxidation velocity, V, is given by

$$V = \frac{y_{us} M_{us}}{y_o M_o} \frac{Y_{oi} C_s}{C_g},$$

(5-1)

where v has been normalized by x_c/t_c, with $x_c = k_{eff}/\dot{m}''_{gi} c_g$ and $t_c = x_c^2 (1-\phi) \rho_{si} c_s / k_{eff}$. The maximum temperature is highly dependent on the magnitude of heat losses from the bottom of the fuel. When a residual ash layer builds below the smolder wave (Case II), such heat losses become negligible as $t \to \infty$, and $\overline{T}_m$ approaches $1/D_{co}$, where D_{co} ($=QY_{oi}/c_g T_i$) is a dimensionless heat release. For the no residual ash case (Case I), as $t \to \infty$, $\overline{T}_m$ is determined by

$$Q_R D_{co}\left[(1+\overline{T}_m)^4 - 1 \right] + \overline{T}_m = D_{co},$$

(5-2)

where Q_R ($= \varepsilon \sigma T_i^4/Q\dot{m}''_{oi}$) is a dimensionless measure of radiation heat losses from the bottom. For several fuels of interest, $Q \approx 12$ kJ/gm of O_2 [28,39]. A plot of T_m versus the inlet oxygen mass flux, $\dot{m}''_{oi}$, parameterized in the initial oxygen concentration, Y_{oi}, for $Q=12$ kJ/gm and $\varepsilon =0.9$, is shown in Fig. 5-1. As $t \to \infty$, the dimensionless pyrolysis speed, $\overline{v}_p = v_p t_c/x_c$, approaches
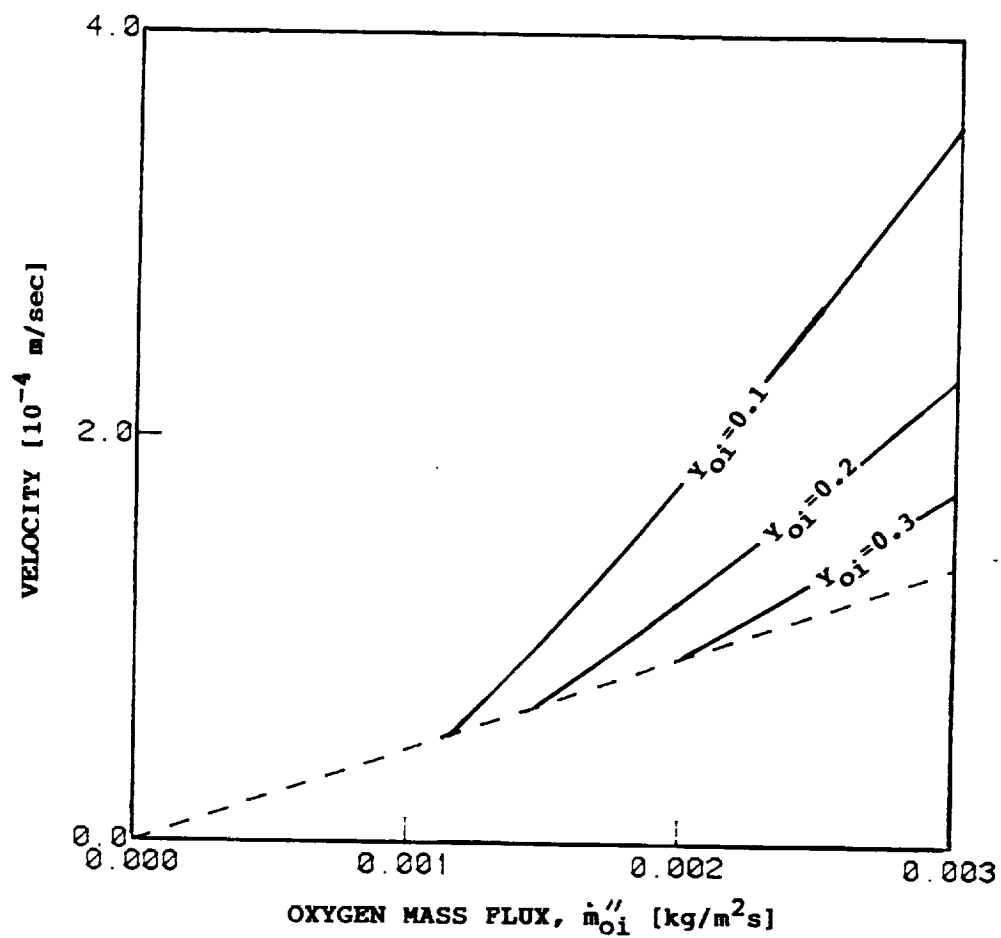
FIG. 5-2: Predicted pyrolysis velocities (——) in the limit t → ∞, and char oxidation velocities (--), as a function of inlet oxygen mass flux, $\dot{m}_{oi}''$, for GM-25 polyurethane.
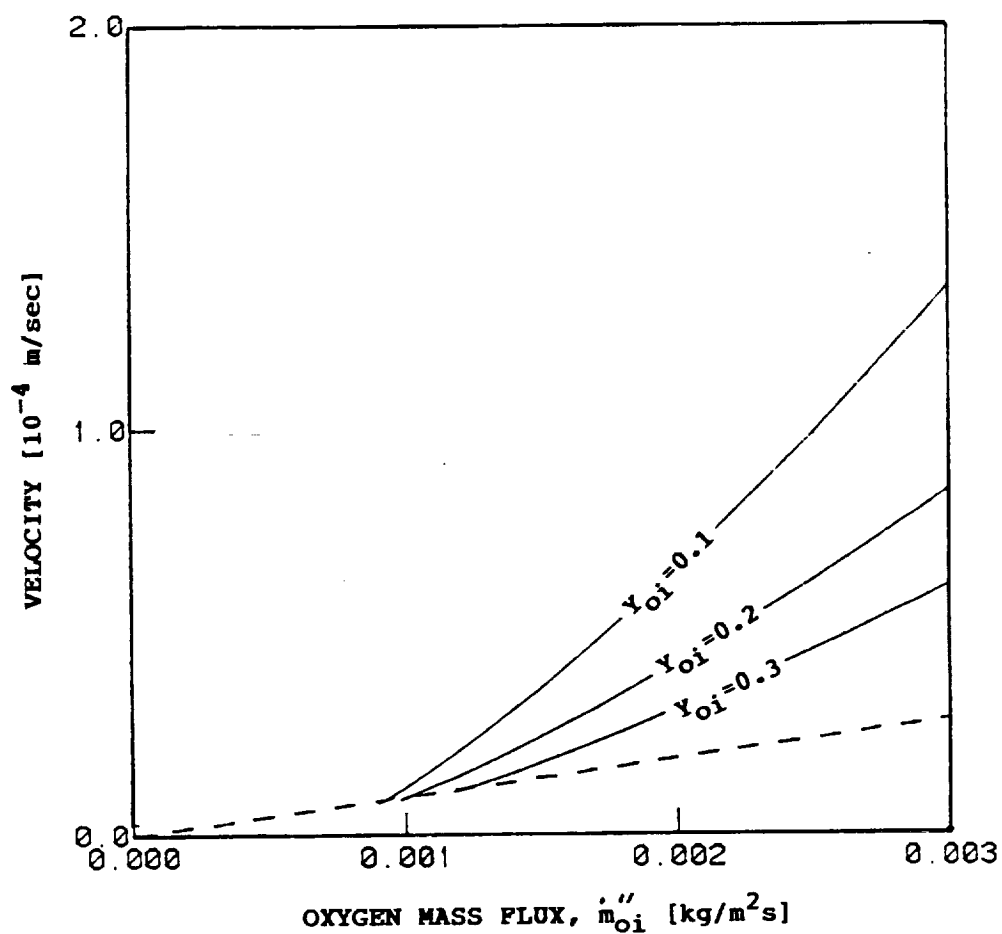
FIG. 5-3: Predicted pyrolysis velocities (—) in the limit $t \to \infty$, and char oxidation velocities (--), as a function of inlet oxygen mass flux, $\dot{m}''_{oi}$, for alpha-cellulose with a void volume fraction of 0.82.
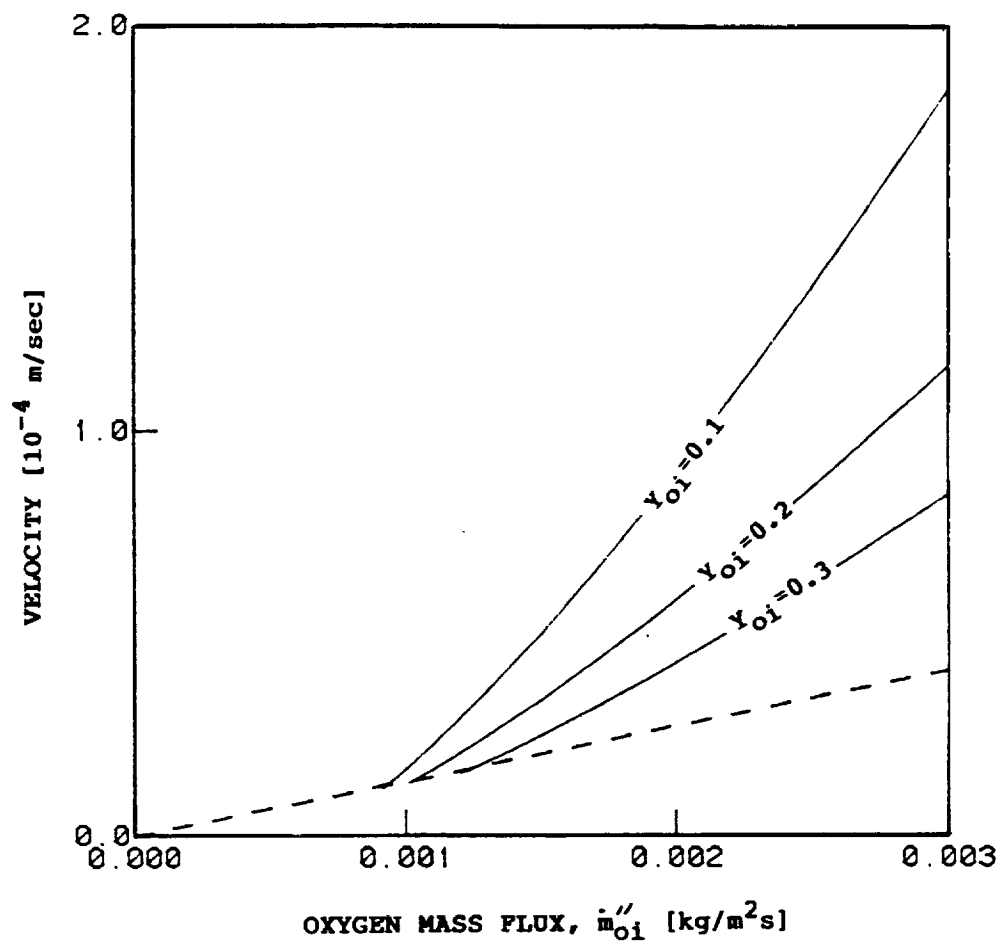
FIG. 5-4: Predicted pyrolysis velocities (—) in the limit $t \to \infty$, and char oxidation velocities (--), as a function of inlet oxygen mass flux, $\dot{m}_{oi}''$, for wood dust with a void volume fraction of 0.8.

$$\bar{v}_p = \frac{(\bar{T}_m - \bar{T}_p) - \mathcal{D}_{cp}V}{(\bar{T}_m - \bar{T}_p) + \mathcal{D}_{cp}} + V \,, \tag{5-3}$$

where D_{cp} $(=Q_p/c_s T_i)$ is a dimensionless measure of the energy consumed by pyrolysis and $\bar{T}_p$ is the pyrolysis temperature. Plots of $v_p(t \to \infty)$ and v versus $\dot{m}_{oi}''$ for GM-25 polyurethane, alpha-cellulose and wood dust are shown in Figs. 5-2, 5-3 and 5-4, respectively. Oxidation velocities, pyrolysis front velocities and maximum temperatures calculated from Eqs. (5-1,5-2,5-3) will be compared with measurements.

Forced cocurrent smoldering experiments will resolve the dependence of the final temperature, T_f, and the smolder velocity , v, on the ambient pressure, P_a. In purely one-dimensional cocurrent smolder, the dimensionless final temperature, $\bar{T}_f = (T_f - T_i)/T_i$, is determined from

$$\tilde{\Lambda} \left[1 + N_R (1 + \bar{T}_f)^3 \right]^{1+a} (1 + \bar{T}_f)^{a+c+2} e^{-\beta'/(1+\bar{T}_f)} = \frac{1}{2} \,, \tag{5-4}$$

where N_R $(=16\sigma \ell_r/3k_{eff})$ is a dimensionless radiation conductivity, $\beta'(=E/RT_i)$ is a dimensionless activation energy and $\tilde{\Lambda}$, which is inversely proportional to the initial oxygen mass flux, $\dot{m}_{oi}''$ (see Table 2-III), is a dimensionless pre-exponential factor. Plots of T_f versus the inlet oxygen mass flux, $\dot{m}_{oi}''$, for GM-25 polyurethane and alpha-cellulose are given in Fig. 2-8. A characteristic smolder velocity, $v_c = Q\dot{m}_{oi}''/(1-\phi)\rho_{si}c_{eff}$, is chosen by

balancing the total energy released with the energy required to preheat the solid and the dimensionless smolder velocity, $\bar{v}=v/v_c$, is given by

$$\bar{v} = \frac{1}{\bar{T}_f} - \frac{1}{D_c} \qquad (5\text{-}5)$$

where D_c $(=QY_{oi}/c_{eff}T_i)$ is a dimensionless heat release. A plot of smolder velocity versus dimensionless pre-exponential, $\tilde{\Lambda}$, for polyurethane is shown in Fig. 2-9. Final temperatures and smolder velocities calculated from Eqs.(5-4,5-5) will be compared with the measurements. As the pressure is lowered, better agreement between predictions and measurements is expected because buoyancy becomes less important.

Comparison of the measured extinction limit in forced cocurrent smoldering with the theory is complicated by the fact that heat losses from the sides of the fuel cylinder often play an important role near extinguishment [2]. When such losses are important, the final temperature is still determined by Eq.(5-4) but the dimensionless smolder velocity, $\bar{v}=v/v_c$, is now

$$\bar{v} = \frac{1}{\bar{T}_f} - \frac{1}{D_c} - q_L\left[1 + N_R(1+\bar{T}_f)^3\right]\left[(1+\bar{T}_f)^4 - 1\right]$$

$$- q_L\int_0^{\bar{T}_f}\left[1 + N_R(1+\bar{T})^3\right]\left[4 + 6\bar{T} + 4\bar{T}^2 + \bar{T}^3\right]d\bar{T} \qquad (5\text{-}6)$$

where q_L $(=4hk_{eff}T^5/d(Q\dot{m}''_{oi})^2)$ is a dimensionless measure of the radial heat losses and d is the diameter of the cylinder. Smoldering can be extinguished either by lowering Y_{oi}, which reduces D_{co}, or by decreasing $\dot{m}''_{oi}$, which increases q_L. As Y_{oi} is diminished, a greater portion of the energy released in the reaction zone is used to preheat the gas and consequently, less energy is available to preheat the solid. Decreasing $\dot{m}''_{oi}$ decreases the total amount of energy released in the reaction zone and once again, less energy is available to preheat the solid. By comparing predicted and measured smolder velocities near extinguishment, the range of validity of the extinction limit defined by setting $\bar{V}=0$ in Eq.(5-6) will be established.

Recall that for each fuel under consideration, an attempt will be made to identify a critical temperature, T_{flame}, above which only flaming is observed. If such a critical temperature can be determined, a flaming criterion for forced cocurrent smolder can be defined by setting $\bar{T}_f=\bar{T}_{flame}$ in Eq.(5-4). For countercurrent smolder, the predicted flaming limit will depend on whether a residual ash layer builds below the smolder wave. When an ash layer forms (Case II), flaming will occur when $D_{co}>1/\bar{T}_{flame}$ (that is, whenever Y_{oi} is above a threshold value). For the no residual ash case (Case I), a flaming limit can be established by setting $\bar{T}_m=\bar{T}_{flame}$ in Eq.(5-2).

CHAPTER 6

CONCLUSIONS

6.1 SUMMARY

Smoldering combustion propagation through very porous solid materials has been modeled. The proposed application is an experiment for use on the Space Shuttle. Due to the microgravity environment, smolder propagation was assumed to be one-dimensional. Two configurations were considered: (1) cocurrent, premixed-flame-like or reverse ; and (2) countercurrent, diffusion-flame-like or forward. Viewed in a frame of reference moving the oxidation zone, the solid fuel and the gaseous oxidizer enter the reaction zone from the same direction during cocurrent smolder, while in the countercurrent configuration, the fuel and the oxidizer enter from opposite directions. Forced and free cocurrent smolder as well as forced countercurrent propagation were examined.

In both configurations, the initial oxygen mass flux, $\dot{m}''_{oi}$, emerges as a key parameter. Because all of the oxygen reaching the smolder zone is consumed, the oxidation velocity, v, increases approximately linearly with $\dot{m}''_{oi}$. For cocurrent smolder, v is determined by a global energy balance between the energy released in the oxidation region and the energy required to preheat the solid and the gas. While for countercurrent smolder, both the oxygen and the

char are completely consumed and consequently, v is proportional to $\dot{m}_{oi}''$ with the proportionality constant determined by stoichiometry.

The fundamental differences between the two configurations follow from the change in the oxygen flow direction. In cocurrent smolder, energy is transferred from the oxidation zone to the pyrolysis region by conduction and radiation. Gas phase convection carries energy upward and out of the system. Provided that the inlet gas velocity varies slowly, cocurrent smolder reaches a steady state. On the other hand, in countercurrent smolder, energy is also transferred from the oxidation zone to the pyrolysis front by gas phase convection. Because convection is a long range "force", the pyrolysis front reaches a steady velocity which is different from the oxidation velocity when radial heat losses are negligible. Thus, countercurrent smolder is unsteady. Because energy convected by the gas phase preheats the solid fuel in countercurrent smolder, temperatures encountered in this configuration are usually higher than those in the cocurrent configuration.

An analytical model of both forced and free cocurrent smolder combustion was presented. Propagation of the smolder wave was assumed to be steady in a frame of reference moving with the wave. Smoldering was represented by a finite-rate, one-step, oxidation reaction and radiation heat transfer was incorporated using a diffusion approximation. The dimensionless equations were very similar to those governing

the propagation of a laminar premixed flame. A straightforward extension of the activation energy asymptotics analysis presented by Williams yielded an expression for a dimensionless eigenvalue, Λ, thus determining the final temperature, T_f. A global energy balance then determined the smolder velocity, v. Explicit expressions were derived for the smolder velocity, v, and the final temperature, T_f. An approximate extinction criterion is identified.

A model of unsteady, forced, countercurrent smoldering combustion was also presented. Smoldering was represented utilizing a two step mechanism consisting of a pyrolysis reaction followed by a char oxidation reaction. A "flame" sheet approximation was used to model the oxidation reaction. It was assumed that pyrolysis occurs at a known temperature, T_p. Because the two reaction zones moved at different velocities, countercurrent smoldering was unsteady. Two cases were considered: (1) no residual ash, $y_a M_a = 0$, and (2) an ash layer forming beneath the oxidation zone, $v_a M_a \neq 0$. The residual ash served as insulation, and its presence lead to high peak temperatures. Explicit expressions were derived for the oxidation velocity, v, the maximum temperature, T_m, and the pyrolysis front velocity, v_p. Results from the cocurrent and countercurrent analyses are summarized in the following section.

6.2 RESULTS

Key results of the forced and free cocurrent and the forced countercurrent analyses included:

6.2.1 Forced Cocurrent Smoldering Combustion

(1.) For a given fuel, the final temperature depends only on the initial oxygen mass flux, $\dot{m}_{oi}''$, increasing logarithmically with $\dot{m}_{oi}''$.

(2.) The smolder velocity, v, is linearly dependent on $\dot{m}_{oi}''$ and at fixed $\dot{m}_{oi}''$, increasing the initial oxygen mass fraction, Y_{oi}, increases v.

(3.) Steady smolder propagation is possible only for $Y_{oi} \geq c_{eff}(T_f - T_i)/Q$, with extinction occurring when all of the energy released in the reaction zone is used to heat the incoming gas.

6.2.2 Forced Countercurrent Smoldering Combustion

(1.) The char oxidation velocity, v, is linearly proportional to inlet oxygen mass flux, with the proportionality constant determined from stoichiometric conditions.

(2.) In the absence of radial heat losses, the pyrolysis front velocity, v_p, approaches a constant value which is, in general, different from v.

(3.1) For the no residual ash case, in limit of long time ($t \rightarrow \infty$), the maximum temperature, T_m, is determined by balancing the energy released in the oxidation region with the energy required to preheat the gas and radiation heat losses.

(3.2) When an ash layer builds below the smolder wave, radiation heat losses from the bottom are negligible in the limit $t \to \infty$ and T_m is much higher than in the no ash case.

(4.) Self-sustained countercurrent smoldering is only possible when $c_g(T_m-T_p)/Q_p > Y_{oi} \mathcal{V}_{us} M_{us} / \mathcal{V}_o M_o$, and solutions cease to exist when the energy convected by the gas phase is insufficient to drive the pyrolysis front.

6.2.3 Free Cocurrent Smoldering Combustion

(1.) The inlet gas velocity, u_i, is proportional to the product of the gravitational acceleration, g, and ambient pressure, P_a.

(2.) The smolder velocity, v, is proportional to the product, gP_a^{λ}.

(3.) The final temperature varies logarithmically with the quantity, gP_a^{2}.

Experiments are needed to test the predictions of the current models. A brief discussion of possible experiments is given in the next section.

6.3 FUTURE RESEARCH

An outline of the experimental study proposed in Chapter 5 follows:

(1.) Experiments will focus on the countercurrent configuration. The char oxidation velocity, v, the maximum temperature, T_m, and the pyrolysis velocity, v_p, will be determined for polyurethane, alpha-cellulose and wood dust. Of special importance is the identification of materials

that leave no residual ash, for flaming combustion is less likely in such materials.

(2.) Further experimental study of forced cocurrent smoldering is anticipated. Both the smolder velocity, v, and the final temperature, T_f, will be determined as a function of the ambient pressure, P_a, at various values of the initial oxygen mass fraction, Y_{oi}, and the inlet gas velocity, u_i.

(3.) An extinction limit for forced cocurrent smoldering will be identified in the parameter space consisting of the regions $Y_{oi} > 0$, $P_a > 0$ and $u_i > 0$.

(4.) For each fuel, an attempt will be made to identify a critical temperature, T_{flame}, above which flaming is observed.

Comparisons between the results of these experiments and the predictions of current models will be used to establish the range of validity of key assumptions in the analyses (such as the one-dimensional propagation approximation). Such comparisons will hopefully lead to refinements in the theory.

REFERENCES

1. Ohlemiller,T.J., "Modeling of Smoldering Combustion Propagation," *Progress in Energy and Combustion Science*, 11, pp.277-310, 1986.

2. Williams,F.A., *Combustion Theory*, Second Edition, The Benjamin/Cummings Publishing Company, Inc., 1985.

3. Beshty,B.S., "A Mathematical Model for the Combustion of a Porous Carbon Particle," *Combustion and Flame*, 32, pp. 295-311, 1978.

4. Gann,R.G. and Cheng,I.T., "Flow Study of Smoldering Charcoal Combustion," American Chemical Society, 172nd National Meeting, Division of Organic Coatings and Plastics, Report #20, 1976.

5. Donaldson, D.T., Yeadon,D.A. and Harper,R.J., "Smoldering Phenomenon Associated with Cotton,"*Textile Research Journal*, 53, pp. 160-164, 1983.

6. McCarter,R.J., "Smoldering Combustion of Cotton and Rayon," *Journal of Consumer Product Flammability*, 4, pp. 346-358, 1977.

7. Kinbara,T., Endo,H. and Sega,S., "Downward Propagation of Smoldering through Solid Materials," *Eleventh Symposium (International) on Combustion*, The Combustion Institute, pp. 525-531, 1967.

8. Ohlemiller,T.J. and Rogers,F.E., "A Survey of Several Factors Influencing Smoldering Combustion in Flexible and Rigid Polymer Foams," *Journal of Fire and Flammability*, 9, pp. 489-509, 1978.

9. Rogers,F.E. and Ohlemiller,T.J., "Studies of the Smoldering Combustion of Flexible Polyurethane Cushioning Materials," *Journal of Fire and Flammability*, 9, pp. 5-13, 1978.

10. Ohlemiller,T.J. and Rogers,F.E., "Minimizing Smolder Tendency in Flexible Polyurethanes," *Journal of Consumer Product Flammability*, 5, pp.59-67, 1978.

11. McCarter,R.J., "Smoldering Combustion of Polyurethane Foam," *Journal of Consumer Product Flammability*, 3, pp. 128-140, 1976.

12. McCarter,R.J., "Smoldering Combustion of Wood Fibers: Cause and Prevention," *Journal of Fire and Flammability*, 9, pp. 119-126, 1978.

13. Kansa,E.J., Perlee,H.E. and Chaiken,R.F., "Mathematical Model of Wood Pyrolysis Including Internal Forced Convection," *Combustion and Flame*, 29, pp. 311-324, 1977.

14. Kailasanath,K. and Zinn,B.T., "Theoretical Investigation of the Smoldering Combustion of Porous Solids," presented at the Fluids Engineering Conference, 1981.

15. Day,M. and Wiles,D.M., "Combustibility of Loose Fiber Fill Cellulose Insulation: The Role of Borax and Boric Acid," *Journal of Thermal Insulation*, 2, pp. 30-39, 1978.

16. Cohen,L. and Luft,N.W., "Combustion of Dust Layers in Still Air," *Fuel*, 34, pp.154-163, 1954.

17. Palmer,K.N., "Smouldering Combustion in Dusts and Fibrous Materials," *Combustion and Flame*, 1, pp. 14-17, 1957.

18. Gann,R.G., Earl,W.L., Manka,M.J. and Miles,L.B., "Mechanism of Cellulose Smoldering Retardance by Sulfur," *Eighteenth Symposium (International) on Combustion*, The Combustion Institute, pp.571-578, 1981.

19. Ohlemiller,T.J. and Lucca,D.A., "An Experimental Comparison of Forward and Reverse Combustion," *Combustion and Flame*, 54, pp. 131-147, 1983.

20. Ohlemiller,T.J., Bellan,J. and Rogers,F.E., "A Model of Smoldering Combustion Applied to Flexible Polyurethane Foams," *Combustion and Flame*, 36, pp.197-215, 1979.

21. Dosanjh,S.S., Pagni,P.J. and Fernandez-Pello,A.C., "Forced Cocurrent Smoldering Combustion," submitted to *Combustion and Flame*.

22. Rogers,F.E. and Ohlemiller,T.J., "Smolder Characteristics of Flexible Polyurethane Foams," *Journal of Fire and Flammability*, 11, pp. 32-44, 1980.

23. Dosanjh,S.S., Peterson,J., Fernandez-Pello,A.C. and Pagni,P.J., "Buoyancy Effects on Smoldering Combustion," *Acta Astronautica IAF-85 Stockholm Special Issue: Microgravity Materials and Fluid Sciences*, 1985.

24. Summerfield,M., Ohlemiller,T.J. and Sandusky,H.W., "A Thermophysical Mathematical Model of Steady-Draw Smoking and Predictions of Overall Cigarette Behavior," *Combustion and Flame*, 33, pp.263-279, 1978.

25. Winslow,A.M., "Numerical Model of Coal Gasification in a Packed," _Sixteenth Symposium (International) on Combustion_, The Combustion Institute, pp.503-514, 1976.

26. Thorness,C. and Roza,R., Lawrence Livermore Laboratory in situ coal gasification program: model calculations and laboratory experiments, Lawrence Livermore Laboratory Preprint UCRL-78302, Livermore, Ca., 1976.

27. Thorness,C., Grens,E. and Sherwood,A., A one-dimensional model for in situ coal gasification, Lawrence Livermore Laboratory Report UCRL-52523, 1978.

28. Moussa,N.A., Toong,T.Y. and Garris,C.A., "Mechanism of Smoldering of Cellulosic Materials," _Sixteenth Symposium (International) on Combustion_, The Combustion Institute, pp. 1447-1457, 1976.

29. Ortiz-Molina,M.G., Toong,T.Y., Moussa,N.A. and Tesero,G.C., "Smoldering Combustion of Flexible Polyurethane Foams and its Transition to Flaming or Extinguishment," _Seventeenth Symposium (International) on Combustion_, The Combustion Institute, pp.1191-1200, 1979.

30. Muramatsu,M., Umemura,S. and Okado,T., "Mathematical Model of Evaporation-Pyrolysis Processes Inside a Naturally Smoldering Cigarette," _Combustion and Flame_, 36, pp. 245-262, 1979.

31. Baker,R.R., "Combustion and Thermal Decomposition Regions Inside a Burning Cigarette," _Combustion and Flame_, 30, pp. 21-32, 1977.

32. Leisch,S.O., Kauffman,C.W. and Sichel,M., "Smoldering Combustion in Horizontal Dust Layers," _The Twentieth Symposium (International) on Combustion_, The Combustion Institute, pp.1601-1610, 1984.

33. Buckmaster,J.D. and Ludford,G.S.S., _Theory of Laminar Flames_, Cambridge University Press, 1982.

34. Siegel,R. and Howell,J.R., _Thermal Radiation Heat Transfer_, McGraw Hill, 1981.

35. Sparrow,E.M. and Cess,R.D., _Radiation Heat Transfer_, McGraw Hill, 1978.

36. Tong,T.W. and Tien,C.L., "Analytic Models for Thermal Radiation in Fibrous Insulation," _Journal of Thermal Insulation_, 4, pp. 27-44, 1980.

37. Hirschefelder,J.O., Curtis,C.F. and Bird,R.B., _Molecular Theory of Gases and Liquids_, John Wiley and Sons, 1954.

38. Williams,F.A., "Mechanisms of Fire Spread," *Sixteenth Symposium (International) on Combustion*, The Combustion Institute, pp. 1281-1293, 1976.

39. Products Research Committee, "Materials Bank Compendium of Fire Property Data," February 1980.

40. Campbell,A.S., "Fire Spread Over Paper," *Journal of Fire and Flammability*, 5, 1974.

41. Kanury,A.M., "Rate of Charring Combustion in a Fire," *Fourteenth Symposium (International) on Combustion*, The Combustion Institute, pp. 1131-1142, 1972.

42. Delichatsios,M.A. and de Ris,J., "An Analytic Model for the Pyrolysis of Charring Materials," Factory Mutual Research Corporation, May 1983.

43. Lunardini,V.J., *Heat Transfer in Cold Climates*, Van Nostrand Reinhold Company, 1981.

44. Kanury,A.M., *Introduction to Combustion Phenomena*, Gordon and Breach Science Publishers, 1975.

45. Shafizadeh,F. and Bradbury,A.G.W., "Smoldering Combustion of Cellulosic Materials," *Journal of Thermal Insulation*, 2, pp. 141-152, 1979.

46. Rogers,F.E. and Ohlemiller,T.J., "Cellulosic Insulation Material - I: Overall Degradation Kinetics and Reaction Rates," *Combustion Science and Technology*, 24, pp. 129-137, 1980.

47. Tye,R.P., "Heat Transmission in Cellulosic Fiber Insulation Materials," *Journal of Testing and Evaluation*, 2, pp. 176-179, 1974.

48. Incorpera,F.P. and DeWitt,D.P., *Fundamentals of Heat Transfer*, John Wiley and Sons, 1981.

49. Private communication from P. Lipowitz.

APPENDIX A

CHEMICAL KINETICS

Reaction mechanisms are presented for the smoldering combustion of alpha-cellulose [28], GM-25 polurethane foam [20], wood dust [32] and cellulosic insulation [46]. Upon being heated, the solid undergoes pyrolysis, leaving behind a black char. Oxidation of this char provides the energy required to sustain smoldering. A typical kinetic model consists of at most two pyrolysis reactions and one oxidation reaction. In all of these models, oxygen is the only gas phase species that participates in the reactions. The subscripts, o, us, c and a, refer to oxygen, unburnt solid, char and ash, respectively.

A.1 ALPHA-CELLULOSE

Moussa et al [28] investigated smoldering combustion propagation in cylindrical, horizontal, alpha-cellulose fuel elements. Degradation of the cellulose was modeled utilizing two competing reactions,

$$\nu_{us}(\text{Unburnt Solid}) + Q_c\nu_{us}M_{us} \longrightarrow \nu_c\text{Char} \tag{A-1}$$

and

$$\nu_{us}(\text{Unburnt Solid}) + Q_{gp}\nu_{us}M_{us} \longrightarrow$$
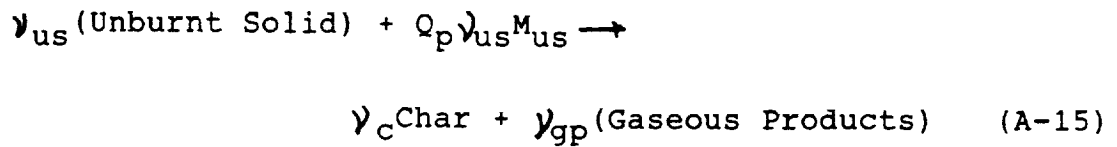
$$\nu_{gp}(\text{Gaseous Products}) \tag{A-2}$$
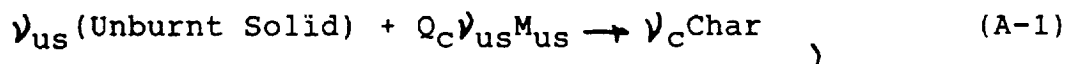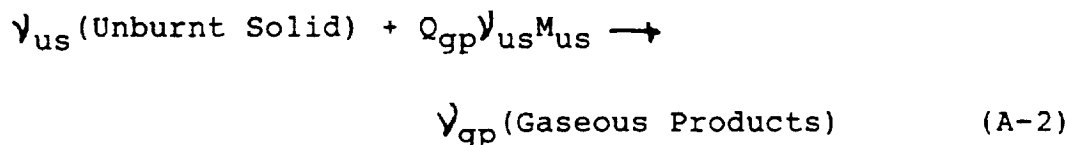
Reaction rates are of the form,

$$\dot{r}''' = Y_{us} \rho_s Z e^{-E/RT} , \qquad \text{(A-3)}$$

where $\dot{r}'''$ is the mass of solid consumed per unit volume per unit time, $Y_{us}\rho_s$ is the density of the unburnt solid, Z is the pre-exponential factor and E is the activation energy. For the charring reaction given in Eq. (A-1), $Z = 10^6$ sec^{-1}, $E = 110$ kJ/mole and $Q_c = 0.37$ kJ/(gm of fuel consumed). While for the gasification reaction in Eq. (A-2), $Z = 5 \times 10^7$ sec^{-1}, $E = 130$ kJ/mole and $Q_{gp} = -0.14$ kJ/(gm of fuel consumed).

Oxidation of the char was depicted by

$$\nu_c \text{Char} + \nu_o O_2 \rightarrow \nu_{gp} (\text{Gaseous Products}) + Q\nu_o M_o . \qquad \text{(A-4)}$$
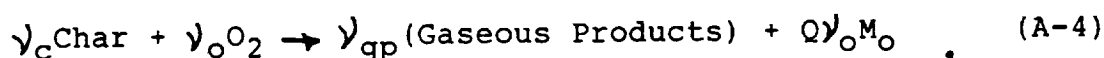
Since the char is comprised primarily of carbon, the above reaction can be approximated by $C + O_2 \rightarrow CO_2$. The oxidation rate was based on the outer surface area of the cylindrical fuel element. This rate is given by

$$\dot{r}''' = (Y_o P_a)^{1/2} Z e^{-E/RT} , \qquad \text{(A-5)}$$

where $\dot{r}'''$ is the mass of char consumed per unit area per unit time, Y_o is the oxygen mass fraction and P_a is the ambient pressure. Moussa et al [28] reported that the following paramter values gave good agreement between the predicted and measured extinction limit: $Z = 10^9$ kg/m^{2}atm$^{1/2}$sec, $E = 180$ kJ/mole and $Q = 12$ kJ/(gm of O_2 consumed).

A.2 GM-25 POLYURETHANE FOAM

Ohlemiller et el [20] modeled the smoldering combustion of polyurethane using a two step mechanism consisting of an oxidative pyrolysis reaction and a char oxidation reaction,

$$\mathcal{Y}_{us}(\text{Unburnt Solid}) + \mathcal{Y}_{o1}O_2 \longrightarrow$$

$$\mathcal{Y}_{c}\text{Char} + \mathcal{Y}_{gp1}(\text{Gaseous Products}) + Q\mathcal{Y}_{o1}M_{o1} \quad (A-6)$$

and

$$\mathcal{Y}_{c}\text{Char} + \mathcal{Y}_{o2}O_2 \longrightarrow$$

$$\mathcal{Y}_{a}\text{Ash} + \mathcal{Y}_{gp2}(\text{Gaseous Products}) + Q\mathcal{Y}_{o2}M_{o2} \quad (A-7)$$
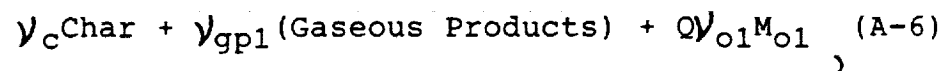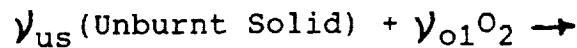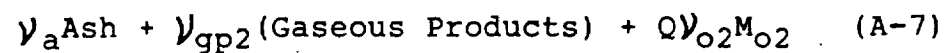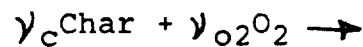
Rates of the reactions in Eqs.(A-6,A-7) are

$$\dot{r}''' = (1-\phi)(Y_o \rho_g)(Y_{us} \rho_s) Z e^{-E/RT}, \quad (A-8)$$

and

$$\dot{r}''' = (1-\phi)(Y_o \rho_g)(Y_c \rho_c) Z e^{-E/RT} \quad (A-9)$$

respectively. For the pyrolysis reaction, $Z= 3.92 \times 10^{11}$ m^3/(kg sec) and $E= 140$ kJ/mole, while for the char oxidation reaction, $Z= 1.42 \times 10^{11}$ m^3/(kg sec) and $E= 126$ kJ/mole. The energy consumed per mass of O_2 consumed, $Q= 7.6$ kJ/gm, was determined by matching predicted and measured smolder velocities. Stoichiometric coefficients are given by: $\mathcal{Y}_{o1}M_o/\mathcal{Y}_{us}M_{us}= 0.085$, $\mathcal{Y}_{c}M_c/\mathcal{Y}_{us}M_{us}= 0.55$, $\mathcal{Y}_{o2}M_o/\mathcal{Y}_{c}M_c= 0.82$, and $\mathcal{Y}_{a}M_a/\mathcal{Y}_{c}M_c= 0.27$. Because the char oxidation is much

faster than pyrolysis [20], Eqs.(A-6,A-7) can be well approximated by

$$\gamma_{us}(\text{Unburnt Solid}) + \gamma_o O_2 \rightarrow$$

$$\gamma_a \text{Ash} + \gamma_{gp}(\text{Gaseous Products}) + Q\gamma_o M_o \quad , \qquad (A-9)$$
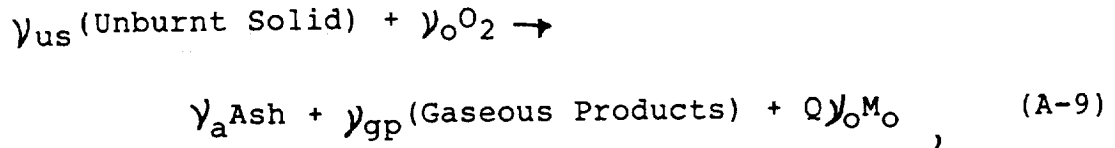
with $\gamma_o M_o / \gamma_{us} M_{us} = 0.54$ and $\gamma_a M_a / \gamma_{us} M_{us} = 0.15$. Moreover, the rate at which the above reaction proceeds is controlled by the (oxidative) pyrolysis rate.

A.3 WOOD DUST

Leisch et al [32] utilized four reactions to model the smoldering combustion of wood dust,

$$\gamma_{us}(\text{Unburnt Solid}) + Q_c \gamma_{us} M_{us} \rightarrow \gamma_c \text{Char} \quad , \qquad (A-10)$$

$$\gamma_{us}(\text{Unburnt Solid}) \rightarrow \gamma_{gp1}(\text{Gaseous Products})$$

$$+ Q_{gp1} \gamma_{us} M_{us} \quad , \qquad (A-11)$$

$$\gamma_c \text{Char} + \gamma_o O_2 \rightarrow \gamma_a \text{Ash} + Q_a \gamma_c M_c \quad , \qquad (A-12)$$

and

$$\gamma_c \text{Char} + \gamma_o O_2 \rightarrow \gamma_{gp2}(\text{Gaseous Products}) + Q_{gp2} \gamma_c M_c \qquad (A-13)$$
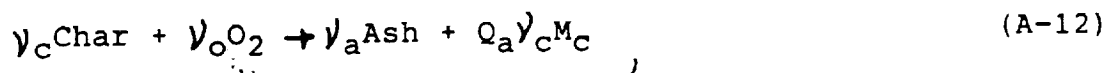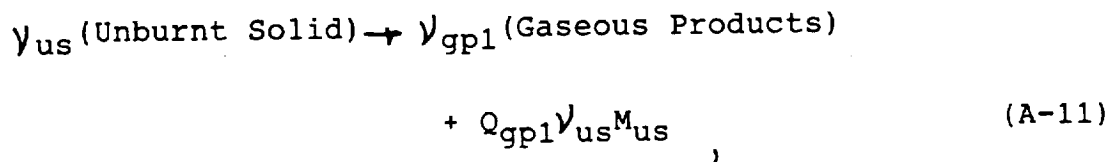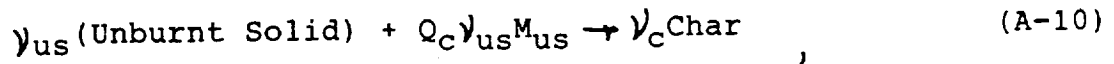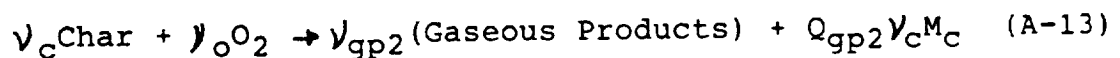
Pyrolysis reaction rates are of the form

$$\dot{r}''' = (\gamma_{us} \rho_s) z \, e^{-E/RT} \quad , \qquad (A-14)$$

where $\dot{r}'''$ is the mass of unburnt solid consumed per unit

volume per unit time. For the charring pyrolysis reaction, $Z = 4.1 \times 10^9 \text{sec}^{-1}$, $E = 105$ kJ/mole and $Q_c = 3.7$ kJ/(gm of fuel consumed). For the gasification reaction given in Eq.(A-11), $Z = 7.8 \times 10^9 \text{sec}^{-1}$, $E = 105$ kJ/mole and $Q_{gp1} = 0.14$ kJ/(gm of fuel consumed). Because the activation energies of these two reactions are equal, Eqs.(A-10,A-11) are equivalent to

$$\gamma_{us}(\text{Unburnt Solid}) + Q_p \gamma_{us} M_{us} \longrightarrow$$

$$\gamma_c \text{Char} + \gamma_{gp}(\text{Gaseous Products}) \qquad (A-15)$$

where $\gamma_c M_c / \gamma_{us} M_{us} = 0.34$ and $Q_p = 1.2$ kJ/(gm of fuel consumed). The rate of the above reaction is still of the form in Eq.(A-14), but with $Z = 1.2 \times 10^{10} \text{sec}^{-1}$ and $E = 105$ kJ/mole.

Oxidation reaction rates are of the form

$$\dot{r}''' = S(Y_o P_a)^{1/2}(Y_c \rho_s) Z e^{-E/RT}, \qquad (A-16)$$

where S is the surface area of solid per mass of solid. For a packing of spherical particles, $S = \pi / \rho_s d_p$, where d_p is an average diameter. Kinetic constants for the ash producing reaction in Eq.(A-12) are: $Z = 1.0 \times 10^4$ kg/m^{2}atm$^{1/2}$s, $E = 126$ kJ/mole and $Q_a = 14.7$ kJ/(gm of char consumed). While for the gasification reaction in Eq.(A-13) $Z = 1.0 \times 10^5$ kg/m^{2}atm$^{1/2}$s, $E = 126$ kJ/mole and $Q_a = 2.1$ kJ/(gm of char consumed). Because the activation energies for the two oxidation reactions are equal,

$$\mathcal{Y}_c \text{Char} + \mathcal{Y}_o O_2 \rightarrow \mathcal{Y}_a \text{Ash} + \mathcal{Y}_{gp}\text{(Gaseous Products)}$$

$$+ Q\mathcal{Y}_c M_c \hspace{4cm} \text{(A-17)}$$
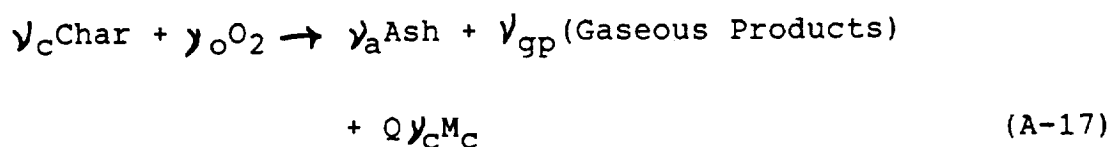
where $\mathcal{Y}_a M_a / \mathcal{Y}_{gp} M_{gp} = 0.1$ and Q= 3.4 kJ/(gm of char consumed). The reaction rate is still if the form in Eq.(A-16), but with Z= 1.1 X 10^5 kg/m^{2}atm$^{1/2}$s and E= 126 kJ/mole.

A.4 CELLULOSIC INSULATION MATERIALS

Rogers and Ohlemiller [46] employed a reaction mechanism consisting of two consecutive oxidative reactions. Reaction rate were of the form

$$\dot{r}''' = \frac{\rho_s^2}{\rho_{si}} \gamma^{0.43} Z e^{-E/RT} \hspace{2cm} \text{(A-18)}$$

For the first reaction, Z= 10^{13}sec^{-1}, E= 110 kJ/mole and Q= 4.2 kJ/(gm of solid consumed), and for the second, Z= 1.25 X 10^9sec^{-1}, E= 165 kJ/mole and 25 kJ/(gm of solid consumed). Ohlemiller and Lucca [19] reported that only the first oxidative reaction is important in cocurrent smolder.

A.5 SUMMARY

Smoldering combustion was represented by a finite-rate, one-step, oxidation reaction in the cocurrent analysis in Chapter 2. This is a reasonable assumption for alpha-cellulose, GM-25 polyurethane, wood dust and cellulosic insulation. These materials have oxidation rates of the

TABLE A-I

Typical kinetic parameters for a oxidation reaction of the form

$$r = Y_o^a \, \rho_g^b \, \rho_s^c \, T^d \, Z \exp(-E/RT).$$

	alpha-cellulose	GM-25 polyurethane	wood dust	cellulosic insulation
a	0.5	1.0	0.5	0.43
b	0.5	1.0	0.5	0
c	0	1.0	1.0	2.0
d	0.5	0	0.5	0
E [kJ/mole]	180	140	126	110
Q [kJ/gm of fuel]	7.7	4.1	3.4	4.2
Z*	6×10^7	1.4×10^{10}	1.1×10^5	2.9×10^{11}

* For GM-25 polyurethane and cellulosic insulation, the units of Z are $m^3/kg\ s$, while for alpha-cellulose and wood dust, the units of Z are $kg^{1/2}/(m \cdot K)^{1/2} s$.

form

$$r = Y_o^a \, \rho_g^b \, \rho_f^c \, T^d \, z \, e^{-E/RT} \, ,$$

where ρ_f is the density of the solid fuel. Typical
values of the reaction orders a,b,c, and d, as well as E, Q
and Z, are given in Table A-I.

APPENDIX B

LOCAL THERMAL EQUILIBRIUM BETWEEN PHASES

In general, two energy equations must be considered, one for the solid and one for the gas. When the solid and the gas are in local thermal equilibrium (that is, $T_s = T_g$), the analysis is considerably simplified. For not only are empirical models for the energy transfer between phases unnecessary, the two energy equations collapse into one equation. In this appendix, a criterion for checking the validity of the thermal equilibrium assumption will be derived using a Biot number analysis.

A gas with velocity, u, flows about a spherical particle of diameter, d_p. The temperature distribution inside the particle can be considered uniform at any given time as long as the Biot number, $Bi = hd_p/k_s$, is much less than one. The surroundings are at a uniform temperature, T_∞, the particle has an initial temperature, T_i, and h is the convection coefficient. At time, t, the tempertature of the particle is

$$\frac{T - T_\infty}{T_i - T_\infty} = e^{-t/\tau} ,$$ (B-1)

where the response time, $\tau = \rho_s c_s d_p / h$, measures the length of time it takes for the particle to come into thermal equilibrium with its surroundings. When τ is much smaller

than the time characteristic of changes in the gas

temperature, x_c/u, the gas and the solid remain in local

thermal equilibrium. That is, $T_s = T_g$ when

$$\frac{u\tau}{x_c} = \frac{\rho_s c_s u d_p}{x_c h} << 1 \quad , \tag{B-2}$$

where x_c is a distance characteristc of changes in

temperature. When the Reynold's number, Re= $u d_p/\nu$, is

small,

$$Nu = \frac{h d_p}{K_g} \approx 2 \, . \tag{B-3}$$

Combining Eqs. (B-2,B-3) gives

$$\frac{\rho_s c_s u d_p^2}{2 x_c k_g} << 1 \quad , \tag{B-4}$$

as the criterion for local thermal equilibrium. Typically,

$x_c \approx 10^{-02}$m, u $\approx 10^{-3}$ m/s, $c_s \approx 1$ kJ/kg and $k_g \approx 0.03$ W/m K. For

polyurethane, $\rho_s \approx 1100$ kg/m^3, and the criterion is

$d_p << 7 \times 10^{-4}$m while for alpha-cellulose, $\rho_s \approx 500$ kg/m^3,

giving $d_p << 10^{-3}$m. It is evident from the electron microscope

photographs of polyurethane and cellulose in Figs.2-2A and

2-2B that the criterion for local thermal equilibrium is

approximately satisfied.

APPENDIX C

DERIVATION OF THE TRANSPORT EQUATIONS

C.1 GENERAL ASSUMPTIONS

The distance characteristic of changes in the pore structure of a permeable material, d_p, is defined as six times the volume of the solid phase divided by its surface area. For a packed bed of spherical particles, d_p is the average diameter of the particles. The equations governing smoldering combustion are amenable to analysis for a particular range of d_p. If d_p is small, on the order of the mean free path of the gas molecules, λ, the diffusion processes become exceedingly complex. There is no hope of using formulas as simple as Fick's law of diffusion or Fourier's law of heat conduction. On the other hand, when d_p is large, of the same order of magnitude as x_c, the distance characteristic of changes in temperature and species concentrations, the particles must be considered individually [1]. When $d_p \ll x_c$, the solid phase can be considered continuous and average quantities, such as a void volume fraction, ϕ, and an effective thermal conductivity, k_{eff}, can be defined. In the following discussion, it is assumed that $\lambda \ll d_p \ll x_c$.

C.2 CONSERVATION OF ENERGY

The solid phase and the gas phase are assumed to be in thermal equilibrium - that is, $T_s = T_g$. A criterion for checking the valididty of this approximation is derived in Appendix B. Consider a volume of space, V , that is stationary relative to the laboratory. The boundary of V is A. Neglecting the work done by viscous forces, the conservation of energy requires that

$$
\left\{ \begin{array}{c} \text{rate of} \\ \text{accumulation} \\ \text{of internal} \\ \text{and kinetic} \\ \text{energy} \end{array} \right\} = - \left\{ \begin{array}{c} \text{net rate} \\ \text{of internal} \\ \text{and kinetic} \\ \text{energy transport out} \\ \text{by convection} \end{array} \right\} - \left\{ \begin{array}{c} \text{net rate} \\ \text{at which} \\ \text{energy} \\ \text{diffuses} \\ \text{out} \end{array} \right\}
$$

$$
+ \left\{ \begin{array}{c} \text{the rate at} \\ \text{which the gas} \\ \text{does work against} \\ \text{surface and body} \\ \text{forces} \end{array} \right\} + \left\{ \begin{array}{c} \text{the rate at} \\ \text{which energy} \\ \text{is released} \\ \text{by chemical} \\ \text{reactions} \end{array} \right\}
$$

where

$$
\begin{array}{c} \text{(gas+solid) internal} \\ \text{and (gas) kinetic} \\ \text{energy stored in V} \end{array} = \int_V \left[(1-\phi)\rho_s e_s + \phi\rho_g e_g + \tfrac{1}{2}\phi\rho_g u^2 \right] dV
$$

$$
\begin{array}{c} \text{internal and kinetic} \\ \text{energy of the gas} \\ \text{phase convected out} \end{array} = \int_A \left[\phi\rho_g (e_g + \tfrac{1}{2}u^2)(\vec{n}\cdot\vec{u}) \right] dA
$$

$$
= \int_V \vec{\nabla}\cdot\left[\phi\rho_g (e_g + \tfrac{1}{2}u^2)\vec{u} \right] dV
$$

energy diffusing out $= \int_A (\vec{n} \cdot \vec{q}) \, dA = \int_V \vec{\nabla} \cdot \vec{q} \, dV$

the rate at which the gas does work against static pressure $= \int_A \phi P(\vec{n} \cdot \vec{u}) \, dA = \int_V \vec{\nabla} \cdot (\phi P \vec{u}) \, dV$

the rate at which gravity does work on the gas $= \int_V \phi \rho_g (\vec{g} \cdot \vec{u}) \, dV$

the rate at which energy is released by chemical reactions $= \int_V \dot{Q}''' \, dV$

In differential form, conservation of energy gives

$$\frac{\partial}{\partial t} \left[(1-\phi)\rho_s e_s + \phi \rho_g e_g + \tfrac{1}{2} \phi \rho_g u^2 \right] = -\vec{\nabla} \cdot \vec{q} + \dot{Q}''' - \phi \rho_g \vec{u} \cdot \vec{g}$$

$$-\vec{\nabla} \cdot \left[\phi \rho_g \left(h_g + \tfrac{1}{2} u^2 \right) \vec{u} \right] . \qquad \text{(C-1)}$$

When the Dufour effect, energy transfer due to concentration gradients, is unimportant, the heat flux is

$$\vec{q} = -K_{eff} \vec{\nabla} T + \vec{q}_{rad} \qquad\qquad \text{(C-2)}$$

The effective thermal conductivity, $k_{eff} = \phi k_g + (1-\phi) k_s$, accounts for energy transfer due to conduction in both solid and gas phases. Neglecting chemical energy, the internal energy of the solid phase is

$$e_s = \int_{T_i}^{T} c_s \, dT \, , \tag{C-3}$$

and the gas phase enthalpy is

$$h_g = \int_{T_i}^{T} c_g \, dT \, , \tag{C-4}$$

where c_g is the gas specific heat (at constant pressure). In most smolder applications, the work done by gravity and the (kinetic and internal) energy stored in the gas phase are negligible [1]. Typically, the ratio of the work done by gravity to the energy convected by the gas, $x_c g / c_g T_i$, is of $\mathcal{O}(10^{-7})$, the ratio of the gas phase kinetic energy to the energy convected by the gas, $u^2 / c_g T_i$, is of $\mathcal{O}(10^{-11})$, and the ratio of the internal energy stored in the gas to that stored in the solid, $\phi \rho_g / (1-\phi) \rho_s$, is of $\mathcal{O}(0.02)$. Equation (C-1) now gives

$$\frac{\partial}{\partial t} \left[(1-\phi) \rho_s e_s \right] = -\vec{\nabla} \cdot \left[\phi \rho_g h_g \vec{u} \right] + \dot{Q}'''$$
$$+ \vec{\nabla} \cdot \left[K_{eff} \vec{\nabla} T \right] - \vec{\nabla} \cdot \vec{q}_{rad} \, , \tag{C-5}$$

which is the basis for Eq.(9) in Chapter 2 and Eqs.(4,5) in Chapter 3.

C.3 CONSERVATION OF SPECIES

C.3.1 Gas Phase

Conservation of gas phase species requires

$$
\left\{ \begin{array}{l} \text{the rate} \\ \text{at which} \\ \text{species i} \\ \text{accumulates} \end{array} \right\} = - \left\{ \begin{array}{l} \text{the net rate at} \\ \text{which species i} \\ \text{is convected} \\ \text{out of V} \end{array} \right\} + \left\{ \begin{array}{l} \text{the rate of} \\ \text{generation of} \\ \text{species i (by} \\ \text{chemical reactions)} \end{array} \right\}
$$

where

$$
\begin{array}{l} \text{the mass of species i} \\ \text{stored in V} \end{array} = \int_V \phi \, \rho_g \, Y_{ig} \, dV
$$

$$
\begin{array}{l} \text{mass of species i} \\ \text{convected out} \end{array} = \int_A \phi \, \rho_g \, Y_{ig} \left[\vec{n} \cdot (\vec{u} + \vec{V_i}) \right] dA
$$

$$
= \int_V \vec{\nabla} \cdot \left[\phi \, \rho_g \, Y_{ig} (\vec{u} + \vec{V_i}) \right] dV
$$

$$
\begin{array}{l} \text{the rate at which species i} \\ \text{is generated} \end{array} = \int_V \dot{w}''_{ig} \, dV
$$

In differential form, conservation of species requires

$$
\frac{\partial}{\partial t} \left[\phi \rho_g Y_{ig} \right] = - \vec{\nabla} \cdot \left[\phi \rho_g Y_{ig} (\vec{u} + \vec{V_i}) \right] + \dot{w}''_{ig} \, , \qquad \text{(C-6)}
$$

When the Soret effect, mass transfer due to temperature gradients, is unimportant, pressure gradient diffusion is negligible and the binary diffusion coefficients of all pairs of species are equal, the diffusion velocity can be

approximated by [2]

$$\vec{V_i} = -D \vec{\nabla} (\log Y_{ig}),$$ (C-7)

Equations (C-6,C-7) are the basis for Eqs.(6,8) in Chapter 2 and Eq.(6) in Chapter 3.

C.3.2 Solid Phase

Noting that the solid is stationary in the laboratory frame of reference, conservation of solid species requires

$$\begin{bmatrix} \text{rate at which} \\ \text{species i} \\ \text{accumulates} \end{bmatrix} = \begin{bmatrix} \text{the rate at which} \\ \text{species i is generated} \\ \text{(by chemical reactions)} \end{bmatrix}$$

where

$$\begin{array}{l} \text{the mass of species i} \\ \text{stored in V} \end{array} = \int_V (1-\phi) \rho_s Y_{is} \, dV$$

$$\begin{array}{l} \text{the rate at which species i} \\ \text{is generated} \end{array} = \int_V \dot{\omega}_{is}'' \, dV$$

In differential form, conservation of solid phase species gives

$$\frac{\partial}{\partial t} \left[(1-\phi) \rho_s Y_{is} \right] = \dot{\omega}_{is}'' \, ,$$ (C-8)

which yields Eq.(7) in Chapter 2 and Eq.(8) in Chapter 3.

PAPER 5

"EXPERIMENTAL OBSERVATIONS OF THE
EFFECT OF BUOYANCY ON CO-CURRENT SMOLDERING"

Newhall, J.L., Fernandez-Pello, A.C., and Pagni, P.J.

PRECEDING PAGE BLANK NOT FILMED

Experimental Observations of the Effect of Pressure and Buoyancy on Cellulose Co-current Smoldering

J. L. Newhall, A. C. Fernandez-Pello and P. J. Pagni

Department of Mechanical Engineering, University of California, Berkeley, CA 94720, USA

An experimental study has been performed to determine the potential effect of buoyancy on the rate of propagation of a co-current smolder reaction through a porous solid fuel, and the range of flow velocities where buoyancy effects are significant. In the co-current smolder reaction, the fuel and oxidizer enter the reaction zone from the same direction. In the present experiments this is accomplished by initiating the reaction at the top of the fuel bed, α-cellulose packed at a void fraction 0.85, so that the smolder wave propagates downward opposing an upward forced flow of air. Since in a stratified density field, buoyancy is proportional to the product of gravity and density difference, buoyancy can be controlled by varying either the gravity vector or the gas density. In this study the latter method is followed, varying gas density through the ambient pressure at which the experiments are performed. The smolder velocity is measured for air flow rates varying from 0.2 to 6 g m^{-2} s^{-1} at constant ambient pressures of 0.6, 0.8 and 1 atm. The results show that for flow rates larger than 1 g m^{-2} s^{-1} the smolder velocity increases linearly with the air flow rate but is independent of pressure. The reaction peak temperature is weakly dependent on flow rate and independent of pressure. For the present experimental conditions the effect of buoyancy is only observed at very low air flow rates. The mechanisms by which it affects the smolder process appears to be by altering the transport of air to the reaction zone from upstream and downstream of the reaction.

INTRODUCTION

Smoldering is defined as a non-flaming, exothermic, surface reaction that propagates through a porous combustible material.[1,2] Although this form of combustion is present in a variety of practical combustion processes, it is particularly important in the fire-safety field because of its role in the initiation of fires. Fires are often triggered by a sudden transition from a slow smoldering reaction to rapid flaming, quickly involving adjacent materials. Furthermore, since it may take place in the material interior and be of low intensity, it can progress undetected for long periods of time, and be difficult to suppress because the porosity of the material prevents the access of the extinguishing agent to the reaction zone. Thus the understanding of the physical and chemical mechanisms controlling smoldering is important not only because smoldering is a fundamental combustion process but because such understanding can be critical to the prevention and control of destructive fires.

The basic mechanisms of smolder propagation are fairly well understood.[1] The heat released during the heterogeneous oxidation of the solid is transferred toward the virgin material by conduction, convection and radiation, supporting the propagation of the smolder reaction. The oxidizer in turn is transported to the reaction zone by diffusion and convection. These transport mechanisms influence not only the rate at which the smolder reaction propagates but also the limiting processes of transition to flaming and extinction. Smoldering is customarily classified into co-current and counter-current configurations, according to the direction in which the fuel and oxidizer enter the reaction zone. In the reference frame of the reaction zone the fuel and oxidizer enter the reaction from the same side in co-current smolder, while in counter-current the fuel and oxidizer enter from opposite sides.

Buoyancy can play a significant role in the above transport mechanisms because of the gas density stratification at the reaction zone. Under natural convection conditions, buoyancy interacts with the transport of heat and mass by diffusion. At low forced-flow velocities it interacts with both diffusion and convection. This leads to another classification of smoldering according to whether the propagation of the smolder front is in the same direction (downward) or opposite direction (upward) as the gravity vector. Most of the experimental work that has been done in the past on smoldering combustion has focused in analyzing the effect oxidant composition and velocity on the smolder reaction rate.[3-9] Except for the work of Dosanjh et al.,[10] which has a limited scope, no systematic study has been done to date of the effect of buoyancy on the smolder combustion process. This is the objective of the present investigation.

Experiments are performed to study the effect of the mass flow rate of oxidant and of the buoyancy force on the propagation velocity and reaction temperature of a downward, co-current, forced-flow smolder reaction. The porous combustible is α-cellulose with a fix void fraction and the oxidant is air. In the experiment the buoyancy force is controlled through the ambient pressure, according to the relation $g(\rho_u - \rho_b) \sim gP(T_b - T_u)$, where the subscripts u and b indicate unburnt and burnt gas conditions. Since the reaction rate can also depend on pressure, the method is best applicable when the chemical reaction is not strongly dependent on pressure. As will be shown later, this appears to be the case for smolder

combustion, thus facilitating the interpretation of the experimental results.

EXPERIMENT

A schematic diagram of the experimental installation is shown in Fig. 1. It consists of a one-dimensional, forced-flow, co-current smolder apparatus and the supporting instrumentation. The apparatus is contained in a pressure vessel 1.8 m in diameter and 3.3 m long that is used to control the experiment pressure. Acrylic windows located at opposite sides of the vessel provide optical access to the test area. The test section containing the porous combustible is a 0.12 m in diameter by 0.16 m high vertically positioned pyrex cylinder. The diameter was selected to reduce any two-dimensional effects to a minimum while maintaining a laboratory scale. To ensure uniform air flow through the test section, the lower end of the cylinder is tapered and filled with glass beads. A wire mesh sits on the beads and also supports the fuel. Small holes placed longitudinally along the side of the cylinder allow the positioning of thermocouples in the porous material.

The air flows into the test section from a 5 l settling tank that is used to provide enough differential pressure to overcome the losses through the flow lines and flow meters. The air-metering system is composed of a Tylan Corporation $1-3 \, l \, min^{-1}$ mass flow meter and controller. The air pressure in the lines after the flow meter and in the test section is slightly above (of the order of 10 Pa) that in the vessel. To keep the vessel pressure constant during the tests and to avoid the flow of combustion products through the vessel main vacuum pump, the exhausts from the test section are collected in a hood and removed from the vessel with a second, smaller, vacuum pump. The vessel's pressure is continuously monitored during the experiments to ensure that the balance between the inlet and outlet flow is maintained.

The fuel (α-cellulose in these experiments) is pre-weighed and placed into a fixed volume in the pyrex cylinder to maintain a constant void fraction of 0.85 throughout the experiments. Five chromel–alumel thermocouple probes 0.8 mm thick (wire diameter 0.12 mm) extending horizontally into the center of the fuel bed are placed 2 cm apart, with the first thermocouple located 2 cm beneath the top of the fuel bed. The thermocouples are connected through a multiplexer to a real-time data-acquisition system, which stores and converts the thermocouple emf into temperature. The temperature histories from each thermocouple are used to calculate the smolder velocity from the lapsed period of smolder reaction passage and the distance between thermocouples. The computed velocity is an average value. At near-extinction conditions, the peak temperature decreases as the smolder front propagates into the fuel bed (Fig. 3). In those cases only the data from the first two thermocouples were used to calculate the smolder velocity. The combustion of the cellulose is initiated at the top of the fuel bed with a methane flame that impinges uniformly on the fuel. The methane is spark ignited with a high-voltage induction coil. Initially flaming occurs but quickly dies down and smoldering commences. The smolder reaction propagates downward opposing the air flow, which is forced upward through the porous combustible. The resulting smoldering configuration is therefore of the downward, co-current type.

RESULTS AND DISCUSSION

Measurements are performed of the velocity of downward co-current smolder propagation through cellulose for air mass flow rates ranging from 0.2 to 6 $g \, m^{-2} \, s^{-1}$ for fixed pressure levels of 0.6, 0.8 and 1 atm. Two characteristic examples of the temperature histories from each
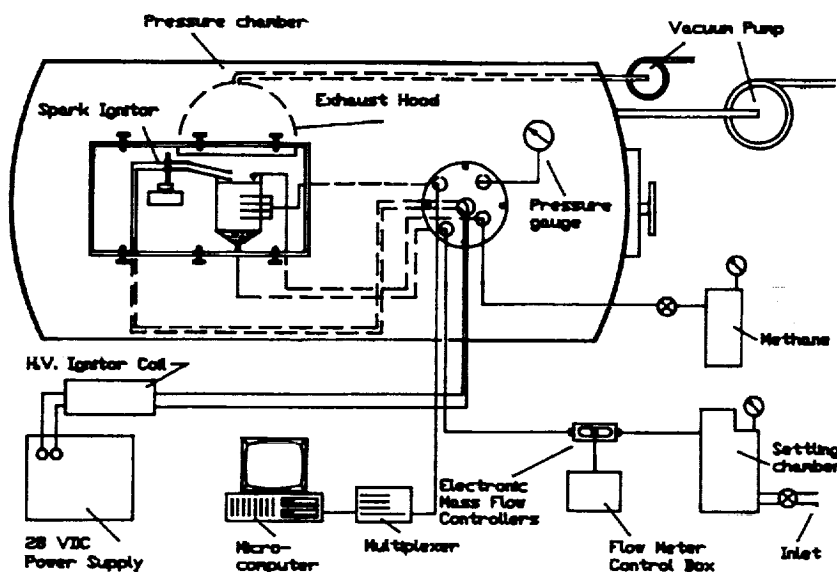
Figure 1. Schematic of experimental installation.

C-3.
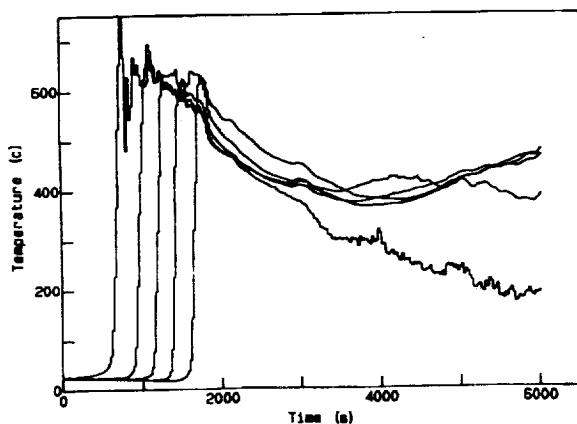
Figure 2. Temperature histories at intervals of 2 cm for an air mass flux of $\dot{m} = 5.7$ g m^{-2} s^{-1} and an ambient pressure of $P = 0.6$ atm.
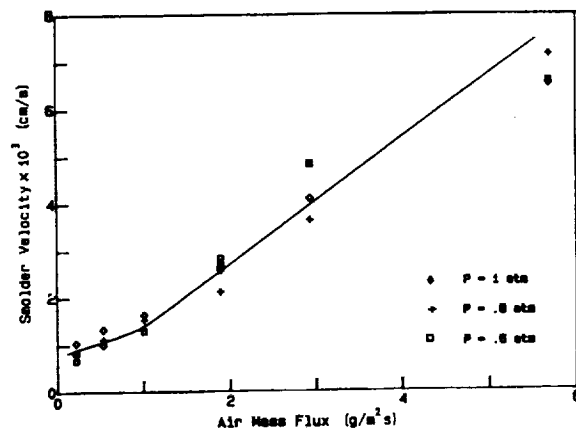

Figure 4. Variation of the smolder velocity with the air mass flow rate for constant pressures of 0.6, 0.8 and 1 atm.

Figure 3. Temperature histories at invervals of 2 cm for an air mass flux of $\dot{m} = 0.213$ g m^{-2} s^{-1} and an ambient pressure of $P = 0.6$ atm.

thermocouple are presented in Figs 2 and 3. The case of Fig. 2 corresponds to a vigorous, constant-velocity, smolder reaction. Figure 3 corresponds to a reaction that is weakening as it propagates through the cellulose and that eventually extinguishes probably for lack of oxidizer. The temperature profiles show how the fuel temperature increases as the reaction zone approaches the thermocouple location. As the reaction proceeds past the thermocouple a peak in temperature is recorded. This temperature is defined in this work as the smolder reaction temperature. After passage of the reaction, the temperature decreases due to heat losses through the test section walls and downstream to the environment. After the reaction zone has reached the bottom of the fuel a second temperature peak is often recorded, generally beginning with the lowest thermocouple. This seems to indicate the onset of a backwardly propagating secondary reaction involving the residual char.

The arrival of the smolder reaction at the thermocouple position is characterized by the maximum in the temperature profile. This maximum, however, is not well defined, which introduces inaccuracies in the definition of

the smolder front arrival time and, consequently, in the calculation of the smoldering velocity. However, if for a given flow rate and pressure the smolder velocity is constant, the measured temperature profiles at each thermocouple location have approximately the same slope. Thus the time for the reaction zone to pass from thermocouple to thermocouple may be calculated by defining a reference temperature common to all the temperature profiles. The reference temperature used in this work was 500°C. The displacement times are then averaged and divided by the known distance between thermocouples to calculate the smolder velocity. The method is not applicable when the smolder velocity is not constant, as is the case represented by the temperature profiles of Fig. 3. These cases require a careful examination of the temperature profiles to interpret the changes that are occurring in the smolder reaction. Since the velocity is not constant, only the first two thermocouples are used to calculate the smolder velocity.

The variation with the air mass flow rate of the measured smolder velocity is presented in Fig. 4 for the three ambient pressures used in these experiments. It is seen that the smolder velocity is approximately linearly proportional to the air mass flux at least for flow rates larger than 1 g m^{-2} s^{-1}. This linear relationship is in agreement with the theoretical predictions of Rogers and Ohlemiller[3] and of Dosanjh and Pagni[11] for forced flow co-current smolder. For mass flow rates less than 1 g m^{-2} s^{-1} the smolder velocity appears to level off, deviating from the linear relationship. This is an indication that at this low flow rate buoyancy may have some effect on the smolder process and that the transport of mass and heat may be controlled by mixed rather than forced convection. A mechanism that may be very important at these flow rates is the convection and diffusion of air from the top back toward the reaction zone. The convection currents are buoyantly generated by the raising post-combustion gases and the diffusion is the result of the difference in oxygen concentration between ambient and the smolder zone.

Results of Fig. 4 also show that for mass flow rates larger than 1 g m^{-2} s^{-1}, the smolder velocity is practically independent of ambient pressure at least for the present

experimental conditions and range of pressures tested. For low flow mass rate it seems that there is a weak pressure dependence of the smolder velocity which increases slightly as the pressure is increased, although the data scatter raises questions about the inferred trend. These results indicate that the smolder reaction itself is not very sensitive to gas pressure and that the observed pressure effect at the lower flow rate is due more to transport mechanisms (i.e. buoyancy) than to chemical kinetic mechanisms.

The dependence of the smolder reaction temperature on the air mass flux is presented in Fig. 5 with pressure as a parameter. The scatter in the data is due to the difficulty of defining the smolder reaction temperature, chosen here as the maximum temperature, and to experimental errors inherent in the technique used to measure the temperature and in the difficulty of packing the cellulose uniformly. These errors include the use of relatively thick thermocouples, the presence of heat losses through the thermocouples leads and uncertainties in the contact of the thermocouple junction with the porous cellulose. For this reason, the temperature data should be used to analyze relative effects and not absolute values. The temperature data of Fig. 5 reveals a moderate dependence of the smolder reaction temperature on the air mass flow rate, decreasing as the flow rate decreases. This result agrees qualitatively with the predictions of Dosanjh and Pagni.[11] With regard to the dependence of the temperature on the gas pressure, no systematic variation is observed within the scatter in the data. Only at very low air flow rates there is indication of a possible weak dependence of the smolder temperature on pressure, decreasing as the pressure decreases.

The weak dependence of the smolder velocity and smolder reaction temperature on the ambient pressure are indicative that the smolder reaction itself may only be weakly dependent on pressure, at least for the range of pressures tested. The observation of Dosanjh et al.[10] that smolder occurs at ambient pressures as low as 0.4 atm provides further confirmation of the above conclusion. The weak dependence of the smolder reaction on pressure may be the result of the surface reaction characteristics of the smolder process, which limits the dependence of the reaction rate on the gaseous species concentrations to

that of the oxidizer only. Another possibility is that since the smolder process is limited by the oxygen supply rate, the kinetics of the oxidation process does not have a strong influence on the rate of smolder propagation.

The weak dependence of the temperature on pressure permits the direct interpretation of the experimental data in terms of the variation of the smolder velocity with buoyancy. Assuming ideal gas behavior, the buoyancy force can be calculated through the relation $g(\rho_u - \rho_b)$ $\sim gP(T_b - T_u)$, where the subscript u indicates ambient conditions and subscript b the conditions after smolder reaction passage. Thus the data from Figs 4 and 5 in conjunction with the above expression can be used to deduce the dependence of the smolder velocity on the buoyancy force. The results are presented in Fig. 6, with the air mass flux as a parameter. It is seen that buoyancy does not appear to influence the smolder velocity except for very low mass flow rates, where the data indicate a weak dependence of the smolder velocity on buoyancy, decreasing as buoyancy decreases. Thus it can be concluded that for the present experimental conditions, buoyancy has only a minor influence on the smolder process, and that theoretical models of forced-flow co-current smoldering are applicable to describe the experiments. The small influence of buoyancy on the present experiments is understandable since the propagation of the smolder front is practically unidimensional, the density stratification is such that gravity has a stabilizing effect, and the motion of the air through the cellulose is deterred by its low porosity. The role of buoyancy should become more important as the void fraction of the fuel is increased or the direction of smolder propagation is changed. With cellulose, however, it is difficult to attain larger void fractions or to perform the experiments for upward propagation.

The present experimental results can be used to compare the predictions of the theoretical models of forced flow co-current smolder because of the minor role that buoyancy places on the process. The analysis of Dosanjh and Pagni[11] gives the following expression for the smolder velocity in terms of the air mass flux:

$$V_s = \frac{QY_0 \dot{m}_a''}{(1-\phi)\rho_{si}c_{ef}(T_b - T_u)} - \frac{\dot{m}_a''}{(1-\phi)\rho_{si}} \qquad (1)$$
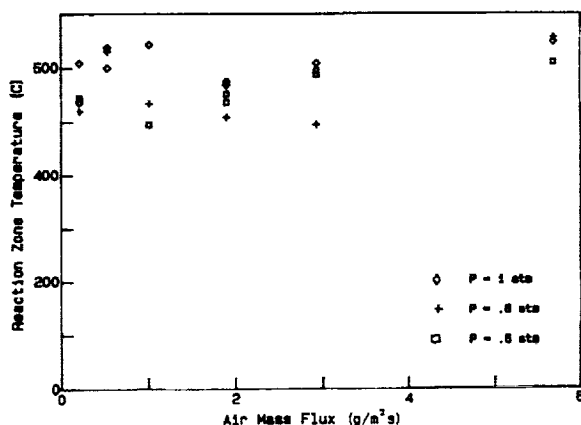

Figure 5. Variation of the peak reaction temperature with the air mass flow rate for constant pressures of 0.6, 0.8 and 1 atm.
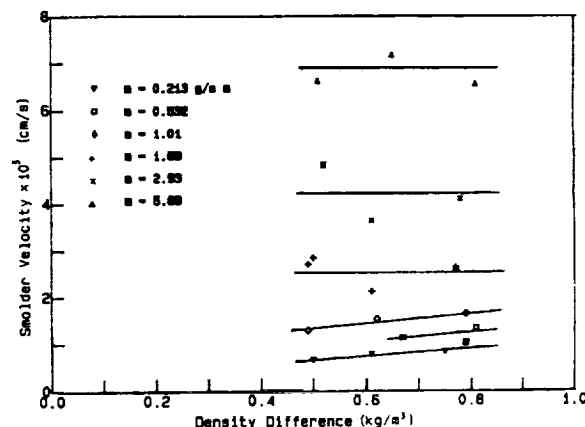

Figure 6. Calculated variation of the smolder velocity with the density difference $(\rho_u - \rho_b)$, i.e. buoyancy, for constant mass fluxes.

where V_s is the smolder velocity and $\dot{m}_a''$ the air mass flux. For the application of Eqn (1) to the present experiments the following data are used:[7,10] cellulose void fraction ϕ $=0.85$: cellulose density $\rho_{si} = 620\ \mathrm{kg\,m^{-3}}$; oxygen mass fraction $Y_0 = 0.23$; effective specific heat $c_{ef} = 1\ \mathrm{kJ}$ $\mathrm{kg^{-1}\,°C}$; reaction temperature $T_b = 600°C$; ambient temperature $T_u = 20°C$; the heat of combustion Q for a cellulose smolder reaction is not well known. Its value for a flaming reaction is around $12\,500\ \mathrm{kJ\,kg^{-1}}$.[7] However, Ohlemiller et al.[8,12] suggest a considerably lower value. Substitution of the above values in Eqn (1) gives a smolder velocity of $V_s = 37\ \dot{m}_a''$ in comparison with the experimental value of $V_s = 11\ \dot{m}_a''$. If a heat of combustion of $Q = 6000\ \mathrm{kJ\,kg^{-1}}$ is used, excellent agreement is obtained between the theory and the experiments. The noted differences in the heat of combustion may be due to the fact that the amount of char consumed affects the calculated value for Q, and this amount is experiment dependent.

Although the value of the heat of combustion has a major influence on the predictions of Eqn (1) there are also other differences between the model and the experiments that can explain the quantitative differences between the predicted and measured smolder velocity. One is the assumption that the char temperature remains constant and equal to the reaction temperature. The experiments, however, show that the temperature drops significantly downstream from the reaction zone (Figs 2 and 3). How quickly and how much the temperature drops seems to depend mainly on the air flow rate. At higher flow rates there is sharper and larger fall in temperature than that found at lower flow rates. This seems to be related to the amount of fuel consumed by the smolder reaction and consequently to the residual material left after the smolder reaction passage. At high mass fluxes there is less residual char/fuel behind the smolder front to insulate the reaction zone. The larger heat losses result in larger temperature drops downstream from the smolder reaction, contrary to the model assumption that the residual material totally insulates the reaction zone. The heat losses to the environment result in lower smolder velocities than those predicted by the model.

Another effect to consider is the assumption in the model that all the oxygen is consumed by the smolder reaction. However, it is not certain that this is true in the experiments, particularly at the higher air fluxes, where all the fuel is consumed and only ash is left behind the reaction. Thus the reaction may not always be oxygen limited as assumed in the model, which also will result in smolder velocities that are lower than those theoretically predicted. Finally, there is the possibility that the actual fuel void fraction is dependent on the air flow rate, increasing with it, which would affect the comparison of the experiments and theory.

CONCLUSIONS

The experiments conducted in this work on the downward propagation of a forced-flow, co-current smolder reaction through porous cellulose show that buoyancy has a minor influence on the propagation velocity and temperature of the smolder reaction. This seems to be the combined result of a relatively low fuel void fraction and the stabilizing influence that gravity has in this smolder configuration. The effect of buoyancy is only observed at very low mass fluxes, which is understandable since inertial forces are then at a minimum. The mechanism by which buoyancy affects the smolder process is, however, not evident. One possibility is the generation of flow non-uniformities due to heat losses to the walls or irregularities in the fuel distribution, which would be enhanced by the gravity. Another potential mechanism is the diffusion and convection of air from the top to the reaction zone. This transport process can only occur at very low forced mass fluxes, when the upward forced convection cannot totally counteract the downward diffusion and convection of air to the reaction zone. The resulting smolder reaction would be a mixed co-current and counter-current downward-propagating reaction.

The above mixed type smolder reaction is quite interesting, since it is likely to occur in practical situations. To observe the relative effect of the transport of air from the top to the reaction a few experiments were performed where an inverted funnel was placed over the test section to accelerate the hot downstream gases and in that way prevent the downward diffusion and convection of air to the reaction. The result was a noticeable reduction in the smolder velocity for a mass flux of $0.5\ \mathrm{g\,m^{-2}\,s^{-1}}$, and the eventual extinction of the reaction for a mass flux of $0.2\ \mathrm{g\,m^{-2}\,s^{-1}}$ and a gas pressure of 0.6 atm. The temperature histories for this last case are those presented in Fig. 3. The temperature profiles show that the smolder reaction was strong when it reached the first thermocouple but that as it progressed downward through the cellulose it weakened. This is evident because the smolder propagation slowed down, the reaction zone widened and the temperature decreased. Finally, at the approximate location of the fourth thermocouple the reaction did not sustain itself and extinguished. This decay of the smolder reaction as it propagated downward through the cellulose clearly demonstrates that diffusion and convection from the top can contribute to sustain the smolder reaction. Their contribution, however, is limited by the build-up of the residual ash/material layer behind the propagating reaction. As this layer grows, or becomes denser, the access of air to the reaction from the top become increasingly restricted until finally the reaction must depend only on the upwardly forced air flow. If this flow is not enough to sustain the reaction, extinction will occur.

It should be again emphasized that the results of this work, particularly those related to the effect of buoyancy, are dependent on the experimental conditions. For example, it is likely that increasing the fuel void fraction, or the oxidant oxygen concentration, will vary the nature of the results. This is because in the former case the drag force would decrease and in the latter the density difference would increase, which in both cases would result in a more favorable situation for the establishment of natural convective flows.

REFERENCES

1. F. A. Williams, *Combustion Theory*, 2nd edn, Benjamin Cummings, New York (1985).
2. T. J. Ohlemiller, Modeling smoldering combustion propagation, *Progress in Energy and Combustion Science* **11**, 277–310 (1986).
3. F. E. Rogers and T. J. Ohlemiller, Cellulosic insulation material—I: Overall degradation kinetics and reaction rates, *Combustion Science and Technology* **24**, 129–37 (1980).
4. R. P. Tye, Heat transmission in cellulosic fiber insulation materials, *Journal of Testing and Evaluation* **2**, 176–9 (1974).
5. F. Shafizadeh and A. G. W. Bradbury, Smoldering combustion of cellulosic materials, *Journal of Thermal Insulation* **2**, 141–52 (1979).
6. M. Day and D. M. Wiles, Combustability of loose fiber fill cellulose insulation: the role of borax and boric acid, *Journal of Thermal Insulation* **2**, 30–39 (1978).
7. N. A. Moussa, T. Y. Toong and C. A. Garris, Mechanism of smoldering of cellulosic materials, *Sixteenth Symposium (Inter-national) on Combustion*, The Combustion Institute, Pittsburgh, pp. 1447–57 (1976).
8. T. J. Ohlemiller and D. A. Lucca, An experimental comparison of forward and reverse combustion, *Combustion and Flame* **54**, 131–47 (1983).
9. R. G. Gann, W. L. Earl, M. J. Manka and L. B. Miles, Mechanism of cellulose smoldering retardance by sulfur, *Eighteenth Symposium (International) on Combustion*, The Combustion Institute, Pittsburgh, pp. 571–78 (1981).
10. S. S. Dosanjh, J. Peterson, A. C. Fernandez-Pello and P. J. Pagni, Buoyancy effects on smoldering combustion, *Acta Astronautica* **13**, 689–96 (1987).
11. S. S. Dosanjh and P. J. Pagni, Forced cocurrent smoldering combustion, *Combustion and Flame* **68**, 131–42 (1987).
12. T. J. Ohlemiller, J. Bellan and F. E. Rogers, A model of smoldering combustion applied to flexible polyurethane foams, *Combustion and Flame* **36**, 197–215 (1979).

PAPER 6*

"EXPERIMENTAL OBSERVATIONS OF THE EFFECT OF BUOYANCY ON THE RATE OF CO-CURRENT SMOLDER PROPAGATION IN CELLULOSE"

Newhall, J.L.

Masters Project, Department of Mechanical Engineering, University of California, Berkeley, 1988.

*Paper 6 could not be included in this summary report. However, the results from this paper are summarized in Paper 5, which is included.

PAPER 7

"GRAVITATIONAL EFFECTS ON CO-CURRENT SMOLDERING"

Torero, J., Kitano, M., and Fernandez-Pello, A.C.

**1990 Spring Meeting, Western States Section and Canadian Section of
The Combustion Institute, April 29 to May 2, Banff, Alberta, Canada, 1990.**

GRAVITATIONAL EFFECTS ON CO-CURRENT SMOLDERING OF POLYURETHANE FOAM

J. Torero, M. Kitano and A. C. Fernandez-Pello
Department of Mechanical Engineering
University of California
Berkeley, CA 94720

ABSTRACT

An experimental study is carried out to determine the effect of buoyancy on the propagation velocity of a free convection smolder reaction through a porous combustible material. Measurements are performed of the smolder velocity through polyurethane foam as a function of its location in the sample, the sample size, and the direction of propagation. The smolder velocity is obtained from the temperature histories of thermocouples placed at fixed intervals along the fuel centerline. Upward and downward burning free convection experiments show that buoyant forces cannot overcome the drag forces in specimen longer than 50 mm. Even in specimen longer than 50 mm extinction did not occur, indicating that the air inside the fuel pores provides enough oxidant for the smolder process to self-sustain. This conclusion is particularly important for a space based environment where gravity and consequently buoyancy could be negligible.

INTRODUCTION

Smoldering is defined as a non-flaming surface combustion reaction propagating through a porous fuel [1]. Although present in a variety of combustion processes, it is of particular interest in the fire safety field because of its role as a potential fire initiation source. Smoldering combustion is an oxygen-limited phenomenon which once established it is very difficult to extinguish. Circumstances that would suppress flaming often favor smolder and it is even possible for a smoldering combustion process to propagate and persist in the absence of any convection (forced or free), therefore it represents a serious fire hazard. Smoldering involves complex processes related to fluid mechanics and heat transfer in a porous media together with surface chemical reactions. Physical factors like fuel surface area per unit volume, permeability to gas flow, rate of heat loss from the reaction zone, and the nature of the ignition source are important in determining the smolder characteristics because they affect the controlling mass and heat transport processes. Chemically, the porous combustible material can sustain complex surface reactions that produce heat and combustion products. The interaction between the physical and chemical processes determines the final characteristics of the smolder reaction.

Most of the work that has been done to date on smoldering combustion has concentrated in analyzing the effects of oxidant composition, velocity and pressure on the smolder reaction [2-8]. The works of Refs. [9,10] are the only ones that specifically address the problem of the potential influence of buoyancy on the smolder reaction. In those works powder Cellulose was used as combustible porous material. The present study is a continuation of the above works, and has as objective to experimentally observe the effect of buoyancy on free convection, co-current, smoldering combustion of Polyurethane foam. The interest of using this material is two-fold; it is a commonly used material, and its structure permits upward burning experiments without collapsing problems as it occurs with Cellulose or other lose materials. The study of buoyancy effects on smoldering is accomplished here by comparing the smolder characteristics of downward and upward smolder propagation. The smolder velocity and temperature are measured at different locations in the sample and compared for different sample sizes and for both orientations.

EXPERIMENT

The fuel used in the experiments is an open cell, unretarded, white polyurethane foam, with a 26.5 Kg/m^3 density and 0.975 void fraction. The porous fuel is contained in a vertical parallelepiped consisting of an aluminum frame and insulation Fiberfax walls whose basic composition is alumina-silica and binders. The parallelepiped dimensions are varied to determine the

effect of scale on the smolder process. The wall material was selected for insulation purposes in an attempt to ensure a one dimensional smolder spread in a region of at least 50 mm in diameter from the sample centerline. The foam ignition is accomplished with an electrically heated igniter placed in close contact with the foam. The igniter is made of a nichrome wire placed in between two, 1 cm thick, porous ceramic honeycomb plates that provide rigidity to the igniter and heating uniformity. To insulate the ignition zone and simulate an ongoing smolder process, a layer of char from an already smoldered foam is placed at the other side of the igniter. The foam ignition requires a supply of 10.3 J/mm² for approximately 10 min. Most of this energy is used to heat up the igniter ceramic plates.

Eight Chromel-Alumel thermocouples 0.8 mm in diameter are embedded at predetermined positions in the porous fuel with their junction placed in the fuel centerline. The rate at which smolder spreads is measured from the temperature histories of the thermocouples, and is calculated from the time lapse of reaction zone arrival to two consecutive thermocouples and the known distance between the thermocouples. This velocity is assigned to be the smolder propagation velocity at the mid point between the two thermocouples. The arrival of the reaction zone is characterized by a maximum in the temperature profile. However, under most experimental conditions this maximum is not sharply defined, and the location of the solder zone is obtained by drawing tangents to the temperature curves and cutting them by a line at a temperature near to the maximum (350°C in this work). The smolder velocity is calculated from the time lapse between two consecutive intersections.

In the downward smoldering experiments the foam is ignited at the top and the smolder propagates downward, and in the upward smoldering ones the foam is ignited at the bottom and the smolder propagates upward. In the former case, the igniter/char layer minimizes the income of air from the top, so air is expected to be naturally induced from the bottom toward the reaction zone and products to leave pass the char toward the top. In the latter case the air is expected to come also from the bottom but flowing through the char layer toward the reaction zone, and the products to flow through the foam toward the top.

RESULTS

Experiments are performed for samples with square cross section 152 mm in the side and heights of 125 mm, 150 mm, 175 mm, 200 mm, and 300 mm (smaller samples were also tested but the results were so influenced by the end effects that did not provided useful information). The measured smolder propagation velocities at different positions along the sample are presented in Fig. 1 for downward and in Fig. 2 for upward smoldering. The origin of the x-axis (labeled Depth) corresponds to the ignition plane. Fig. 1 shows that in downward smoldering there is an initial zone, approximately two inches deep, where heat transfer from the igniter results in a slightly higher smolder velocity than in the sample center. This zone is followed by another one where an approximately constant smolder velocity is observed. The length of this region increases with the foam length. Then there is a final zone two inches deep that is characterized by a strong increase in the smolder velocity. For upward burning (Fig. 2) it can be observed a slightly longer igniter affected zone that is followed by another zone were the spread rate stays almost constant, and again a final zone were the smolder velocity increases sharply.

For downward smolder, the buoyant plume generated by the hot combustion gases is not able to overcome the pressure drop created by the foam in the initial two zones, therefore the reaction sustains itself by mainly using the air contained inside the foam pores. The smolder velocity in these zones becomes smaller when the length of the sample is increased, which indicates that there is always a small amount of air flowing through the fuel from the bottom, either by diffusion or natural convection. In the last two inches of foam the buoyant plume is able to overcome the pressure drop and naturally induced air reaches the reaction zone, enhancing its smolder propagation velocity.

For upward burning, the reaction products are not able to push their way upward out of the foam, and thus the oxygen cannot be buoyantly drawn from the bottom due to the elevated pressure generated inside the foam by the trapped products. The products dilute the oxygen

concentration in the foam porous, and therefore a decrease in the reaction rate along with a decrease in the smolder velocity occurs. The temperature distributions along the fuel sample presented in Fig. 3 clearly show that for upward smolder there is a decrease in the reaction temperature along the middle region of the sample. However, in this configuration the products also preheat a larger region of the unburnt fuel. The balance between the lower smolder temperature and the larger preheated region results in an almost constant spread rate, as it is shown in Fig. 4. Finally, as the fuel is burnt the pressure drop inside the foam decreases letting air flow through the sample and thus increasing the oxygen concentration and consequently the smolder temperature and velocity.

It is important to note that for small samples the end effect is going to be similar for both upward and downward smolder. However, as the size of the sample is increased the buoyant forces become larger in the upward case, which results in an earlier overcome of the pressure drop and an earlier increase in the smolder velocity (Fig. 4). It should be also pointed out that the larger smolder velocities in the constant zone obtained for the 300 mm sample are due to end effects caused by draft in the hood were the experiments are conducted and not to an actual fuel geometry effect. In this case the sample was too long for the hood being used in the tests and the influence of the drafts that the hood generates was bigger than in the other smaller samples. A series of experiments were also carried out without the char layer at one of the igniter sides. For both downward and upward configurations smoldered self-sustained initially; the downward smolder with a constant velocity of 5.10^{-3} cm/sec until it extinguished due to heat losses, and the upward with a decreasing rate that reached a minimum of 1×10^{-3} cm/sec before extinguishing due to depletion of oxygen and heat losses.

CONCLUSION

The results of this work show that for the present fuel and test conditions buoyancy has only a limited role in one dimensional smolder combustion because the buoyant forces generated by the postcombustion gases are not capable of overcoming the pressure losses generated in the porous fuel interior. They also show that the air contained in the fuel pores is capable of sustaining a smolder reaction that, although weak, is self-propagating. Under these conditions both upward and downward co-current smolder have similar smolder velocities. This result is of particular interest for the prediction of smolder in a space based environment.

ACKNOWLEDGEMENTS

REFERENCES

1. Ohlemiller, T.J., *Prog. in Ener. & Comb. Sci.*, 277, 1986.
2. Summerfield, M. and Mesina, N., *Prog. in Astro. and Aero.*, 129, 1981.
3. Rogers, F.E. and Ohlemiller, T.J., *Comb. Sci. and Tech.*, 24, 129, 1980.
4. Shafizadeh, F. and Bradbury, A.G.W., *J. Therm. Insul.*, 2, 141, 1979.
5. Day, M. and Wiles, D.M., *J. Therm. Insul.*, 2, 30, 1978.
6. Moussa, N.A., Toong, T.Y. and Garris, C.A., *16th Symp. (Int.) on Comb.*, 1447, 1976.
7. Ohlemiller, T.J. and Lucca, D.A., *Comb. Flame*, 54, 131, 1983.
8. Gann, R.G., Earl, W.L., Manka, M.J., and Miles, L.B., *18th Symp. (Int.) on Comb.*, 571, 1981.
9. Dosanjh, S.S., Peterson, J., Fernandez-Pello, A.C., and Pagni, P.J., *Acta Astro.*, 13, 689, 1987.
10. Newhall, J., Fernandez-Pello, A.C., and Pagni, P.J., *J. Fire Mat.*, (in press) 1989.

PROPAGATION VELOCITIES
(Free Convection-Downward Burning)
(Foam Length: ◇ -125mm, □ -150mm, + -175mm, x -200mm, ▽ -300mm)

Figure 1

PROPAGATION VELOCITIES
(Free Convection-Upward Burning)
(Foam Length: □ -150mm, + -175mm, x -200mm, ▽ -300mm)
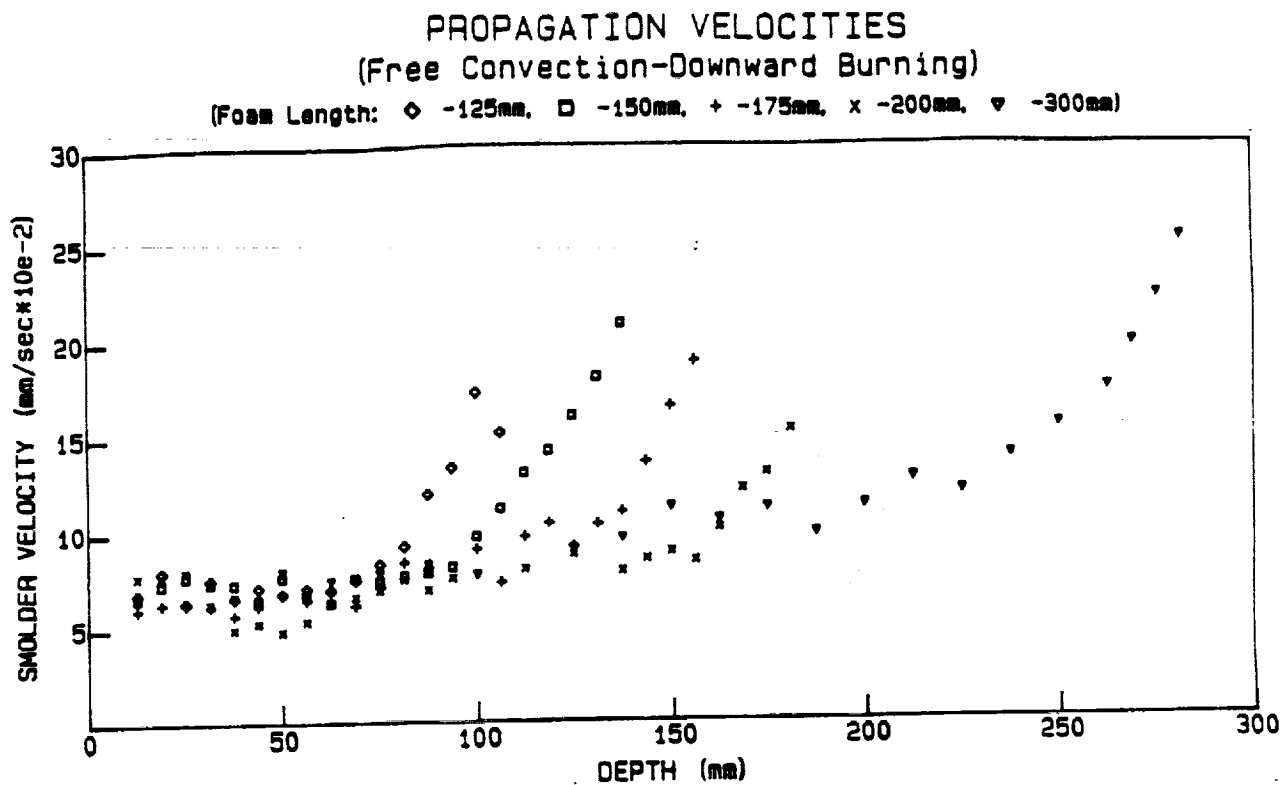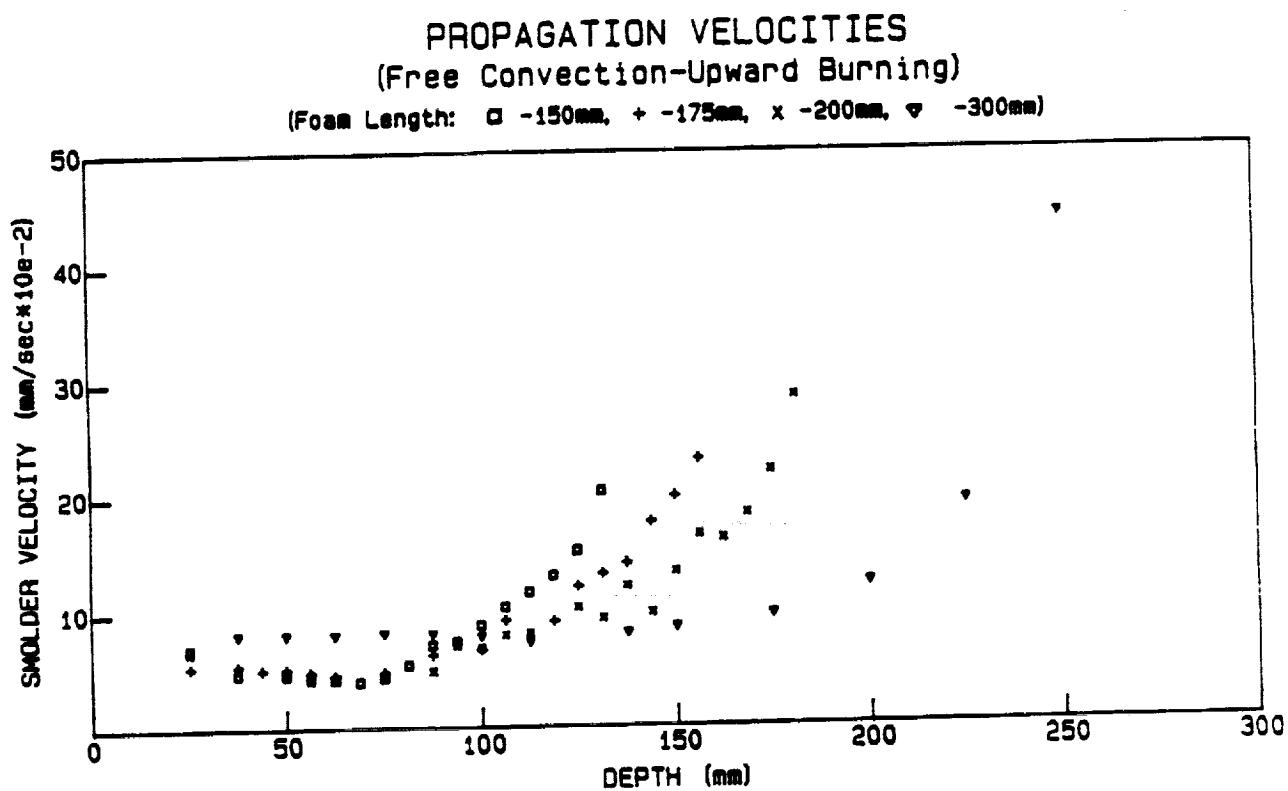
Figure 2

COMPARED MAXIMUM TEMPERATURES
(300 mm Sample)
(+ -Downward Burning, x -Upward Burning)
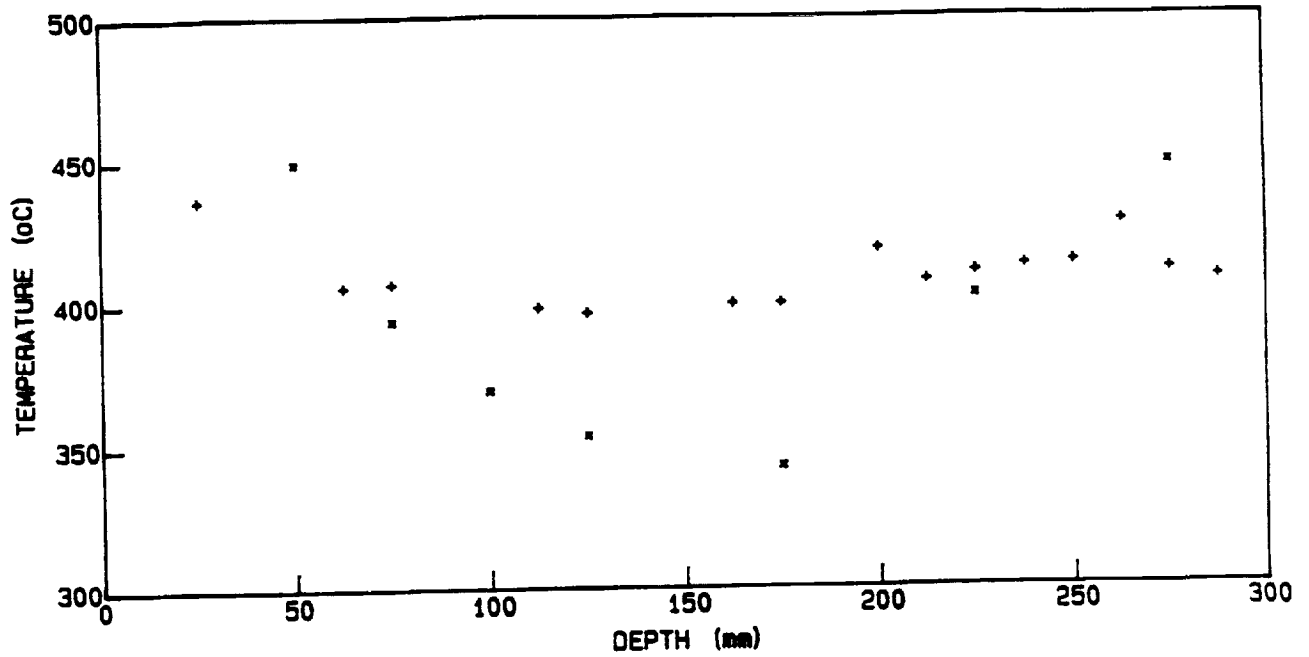
Figure 3

COMPARED PROPAGATION VELOCITIES
(300 mm Sample)
(+ -Downward Burning, x -Upward Burning)
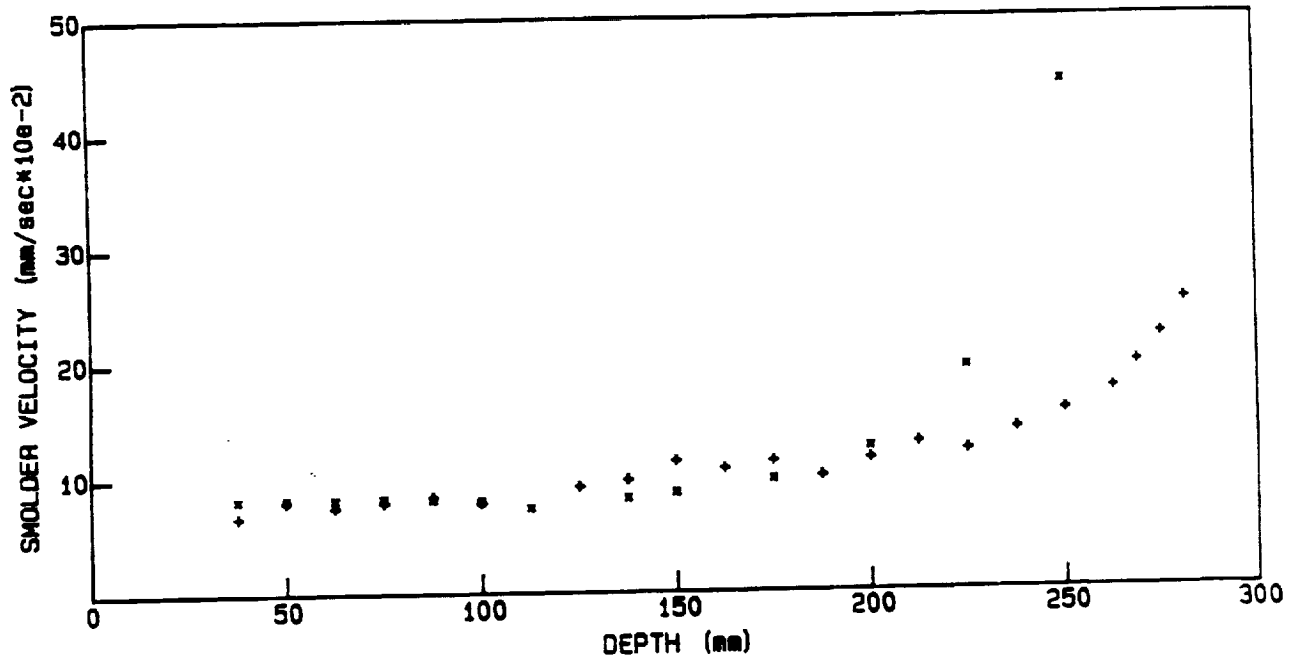
Figure 4

PAPER 8

"MIXED FLOW SMOLDERING OF POLYURETHANE FOAM"

Torero, J., Kitano, M. and Fernandez-Pello, A.C.

MIXED FLOW SMOLDERING OF POLYURETHANE FOAM

J.L. Torero, M. Kitano and A.C. Fernandez-Pello
Department of Mechanical Engineering
University of California
Berkeley,CA94720

1

ABSTRACT

An experimental study is carried out of the effect on the propagation velocity of a smolder reaction of a forced flow of oxidizer opposing the direction of smolder propagation. The experiments are conducted with a high void fraction polyurethane foam as fuel and air as oxidizer, in a geometry that approximately produces a one-dimensional smolder propagation. Measurements are performed of the smolder propagation velocity and smolder reaction temperature as a function of the flow velocity, location in the sample and direction of propagation (downward and upward). For both downward and upward smoldering three zones with distinct smolder characteristics are identified along the foam sample. An initial zone near the igniter were the smolder process is influenced by heat from the igniter, an intermediate zone where smolder is self-sustained and free from external effects, and a third zone near the sample end that is strongly affected by convective currents. The smolder reaction propagation velocity and temperature have a direct correspondence and are different in each one of these three zones. The variation with the opposed forced air flow of the smolder propagation velocity and temperature shows that both parameters reach a maximum at flow velocities of approximately 2.5 mm/sec. The analysis of the results confirm that the smolder process is controlled by the competition between the supply of oxidizer to the reaction zone and the loss of heat from the reaction zone. At low flow velocities oxygen depletion is the dominant factor controlling the smolder process, and the smolder velocity and temperatures are small. Increasing the flow velocity strengthens the smolder reaction resulting in larger smolder velocities and temperatures. At even larger flow velocities convective cooling becomes dominant causing the extinction of the smolder reaction. These competing mechanisms play a very important role in the end region of the sample where buoyancy generated currents result in the strong enhancement of the reaction or in its extinction, depending on whether oxygen supply or convective cooling is the controlling smolder mechanism. Comparison between downward and upward smoldering corroborates the above observations.

INTRODUCTION

Smoldering is defined as a non-flaming, surface combustion reaction propagating through a porous fuel [1]. Although present in a variety of combustion processes, it is of particular interest in the fire safety field because of its role as a potential fire initiation source. Smoldering combustion is a weakly reacting phenomenon which once established is difficult to detect and extinguish because it propagates through the interior of the fuel. Circumstances that would suppress flaming often favor smolder and it is even possible for a smoldering combustion process to propagate and persist in the absence of any convection (forced or free), therefore it represents a serious fire hazard. Smolder involves complex processes related to fluid mechanics and heat transfer in a porous media, together with surface chemical reactions. Physical factors like fuel surface per unit volume, permeability to gas flow, rate of heat loss from the reaction zone, and the nature of the ignition source are important in determining the smolder characteristics. Chemically the porous combustible material can sustain complex surface reactions and produce heat and combustion products. The interaction between the physical and chemical processes determines the final characteristics of the smolder reaction.

Most of the work that has been done to date on smoldering combustion has concentrated in analyzing the effect of oxidant composition, velocity and pressure on the smolder reaction [2-9]. The present work is part of an ongoing study that has as objective understanding the effect of buoyancy on the smolder process. It extends the works of Refs.[10,11] which used powder cellulose as combustible porous material, and studied the effect of buoyancy on the smolder process by changing the environmental conditions. Here Polyurethane foam is used as fuel, and the effect of buoyancy is determined by comparing the smolder parameters in downward and upward propagation. The interest of using this material is two fold; it is a commonly used material, and its structure permits upward burning experiments without collapsing problems as it occurs with cellulose and other loose materials.

The experiments are conducted in the opposed flow configuration, for both downward and upward smolder propagation . In this type of smolder the reaction zone and the forced oxidizer flow move in opposite directions. This type of smoldering is also referred to as co-current smoldering because if the reaction front is considered as stationary both the fuel and oxidizer reach the reaction zone in the same direction. In the downward smoldering experiments the foam is ignited at the top and smolder propagates downwards, and in upward smoldering the foam is ignited at the bottom and the smolder propagates upward. In downward smoldering the gravitational acceleration is in the same direction as that of smolder propagation, and for upward smoldering in opposite directions. Therefore, when the upward and

downward experiments are compared, the difference between the two can be attributed to gravity.

EXPERIMENT

A schematic diagram of the experimental installation is shown in Fig. 1. The porous fuel is contained in a 300mm long vertical duct with a 150mm side square cross section. The duct walls are made of insulating 10mm thick Fiberfax sheet mounted on an aluminum frame. . The oxidizer gas flows to the test section through a diffuser fitted at one end of the duct, after being metered with a Tyland mass controller. The fuel ignition is accomplished with an electrically heated igniter placed in close contact with the foam. The igniter consists of a Nichrome wire placed in between two, 5 mm thick, porous ceramic honeycomb plates that provide rigidity to the igniter and heating uniformity. To insulate the ignition zone and simulate and ongoing smolder process, a layer of char from an already smoldered foam is placed at the other side of the igniter.

The foam ignition is accomplished by applying an electrical energy of 10 J/mm2 for approximately 15 min. Most of this energy is used, however, to heat up the igniter ceramic plates to an approximate temperature of 400 C. During this heating period the air flow is turned off to avoid the flaming of the char or even the virgin material. The heating period is selected to ensure the self supported propagation of the smolder reaction. Once the ignition heating period is completed, the igniter current is turned off and the flow of air is turned on initiating the self sustained smolder process.

The rate of smolder propagation is obtained from the temperature histories of eight Chromel-Alumel thermocouples 0.8 mm in diameter that are embedded at predetermined positions in the porous fuel with their junction placed in the fuel centerline. The smolder velocity is calculated from the time lapse of the reaction zone arrival to two consecutive thermocouples, and the known distance between the thermocouples. The arrival of the reaction zone is characterized by a maximum in the temperature profile, although under most experimental conditions this maximum is not sharply defined. For this reason the location of the smolder zone is defined by the intersection of the tangent to the temperature curve at the inflexion point and a horizontal line at a temperature near to the maximum (350 C in this work).

All the experiments are conducted with 150mm side cubes of an open cell, unretarded, white polyurethane foam, with a 26.5 Kg/m3 density and 0.975 void fraction. The foam sample width was selected to ensure a one dimensional smolder propagation in a region of at least 50 mm in diameter from the sample center line, and the length to permit the observation of self propagating smolder without the influence of end effects. House compressed

air is used as oxidizer. For the downward experiments the igniter and char are placed on top of the foam sample and the air flow is introduced at the bottom. For the upward experiments the apparatus is simply rotated 180 degrees. The smolder process is characterized from the propagation velocity and reaction zone temperatures.

RESULTS AND DISCUSSION

DOWNWARD SMOLDERING

The variation of the downward smolder propagation velocity through the sample length is presented in Fig. 2. for several opposed air flow velocities. The data for a given flow velocity permits the identification of three regions within the foam sample with different smolder characteristics. An initial zone (I) approximately 70mm in length from the igniter where the smolder process is strongly affected by the heat from the igniter, and the smolder velocities are high. A second zone (II) approximately 50mm long in the middle of the sample where the smolder process is self sustained and free from end effects, and where the smolder velocity is fairly uniform. A third zone (III) at the end of the sample where the smolder is affected by buoyantly induced flows that cause an increase of the smolder velocity or a decrease depending on the initial strength of the reaction. The characteristics of the smolder reaction at each zone depend on the air flow rate. For comparison purposes, also included in Fig. 2 is the data from a smolder experiment in natural convection [13]. It is seen that the smolder propagation velocities are practically identical to those of case C, which implies that free convective currents generated through the sample during the downward smolder propagation are of the order of 0.9mm/sec.

The smoldering in the zone II is the most representative of a forced flow opposed smoldering, at least from the point of view of modeling, since is free from external effects. The smoldering in the other zones, however, are also interesting because they provide additional information about the process, and describe situations that may occur in practice. The smolder in zone I is representative of a situation where smoldering is supported by an external heat source (an electrical appliance for example). The smolder in zone III is of particular interest from the point of view of buoyant effects on smoldering. In this zone the sample thickness, and consequently its drag resistance, are small enough to permit the generation of buoyant flows through the virgin foam and remaining char. These flows may play an important role in the smolder process in this zone because their velocities may be considerably larger than those of the forced flow.

The variation of the maximum smolder reaction zone temperature along the foam sample is presented in Fig. 3 for the air flow velocities tested. Although less well defined, the data also

indicates the presence of the three zones described above. The temperatures in zone I are generally higher due to the igniter influence, and in region III lower due to convective heat losses to the external environment. Comparison between the results of Figs. 2 and 3 shows that there is a one to one correspondence between the smolder reaction temperature and the smolder velocity, with the smolder velocity being higher when the smolder temperature is higher. It is also observed that small variations in smolder reaction temperature results in large variations on the smolder propagation velocity.

The effect of the forced air flow velocity on the smolder propagation velocity is presented in Fig. 4, for the three zones indicated above. The smolder velocities are obtained from the results of Fig. 2 and are averaged values of the smolder velocities at each zone. It is seen that the smolder velocity presents a maximum for an air flow rate of approximately 2.5mm/sec, although the exact value of the flow rate varies with the zone under consideration. The value of the maximum velocity is also different for the three zones, and is highest in the zone III. The variation of the maximum smolder reaction temperature with the air flow rate is presented in Fig. 5, for the three zones. It is seen that the smolder temperature also presents a maximum at approximately 2.5mm/sec, again corroborating the correspondence between the temperature of the smolder reaction and its propagation velocity.

The above results point out to a smolder process that is controlled by the competition between the supply of oxidizer to the reaction zone and the loss of heat from the reaction zone. The presence of two smolder controlling mechanisms, chemical kinetics and heat losses, has been suggested before by Ohlemiller et.al. [1,9,12] in a study of the effect of oxygen concentration and pressure on the smolder of polyurethane foam. To understand how these two controlling mechanisms affect the characteristics of the smolder process is convenient to analyze the smolder data in zone II first. The temperature data of Fig. 3 shows that for low air flow velocity (B) the reaction zone temperature is low, which indicates the presence of a weak smolder reaction due to the low supply of oxidizer. This results in a very small smolder propagation velocity (Fig. 2, line B). As the air flow velocity is increased (C,D,E,F), the smolder reaction temperature and velocity first increase, reach a maximum, and then start to decrease. The increase in the smolder temperature and velocity is due to the increased supply of oxidizer to the reaction zone and the resulting enhancement of the chemical reaction. The larger amount of heat generated by the smolder reaction compensates for the larger convective heat losses caused by the larger air flow rate. As the air velocity is increased, eventually the heat generation and heat losses balance each other and the smolder reaction reaches a maximum in temperature and velocity (E). If the air flow rate is increased further the heat losses overcome the heat generation and the smolder temperature and velocity start to decrease (F). For larger air flow rates the heat losses dominate and cause the weakening and final extinction of the

6

smolder reaction (G,H).

The above discussed controlling mechanisms also apply to the other two zones, although the external effects modify somewhat the balance between then. In zone I the fuel is preheated by the igniter and when air is made available, the smolder reaction becomes very vigorous with high temperatures and propagation velocities. However, as the smolder reaction moves away from the zone of igniter influence, the cooling effect of the increased air flow becomes dominant and the reaction temperature and velocity decrease rapidly until the reaction stabilize itself or is extinguished. In zone III, the onset of buoyant currents affects the characteristics of the ongoing smolder reaction by either enhancing the reaction (cases C and D) or by weakening it (cases B,E and F). The mechanisms by which these buoyantly generated currents affect the smolder reaction is not totally understood although it appears that if the reaction is strong the added supply of air is dominant over the convective cooling. However, if the reaction is already weak, the heat losses are dominant weakening the reaction even further.

UPWARD SMOLDERING

The variation of the upward smoldering propagation velocity through the foam sample length is presented in Fig. 6 for the same opposed air flow velocities used in the downward smolder tests. Here also three zones can be identified with different smolder characteristics. The location of the zones and the variation of the smolder velocity in each zone are very similar to those observed in downward smolder. Also included in Fig. 6 is smolder velocity data for upward free convection smoldering, and it is seen that the smolder velocities are similar to those of case C, corroborating the previously stated observation that buoyancy generates air flows through the this type and size of foam of the order of 0.9 mm/sec.

The variation of the smolder velocity with the forced air flow rate in each of the three zones are presented in Fig. 4 together with the downward data to facilitate comparison of the results. It is seen that the effect of the forced air flow on the upward smolder velocity is similar to that of the downward smoldering with the smolder velocity first increasing, and then decreasing as the air velocity is increased. The air velocity that produces the maximum smolder velocity is also approximately the same as that measured for downward smoldering except in zone III where it occurs at slightly higher velocities. The almost identity between the downward and upward smolder velocities in zones I and II indicates that in these experiments buoyancy does not affect the smolder process in zones deep in the foam interior . It does, however, have a noticeable influence in zone III, which corroborates that the end effects observed in the

7

donward dataata are the result of buoyantly generated air flows.

The variation of the maximum smolder reaction temperature along the foam sample is presented in Fig. 7 for the same air flow velocities used in the downward tests. The temperature distributions are also similar to those observed for downward smoldering, although the upward smolder temperatures are generally higher than those for downward smolder, particularly in zones I and III. This is clearly seen from the data of Fig. 5 where the variation of the smolder temperature at the three sample zones with the air flow velocity is presented together with the data for downward smoldering.

The above results indicate that for opposed upward smoldering the competition between the supply of oxidizer to the reaction zone and the heat losses from the reaction zone also determine the characteristics of the smolder process. They also show that the smolder processes for downward and upward propagation are identical when buoyancy is unimportatnt, as it could be expected. When buoyancy participates in the process, as is the case in zone III, there are differences between the smolder in the two configurations that are worth discussing. In upward smoldering the buoyantly generated gas heats up as it flows upward past the elevated temperature char and preheats the virgin fuel ahead of the smolder zone, which tends to produce larger smolder velocities than in downward smoldering. However, these upwardly moving gases also contain combustion products that can reduce the supply of oxidizer to the reaction zone and cause the weakening of the smolder reaction. Depending on which effect is dominant, the buoyant flow can enhance or deter the progress of the smolder reaction, as it can be observed comparing the results of Figs. 4 and 5.

CONCLUDING REMARKS

By studying the effect of a forced flow of oxidizer on a smoldering reaction propagating downward and upward through a high void fraction porous fuel, the present work has helped to identify the controlling mechanisms of opposed smoldering combustion, and to determine the potential importance of buoyancy on the process. Particularly interesting is the verification that in this type of smoldering, the competition between oxygen supply and heat losses determines, in conjunction with the initial state of the reaction, the fate of the smolder reaction. Both at very low and (relatively) large air velocities the smolder reaction is weak due to respectivelly lack of oxidizer or excessive heat losses.

The range of air velocities that produce a stronger smolder-

ing reaction are surprisingly small (of the order of 2mm/sec) in comparison to those in other combustion processes. For this reason buoyancy can have a very important role in the smolder process since buoyantly generated air currents can be larger than those that has been observed to produce the extinction of the smolder reaction. In fact this is one of the reasons why unassisted smolder is difficult to be sustained if the sample is small. For large size samples, the buoyant flows do not penetrate the fuel interior as readily because of the large drag losses, and the porous fuel itself insulates the reaction from external convective cooling, which helps the establishment of the smolder reaction, particularly if enough oxidizer is available at the reaction zone.

REFERENCES

1. Ohlemiller, T.J., Prog. in Ener.& Comb. Sci.,277, 1986.2. Summerfield, M. and Mesina, N., Prog. in Astro. and Aero.,29, 1981.
3. Rogers, F.E. and Ohlemiller, T.J., Comb. Sci. & Tech., 24, 129, 1980.4. Shafizadeh, F. and Bradbury, A.G.W., J. Ther. Insul.,2, 141, 1979.
5. Day, M. and Wiles, D.M., J.Therm. Insul., 2, 30, 1978.6. Moussa, N.A., Toong, T.Y. and Garris, C.A., 16th Symp. (Int.) Comb., 1447, 1976.
7. Ohlemiller, T.J. and Lucca, D.A., Comb. Flame, 54, 131, 1983.8. Gann, R.G., Earl, W.L.,Manka, M.J. and Miles, L.B., 18th Symp. (Int.)   Comb., 571, 1981.9. Ohlemiller, T.J., Bellan, J. and Rogers, F., Comb. and Flame, 36, 197, 1979.
10. Dosanjh, S.S., Peterson, J., Fernandez-Pello, A.C., and Pagni, P.J., Acta Astro., 13, 689, 1987.
11. Newhall, J., Fernandez-Pello, A.C., and Pagni, P.J., J. Fire Materials., (in press) 1989.
12. Ohlemiller, T.J., Comb. Flame, 81, 354, 199013. Torero, J., Kitano, M. and Fernandez-Pello, A.C., 1990 Spring   Joint Meeting, WSS/CS/Comb. Inst., April 1990, Banff, Canada

LIST OF FIGURES

IGNITER CROSSECTION

TEST AREA CROSSECTION

MICRO-COMPUTER

MULTIPLEXER

POROUS FUEL

THERMOCOUPLES

CHAR

GLASS BEADS

G.C.PROBE

TEST SECTION

IGNITER

GAS CHROMATOGRAPH

CONTROLLED MASS FLOWMETER

AIR

AIR FLOW
VELOCITY
(mm/sec)
—○— 0.00
—●— 0.30
—■— 0.48
—□— 1.70
—▲— 2.80

DISTANCE FROM IGNITION (mm)

SMOLDERING VELOCITY (mm/sec)

AIR FLOW
VELOCITY
(mm/sec)
○— 0.00
●— 0.30
■— 0.48
□— 1.70
▲— 2.80

DISTANCE FROM IGNITION (mm)

TEMPERATURE (°C)

Torero et al.
Figure 3

Torero et al.
Figure 5

Torero et al.
Figure 8

PAPER 9

"FORWARD SMOLDERING OF POLYURETHANE FOAM"

Torero, J. Kitano, M. and Fernandez-Pello, A.C.

FORWARD SMOLDERING OF POLYURETHANE FOAM

J.L.Torero, M.Kitano and A.C.Fernandez-Pello
Department of Mechanical Engineering
University of California
Berkeley, CA94720

ABSTRACT

An experimental study is carried out of the effect on the propagation velocity of a smolder reaction of oxidizer forced to flow in the same direction of smolder propagation. The experiments are carried with a high void fraction polyurethane foam as fuel and air as oxidizer, in a geometry that approximately produces a one-dimensional smolder propagation. Measurements are performed of the smolder propagation velocity and smolder reaction temperature as a function of the flow velocity, location in the sample and direction of propagation (downward and upward). For both upward and downward smoldering three zones with distinct smolder characteristics are identified along the foam sample. For forward burning the air is forced through the igniter, therefore an initial zone near the igniter where the smolder process is influenced by heat from the igniter, and intermediate zone where smolder is self-sustained and free from external effects, and a third zone near the sample end that is strongly affected by convective currents. The smolder reaction propagation velocity and temperature have a direct correspondence and are different in each one of these three zones. The variation with the forced air flow of the smolder propagation and temperature shows that both parameters increase with the flow rate reaching, in the case of upward smolder, transition to flaming at flow velocities of approximately 15 mm/sec. At very small flow rates (smaller than 2.5 mm/sec) extinction is experienced under different conditions. The analysis of the results confirm that the smolder process is controlled by the competition between the supply of oxidizer to the reaction zone and the loss of heat from the reaction zone. Forward smoldering shows a clear effect of gravity for flows smaller than approximately 3.0 mm/sec, at low flow rates oxygen depletion is the dominant factor controlling the smolder process, air is forced through the igniter therefor convective heat losses to the air flow are less significant letting us observe the effect of gravity in the transport of oxidizer. For opposed flow previously reported experiments showed that increasing the flow velocity strengthens the smolder reaction resulting in larger velocities and temperatures, but for flows over 2.5 mm/sec convective cooling to the air becomes dominant leading to extinction. For this configuration the air flow carries the reaction heat to the virgin fuel resulting in temperatures and velocities increasing monotonically with the flow rate, giving a more clear image of the effect of gravity and the competition between oxidizer transport and heat losses. The convective currents acting at the end of the sample show a different view of this competition, which is transition to flaming; smolder would not transition to flaming in downward burning where convective currents will significantly oppose the forced flow, instead transition to flaming will occur in upward burning where convective currents act in the same direction of the forced flow. Comparison between downward and upward smoldering corroborates the above observations.

INTRODUCTION

Smoldering is defined as a non-flaming, surface combustion reaction propagating through a porous fuel [1]. Although present in a variety of combustion processes, it is of particular interest in the fire safety field because of its role as a potential fire initiation source. Smoldering combustion is a weakly reacting phenomenon which once established is difficult to detect and extinguish because it propagates through the interior of the fuel. Circumstances that will suppress flaming often favor smolder and it is even possible for a smoldering combustion process to propagate and persist in the absence of any convection, therefore it represents a serious fire hazard. Smolder involves a complex process related to fluid mechanics and heat transfer in a porous media, together with surface chemical reactions. Chemically the porous combustible material can sustain complex surface reactions and produce heat and combustion products. The interaction between the physical and the chemical processes determines the final characteristics of the smolder reaction.

Most of the work that has been done to date on smoldering combustion has concentrated in analyzing the effect of oxidant composition, velocity and pressure on the smolder reaction [2-9]. The present work is part of an ongoing study that has as objective understanding the effect of buoyancy on the smolder process. It extends the works of references [10,11] which used powder cellulose as combustible porous material and of references [13,14] which used the same polyurethane foam; all of these studied the effect of buoyancy on the smolder process by changing the environmental conditions. Here

Polyurethane foam is used as fuel, and the effect of buoyancy is determine by comparing the smolder parameters in downward and upward propagation. The interest of using this material is two fold; it is a commonly used material, and its structure permits upward burning experiments without collapsing problems as it occurs with cellulose and other loose materials.

The experiments are conducted in the forward flow configuration, for both downward and upward smolder propagation. In this type of smolder the reaction zone and the forced oxidizer flow move in the same direction. This type of smoldering is also referred to as counter-current smoldering because if the reaction front is considered as stationary the fuel and oxidizer reach the reaction zone in opposite directions. In the downward smoldering experiments the foam is ignited at the top and smolder propagates downward, and in upward smoldering the foam is ignited at the bottom and the smolder propagates upward. In downward smoldering the gravitational acceleration is in the same direction as that of smolder propagation, and for upward smoldering in opposite direction. Therefore when the upward and downward experiments are compared, the difference between the two can be attributed to gravity.

EXPERIMENT

A schematic diagram of the experimental installation is shown in Fig. 1. The porous fuel is contained in a 300 mm long vertical duct with a 150 mm side square cross section. The duct walls are made of insulating 10 mm thick Fiberfax sheet mounted on an aluminum frame. The oxidizer gas flows to the test section through a diffuser fitted at one end of the duct, after being metered with a Tyland mass controller. The fuel ignition is accomplished with an electrically heated igniter placed in close contact with the foam. The igniter consists of a Nichrome wire placed in between two, 5 mm thick, porous ceramic honeycomb plates that provide rigidity to the igniter and heating uniformity. To insulate the ignition zone and simulate an ongoing smolder process, a layer of char from an already smoldered foam is placed at the other side of the igniter. For the forward smoldering experiments the section containing the igniter and the char is placed at the diffuser exit upstream from the section containing the virgin foam.

The foam ignition is accomplished by bringing the temperature of the igniter up to approximately 500 °C. For these specific experiments the power needed was of approximately 10 J/mm² during a period of 15 minutes. Most of the energy is used, however, to heat up the igniter ceramic plates to the temperature mentioned above. Since the air flows through the igniter before reaching the fuel, the air flow is turned off, during the heating period, to avoid extending the igniter influence to a larger fraction of the virgin material, and to standardize the ignition process that if performed with the air flow on, will

depend on the flow rate. The heating period is selected to ensure the self supported propagation of the smolder reaction. Once the ignition heating period is completed, the igniter current is turned off and the flow of air is turned on, initiating the flow assisted smolder process.

The rate of smolder propagation is obtained from the temperature histories of eight Chromel-Alumel thermocouples 0.8 mm in diameter that are embedded at predetermined positions in the porous fuel with their junction placed in the fuel centerline. The smolder velocity is calculated from the time lapse of the reaction zone arrival to two consecutive thermocouples, and the known distance between the thermocouples. Although the arrival of the reaction zone is characterized by a maximum in the temperature profile, under most experimental conditions this maximum is not sharply defined, and the location of the smolder zone is defined by the intersection of the tangent to the temperature curve at the inflexion point and a horizontal line at a temperature near to the maximum (350 °C in this work).

All the experiments are conducted with 150 mm side cubes of an open cell, unretarded, white polyurethane foam, with a 26.5 Kg/m^3 density and 0.975 void fraction. The foam sample width was selected to reduce the effect of the cold walls on the smoldering reaction thus helping to obtain one dimensional smolder propagation in a region of at least 50 mm in diameter from the sample centerline. The length is enough to permit the observation of self propagating smolder without the influence of the igniter and end effects. House compressed air is used as oxidizer. For the downward experiments the igniter and

char are placed on top of the foam sample and the air flow is introduced through the igniter. For the upward experiments the apparatus is simply rotated 180 degrees. The characteristics of the smolder process are determined from the propagation velocity and the reaction zone temperatures.

RESULTS AND DISCUSSION

The analysis of the data is done by dividing the foam sample in three different zones (Fig.2). An initial zone (I) of length dependant on the flow rate, but that is never more than 50 mm away from the igniter, where the smolder process is affected by the heat from the igniter. A second zone (II) covering approximately the central 60 mm of the sample, where the smolder process is self sustained and relatively free from end effects. A third zone (III) at the end of the sample where the smolder is affected by the ambient air and by the small size of the virgin fuel left for smoldering. The extent and characteristics of the smolder reaction at each zone depend on the air flow rate. Since during the period of ignition there is no forced air flow through the foam this region is not representative of the type of smoldering studied here, therefore the data from the first 35 mm of the sample is not presented. Also since the velocities are obtained from the temperature histories of two thermocouples and assigned to the midpoint between the two, the corresponding figures (Fig.2 and Fig.7) do not show data points for the first 50 mm.

The smoldering in zone II is the most representative of a forced flow, forward

smoldering, at least from the point of view of modeling, since external effects are limited. The smoldering in the other zones, however, are also interesting because they provide additional information about the process, and describe situations that may occur in practice. The smoldering in zone I is representative of a situation where smoldering is supported by an external heat source. As it will explain later, the smolder in zone III is of particular interest from the point of view of buoyant effects on smoldering. In this zone the length of the virgin fuel, and consequently its drag resistance, are small enough to permit the generation of buoyant flows through the virgin foam and remaining char. These buoyant flows may play an important role in the smolder process in this zone because their velocities may be similar or even larger than those of the forced flow.

In smoldering the heat transfer from the smoldering reaction to the adjacent material, and the oxygen supply to the reaction zone are the two main mechanisms that control the smolder reaction characteristics [1,9,12,13,14]. In the forward flow configuration heat is being carried away from the reaction zone towards the virgin foam by the flow after passing through the char. As a consequence the heat transferred to the virgin fuel is enhanced as the flow rate is increased, which favors the propagation of the smolder reaction. The oxidizer transport effect of the forced flow is two fold; increasing the flow rate increases the oxygen supply to the reaction zone , on the other hand the products of combustion are carried into the virgin foam mixing with the oxidizer inside the pores and diluting the oxygen concentration. Furthermore, the oxidizer is reaching the reaction zone through the char which while preheating the air may also cause its depletion due to secondary reactions. Another process that takes place under certain flow conditions is the onset of secondary

reactions in the char, the fresh oxidizer moving through the char will encounter hot char generating secondary smolder reactions behind the smoldering front that will propagate in an opposed manner. This will result in the depletion of the oxidizer reaching the smolder wave from the char, this effect significantly decreases the smoldering reaction strength. The final characteristics of the smolder reaction in a given case depend on the relative importance of each one of these effects.

DOWNWARD SMOLDERING

The variation of the downward smolder propagation velocity and of the maximum smolder reaction temperature through the sample length are presented in Figs. 2 and 3 respectively, for several opposed air flow velocities. The results of figures 2 and 3 are better analyzed if the processes involved in each zone are treated separately. Although the boundaries between the different zones cannot be clearly determined, the following trends are identified from the measurements. Since the smoldering in zone II is the most representative of a forced flow we will begin by describing this zone. With no flow (A) the smolder velocities for this zone remains almost constant decaying in the last 30 mm of the sample. When the air flow is increased to 0.3 mm/sec (B) extinction is observed very early in the sample, a further increase in the flow velocity (C) shows again a slowly propagating reaction that reaches extinction in the last 30 mm of the sample. And for higher flow velocities the smolder velocity increase monotonically with the flow velocity. Smolder

velocities are not constant for flow velocities greater than 1.7 mm/sec (D) instead it is observed that the smolder velocities increase towards the end of the sample. The smolder reaction temperatures follow a different trend. For no flow temperature remains almost constant and below 350°C along all zone II, which is indicative of a very weak smolder reaction (13,14). For case (B) it can be observed that the temperature drops down along the fuel sample until the reaction finally extinguishes. As the flow velocity is increased above values of 0.9 mm/sec (C) the maximum reaction temperatures keep increasing as the air flow velocity is increased. The temperatures for a given flow rate shows that the reaction temperatures decay through zone II.

These results are explained by the interaction of the above indicated heat and mass transfer mechanisms. For the case with no forced flow the smoldering reaction propagates into the virgin foam which contains oxidizer in its pores. This is mainly a self sustained process where the biggest contribution of oxidizer to the reaction comes from the air in the foam pores. When air velocities of the same order of magnitude as the smoldering velocities are forced through the sample (B), the air flow pushes the products of the reaction along with the smoldering front, which causes a significant dilution of the oxidizer and results in the observed extinction. As the air velocity is increased above the smoldering velocity, the forced flow carries the products away from the reaction and brings to the reaction zone more oxidizer, which results in an increase in the smolder velocity as the flow is increased.

The smolder velocity data for a specific flow velocity show that the smolder propagates faster as the smoldering reaction progresses through the sample. The rate of

propagation increases as the air flow is increased. This is the result of the forced flow carrying the hot products from the smoldering reaction into the virgin fuel, which preheat the foam and consequently increase the smolder velocity. The further away from ignition the longer the preheating period and therefore the higher the temperature of the fuel encountered by the smoldering front.

The temperature data of Fig.3 shows that for most flow rates the smolder reaction temperatures decrease as the reaction moves through the sample. The decrease in temperature is brought by the continuous, although weak, reaction of the char together with the onset of stronger secondary reactions mentioned above. This reactions consume part of the oxygen from the air flowing through the char and as a consequence the air reaching the primary smolder reaction zone has a smaller oxygen concentration which results in weaker, lower temperature, smaller reactions. Secondary reactions are very weak at low flow velocities and may extinguish due to convective heat losses. The strength of these secondary reactions is enhanced as the forced flow is increased due to the increased availability of oxidizer. It is interesting to note that although the temperature decreases the smolder velocity increases, which indicates that for most flow rates the preheating effect is dominant over the decrease in oxidizer. However, as the air flow is increased and the strength and duration of this secondary reactions increase, they consume more oxidizer until the preheating effect is canceled and the smolder velocity starts to decrease as occurs in case (I). The maximum reaction temperatures of these secondary reactions are much higher than the typical smoldering temperatures, usually above 500°C.

The same mechanisms described for zone II basically apply for zone I. In zone I the heat from the igniter represents an extra source of heat and introduces a transient period where the process transitions from the no flow ignition heating regime to the forced flow described above. This transition period becomes less important as the air flow is increased but the increase in oxidizer supply results in secondary reactions that will be present in the char near the reaction zone and near the igniter, resulting in the dilution of the oxidizer reaching the smolder reaction. For small flow rates the products accumulated during the ignition period are pushed into the smolder reaction zone resulting in a decrease in both temperatures and smoldering velocities, this effect decreases with the increase in air flow, but as it becomes less significant the secondary reactions appear depleting the oxygen concentration reaching the reaction zone. Only for the largest air flow (I) it is observed that the heat carried from the hot secondary reaction has an effect on the smoldering reaction in zone I, increasing both reaction temperature and velocity.

In zone III the amount of virgin foam is small enough that buoyant recirculation can be generated. These recirculation flows bring additional air to the reaction zone which results in the trends observed in Figs. 2 and 3 for zone II to be magnified. From Fig.2 it can be seen that for all flow rates the smolder velocities increase strongly as the smolder front reaches the end of the sample. The data of Fig.3 shows also an apparent increase in the maximum reaction temperature in the last centimeter of the sample indicating the presence of added oxidizer from the ambient air. For smolder velocities higher that 0.5 [mm/sec] and in the last 50 mm of fuel the combined flow rate of the forced flow and buoyantly induced recirculating flows (due to the decrease in drag) is big enough so as to make the products

concentration in the total flow very small leading to an enhancement in the reaction, at this point we start observing weak secondary reactions moving upward in an opposed flow configuration. A continuous secondary reaction can be observed in the char for flow rates between 2.8 and 7.8 [mm/sec].This secondary reaction is weak and can not propagate opposed to the forced flow due to heat losses to the incoming flow. The secondary reaction will use up some of the oxygen that used to reach the smoldering reaction, resulting in a further decrease in the reaction temperature. The process at this stage becomes extremely complicated, we have virgin foam heavily preheated, more and more significant buoyant flows coming from the bottom and opposing the forced flow that result on an overall increase in the smolder velocity, for flows smaller than 10 [mm/sec] (Fig.2 and 4) and an overall decrease in the reaction temperatures (Fig. 3 and 6). As we increase the flow rate the secondary reactions increase in strength and start to propagate upwards, becoming, for flows greater that 14 [mm/sec], the dominant reaction using large fractions of the incoming oxidizer. Smoldering velocities decrease and stabilize around 0.9 [mm/sec] and reaction temperatures are kept high by the heat generated from the secondary reaction which is basically a much stronger process.

The effect of the forced air flow velocity on the smolder propagation velocity is presented in Fig.4, for the three zones indicated above. An expansion of the data at low air velocities is presented in Fig.5. The smolder velocities are obtained from the results in Fig.2 and are averaged values of the smolder velocities at each zone. From Fig.5 it is seen that in zones I and II the smolder velocity has a minimum at a flow velocity of approximately 4 [mm/sec], and increases monotonically with the flow velocity for larger flow rates. Zone

III shows a minimum at 4 [mm/sec] and a maximum at approximately 7 [mm/sec] (Fig.4). For downward smoldering, buoyant flows generated by the density stratification move upward while the forced flow moves downward, therefore they will distort the flow when the forced velocity is smaller or equal to the buoyant one which results in smaller smolder rates due to the accumulation of the products in the reaction zone. For greater air velocities, the forced flow becomes the dominant transport mechanism and the smolder velocity increases with the flow rate due to the increase in oxygen supply to the reaction. This is confirmed by the results from previous experiments in the opposed configuration [14] where it was determined that buoyant flows were of the order of 1 [mm/s], which corresponds approximately to the values observed in Fig. 5. The reaction in zone I is particularly weak at low flow velocities because the reaction products generated during the ignition period remain stagnant around the reaction zone diluting the oxidizer in the fuel pores. In some cases the competition between the oxidizer supply to the reaction zone and the convective heat losses from the reaction zone yields in favor of the heat loses and results in the extinction of the reaction (case B). The fact that this extinction is buoyantly originated is further verified by the results from zone III and for upward propagation described below.

UPWARD SMOLDERING

The variation of the upward smoldering propagation velocity along the foam sample length is presented in Fig.7 for the same forward air flow velocities used in the downward smoldering tests. Here also the three zones indicated above are used to describe the data.

Zone II has almost constant velocities for small flow rates and the velocities in zone III increase as the smoldering front reaches the end of the sample. In Fig.8 it can be observed that for small flow velocities temperatures are constant through zones I and II and that as the flow velocities is increased temperatures are highest in zone I and decay through zones II and III for flow rates larger than approximately 6 [mm/sec].

The basic mechanisms that explained the results for downward burning also apply for upward burning, and the differences can be attributed to gravity. In upward burning both the buoyant and forced flow move in the same direction in the central core of the fuel, and therefore the combustion products are always driven ahead of the reaction. As a result the smolder velocities for all flow velocities increase monotonically with the flow rate and extinction is not observed even at the lowest flow velocities. Another important aspect that results from buoyancy acting in the same direction as that of the forced flow is the decrease in mixing between products and oxidizer. In downward burning since buoyant flows and forced flows move in opposite directions, recirculation current are enhanced and therefore mixing between products and oxidizer is also enhanced, for upward burning both flows act in the same direction therefore the products travel through the fuel, and mixing is less significant.

For upward smolder we also observe secondary reactions of similar characteristics to the one observed for downward smolder. These reactions produce the same effect on the smolder wave as before. In this case, however, these secondary reactions bring up a very important aspect to the smolder process, transition to flaming. In upward smolder the

products leave the smolder reaction zone through the virgin fuel, therefore the char that will act as fuel for the secondary reaction receives fresh and unobstructed oxidizer flow. Since the limiting parameter for a smolder reaction to transition to flaming is the oxidizer concentration, if the reaction is strong enough upward burning will have a greater tendency to flaming. The experiments confirmed this hypothesis, and the secondary reaction transition to flaming for 14 [mm/sec] flow rate.

The variation of the upward smolder velocity with the forced air flow rate is presented in Fig.4 and 5. From these figures it can be observed that the significance of buoyancy in zone I extends to flows approximately 14 [mm/sec]. Buoyancy increases the transport of hot gases from the reaction region to the virgin foam nearby. This is particularly significant in zone I where a slight increase in oxygen supply will result, due to the preheating effect, in a significant increase in the propagation velocity, as observed for flow rates over approximately 6 [mm/sec]. During the ignition period in upward burning the products will move towards the virgin fuel, instead in downward burning they will move towards the char, therefore the concentration of smolder and temperature of the virgin foam, at the time when the forced flow is initiated, are higher in the upward burning configuration. These results can be observed in Fig. 4, 5 and 6 where we see that for upward burning, velocities increase monotonically with flow rate and the initial region of extinction present in downward smolder does not appear. In zone II the reaction is free from the igniter effect and the effect of buoyancy is reduced to flows below 2.8 [mm/sec]. The smolder velocities for zone II have values smaller to the ones of zone I (up) and higher to those of zone I (down) showing how the influence of the igniter magnifies the buoyant

effect.

In zone III the influence of buoyancy is very significant, forced flow and buoyantly generated flows appear to be of the same magnitude, for small flow rates after the period where extinction is observed in downward smolder, propagation is much faster in the downward configuration even though reaction temperatures are always much lower. In downward burning buoyancy opposes the forced flow generating recirculating currents that seem to enhance both mixing of products and oxidizer as well as localizing the heat transfer from the reaction zone to the virgin fuel, instead in upward burning mixing is less intense and the heat is carried to a much larger region of the fuel. More mixing results in a more diluted oxidizer and therefore in lower temperatures for downward smoldering and more localized heat transport in a smaller smolder velocity for upward burning. As we increase the flow rate this complicated scenario brings a transition range of flows between 4 and 8 [mm/sec] where is not clear which effect is dominant and resulting in a clear higher temperature for upward smolder and smolder velocities which tend to match for flow rates over 5 [mm/sec].

CONCLUDING REMARKS

By studying the effect of a forced flow of oxidizer on smoldering reaction propagating downward and upward through a high void fraction porous fuel, the present work has helped to identify the controlling mechanisms of forward smoldering combustion, and to determine the potential importance of buoyancy on the process. Particularly interesting is the

verification that in this type of smoldering, the competition between oxygen supply and heat transport determines, in conjunction with the initial state of the reaction, the fate of the smolder reaction. Heat transport mechanisms are always favorable in this type of smoldering, but even under this favorable conditions lack of oxidizer can lead to weak reactions and even to extinction.

The favorable heat transfer conditions enable us to observe the process of transition to flaming, which occur for flows over 14 [mm/sec]. Buoyancy plays an important role in this process, the main limiting factor in transition to flaming is the lack of oxidizer, the large drag loses induced by the foam do not enable enough oxidizer to reach the reaction zone so only when the smolder reaction propagates in the char that is more porous flaming can occur. Even then the oxidizer content has to be high and the enhanced mixing between oxidizer and products in downward smolder inhibits flaming. This work is very important because it shows the requirements that any future transition to flaming experiment in this kind of material has to have.

ACKNOWLEDGEMENTS

REFERENCES

1. Ohlemiller,T.J., Prog. in Ener.& Comb. Sci., 277, 1986.

2. Summerfield, M. and Mesina, N., Prog. in Astro. and Aero., 129, 1981.

3. Rogers, F.E. and Ohlemiller, T.J., Comb. Sci. & Tech., 24, 129, 1980.

4. Shafizadeh, F. and Bradbury, A.G.W., J.Ther. Insul.,2,141,1979.

5. Day, M. and Wiles, D.M., J.Therm. Insul., 2, 30, 1978.

6. Moussa, N.A., Toong, T.Y. and Garris, C.A., 16th Symp. (Int.) Comb., 1447,1976.

7. Ohlemiller, T.J. and Lucca, D.A., Comb. Flame, 54, 131, 1983.

8. Gann, R.G., Earl, W.L., Manka, M.J. and Miles, L.B., 18th Symp. (Int.) Comb., 571, 1981.

9. Ohlemiller, T.J., Bellan, J. and Rogers, F. , Comb. and Flame, 36, 197, 1979.

10. Dosanjh, S.S., Peterson, J., Fernandez-Pello, A.C., and Pagni, P.J., Acta Astro., 13, 689, 1987.

11. Newhall, J., Fernandez-Pello, A.C., and Pagni, P.J., J. Fire Materials, 14, 145, 1989.

12. Ohlemiller, T.J., Comb. Flame, 81, 354, 1990

13. Torero, J.L., Kitano, M., and Fernandez-Pello, A.C., 1990 Spring Joint Meeting, WSS/CS/Comb. Inst., April 1990, Banff, Canada.

14. Torero, J.L., Kitano, M., and Fernandez-Pello, A.C., Fall Meeting, WSS/Comb. Inst., October 1990, San Diego, CA.

LIST OF FIGURES

FIGURE 1

EXPERIMENTAL FACILITY

FIGURE 2
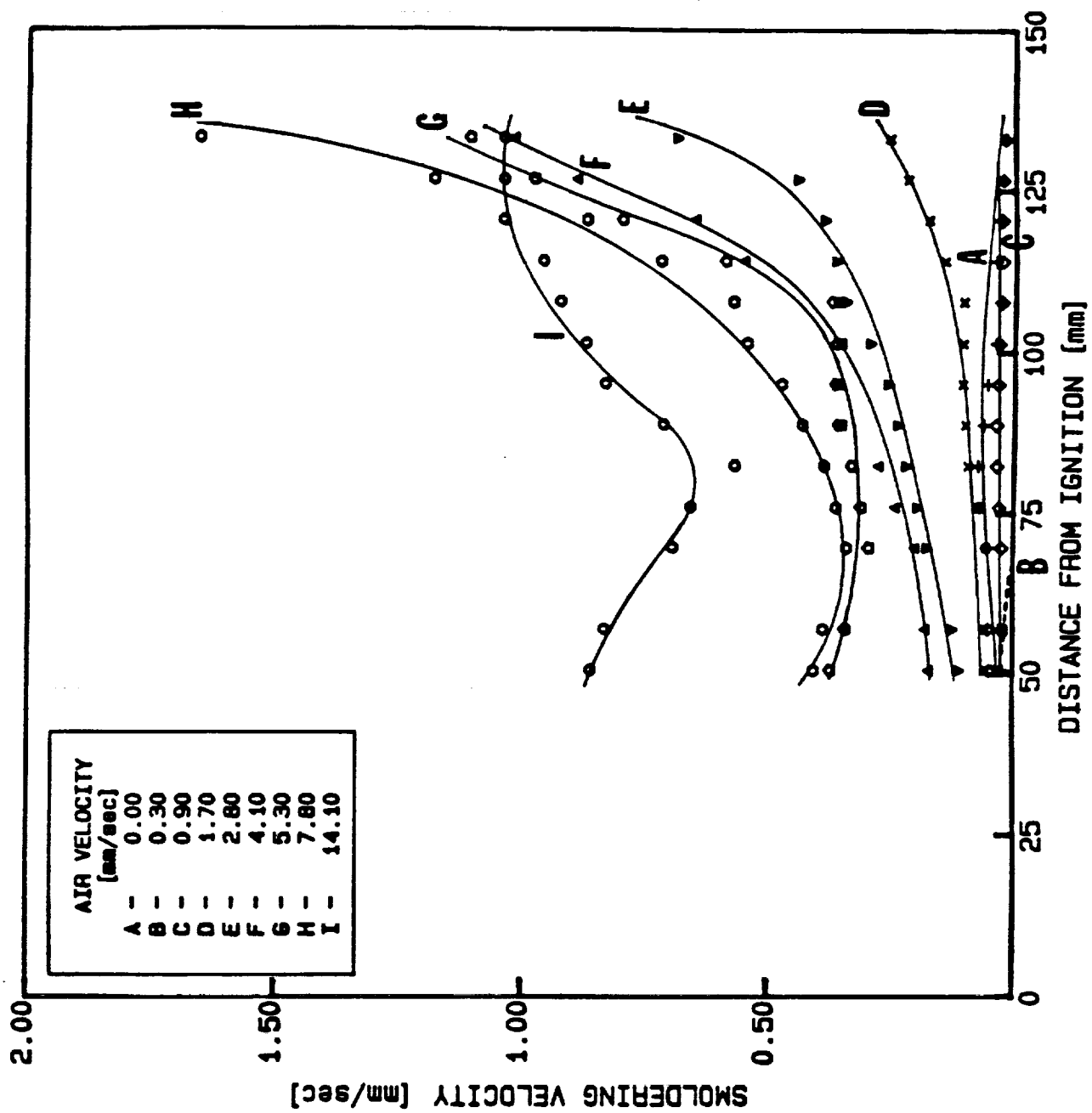
FIGURE 3
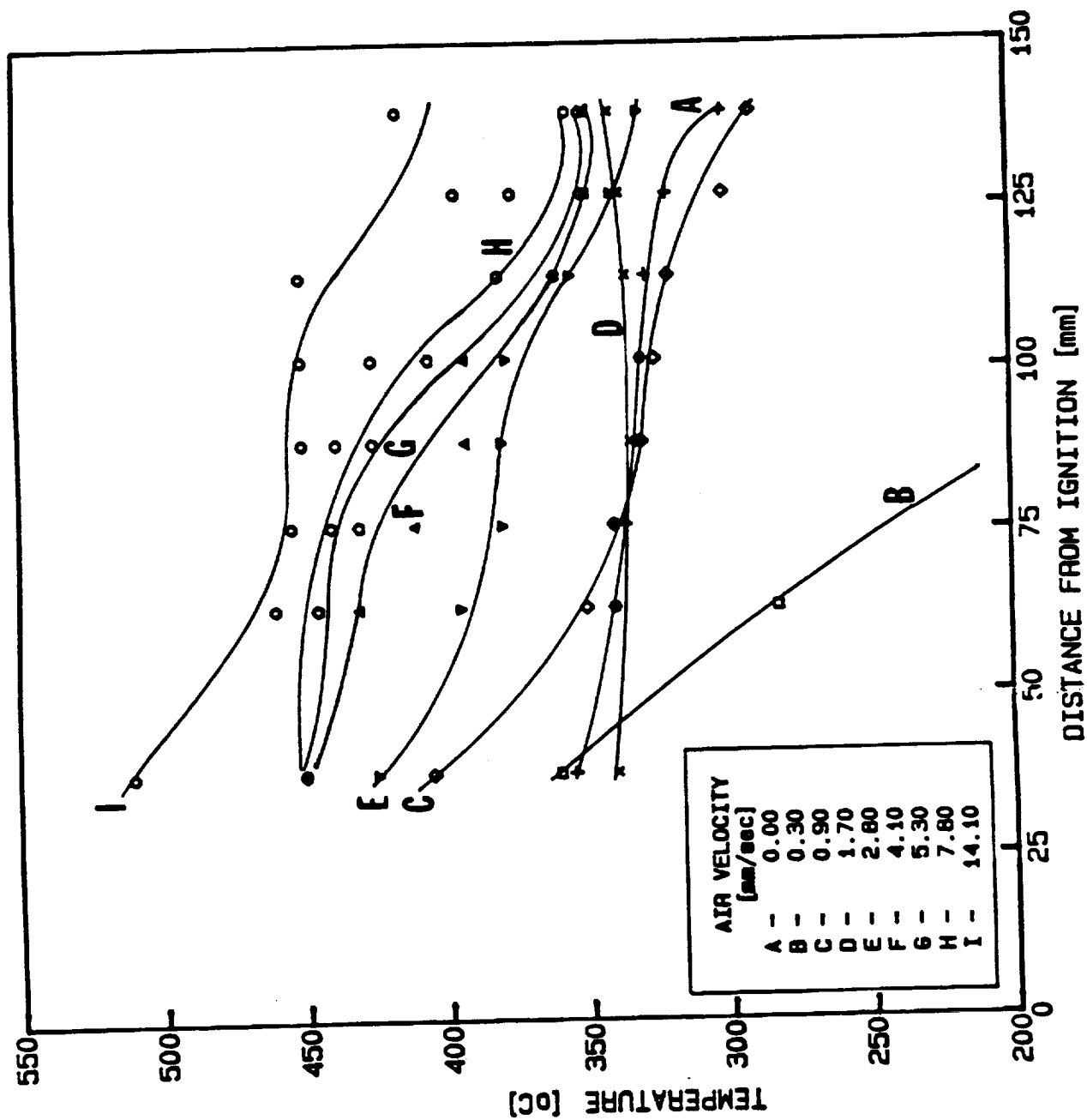
FIGURE 4
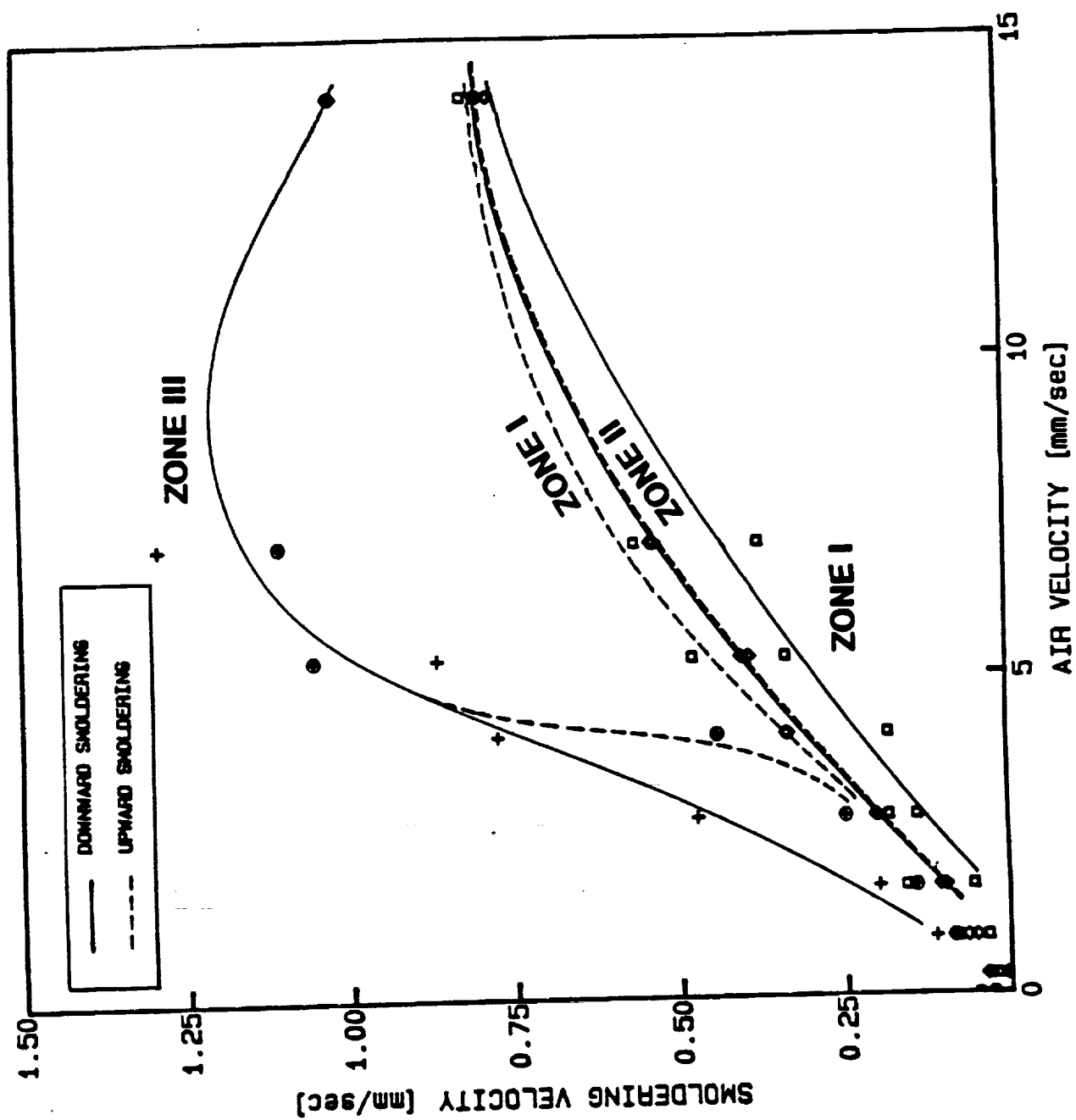
FIGURE 5

FIGURE 6

FIGURE 7

AIR VELOCITY
[mm/sec]
A – 0.00
B – 0.30
C – 0.90
D – 1.70
E – 2.60
F – 4.10
G – 5.30
H – 7.80
I – 14.10

SMOLDERING VELOCITY [mm/sec]

DISTANCE FROM IGNITION [mm]
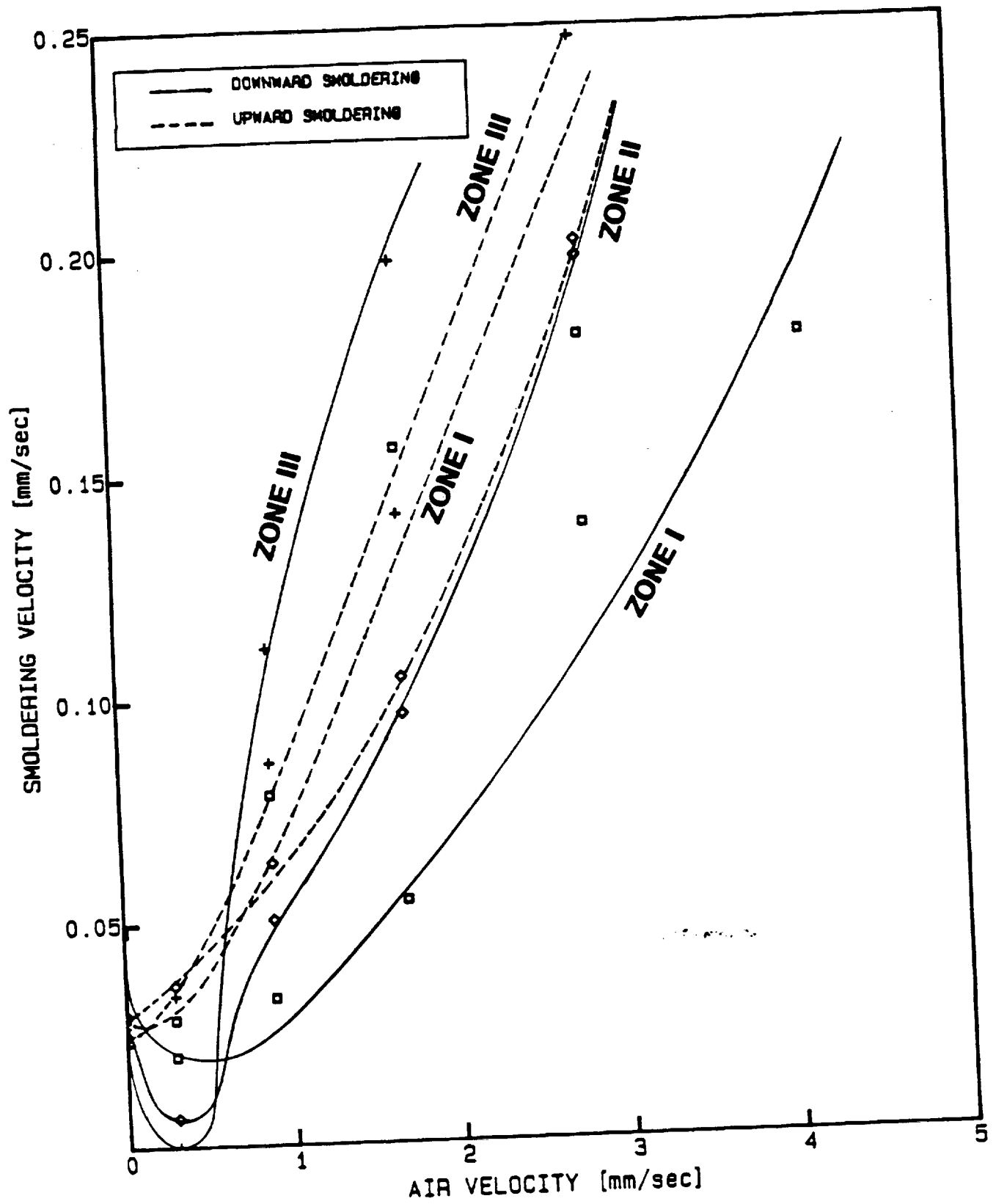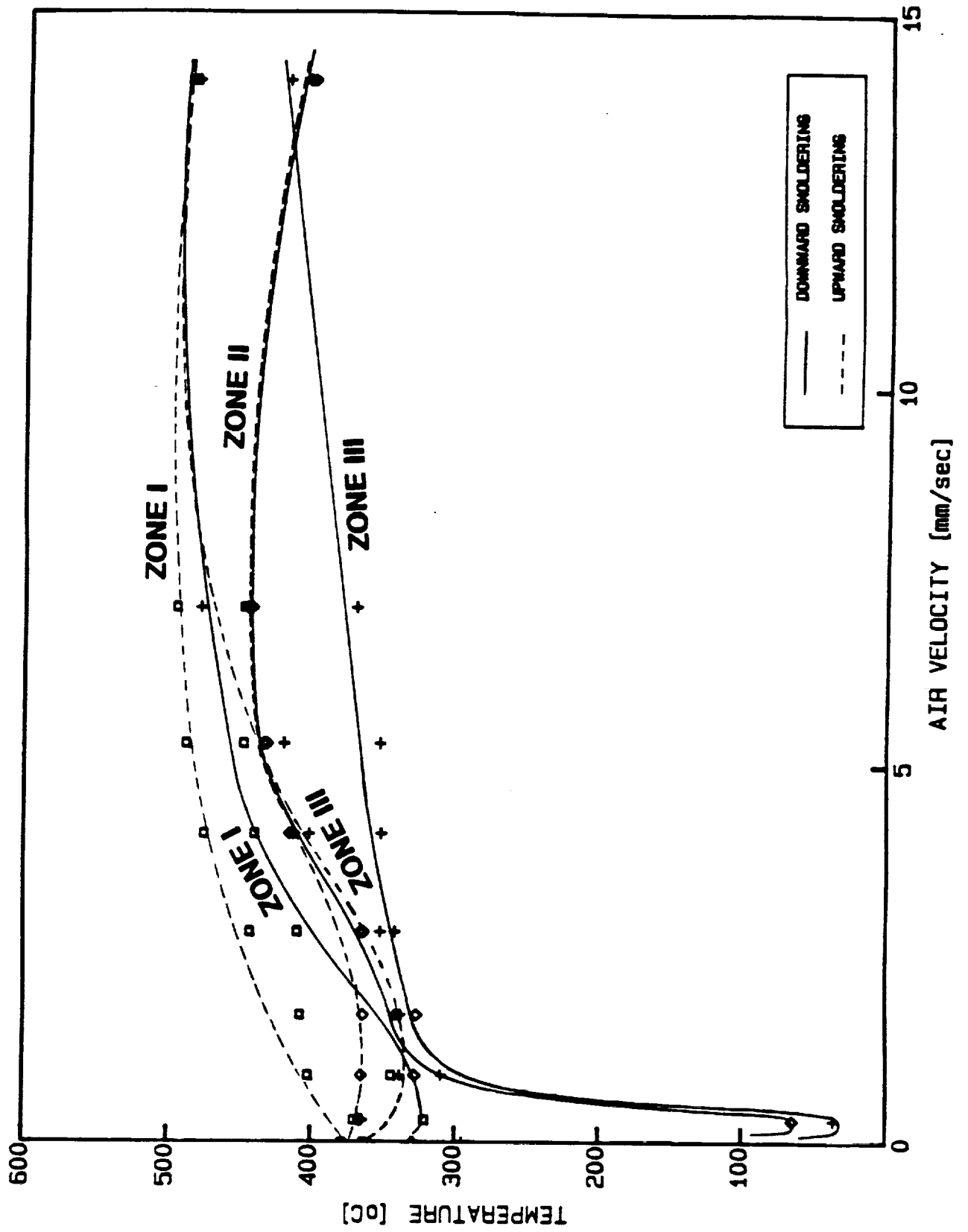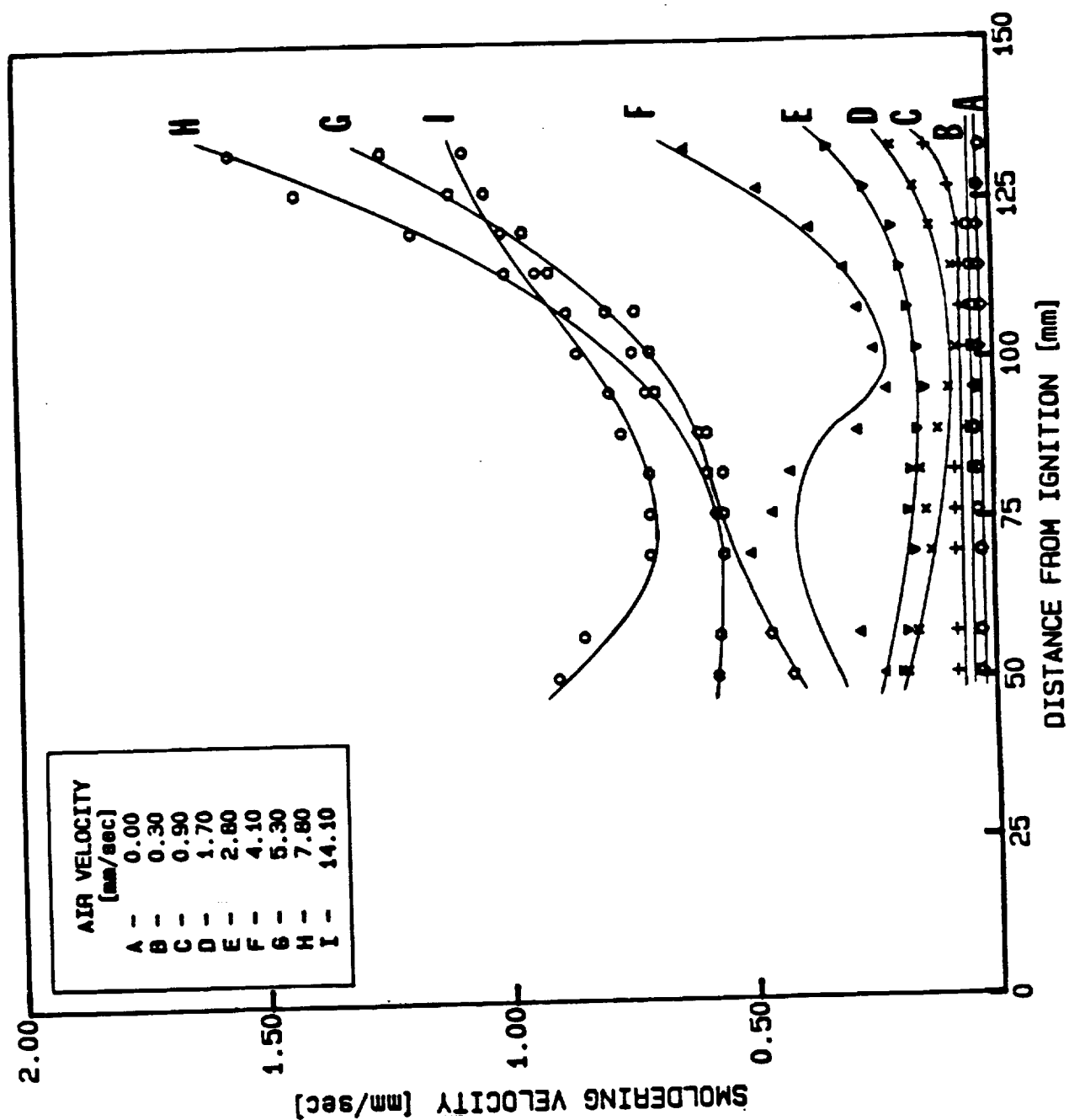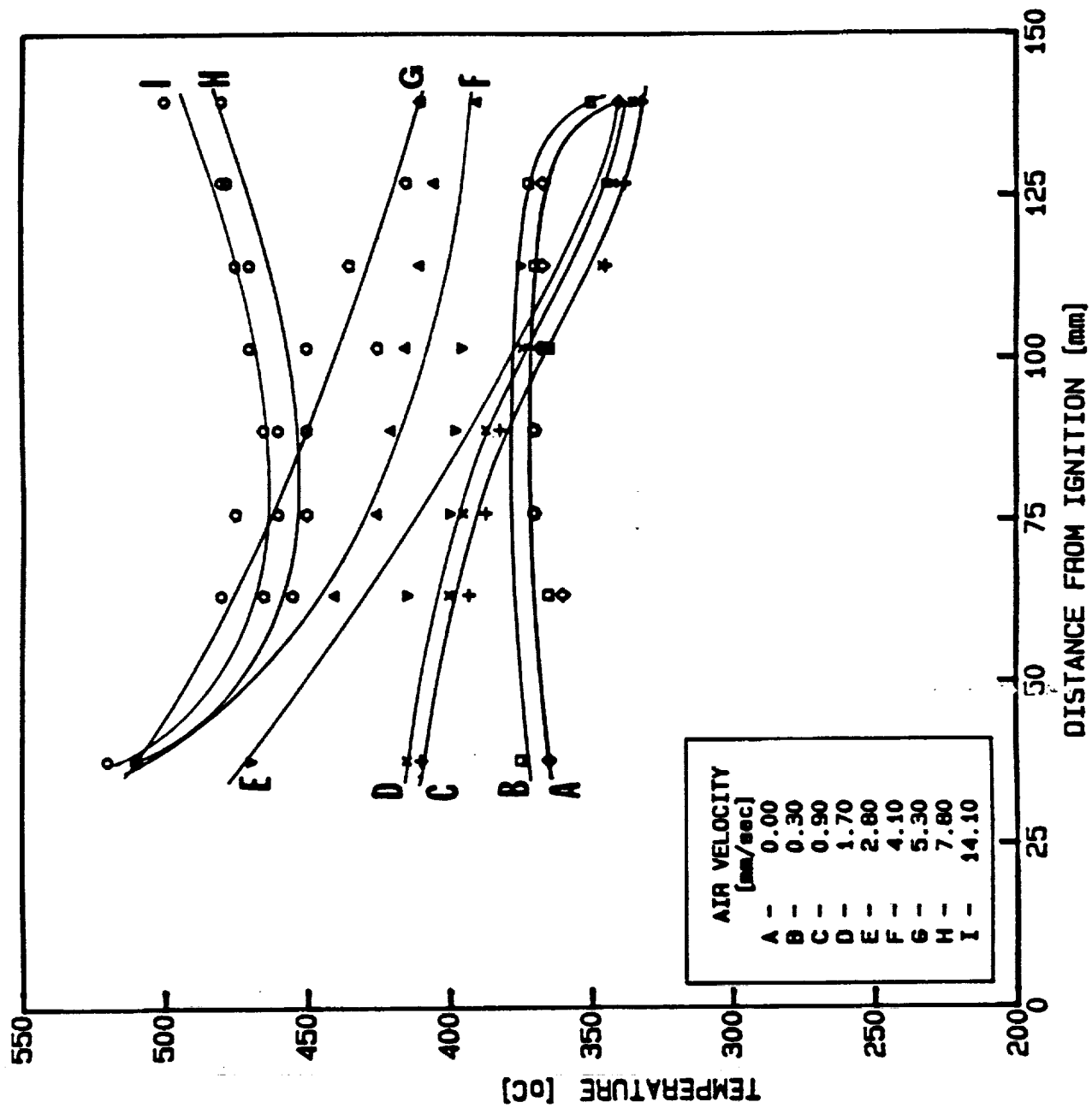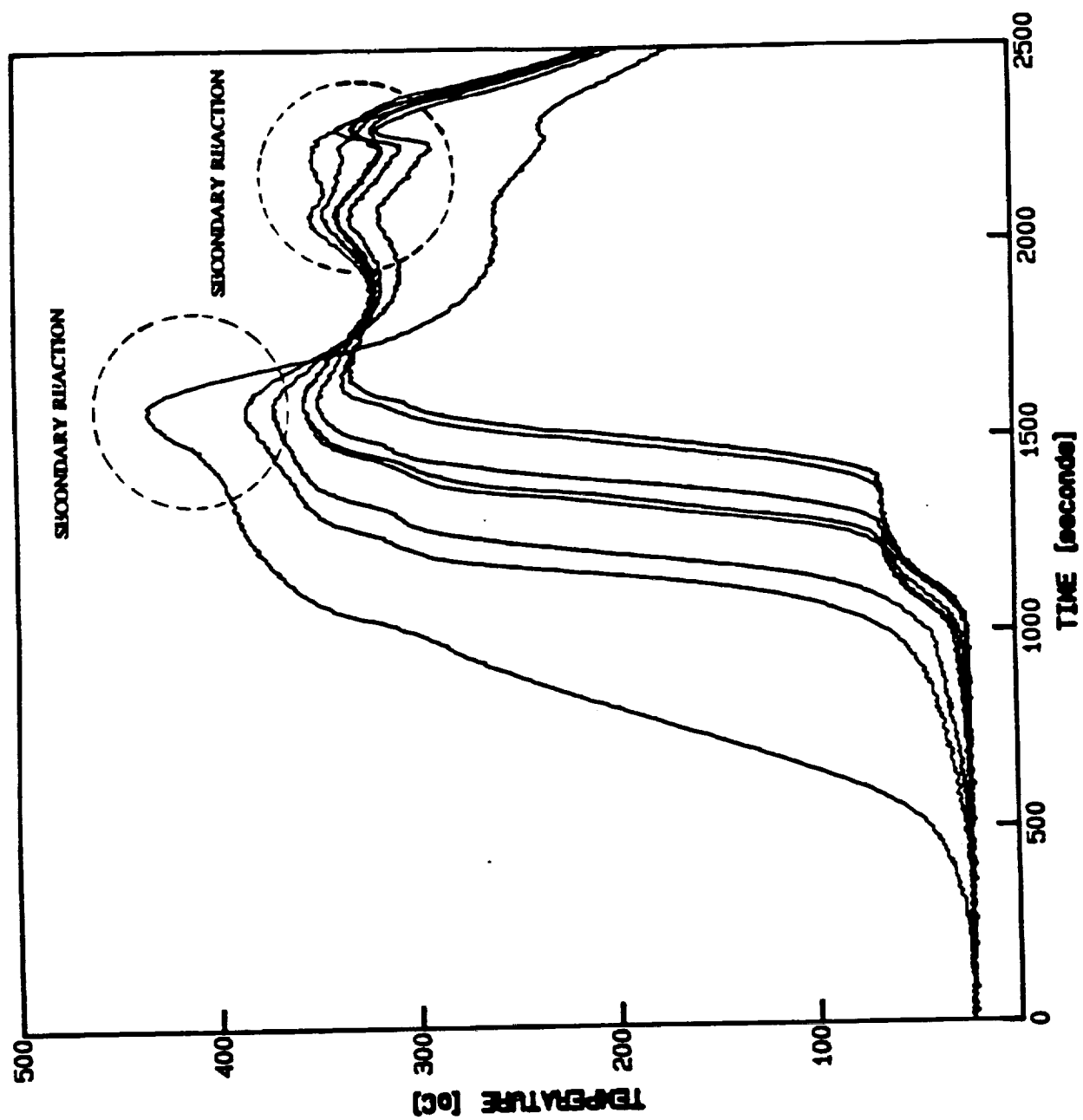
FIGURE 8

FIGURE 9

FIGURE 10
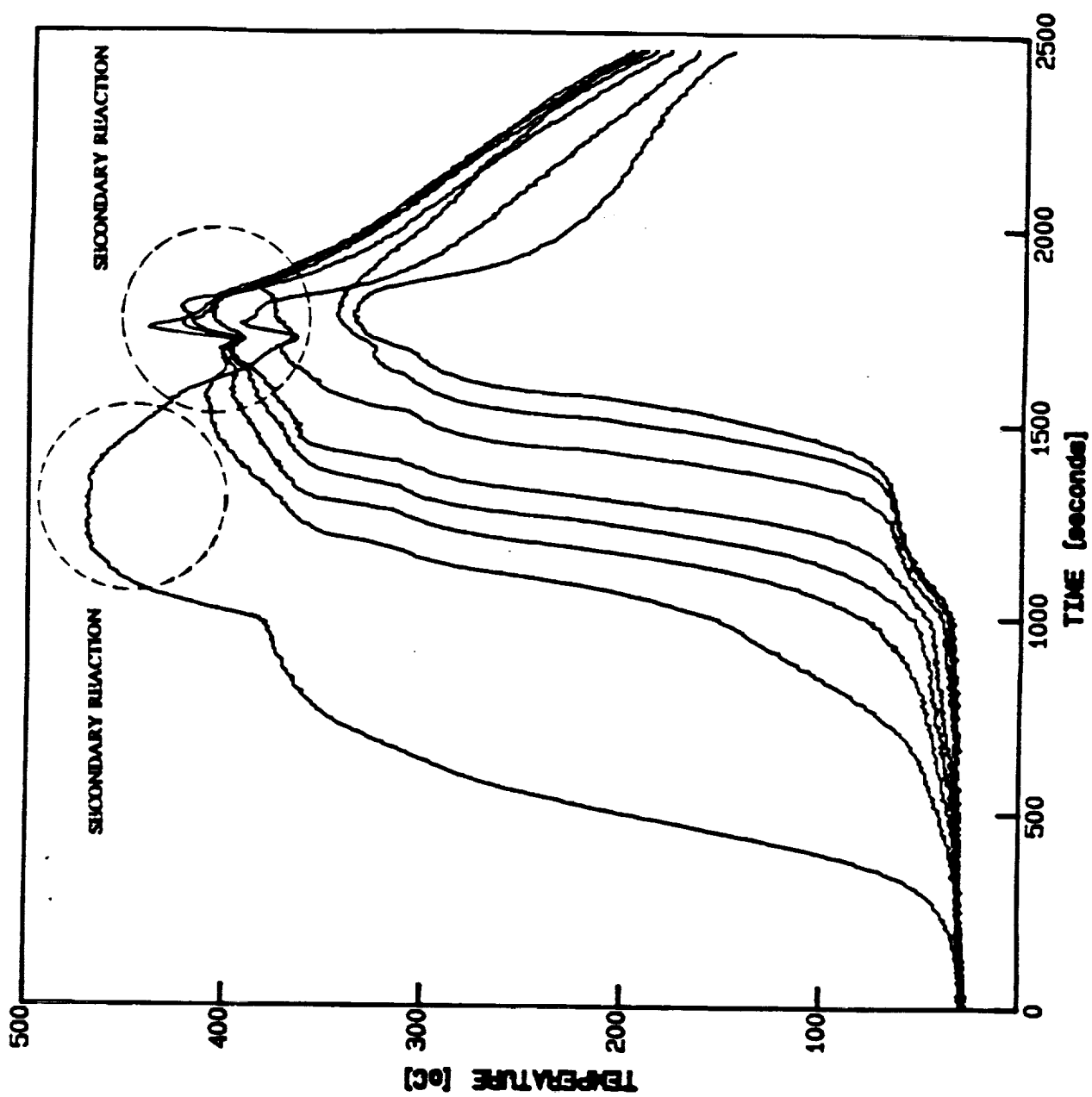
PAPER 10

"SMOLDERING COMBUSTION UNDER LOW GRAVITY"

Cantwell, E. and Fernandez-Pello, A.C.

AIAA-90-0648
**Smoldering Combustion Under Low Gravity
Conditions**

Elizabeth R. Cantwell
NASA Ames Research Center
Moffett Field, CA
and
A.C. Fernandez-Pello
University of California at Berkeley
Berkeley, CA

28th Aerospace Sciences Meeting
January 8-11, 1990/Reno, Nevada

Abstract

A study is being conducted on the effects of buoyancy in smoldering combustion, and the expected behavior of smolder under low gravity conditions. Initial experiments, on one-dimensional smoldering of polyurethane foam have been conducted, both in ground-based and drop tower facilities, to provide information for the design of space-based experiments. Results from these experiments are presented and discussed in light of our understanding of the various competing physical processes controlling smoldering combustion. These results show that for low forcing flow rates, smolder behaves differently in the absence of gravity than at normal gravity.

1. Introduction

Smolder is defined as a non-flaming, exothermic surface combustion reaction[1]. Smoldering commonly occurs in porous and permeable combustible materials, and is distinguished from other combustion reactions by its low temperatures, lack of flame and slow propagation velocities. After smolder has been initiated, it propagates through the fuel by transferring heat, released during heterogeneous oxidation of the fuel, toward the virgin material. Heat is transferred by conduction, convection and radiation. Heat losses may be due to heating up the virgin fuel as well as conduction and convection to the ambient environment. Additionally, oxidizer, transported to the reaction zone by diffusion and convection, must be present in sufficient quantity to allow the reaction to proceed.

Smolder has been the subject of much interest and study because it is acknowledged as a significant fire safety hazard[1]. It can play a role in the initiation of unwanted fires, which may be triggered by a sudden transition from smolder to flaming. Smolder may progress for long periods of time undetected (because of its low intensity) until a sudden transition to flaming occurs.[1,4,8]

The terminology of smoldering for one-dimensional configurations is shown in Figure 1. Cocurrent smolder applies to the situation where, when viewed in a frame of reference attached to the smolder wave, both the fuel and the oxidizer enter the reaction zone from the same direction. Countercurrent smolder is therefore the situation where fuel and oxidizer enter the reaction zone from opposite directions. The interaction of the physical processes which control smoldering is quite complex, and models developed so far have been limited. An excellent review of smolder combustion modeling is that of Ohlemiller[1]. A limited number of experimental and theoretical

studies on the effect of buoyancy on steady smolder have been published[3]. With the exception of the works of Ohlemiller and Sato[11,12], relatively little work has been done in the areas of ignition data and analysis and transition to flaming modeling.

Since smolder is possible at air/fuel ratios only a few percent of stoichiometric[10], heat release and smolder velocities may be, relatively, quite low. Convective flow of gases, either free or forced, may therefore have a significant effect on smolder. In an effort motivated primarily by the need to understand the possible behavior of smoldering combustion in a space-based environment where natural convection will not be present, we have been studying the role of buoyancy in smolder initiation and propagation through porous combustible materials.

We have conducted a short program of microgravity experiments on smoldering combustion, using a drop tower, to obtain preliminary information on smolder behavior in this environment. These results are primarily qualitative, as the slow process of smolder allows only limited data to be obtained in the 2.2 seconds available in the drop tower. In this paper we will report on experimental results from both normal and low gravity studies. All configurations involve one-dimensional cocurrent smolder, either upward burning or downward burning. Results show that buoyancy does influence smolder propagation, as would be expected from a process so sensitive to convective mass and energy transfer, and we can begin to identify regions of parameter space where the role of buoyancy is most significant. Results also provide qualitative information for the role buoyancy plays in smoldering.
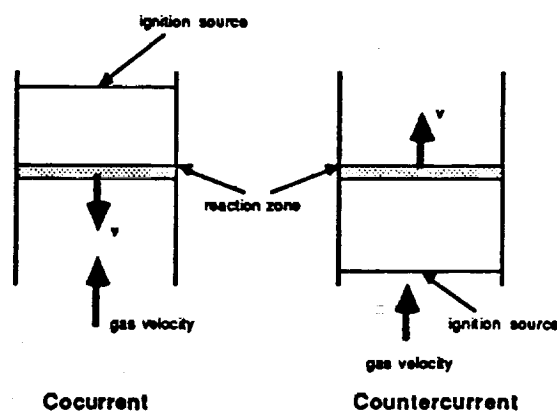

Figure 1

2. Experiment

All tests, at both normal and micro-gravity, were conducted on cubic samples of polyurethane foam, four inches on a side. Figure 2 shows a schematic of the general test apparatus. The sides of the test apparatus holding the foam were well insulated. For free flow conditions, top and bottom were left open. For forced flow conditions, one end was fitted to an air duct. Compressed standard air was used, and flow was controlled by either a Matheson 603/604 rotameter (ground tests) or a precision metering valve (drop tower tests).

Polyurethane foam was chosen as our fuel because it maintains its shape as it smolders (a critical issue for conducting both upward and downward burning tests at normal gravity) and it is a realistic test fuel for spacecraft fire hazards. Smoldering combustion of polyurethane foam has been studied extensively[4,5,6,7,8]. Smolder was initiated from the top (downward burning) or from the bottom (upward burning). Repeatable smolder initiation in polyurethane samples of this size and geometry proved to be a delicate task. After much trial and error, the procedure evolved to the following: A nichrome wire coil, through which a 10V current was passed, was placed against 3 layers of cotton linen (1 1/2 " square) centered in the open end of the sample. The wire, which heated to 450° C, was left on for 40 seconds to ensure that the top cloth layer had begun to smolder. Smolder proceeded through the three layers of cloth and into the foam sample below.

Temperature data were taken with K-type thermocouples placed at fixed distances along the centerline of the samples. The temperature histories of the thermocouples was used to determine both peak temperature and smolder velocity as a function of air flow rate. Smolder velocity was determined by taking the ratio of the distance between two thermocouples and the delay time of arrival of the smolder front between these thermocouples. Both sources of information were used to analyze the characteristics of the smolder propagation through the samples, and their variation with the environment.

3. Results

3.1 Downward Cocurrent Smolder at Normal Gravity

These tests were conducted on samples, as described above, in a chemical fume hood. In these tests, samples were ignited at the top and smoldered downward. When a forcing flow was applied, it was ducted upward through the samples from the bottom (see Figure 2). Peak temperatures measured by the topmost and bottommost thermocouples are plotted vs. a range of forced flowrates in Figure 3. Smolder velocities obtained with data from the topmost thermocouple pair and the bottommost thermocouple pair are plotted vs. forced flowrates in Figure 4. The topmost thermocouple is expected to be highly influenced by the ignition region, while the bottommost thermocouple represents a region independent of the
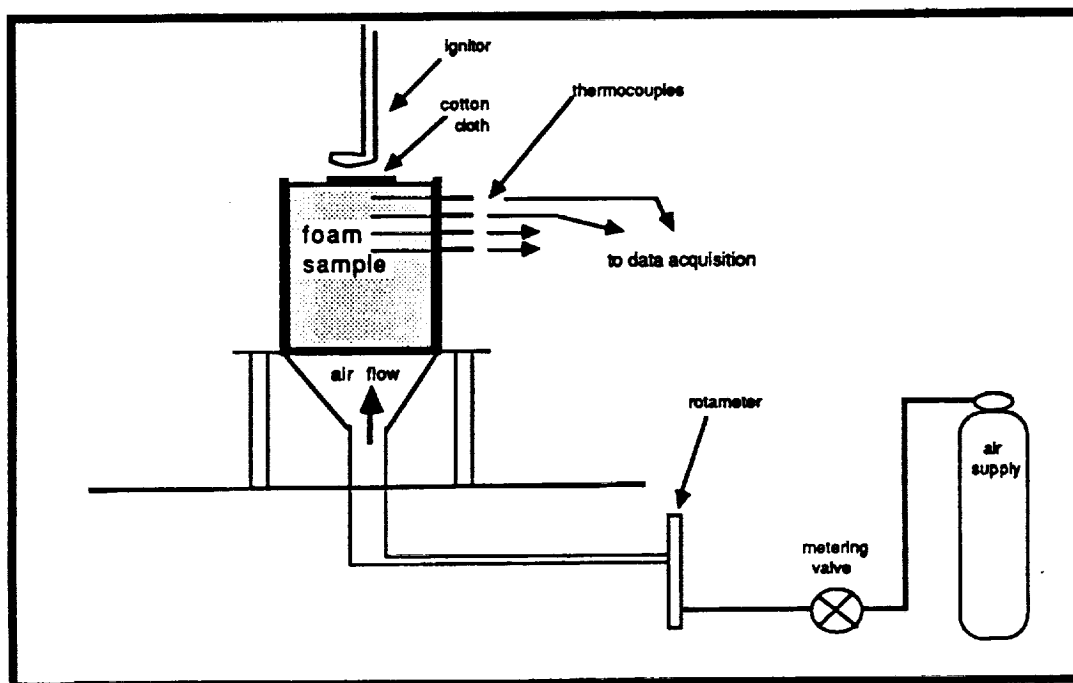

Figure 2

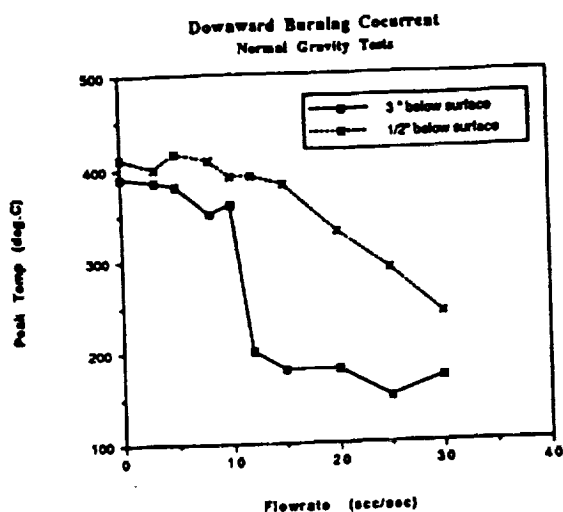**Downward Burning Cocurrent**
Normal Gravity Tests

Figure 3

ignition source. Note that Figure 4 reflects a nearly constant smolder velocity derived from the topmost thermocouple pair. This is another indication of the steadying effect of the ignition region.

In comparing Figures 3 and 4, it can be seen that there is a correspondance between peak temperature and smolder propagation velocity. In both figures, the uppermost temperature or velocity shows a region which, although affected by flowrate (higher flowrates produce cooler ignition regions), is clearly most strongly dependent on the fact that it is near the ignition zone. The bottommost thermocouple shows a strong drop at 12 scc/sec flowrate, true also for smolder velocity away from the influence of the ignition zone. This is at least partially the result of forced flow cooling. In addition, there is the possibility that this is where entrainment due to buoyancy is overcome by the forcing flow.

Downward Burning Cocurrent
Normal Gravity Tests
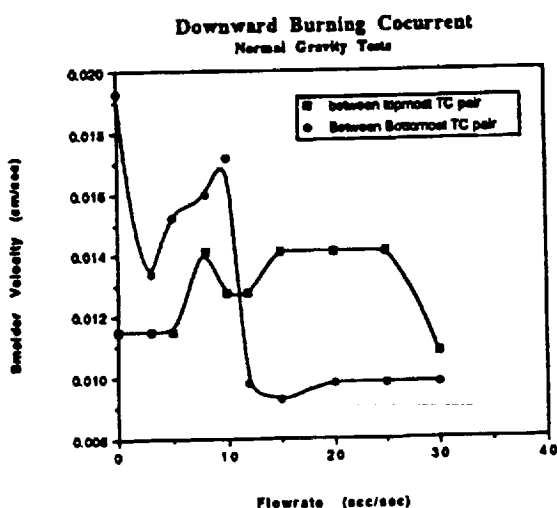
Figure 4

3.2 Upward Cocurrent Smoldering at Normal Gravity

In this case, samples were ignited at the bottom, smoldering upward, with forced air flowing downward through the samples for those cases where forcing flow was applied. For this configuration, the effect of buoyancy is more complex. Figure 5 shows peak temperatures measured by the topmost and bottommost thermocouples plotted against a range of flowrates. As can be seen in this figure, peak temperature drops drastically when flowrate is increased slightly, then climbs again in the range 25-40 scc/sec, then falls off at higher flow velocities. In these tests, buoyancy acts in a direction opposite to that of the forcing flow, moving combustion products upward into the porous foam. Since this is the case, we expect to see a region in flowrate space where the two flow effects counteract one another, and recirculation effects may be generated within the fuel bed. From Figure 5, we can see that at higher flow rates, forcing flow overcomes any effect due to buoyant flow, as was true in the downward burning case (see Figure 3). For the range of flowrates below that, we can now see the effects of buoyancy competing with forcing flow (rather than combining, as in downward burning).

3.3 Low Gravity Tests

Two series of tests were conducted under low gravity conditions - an ignition series and a steady smolder series. As mentioned previously, because of the short duration of each test, changes in smolder characteristics when g level was abruptly changed from one to almost zero were noted. All these tests were conducted in the 2.2 Second Zero-Gravity Facility at NASA's Lewis Research Center in Cleveland, Ohio. A schematic of this facility if shown in Figure 6. In this facility, 2.2 seconds of acceleration levels of about 10-5 g are achieved by allowing an experimental package to free-fall in the 89 ft. tower. The package is enclosed within a free-falling drag shield, designed with a low drag coefficient. Since the package and the drag shield fall freely and independently of each other, the package experiences drag due only to it's small velocity relative to the shield. At the end of a drop test, spikes on the bottom of the drag shield penetrate a 7-ft. deep bed of sand at the base of the tower, bringing the package to rest. Maximum decelerations are about 30 g.

Upward Burning Cocurrent
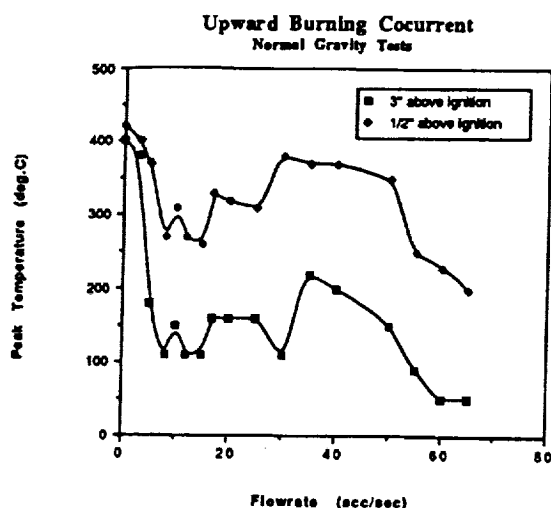**Normal Gravity Tests**

Figure 5

Figure 7 shows a schematic of the drop package, whose overall measurements were 36 by 16 by 30 inches. All data acquisition, power and timing equipment were mounted on the drop package itself. Either two or five K-type thermocouples, ungrounded junction of diameter .001", were used for these tests. For the ignition tests, two thermocouples were use, one just under the foam surface and another 1/4" below that. For the steady smolder tests, five thermocouples were used, placed at 1/2" intervals through the foam. Note that the purpose here was not to measure smolder velocities. We initiated a drop after steady smolder was established, and then looked at changes registered by any of the five thermocouples as single entities. Temperature data were taken and stored with a small on-board data acquisition and control computer. The efm for each thermocouple was recorded 20 times per second, and at the end of

each drop the data were transferred to a PC for reduction and analysis. The smolder apparatus was mounted at the center of a 10 in. diameter, and 2 foot tall combustion chamber. Air flow, from a regulated pressure cylinder on the rig, was controlled by a precision metering valve. The metering valve was calibrated on the ground, and the calibration was checked at the end of each days drops. Air entered the combustion chamber through ports mounted on its floor, and was ducted into the apparatus and through the foam. Volumetric flow rates were very small, and did not affect the pressure in the combustion chamber over the lengths of time that these tests were conducted.

Samples were ignited in 1 g and then dropped. For the tests designed to look at ignition, the drop occurred after a ninety second wait, which was determined from ground tests to be enough time for the foam to just begin to smolder. Tests conducted to see if information could be gained from looking at the 1 g to 0 g transition in steady smolder had a 5-7 minute wait after ignition. This was necessary to allow the smolder front to move into the body of the foam sample. The drop in these tests occurred when the smolder front just reached a particular thermocouple.

3.3.1 Low Gravity Ignition Tests

14 tests were conducted, using five different forcing flow rates over the range of 0-20 scc/sec. For these tests, the samples were ignited in 1 g and then dropped while still in the ignition phase (i.e., self-sustaining smolder was achieved in the cotton cloth but not in the foam itself). What is derived from these tests is information on how temperature

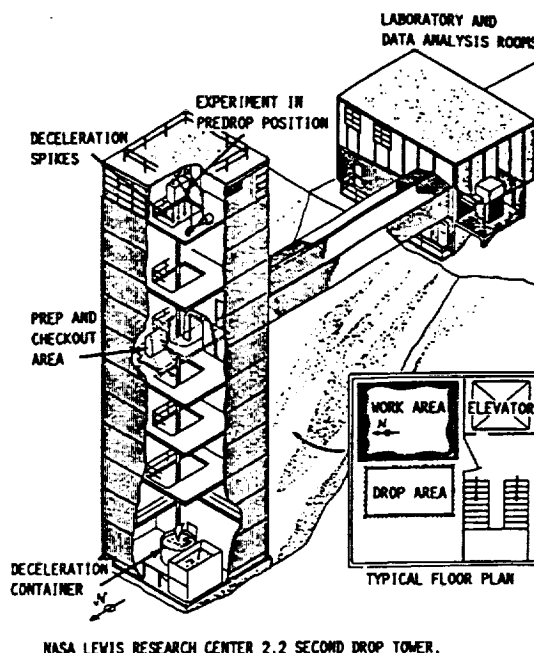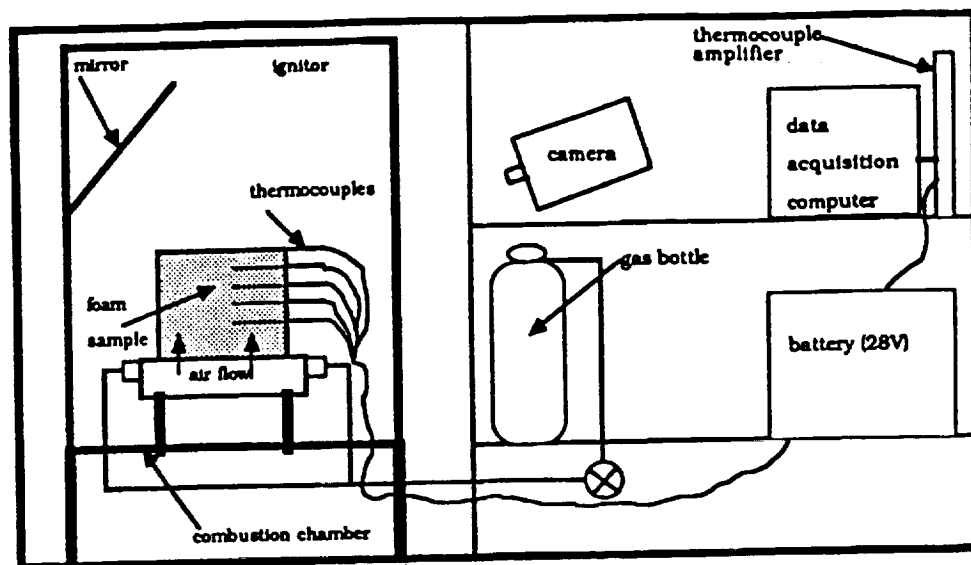NASA LEWIS RESEARCH CENTER 2.2 SECOND DROP TOWER.

Figure 6

Figure 7

changes in the immediate vicinity of ignition as we go from 1 g to 0 g. Figure 8 shows a representative graph of temperature vs. time results for a single one of these drops. Graphical representation of the overall results in shown in Figure 9. Figure 9 shows the average change in slope of the recorded temperature (°C/sec) from before drop initiation through the duration of the drop. This figure clearly shows that there is a significant change at lower flowrates, and that this change becomes negligible as the flowrate increases (somewhere after 8scc/sec). This indicates that forced flow conditions are dominant at larger flowrates, in qualitative agreement with the normal gravity data.
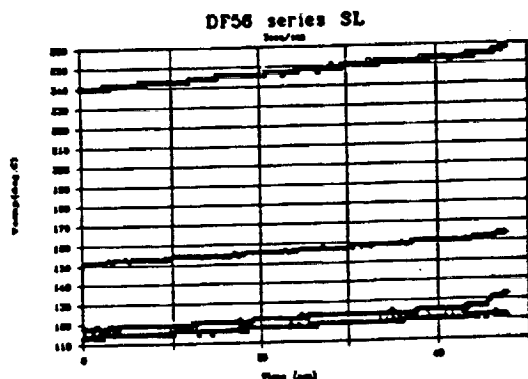
Figure 8

3.3.2 Low Gravity Steady Smolder Tests

14 tests were conducted over three flowrates. These tests had the same apparatus as the ignition series, but with more thermocouples, as was explained earlier. In these cases, The drop package sat at the top of the tower for 5-7 minutes between ignition and dropping, to allow steady smolder to become established in the samples. The drop was initiated when the smolder wave reached one of the thermocouples. This was accomplished by having the on-board computer send a signal when the temperature recorded by the third thermocouple reached levels expected in the smolder front. These results are far more difficult to interpret than the ignition cases because there is not the uniformity seen in the ignition series. There were three types of results from these tests. They will be described here and discussed qualitatively in the next section. In three cases, oscillations in temperature can be observed at the reaction zone after the package drops. These are not artifacts of the data acquisition system. There are also four definite, clear cases, for low flow rates, where the temperature at both the reaction zone thermocouple and the topmost thermocouple goes up after the drop. This parallels the results of the ignition series tests. The rest of the drops show little or no changes at any of the thermocouples. This may well have resulted from errors in drop signal timing or delays in the drop sequence causing the drop to occur with the reaction front not located right at a thermocouple.

4. Discussion and Conclusions

In comparing the two configurations of normal gravity studies, it should be noted that, while both are cocurrent, in one case (downward burning) the
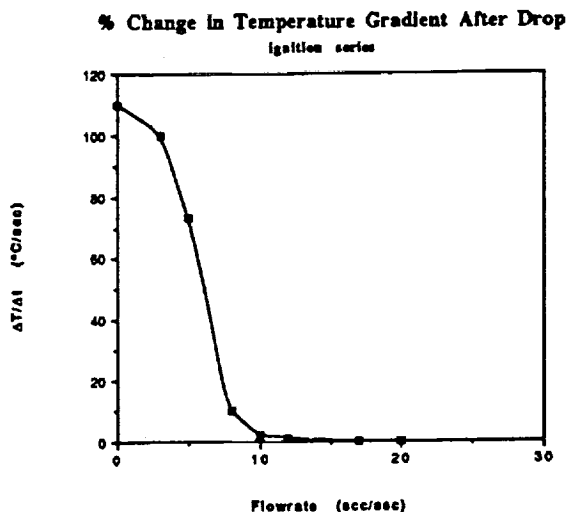
% Change in Temperature Gradient After Drop

Ignition series

Figure 9

forcing flow acts in the same direction as flow due to buoyancy, and in the other case (upward burning) they act in opposite directions. For the downward burning case, at low forcing flow velocities, there will be a buoyant plume above the hot smoldering region that will carry away hot products and entrain fresh cooler air, bringing it into the smolder region. For larger values of forcing flow, flow effects due to buoyancy will be overpowered. It is expected that, for forced flowrates above a threshold value, buoyancy will not play a role. For the upward burning case as well, we expect to see buoyancy playing a role at lower flowrates, and being overcome by forcing flow effects after some threshold. Figures 3, 4 and 5 all indicate that there appears to be a region where buoyancy does play a clear role in smoldering propagation. That region is 5-15 scc/sec for the geometry and fuel we are studying.

The smolder process itself is very slow, and occurs (in steady state) in a time frame far longer than two seconds (approximately 20 minutes for complete burning in the sample size we had). Our objective in using the Drop Tower has been to obtain trends and to examine the changes which occur in a smoldering sample during the transition from normal to low gravity. While somewhat limited data have been obtained, this preliminary level of information is critical for the design of future, longer time scale experiments in low gravity, particularly for the development of smolder initiation techniques in low gravity.

As was seen from the normal gravity tests in this program, buoyancy driven convective heat and mass transfer do play a role in smoldering combustion. In the ignition phase, buoyancy affects both the heat transfer from the ignition source and the mass flux of oxygen to the smolder initiation zone. An understanding of the differences we can expect in

initial temperature and location of combustion products for 1 g and 0 g cases is necessary in order to design an ignition system for space-based experiments.

As can be seen from Figure 9, low gravity vs. one gravity trends cease to show differences for higher forced flowrates, but do reflect changed for the lower flowrates. the region where differences occur encompasses the same range as was observed in the normal gravity downward burning tests (see Figure 4). These tests indicate that there is a definite region where smoldering combustion will behave differently in the absence of gravity than it does at one g, and that this difference may affect the whole process of ignition to smolder. What is interesting to note is that, over the time scale of these tests (2.2 sec.) the system responds more to the influence of heat loss changes than it does to any changes in the oxygen flux. This clearly affected the results of the low gravity steady smolder series of tests, where at least part of the problem was that the characteristic time for steady smolder inside a porous body to be affected by changes in buoyant currents is much longer than for smolder initiation. It is also true, however, that the steadying effects that we saw in the normal gravity tests from the ignition zone will not necessarily be present at the location of most of the thermocouples in these tests.

From our ground tests, where we studied one-dimensional cocurrent smolder, we have identified a range of low flowrates where buoyancy affects smolder propagation, for the fuel and geometry we are studying. The results of our preliminary low gravity tests, looking at the same fuel and geometry in a 2.2 second drop tower, indicate that there are differences in the behavior of smolder over the same range of low flowrates, when compared with normal g tests. In order to truly verify these results for steady smolder over the range of flowrates which should be studied, we need to move to a facility which allows longer periods of low gravity.

References

1. Ohlemiller, T. "Modeling of Smoldering Combustion Propagation", Progress in Energy and Combustion Science, 11, pp.277-310, 1986

2. Dosanj, S.S., Pagni, P.J. & A.C. Fernandez-Pello, "Forced Cocurrent Smoldering Combustion", Combustion and Flame, 68, pp.131-142, 1987

3. Dosanj, S.S., Peterson, J., Fernandez-Pello, A.C. & P.J. Pagni, "Buoyancy Effects on Smoldering Combustion", Acta Astronautica, 13, pp.689-696, 1987

4. McCarter, R.J., "Smoldering Combustion of Polyurethane Foam", Journal of Fire and Flammability, 3, pp.128-140, 1976

5. Ohlemiller, T. & F.E. Rogers "A Survey of Several Factors Influencing Smoldering Combustion in Flexible and Rigid Polymer Foams", Journal of Fire and Flammability, 9, pp.489-509, 1978

6. Rogers, F.E. and T. Ohlemiller "Smolder Characteristics of Flexible Polyurethane Foams", Journal of Fire and Flammability, 11, pp.32-44, 1980

7. Ohlemiller, T., Bellan, J. and F.E. Rogers "A Model of Smoldering Combustion Applied to Flexible Polyurethane Foams", Combustion and Flame, 36, pp.197-215, 1979

8. Ortiz-Molina, M.G., Toong, T.Y., Moussa, N.A., and G.C. Tereso, "Smoldering Combustion of Flexible Polyurethane Foams and Its Transition to Flaming or Extinguishment", Seventeenth Symposium (International) on Combustion, The Combustion Institute, pp.1191-1200, 1979

9. Jumper, G.Y. and R.L.P. Custer "Ignition in Microgravity", AIAA-89-0180, 27th Aerospace Sciences Meeting, AIAA, Reno, Nevada, January, 1989

10. Summerfield, M., Messina, N.A. & L.S. Ingram, "Definition of Smoldering Experiments for Spacelab", NASA CR-159528, January, 1979

11. Ohlemiller, T.J., "Forced Smolder Propagation and Transition to Flaming in Cellulosic Insulation", NBS Report NBSIR 85-3212, October 1985

12. Sega, S., Sato, K., Takaoka, F. & K. Saburi "Transition From Smolderinng to Flaming with High Temperature Air Flow", Annual Meeting of the Japanese Association of Fire Science and Engineering, pp.145-148, 1988

PAPER 11

"SMOLDERING COMBUSTION UNDER LOW GRAVITY CONDITIONS"

Cantwell, E.R., and Fernandez-Pello, A.C.

Smoldering Combustion Under Low Gravity Conditions

E.R. Cantwell and A.C. Fernandez-Pello
Department of Mechanical Engineering
University of California
Berkeley, Ca. 94720

ABSTRACT

Smoldering combustion experiments have been conducted in normal gravity, in a Drop Tower (the NASA Lewis Research Center 2.2 second drop tower) and in an aircraft following a parabolic trajectory (NASA KC-135), to observe the effects of buoyancy (and the absence of buoyancy) on opposed smoldering of samples of polyurethane foam. In opposed smolder the smolder reaction propagates in a direction opposed to that of the forced oxidizer flow. Initial information on smolder behavior in a microgravity environment has been obtained and compared with normal gravity tests. The slow process of smolder (approximately 1 mm/sec) allowed somewhat limited data acquisition in the drop tower tests (where 2.2 seconds of microgravity are available). In the KC-135 tests (30 seconds of low gravity for up to 40 parabolas), considerably more data was obtained, as a single sample was smoldered for an entire flight, with data acquisition occurring during both high-g and low-g portions of each flight. The experimental results show that buoyancy affects both species transport and transfer of heat to and from the reaction zone. Results from parabolic flight tests indicate that at the reaction zone transport of O_2 is dominant, and the consequent reaction temperature decreases in microgravity. Away from the reaction zone, temperature increases in microgravity due to the lack of convective cooling. All of these effects are less noticeable as the flow velocity is increased, and as the reaction propagates more toward the interior of the foam samples.

INTRODUCTION

This paper summarizes a preliminary analysis of the results of a study of smoldering combustion under low gravity conditions. Smolder is defined as a non-flaming, exothermic surface combustion reaction[1]. It commonly occurs in porous and permeable combustible materials, and is distinguished from other combustion reactions by its low temperatures, lack of flame and slow propagation velocities. After smolder has been initiated, it propagates through the fuel by transferring heat, released during heterogeneous oxidation of the fuel, toward the virgin material. Heat is transferred by conduction, convection and radiation. Additionally, oxidizer, transported to the reaction zone by diffusion and convection, must be present in sufficient quantity to allow the reaction to proceed. An excellent review of smolder combustion modeling is that of Ohlemiller[1]. A limited number of experimental and theoretical studies on the effect of buoyancy on steady smolder have been published[2,3]. Since smolder is possible at air/fuel ratios only a few percent of stoichiometric[3], heat release and smolder velocities may be, relatively, quite low. Convective flow of gases, either free or forced, may therefore have a significant effect on smolder. In an effort motivated primarily by the need to understand the possible behavior of smoldering combustion in a space-based environment where natural convection will not be present, we have been studying the role of buoyancy in smolder initiation and propagation through porous combustible materials. The particular fuel used for all of these studies is polyurethane foam, which has been studied previously for it's smoldering properties[5,6,7,8,9].

In the current investigations, smoldering combustion experiments have been conducted in normal gravity, and at low gravity in a Drop Tower (the NASA Lewis Research Center 2.2 second drop tower) and in an aircraft following a parabolic trajectory (NASA KC-135), to observe the effects of buoyancy (and the absence of buoyancy) on opposed smoldering of samples of polyurethane foam. Initial information on smolder behavior in a microgravity environment has been obtained and compared with normal gravity tests. The slow process of smolder (approximately 1 mm/sec) allowed only limited data acquisition in the drop tower tests (where 2.2 seconds of microgravity are available). In the KC-135 tests (30 seconds of low gravity for up to 40 parabolas), considerably more data was obtained, as a single sample was smoldered for an entire flight, with data acquisition occurring during both high-g and low-g portions of each flight. The results of

the KC-135 investigations will be the focus of this paper. The other investigations have been reported on in detail in a previous paper [4], and will only be summarized here.

EXPERIMENTAL DETAILS

All tests involve downward propagation of reverse or opposed smolder of polyurethane foam. Figure 1 shows a schematic of opposed downward smolder. In this configuration, the smolder reaction is ignited at the top of the fuel sample and propagates downward against an opposing flow of air. All tests, at both normal and low gravity, were conducted on cubic samples of polyurethane foam, four inches on a side. Figure 2 shows a schematic of the test apparatus used for all of these experiments. A foam sample was ignited at the top. The sides of the test apparatus holding the foam were well insulated. One end of the foam container was fitted to an air duct through which a flow of air forced. Compressed standard air was used, and flow was controlled by either a Matheson 603/604 rotameter (ground tests) or a precision metering valve (drop tower tests and KC-135 tests).Ground tests were conducted in a chemical fume hood, and in both the Drop Tower and KC-135 a combustion chamber (1.5'X1.5'X3') was used.

Polyurethane foam was chosen as our fuel because it maintains its shape as it smolders and it is a realistic test fuel for spacecraft fire hazards. Smolder was initiated from the top in the following manner: A nichrome wire coil, through which a 10V current was passed, was placed against 3 layers of cotton linen (1 1/2 " square) centered in the open end of the sample. The wire was left on for approximately 40 seconds to ensure that the top cloth layer had begun to smolder. Smolder proceeded through the three layers of cloth and into the foam sample below. It appears that the role of the cotton is to keep the smolder initiation region sufficiently insulated to prevent heat losses which may cause the reaction to extinguish. This proved a reliable and repeatable method for smolder initiation for all phases of this testing.

Temperature data were taken with K-type thermocouples placed at 1/2" intervals along the centerline of the samples. The temperature histories of the thermocouples was used to determine both peak temperature and smolder velocity (in the cases where data was sufficiently steady to derive it) as a function of time and air flow rate. Smolder velocity was determined by taking the ratio of the distance between two thermocouples and the delay time of arrival of the smolder front between these thermocouples. Both sources of information were used to analyze the characteristics of the smolder propagation through the samples, and their variation with the environment. In particular, for the KC-135 experiments, samples were ignited in normal gravity just prior to the initiation of the first parabola. In order to obtain low gravity, the KC-135 flies a series of parabolas consisting of a 2G acceleration upwards followed by a low gravity period of about 30 seconds. During each flight, a single sample was ignited and smoldered until it extinguished or was extinguished (~1 hr).

RESULTS FROM PREVIOUS WORK

From our ground tests, where studies were conducted on one-dimensional reverse smolder, a range of low flow rates where identified where buoyancy affects smolder propagation, for the fuel and geometry we are using. Figure 3 shows smolder velocity vs. forced flow velocity for downward smolder. The data leads to the identification of a range of low flow rates where buoyancy may be the mechanism causing differences in the results. Preliminary low gravity tests conducted in a drop tower, looking at the same fuel and geometry, indicated that there were differences in the behavior of smolder near the ignition zone over the same range of low flow rates when compared with normal gravity results. Figure 4 shows results from these tests. Though this preliminary work showed some apparent trends, it was clear that, because of the very slow propagation rates of smolder, longer low gravity times were needed to begin to define better the actual behavior of smolder in a low gravity environment.

RESULTS FROM CURRENT WORK

A series of four flights on the KC-135 were completed, each one with fixed experimental conditions. Two of the experiments with forced flow velocities of 0.14 and 0.22 cm/sec provided good data. A third experiment with forced flow of .05 cm/sec provided a small amount of additional data. A description of these results follows.

Near the reaction Zone

Figure 5 shows a sample of a complete days flight (0.14 cm/sec) with a thermocouple trace and acceleration data overlaid together vs. time. In this particular case, the smolder reaction is approaching and passing by the thermocouple as this set of parabolas is flown. Data like this was obtained for all three forced flow rates described above. As well, data from thermocouples ahead of the reaction (virgin foam) and behind the reaction zone (the char region) were obtained for 0.14 and 0.22 cm/sec. From these data sets, it was determined that, at least for the region quite close to the reaction zone, there are several time intervals which are evident. The first, called transition 1, was the time lag between the onset of 0G and an abrupt change in the sign of the temperature gradient. Transition 2 is the time lag between the end of 0G and the next change in sign of the temperature gradient. The trends of these time lags are summarized in Table 1.

	Forced Flow Rate	Parabola #	Transition 1 (sec)	Transition 2 (sec)
thermocouples				
1/2" from top	.05 cm/sec	1	...	...
surface		2	3.2	2.5
		3	2.5	2.5
		4	2.5	2.5
	.14 cm/sec	1	5	5
		2	3.5	3.4
		3	3.4	2.8
		4	1.8	0
		5	1.8	1.8
		6	7	...
	.22 cm/sec	1	8	4
		2	2.5	2.5
		3	1.2	1.2
		4	6.5	5.0
thermocouple				
1 1/2" from				
top surface	.14 cm/sec	2	8.5	5.3
		3	5.3	4.2
		4	4.0	4.2
		5	6.1	5.1
	.22 cm/sec	1	9.8	5.0
		2	4.2	4.0
		3	4.0	2.5
		4	12	10

<center>Table 1</center>

Note that when smolder occurs further inside the porous body the time it takes to be affected by changes in gravity is longer. This is due to the resistance presented to the air passing through a longer sample prior to reaching the reaction zone. It appears that the effect of flow rate is that higher forcing flows have longer time lags for either transition. This makes sense qualitatively, since the effects of buoyancy are a more significant portion of the overall process for lower forcing flow rates.

In addition to time lags, lines have been fit to the data for the periods just prior to entering 0G and in 0G. These are tabulated as slopes ($\partial T/\partial t$) in Table 2, and Figure 6

shows an example of what portions of the thermocouple traces these values are derived from. As shown in Table 2, for lower forced flow rates in regions near the reaction zone, temperature rises faster just prior to the initiation of 0G (this is the pull-up, where acceleration is 2G's) and falls faster during 0G (this is shown graphically in Figure 7). This shows that, for the higher forced flow velocities, the effects of 2G or 0G are less and less noticeable. This is an indication that we are moving toward pure forced flow dominated smolder.

Forced Flow Rate	Thermocouple Location	$\partial T/\partial t$ Prior to 0G	$\partial T/\partial t$ in 0G
near reaction zone			
.05 cm/sec	1/2"	+.945	-1.93
.14 cm/sec		+.690	-1.58
.22 cm/sec		+.355	-1.26
.14 cm/sec	1 1/2"	+.904	-0.71
.22 cm/sec		+1.16	-0.80
away from reaction zone			
virgin foam			
.05 cm/sec	1 1/2"	-.148	+.263
.14 cm/sec	2"	-.019	+.289
.22 cm/sec	2"		
char regions			
.14 cm/sec	1/2"	-.228	+.480
	1 1/2"	-.113	+.658
.22 cm/sec	1/2"		
	1 1/2"		

Table 2 - Averages of $\partial T/\partial t$ Over Four Parabolas

Away From the Reaction Zone

Figure 8 shows thermocouple and acceleration traces which are an example of results from the char region. As can be seen from this figure, as well as Table 2, the effect of the 2G pull-up is minimal but during 0G the temperature clearly goes up. There is no discernable time lag for data from these regions, and the effect of forced flow rate seem to be that the temperature rise during 0G is smaller the higher the forced flow velocity. Qualitatively, this makes sense, since the higher the forced velocity, the smaller the percentage of overall convective heat loss that is due to buoyant convection. What is clear is that in these regions away from the reaction zone the reduced heat losses in 0G result in higher fuel temperatures.

CONCLUDING REMARKS

These data show significant variation, for smolder behavior in 0G, from that in a normal or higher gravity environment. For all forced flow rates examined, there is a greater change in smolder during 0G than during 2G accelerations. While the 2G pull-ups seemed to enhance smolder (see Figure 6), the reaction itself was always significantly depressed in 0G. The peak smolder temperature seen during these experiments was somewhat higher than that seen in ground-based experiments on smoldering polyurethane foam[6]. This is due to the high G maneuvers, which enhance oxygen flow to the reaction zone. This, and the response of the reaction to 0G indicate that this strong smolder reaction is oxygen supply limited. These tests give some possible evidence that smolder will simply extinguish in low gravity environments. But there are several factors which must still be better understood. The tests also show an apparent insulating effect, seen in the temperature rise in char regions during 0G, which may contribute to smolder sustainability at a lower temperature than those in these tests. The KC-135 environment will never allow examination of this because the 2G pull-ups enhance the smolder reaction prior to each 0G

period. This would of course be dependent on sufficient available oxygen to sustain a low temperature smolder reaction, since there is, particularly in high porosity fuels such as low density foams, a strong coupling between heat transfer and oxygen supply in a smolder reaction.[10]. It is unknown at this time whether there is sufficient oxygen in the pores of a foam fuel to sustain smolder (i.e. a purely diffusion controlled reaction).

REFERENCES

1. Ohlemiller, T. "Modeling of Smoldering Combustion Propagation", Progress in Energy and Combustion Science, 11, pp.277-310, 1986

2. Dosanj, S.S., Peterson, J., Fernandez-Pello, A.C. & P.J. Pagni, "Buoyancy Effects on Smoldering Combustion", Acta Astronautica, 13, pp.689-696, 1987

3. Summerfield, M., Messina, N.A. & L.S. Ingram, "Definition of Smoldering Experiments for Spacelab", NASA CR-159528, January, 1979

4. Cantwell, E.R. and Fernandez-Pello, A.C., " Smoldering Combustion Under Low Gravity Conditions", AIAA paper # 90-0648 ,AIAA 28th Aerospace Sciences Meeting, Reno Nevada, January, 1990

5. McCarter, R.J., "Smoldering Combustion of Polyurethane Foam", Journal of Fire and Flammability, 3, pp.128-140, 1976

6. Ohlemiller, T. & F.E. Rogers "A Survey of Several Factors Influencing Smoldering Combustion in Flexible and Rigid Polymer Foams", Journal of Fire and Flammability, 9, pp.489-509, 1978

7. Rogers, F.E. and T. Ohlemiller "Smolder Characteristics of Flexible Polyurethane Foams", Journal of Fire and Flammability, 11, pp.32-44, 1980

8. Ohlemiller, T., Bellan, J. and F.E. Rogers "A Model of Smoldering Combustion Applied to Flexible Polyurethane Foams", Combustion and Flame, 36, pp.197-215, 1979

9. Ortiz-Molina, M.G., Toong, T.Y., Moussa, N.A., and G.C. Tereso, "Smoldering Combustion of Flexible Polyurethane Foams and Its Transition to Flaming or Extinguishment", Seventeenth Symposium (International) on Combustion, The Combustion Institute, pp.1191-1200, 1979

10. Ohlemiller, T.J., "Forced Smolder Propagation and Transition to Flaming in Cellulosic Insulation", Combustion and Flame, 81, pp. 354-365, 1990
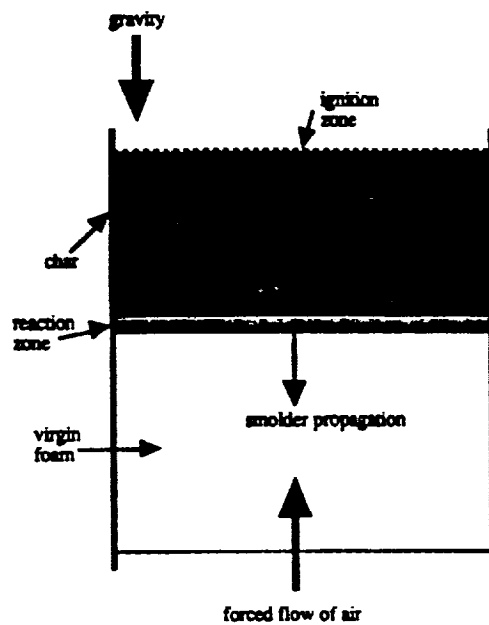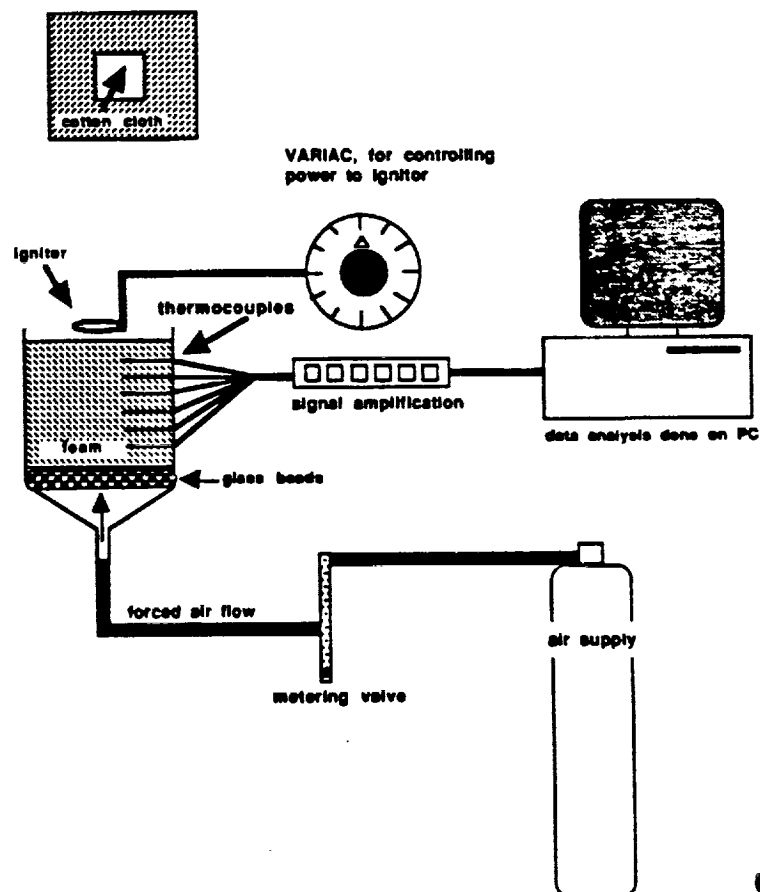
Figure 1   Opposed Downward Smolder

Figure 2   Test Apparatus Used for Opposed Smolder

Figure 3
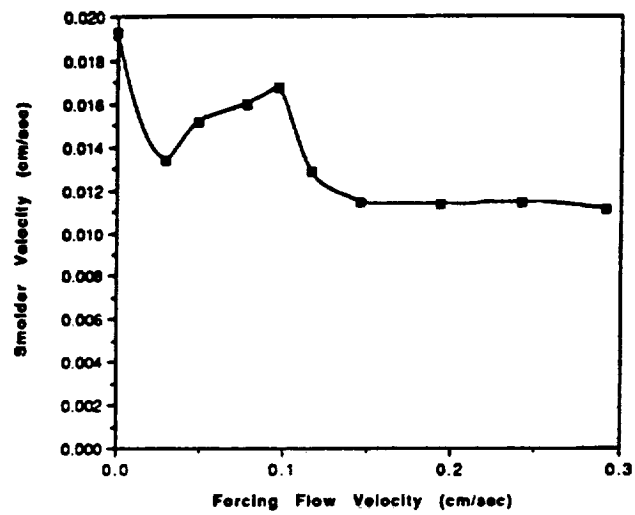## Data From Normal Gravity Tests
Downward Opposed Smolder

Figure 4
Data From Drop Tower Tests
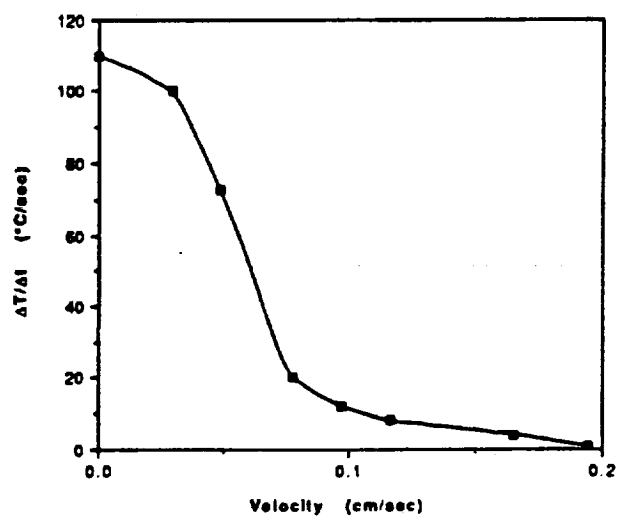### $\partial T/\partial t$ (°C/sec) During Drop

Figure 5
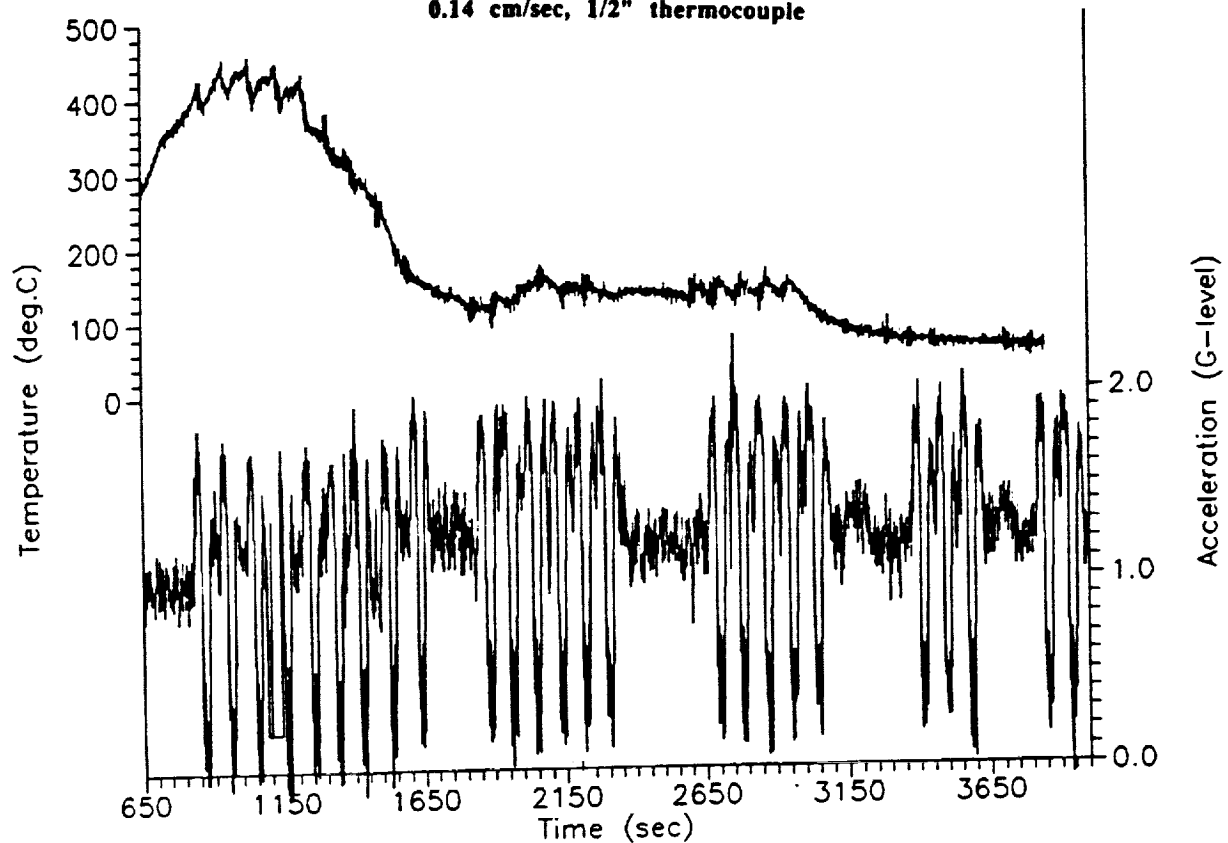**Data From An Entire Flight**
0.14 cm/sec, 1/2" thermocouple

Figure 6
Close-Up of 0.14 cm/sec Data
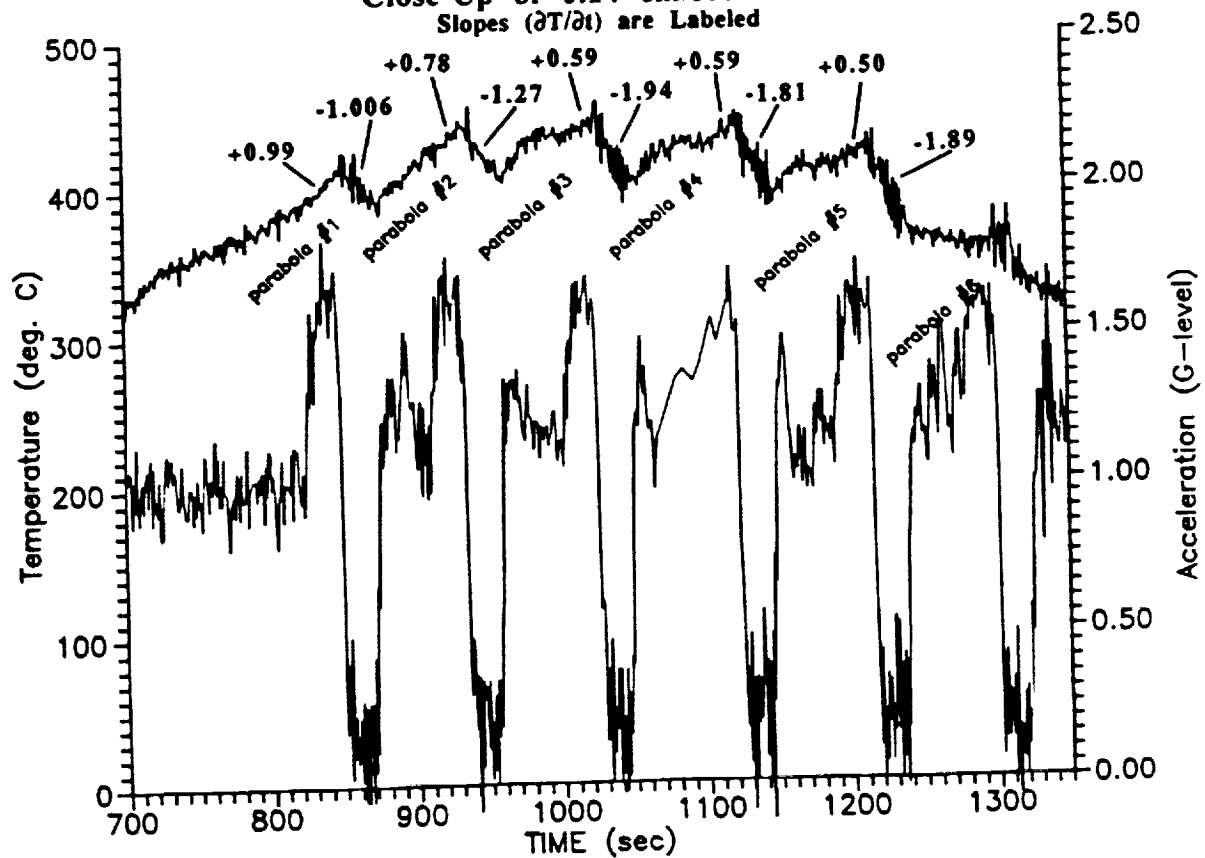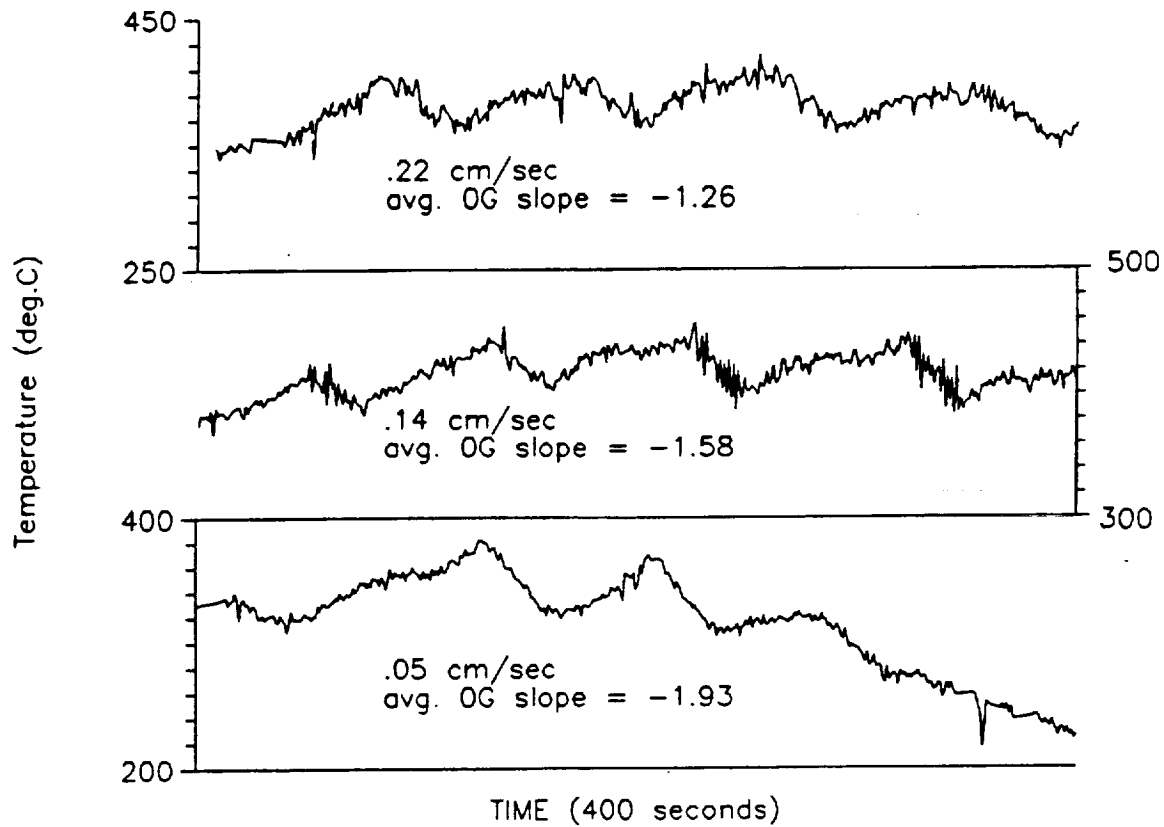Slopes ($\partial T/\partial t$) are Labeled
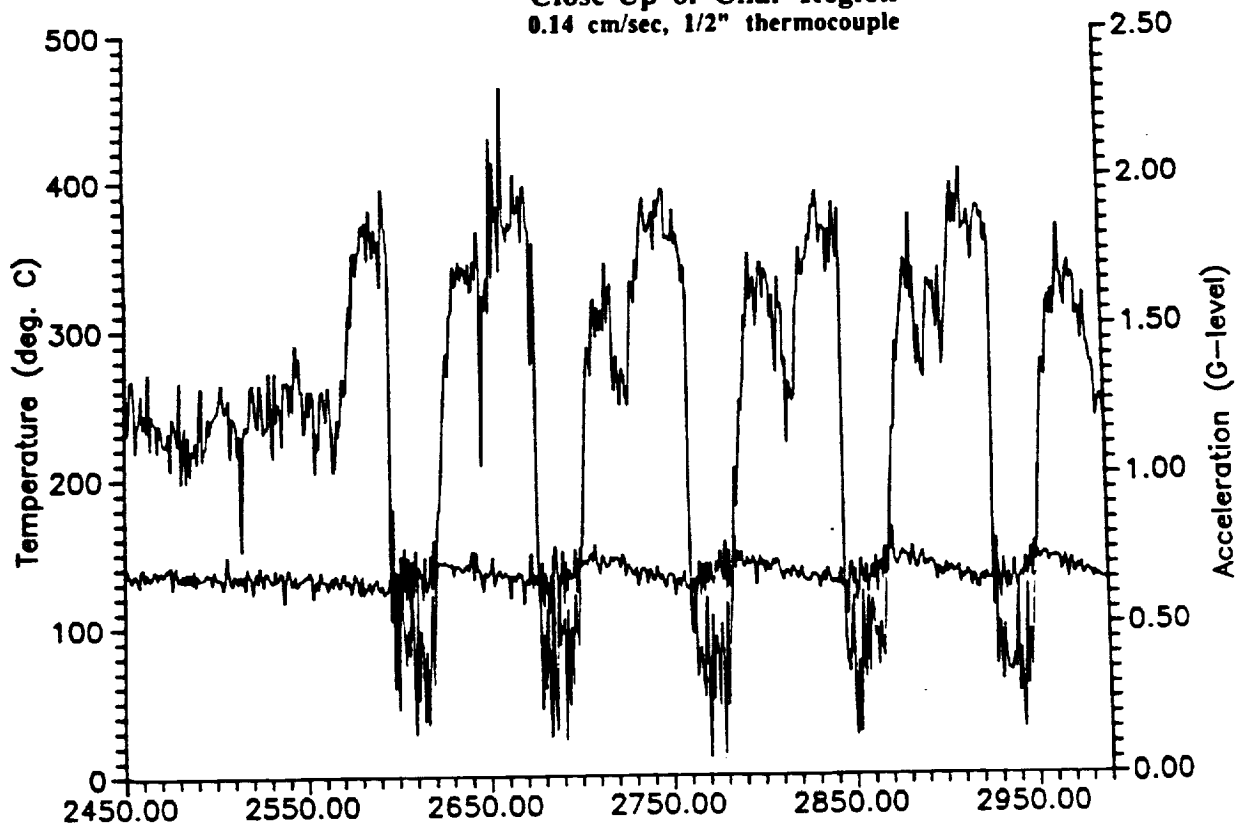
Figure 7
Comparative Close-Ups
1/2" Thermocouple

.22 cm/sec
avg. 0G slope = −1.26

.14 cm/sec
avg. 0G slope = −1.58

.05 cm/sec
avg. 0G slope = −1.93

TIME (400 seconds)

Figure 8
Close-Up of Char Region
0.14 cm/sec, 1/2" thermocouple

REPORT DOCUMENTATION PAGE

1. AGENCY USE ONLY (Leave blank)	2. REPORT DATE	3. REPORT TYPE AND DATES COVERED
	August 1995	Final Contractor Report

4. TITLE AND SUBTITLE

A Fundamental Study of Smoldering With Emphasis on Experimental Design for Zero-G

5. FUNDING NUMBERS

WU–962–22–00
G–NAG3–443

6. AUTHOR(S)

Carlos Fernandez-Pello and Patrick J. Pagni

7. PERFORMING ORGANIZATION NAME(S) AND ADDRESS(ES)

University of California, Berkeley
Department of Mechanical Engineering
Berkeley, California 94720

8. PERFORMING ORGANIZATION REPORT NUMBER

E–9837

9. SPONSORING/MONITORING AGENCY NAME(S) AND ADDRESS(ES)

National Aeronautics and Space Administration
Lewis Research Center
Cleveland, Ohio 44135–3191

10. SPONSORING/MONITORING AGENCY REPORT NUMBER

NASA CR–198378

11. SUPPLEMENTARY NOTES

Project Manager, Dennis P. Stocker, Space Experiments Division, NASA Lewis Research Center, organization code 6711, (216) 433–2166.

12a. DISTRIBUTION/AVAILABILITY STATEMENT

Unclassified - Unlimited
Subject Category 29

This publication is available from the NASA Center for Aerospace Information, (301) 621–0390.

12b. DISTRIBUTION CODE

13. ABSTRACT (Maximum 200 words)

A research program to study smoldering combustion with emphasis on the design of an experiment to be conducted in the Space Shuttle was conducted at the Department of Mechanical Engineering, University of California, Berkeley, under NASA sponsorship. The motivation of the research is the interest in smoldering both as a fundamental combustion problem and as a serious fire risk. Research conducted included theoretical and experimental studies that have brought considerable new information about smolder combustion, the effect that buoyancy has on the process, and specific information for the design of a space experiment. Experiments were conducted at normal gravity, in opposed and forward mode of propagation and in the upward and downward direction to determine the effect and range of influence of gravity on smolder. Experiments were also conducted in microgravity, in a drop tower and in parabolic aircraft flights, where the brief microgravity periods were used to analyze transient aspects of the problem. Significant progress was made on the study of one-dimensional smolder, particularly in the opposed-flow configuration. These studies provided the background for a continuation research program currently underway on smoldering, also supported by NASA. They also provided enough information to design a small-scale space-based experiment and that was successfully conducted in the Spacelab Glovebox in the June 1992 USML-1/STS-50 mission of the Space Shuttle Columbia.

14. SUBJECT TERMS

Smoldering; Combustion; Microgravity; Polyurethane foam; Buoyancy

15. NUMBER OF PAGES

274

16. PRICE CODE

A12

17. SECURITY CLASSIFICATION OF REPORT	18. SECURITY CLASSIFICATION OF THIS PAGE	19. SECURITY CLASSIFICATION OF ABSTRACT	20. LIMITATION OF ABSTRACT
Unclassified	Unclassified	Unclassified	